Nanocellulose-based Composite Hydrogels for Water Remediation

by

Yufei Nan

A dissertation submitted to the Graduate Faculty of
Auburn University
in partial fulfillment of the
requirements for the Degree of
Doctorate of Philosophy

Auburn, Alabama
December 9, 2023

Keywords: water treatment, nanocellulose, hydrogel adsorbent, adsorption, particle size

Approved by

Dr. Maria S. Peresin, Chair, Associate Professor of Forest Biomaterials, Auburn university
Dr. Zhihua Jiang, Associate Professor of Chemical Engineering, Auburn University
Dr. Brian K. Via, Region Bank Professor of Forest Products, Auburn University
Dr. Daniel C. Whitehead, Associate professor of Chemistry, Clemson University
Dr. Yucheng Peng, Assistant professor of Sustainable Bioproducts, Auburn University
Dr. Yucheng Feng, University reader, Professor of Soil Microbiology, Auburn University

Abstract

Water quality issues caused by chemical contaminants are a major challenge that humanity is facing in the twenty-first century. Designing an environmentally benign bio-adsorbent material for the removal of pollutants from water resources was a sustainable strategy to ensure water safety. Nanocellulose is an attractive candidate for water remediation owing to abundant renewable resources and tunable physicochemical characteristics. However, most of them are synthesized by chemical cross-linkers, which usually cause a second pollution and extra cost. Moreover, most nanocellulose composites adsorbents are available in powder form, which present poor separability and recyclability.

In order to address these issues, the main objective of this dissertation is to design and synthesize stable nanocellulose-based 3-D composite hydrogels by self-assembly mechanisms for water remediation. Their chemical, morphology, and surface properties were characterized, and their adsorption behavior for toxic dyes, heavy metal ions, oil spills was investigated in terms of the optimal functionalized polymer content, pH effect, kinetics, and isotherm models. The results show that after functionalization, their adsorption capability for toxic dyes, metals ions and oils are all significantly increase, especially for toxic dyes due to the electrostatic attraction mechanism. This work not only provides a simple and cost-effective synthetic route to nanocellulose-based 3-D composite adsorbents, but also offers valuable clues for the removal of multiple water pollutants.

Acknowledgments

Firstly, I want to give special thanks to my advisor Dr. Maria Soledad Peresin for her constant encouragement and guidance not only on research, but also on academic and professional development throughout my PhD. Thank you for organizing parties or events on special holidays, which make me feel less alone during those festivals and allow me to experience the culture and traditions of various countries. I am also grateful to my committee members Dr. Zhihua Jiang, Dr. Brian K. Via, Dr. Daniel C. Whitehead, and Dr. Yucheng Peng, thank you for spending your time and patience as well as providing insightful comments on my research projects and the dissertation.

I would like to thank Dr. Xinyu Zhang for allowing me to do part of my research in his lab and thank Haishun Du for guiding me to finish them. Thanks to Dr. Sushil Adhikari for allowing me to use Element Analyzer in his lab and thanks to Tawsif Rahman for training and help. Thank Dr. Michael Miller for the SEM training and guiding for some tests. Thanks to Dr. Zeki Billor for the ICP-MS test. And thanks to Dr. Mi Li and his student Kailong Zhang in University of Tennessee Knoxville for supporting the iGC-SEA test.

I want to thank my lab mates, Diego Gomez-Maldonado, Maria Celeste Iglesias, Javier Hernandez Diaz, Sydney Brake, Diego Alejandro Cuartas Marulanda, Laura Alvarez Marin, Duber Esmely Garces Martinez, Daniel Owusu Sekyere. I want to specially thank Diego Gomez-Maldonado for guiding me to do my research, write my paper, as well as academic and professional development. Thanks, Diego, for always responding to me with any questions. I want to specially thank Fatimatu for modifying dissertation and giving support and encourage during dissertation writing time. I also want to specially thank Sydney and Nate for accompanying me, supporting me, and sharing

life with each other as well as inviting me to attend her/his family activities. Thank both of you for treating me as a family member. Thank Nate for helping address lots of issues in life.

I also want to specially thank my best friend Wenjing Ren and Na Guo for accompanying me and encouraging me at any time and sharing life with each other. Thank all my other friends, Zihao Bian, Teng Zhao, Yongfa You, Naiqing Pan, Xiaoyong Li. Thank you all of you are here and spend time with me.

I am very grateful to my families for their endless love, constant moral support, and encouragement throughout the years. Thanks to my mom, you are always in my mind, and you are the source of strength and spiritual support in my struggle.

I also want to thank myself for being brave and persistent. Thanks to myself for always thinking of ways to solve problems. Thanks to myself for being kind and always thinking about how to bring warmth to others.

Last but not least, I want to thank Dr. Flowers, the dean of the graduate school gave me the chance to come here and have all these experiences.

Table of Contents

List of Figures

List of Tables

List of Publications and Contributions

Peer-reviewed articles in archived literature

- **Nan, Y**.; Gomez-Maldonado, D.; Iglesias, M.C.; Whitehead, D.; Peresin, M.S. **(2023)**. Revalorization of soybean hulls as TEMPO oxidized cellulose nanofibers and polyethylenimine composite hydrogels. Cellulose, 30, pages 3639–3651. **(IF=6.12).**
- **Nan, Y.;** Gomez-Maldonado, D.; Whitehead, D.; Yang M.; Peresin, M.S. **(2023)**. Comparison between nanocellulose-polyethyleneimine composite synthesis methods towards multiple water pollutants removal: A review *Journal of Biological Macromolecules*, *232*(2023). 123342. **(IF=8.03).**

Peer-reviewed articles in preparation

- **Nan, Y.**; Gomez-Maldonado, D.; Iglesias, M.C.; Whitehead, D.; Yang, M.; Peresin, M.S. (2023). Investigating Interaction Mechanisms Between Cellulose-Polyethylenimine Hydrogels and Methyl Blue Dyes. (Submitted to *ACS Applied Materials & Interface*s 09/25/2023). (**IF=9.5**).
- **Nan, Y.;** Gomez-Maldonado, D.; Zhang K.; Du, H.; Whitehead, D.; Li, M.; Zhang, X.; Peresin, M.S. **(2023)**. Polyethyleneimine functionalized graphene oxide and cellulose nanofibril composite hydrogels for removal of water pollutants. *Carbohydrates Polymer***.** (**IF=11.2**).
- **Nan, Y.**; Gomez-Maldonado, D.; Zhu, J.; Yang, M.; Peresin, M.S. (2023). The effect of nanocellulose particle size on its surface properties and adsorption behavior of toxic dyes. In preparation.

Chapter 1. Introduction

Water contamination caused by harmful chemical compounds from industrial and municipal wastewater has become a global environmental concern. These compounds mainly include traditional toxic dyes, metal ions, spilled oils and emerging contaminants (ECs) [1, 2]. ECs are those that have been recently detected in natural environments, including pharmaceutical organic contaminants, personal care products (PCPs), endocrine disrupting compounds (EDCs), surfactants, pesticides, flame retardants, and industrial additives among others with the development of the times [2]. Most of the abovementioned contaminants are toxic, non-biodegradable and carcinogenic and their accumulation posed serious threats to human health and ecosystems. Therefore, it is important to remove these contaminants from the water prior to disposal or reuse.

Some methods have been developed over the years to remove contaminants from water. These methods include membrane filtration [3], coagulation [4], solvent extraction [5], photocatalytic degradation [6], chemical oxidation and reduction [7], biological oxidation [4], and adsorption [8]. Among these, adsorption has been considered the most commonly used method because of low cost, low energy consuming, simple, and easy operation procedure, and wide variety of adsorbent materials [9-11]. Currently, substantial research has focused on preparing novel eco-friendly adsorbents with large adsorption capacity, fast adsorption rate, facile separation, and reused property.

Generally, ideal raw materials for the development of adsorbent should meet certain requirements: (1) should be eco-friendly, (2) be inexpensive, (3) have good mechanical and structural integrity to overcome water flow for a long period, (4) show high adsorption capacities with high rates, (5)

have a large surface area and (6) possess a regeneration aptitude using cost-effective approaches [12]. Compared with metal–organic frameworks, or carbon and petroleum-based polymers, biopolymer-based materials are gaining more attention as adsorbents due to their cost effectiveness, renewability and biodegradability [13]. Cellulose is the most abundant bio-based polymer on the earth, with an annual production estimated as over 7.5×10^{10} tons [14]. This polymer possesses unique chemical, physical, and mechanical properties, which have been suggested its use for the production of a wide range of materials [15]. Moreover, it is easier to cleave cellulose hierarchical structure to obtain nanocellulose (NC) in the form of nanocrystals (cellulose nanocrystals, CNCs) and nanofibers (cellulose nanofibers, CNFs) through the development of emerging technologies, allowing for mor complex material design [16]. In this case, when the size is reduced to the nanoscale, the high specific surface area contributes to enhance the adsorption capacity of materials developed using these CNMs [12].

However, there are limitations to the application of nanocellulose (NC) absorbents. The pure NC adsorbents are easily disintegrated in water, which makes handling difficult during separation and reusing [17-19]. Besides, the adsorption capacity is relatively low due to the low electrostatic activity of hydroxyl groups [19]. The presence of abundant-OH groups in the NC structure also makes it difficult to be dispersed evenly in nonpolar solvents with inadequate interfacial adhesion with hydrophobic matrixes. This property makes NC susceptible to aggregation, reducing the surface area available for adsorption processes [20, 21]. Moreover, much reported NC-based adsorbent focuses on single water pollutants, which limit their practical settings because most of the water resources such as rivers, lakes, and even oceans contain complex mixtures of pollutants, including dyes, spilled oils, organic solvents, and heavy metals [22]. The chemical modification of cellulose nanomaterials can improve the adsorption capacity of adsorbents to pollutants in

aqueous solution and determine their selectivity for specific pollutants or multiple pollutants because there are more active binding sites after modification.

Numerous modification methods have been used to introduce various functional groups onto NC surface, such as silylation, carboxylation, acetylation, sulfonation, phosphorylation, and amidation, or grating with related polymers, as well as formation composites to increase adsorption performance for water treatment. Among all of them, introducing the amine groups has shown great potential for adsorption more types of water pollutnants, including metal ions, toxic dyes, some emerging contaminants and also can be used for carbon capture. Moreover, the charged amine groups in adsorbents can be protonated and deprotonated via adjusting the pH to enable the adsorption and desorption of contaminants, thus realizing the regeneration of the adsorbent [11]. Branched PEI, contains abundant primary, secondary, and tertiary amino groups on its molecular chain, and is an ideal water-soluble polymeric amine [23-25]. These active amino groups can be crosslinked by carboxy group, aldehyde, or epoxy group to fabricate hydrogels, membranes, and fibres polymers to develop bio-sorbents for treating wastewater. Therefore, PEI and nanocellulose composites could be show a promising composite in water remediation [11, 23, 26].

Combing cellulose or nanocellulose matrices with PEI has led to the production of a wide range of composites for water remediation and have shown supper adsorption capability for different kinds of pollutants than other adsorbents [16]. However, current research mainly synthesizes PEI-nanocellulose composites by chemical crosslinking with bridging agents or high temperature heating to promote the crosslinking of amino and carboxyl groups [16, 27]. The use of chemical crosslinker not only increase the cost but also could cause second contamination because the most frequently used cross-linkers are toxic, like glutaraldehyde (GAL) and epichlorohydrin (EPI) [16, 28-31]. Some of research reported without use of additional cross-linker or additive, directly cross-

links PEI and NC pre-functionalized by 2,2,6,6-tetramethylpiperidine 1-oxyl (TEMPO) by thermal processes, but this method requires freezing dry and then heating (more than 100 °C), which are high energy consuming processes [32-35]. Moreover, it was found that NC-PEI composite adsorbents typically come in powders or aerogels form. For the powders, they have poor separability and recyclability, thus making wastewater remediation a costly process [36]. Aerogel materials are highly interconnected porous and ultralight bulk solids. Their high porosity, large specific surface area, and ease of separation from aqueous solutions make them efficient sorbent for the removal of heavy metal pollutants [36-38]. Nevertheless, the formation of aerogels requires freeze-drying, which is a process that consumes a lot of energy, which increases the cost of the absorbent and carbon footprint. Therefore, it is necessary to synthesize 3-D porous nanocellulose based composites without the need for freeze-drying or chemical crosslinking to replace aerogel as an adsorbent. Hydrogels can overcome the problems from powders and aerogels.

In addition, existing research mainly focused on using those composites to remove a single type of contaminant from water. It is essential to realize that water pollution is a complex process in reality, given that it is not dealing generally with a single type of contaminant, but the co-occurrence of more than a single pollutant in the water systems [39, 40]. A paradigm shift from single pollutant to multi-pollutant control is crucial to tackle these water purification challenges.

Based on the above, the main aim of this work is to design and synthesize stable CNM-PEI 3-D composites hydrogels through self-assembling mechanisms for the removal of multiple pollutants from water resources.

This dissertation consists of seven Chapters. **Chapter 1** is the present introduction. In **Chapter 2**, presents the background and literature review. First, detailed information regarding the water

pollution problems caused by traditional and emerging chemical pollutants as well as current technologies for removing these pollutants and their advantages and disadvantages are discussed. Potential use of nanocellulose based materials for water remediation based on their sustainable and non-toxic properties, abundant resources, hierarchical structure, molecular structure with rich hydroxyl group as well as unique morphological and chemical properties produced by different processing techniques are presented. The limitations of nanocellulose in water remediation and current countermeasures are also presented in addition to the great potential of CNM/PEI composites in addressing this limitation. Additionally, a literature review summary of the application of CNM/PEI composites in water remediation and current problems are presented. The final part of this chapter focuses on the research aim and objective**. Chapter 3** focuses on the design and synthesis of stable hydrogels from CNF and PEI. This work relies on utilizing an agricultural by-product – soybean hulls – as a readily available raw material to produce CNFs to prepare hydrogels with PEI by self-assembling or physical interaction. Then immersed into a PEI solution for further functionalization by physical adsorption. The effect of concentration and pH of PEI solutions was investigated. In addition, the adsorption efficiency of the hydrogels for the capture of methyl blue dyes and Cu (II) ions from water was tested to explore the potential application of this new material for water remediation. **Chapter 4** is focused on the investigation of the effect of pH on the removal mechanism of methyl blue by the TCNF/PEI hydrogels at different pH. **In Chapter 5,** to further increase mechanical properties and adsorption capability of TCNF/PEI composites hydrogel to expend the scope of application, graphene oxidize (GO) as an adsorption site was introduced into TCNF/PEI composites hydrogel to design a new TCNF/GO/PEI composite hydrogel to target multiple water pollutants. To test the adsorption capability of the resulting TCNF/GO/PEI hydrogels for multiple water pollutants, the methyl

anionic dyes, methylene blue cationic dyes, Cu (II) ions, and soybean oils were used as references. **Chapter 6** focuses on exploring the effect of nanocellulose particle size on nanocellulose-based hydrogels' surface properties and adsorption behavior for toxic dyes. Finally, **Chapter 7** outlines the main research conclusions and recommendations for future work.

Chapter 2. Background and literature review

2.1 Background

2.1.1 Water scarcity and water pollution

Water scarcity is a major challenge that humanity is facing in the twenty-first century [41-43]. The shrinkage in available sources and reduction in quality can be correlated to various reasons, like rampant urbanization, industrialization, and uncontrolled population growth [44, 45]. Presently, more than 780 million people globally are unable to access safe water for drinking purposes, whereas more than 5 million people lose their lives due to water-related diseases. These losses equal ten times the number of people that are killed in wars every year on an average [45]. It has been reported that two-thirds of the world's population is expected to live in countries with moderate or severe water crises by 2025, which is of great concern [46].

Water pollution is one of the main causes of reduction in water quality [47] (worldwide global water contamination and their findings are as shown in **Fig. 2-1** [48]). This usually occurs when unwanted materials such as agricultural, industrial, and municipal effluents which contain various harmful chemical compounds such as heavy metal ions, toxic organic dyes, spilled oils, and emerging contaminants (ECs) are released into the water bodies [47, 49]. ECs mainly include pharmaceutical organic contaminants, personal care products (PCPs), endocrine disrupting compounds (EDCs), surfactants, pesticides, flame retardants, industrial additives, among others [50, 51]. The accumulation of all these contaminants causes serious adverse effects for human health and ecosystems. Therefore, it is urgent to develop efficient technology to remove these pollutants.

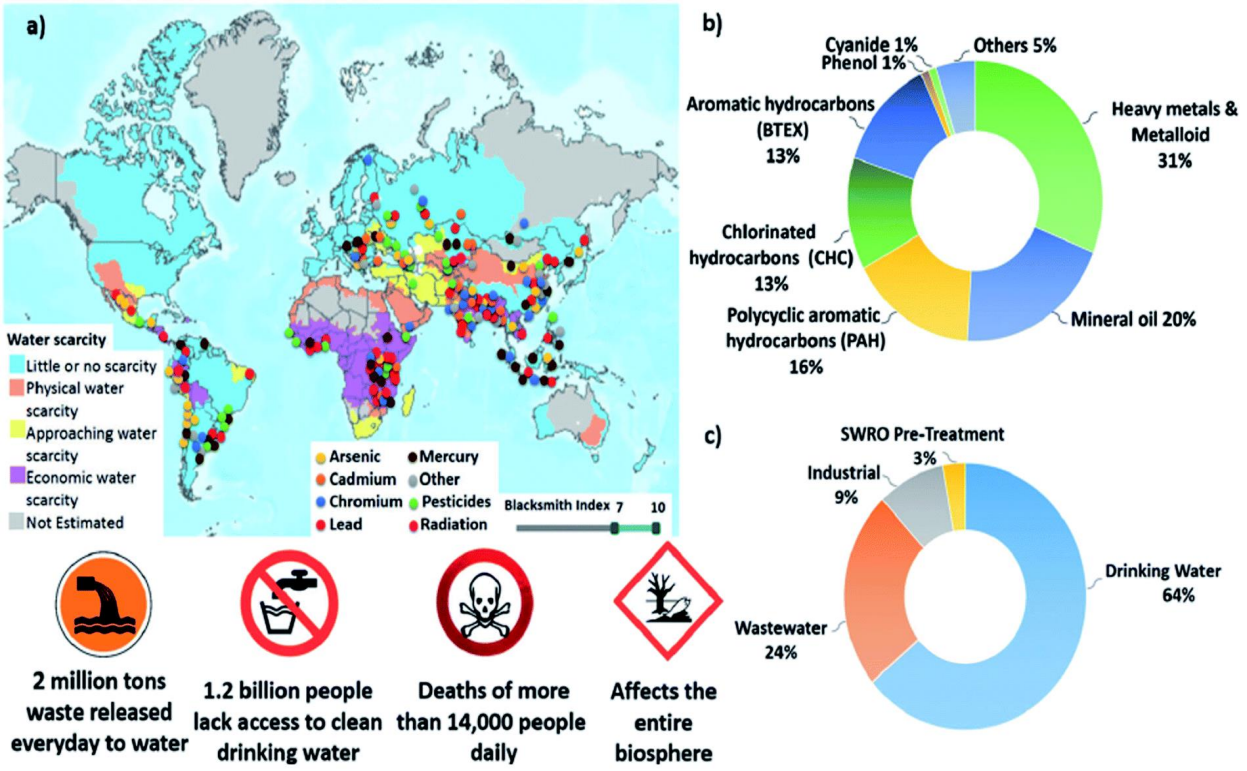

Figure 2-1. Summary of worldwide global water contamination spread in numbers. (a) Superimposed geographical distribution of water scarcity and of contamination by the type of major contaminants, including heavy metals, pesticides, and radionuclides. (b) Normalized composition of water contaminants in treated and recycled water streams. (c) Normalized volume of treated water by field of use [48].

2.1.2 Current technologies used for removal water pollutants

A number of technologies have been developed for the removal of water contaminants [52], and are classified as shown in **Fig. 2-2** [53]. The most commonly employed technologies are coagulation/flocculation [54, 55], membrane filtration [56, 57], photocatalysis [58], chemical oxidization or reduction [59], biodegradation [60], and adsorption [61]. Nevertheless, these technologies present their own advantages and disadvantages, summarized in **Table 2-1**.

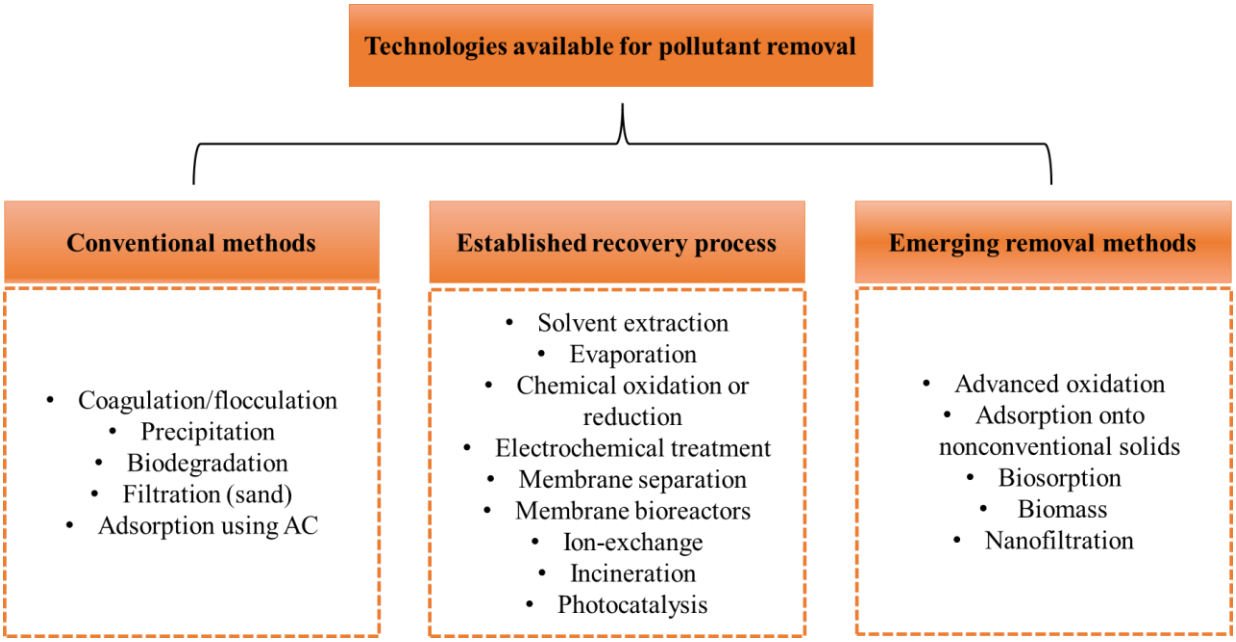

Figure 2-2. Classification of technologies available for pollutant removal and examples of techniques [53].

Table 2-1. Advantages and disadvantages of mostly used technologies for water remediation.

Mostly used water treatment technologies	Advantages	Disadvantages	References
Coagulation or flocculation	Simplicity. Inexpensive capital cost. Rapid and efficient.	Production biodegradation toxic sludge. In effectiveness in removing heavy metals and emerging contaminants.	[53, 54]
Membrane filtration	Rapid and straightforward techniques. Suitable for all types of pollutants. Allows continuous separation. Enables easy upscaling hybrid processing.	Maintenance and operation costs. Low membrane lifetime. High energy requirements.	[53, 56, 57]
Chemical oxidization or reduction	Simple, rapid, efficient and have multiple	high cost By-products	[53, 59, 62]
Photocatalysis	High efficiency. Versatility. A wide range of pollutants.	Relies on light source to activate catalyst. Formation of dioxins and pollutants.	[53, 58]
Biodegradation	Simple.	Slow processing.	[53, 63]

	Environmentally friendly. Economically attractive operation	Favorable environment needed. Generation of biological sludge and uncontrolled degradation products	
Adsorption	Low-cost. High efficiency. Ease of operation. More choice of adsorbent substrates. The possibility to recover the absorbent. Competitive and efficient in low concentration.	Disposal of adsorbent after adsorption	[53, 64-66]

The coagulation–flocculation process is one of the most important and widely used treatment processes of industrial wastewater due to its simplicity and effectiveness [53, 54]. Its main aim is to agglomerate fine particles and colloids into larger particles to reduce turbidity, natural organic matter, and other soluble organic and inorganic pollutants in the wastewater. In addition, this process is simple, inexpensive cost, rapid and efficient for removal insoluble contaminants, such as pigments and colloidal particles [53, 65]. However, there are limitations for the coagulation–flocculation process, including toxicity and health hazard posed by inorganic coagulants, the production of large amounts of toxic sludge, and ineffectiveness in removing heavy metals and ECs [67].

Membrane filtration is a separation process that uses a semi-permeable membrane to separate particles or substances based on their size and molecular weight [56, 57]. It is a rapid and straightforward techniques, suitable for most types of pollutants, which allows continuous separation under mild conditions, and enabling an easy upscaling hybrid processing [56]. However, this technology has some drawbacks, which include maintenance and operation cost, concentration polarization and membrane fouling, low membrane lifetime, and high energy requirements [53, 56].

Photocatalysis is a promising technology for water treatment that utilizes light and catalysts to degrade pollutants and contaminants [58]. Photocatalysis offers high efficiency, versatility and can be applied to a wide range of pollutants [68]. The challenge in this process relies on the light source to activate the catalyst and initiate the degradation of pollutants. It also leads to the formation of dioxins, metals, and other pollutants as by-products [53].

Chemical oxidation and reduction are two important processes used in water treatment to remove contaminants and improve water quality [59]. Chemical oxidation involves the use of oxidizing agents or reducing agents to convert contaminants in water into less harmful or more easily removable forms [62]. Some commonly used oxidizing agents include chlorine, ozone, hydrogen peroxide, and potassium permanganate. The reducing agents mainly include sodium bisulfite, sodium metabisulfite, and sulfur dioxide. Chemical oxidation and reduction methos are also simple, rapid, efficient and have multiple approaches concerning oxidizing and reducing agents. However, chemicals are required, therefore, an additional cost is added to the treatment of waste [62]. Additionally, potentially toxic by-products will be produced during the processing, which then will be needed to be addressed [53].

Biodegradation involves the breakdown of pollutants into various byproducts by microorganisms, including fungi, bacteria, yeasts, and algae [63]. It is simple environmentally friendly, economically attractive operation [53, 63]. Nevertheless, there are some limitations, such as slow processing, the requirement of a favorable environment needed, the generation of biological sludge and uncontrolled degradation products [53, 65].

Adsorption is a process of mass transfer in which dissolved contaminants are transferred from the liquid phase to the adsorbent surface to purify the water [64-66]. Adsorption is currently popular

for water treatment purposes because of the following advantages: low-cost, high efficiency, ease of operation, the possibility of using virous materials as adsorbent substrates, and the possibility to recover the adsorbent and the adsorbate [64]. Importantly, adsorption is competitive and efficient when the concentration of the contaminants in the water ranges from ng L^{-1} to mg L^{-1}. The removal efficiency of adsorption can go up to 99.9%. The United States Environmental Protection Agency (USEPA) declared the adsorption process as one of the most excellent and best wastewater treatment techniques available [65, 69]. However, the regeneration of the absorbent is required [70]. Presently, research is devoted to the pursuit of ideal adsorbent materials.

2.1.3 Nanomaterials for generation of adsorbents

Generally, ideal materials for the adsorption of pollutants should meet several requirements: (1) it should be inexpensive, (2) have good mechanical and structural integrity to overcome water flow for a long time, (3) show high adsorption capacities with high rates, (4) have a large surface area, (5) possess a regeneration aptitude using cost-effective, and (6) biodegradation and eco-friendliness [71-73]. A wide variety of materials have been developed for water remediation application and their classification as shown in **Fig. 2-3.** Among all, nanomaterials have been recognized potential adsorbents for wastewater treatment in the last decade mainly because they present higher adsorption capacities, and better binding affinities than their macroscale counterparts [71, 74, 75].

At the nanoscale, an additional advantage is realized because of the small size, expansion of the specific surface, the dominance of interfacial phenomena and the ability to tailor surface criteria via surface different modification technologies [76-78]. This opens the way for nanomaterials toward wider applicability such as in water remediation. Silica nanoparticles [79], nano zeolites [80], activated carbon (AC) [53, 81], graphene and graphene oxide (GO) [82-84], metal-organic

frameworks (MOFs) [85] and nanocellulose attract more attention due to their unique properties for water remediation. The advantages and disadvantages of these materials for water remediation are summarized in **Table 2-2** and will be discussed in the following section.

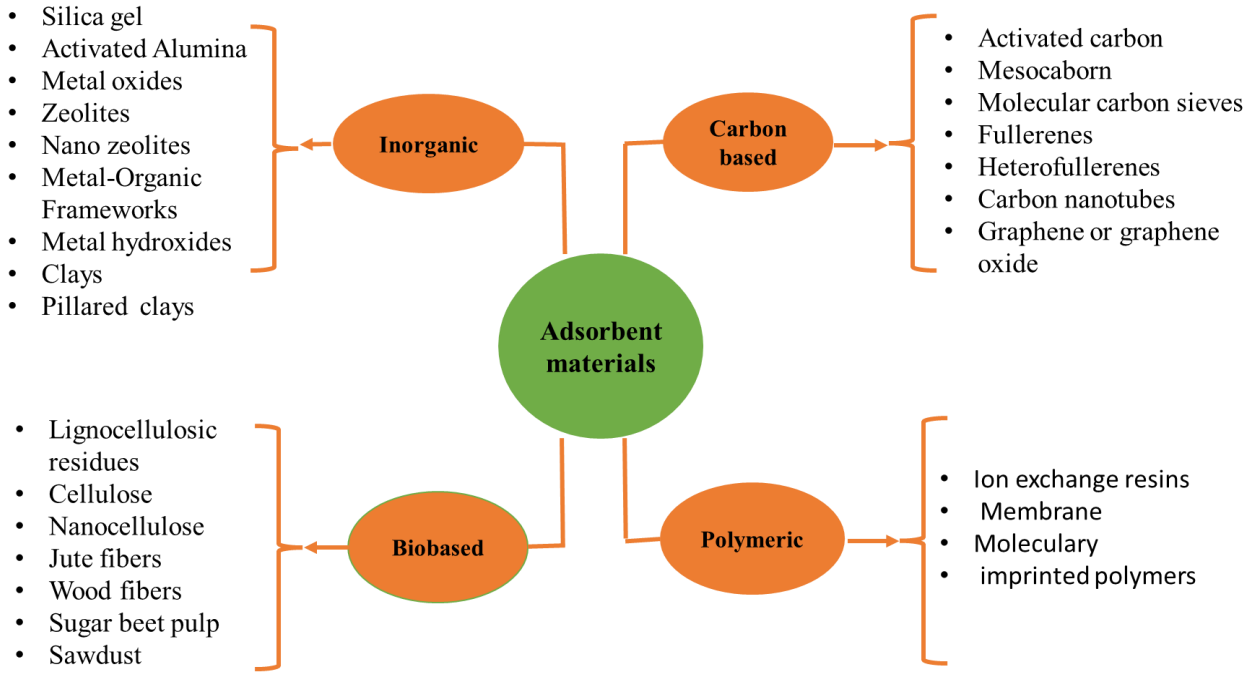

Figure 2-3. The classification of current materials for adsorbents [71].

Table 2-2. Main advantages and disadvantages of mostly used nanomaterials for adsorbents.

Mostly used nanomaterials for adsorbents	Advantages	Disadvantages	References
Silica	High surface area (>1000 m^2 g^{-1}) Large pore volume Tunable sizes and properties Ease of surface functionalization	Price and availability	[86-88]
Nanosized Zeolites	Larger specific surface area (some zeolite-based materials >1000 m^2 g^{-1}) Higher thermal stability and lattice stability, Easily tunable size and properties	Limited in possibilities of functionalization	[89-92]

Nano structured Activated Carbon (AC)	High surface area (ranges from 500 to 1500 $m^2 g^{-1}$) Well-developed internal microporosity Wide spectrum of surface functional groups	Difficult separation from water bodies High cost Non-recyclability High energy consumption for producing	[53, 81, 93]
Graphene and Graphene Oxide (GO)	Large specific surface area (2630 $m^2 g^{-1}$) Great electrical and thermal conductivity High chemical stability Excellent mechanical, thermal and optical properties	Production of high-quality graphene is expensive	[82-84]
Metal-Organic Frameworks (MOFs)	Possess wide range of window opening/pore cavity and different functionalities	Low stability Poor recyclability High cost for fabrication	[85]
Nanocellulose	High specific area (~1000 m^2 g–1) High adsorption capacity Low cost Sustainability Non-toxic material 100% biodegradable	Making processing is challenging Limitation for multiple water pollutant adsorption	[71, 94]

Silica nanoparticles are one of the most commonly used nano adsorbent for water purification due to its high surface area (>1000 $m^2 g^{-1}$) [95], large pore volume, tunable sizes and shapes, and ease of surface functionalization. In addition, it has attractive physicochemical properties, such as abundant surface chemistry, colloidal stability, high dispersity, and thermal stability [86-88]. However, the disadvantage of nano silica is its price and availability in certain countries. Some countries have to import nano silica to be used in concrete industry [96].

Nanosized zeolite has attracted more and more attention in the last decades because of its inherent properties, such as shorter diffusion channel, larger specific surface area (some specific nanosized zeolite based materials presents >1000 $m^2 g^{-1}$), higher thermal and lattice stability, easier shaping

and tunable physical and chemical properties than regular ones [89-92]. However, they are limited in terms of possibilities of functionalization, which is mainly achieved by tuning the Si/Al ratio.

AC nanoparticle is a widely used adsorbent due to its exceptionally high surface area (ranges from 500 to 1500 $m^2 g^{-1}$), well-developed internal microporosity, a wide spectrum of surface functional groups, and high adsorption capacity [53, 81]. Nevertheless, AC generates secondary pollution because of the difficulty in its separation from water bodies, cost-ineffective due to non-recyclability, and high energy consumption because of production by heating carbonaceous materials at high temperatures [53, 81, 93].

Graphene or graphene oxide (GO) possesses impressive properties, such as large specific surface area (2630 $m^2 g^{-1}$), good electrical and thermal conductivity, high chemical stability, as well as excellent mechanical, thermal and optical properties, [82-84]. These features make graphene a multifunctional material so that can be applied in many different fields. However, production of high-quality graphene is expensive, which is a big challenge for the graphene or GO-based materials [97].

MOFs are a class of highly porous materials composed of metal ions or clusters coordinated with organic linkers [85]. Their tunable structure offers significant chemical and structural diversity, allowing for precise control over pore size and functionality, and enabling the adsorption of specific molecules. Compared with activated carbons (ACs), zeolites, or other porous materials, many MOFs possess a wide range of window opening/pore cavities and different functionalities, which enable them to accept several types of compounds inside their cavities [98]. Despite such significant efforts, there are still many scientific issues and challenges in the removal purification

of pollutants, such as low stability and poor recyclability, and high cost for the fabrication of MOFs [85].

Cellulose is an attractive alternative material for different applications, especially for water remediation owing to its low cost, low toxicity, high natural abundance, and biodegradability. When the size is minimized to the nanoscale [99], its intricate architecture imparts a unique combination of stiffness, strength, and toughness, and that it combines intriguing features from its nanoscale elements, such as high strength and modulus and large aspect ratios. The high specific area contributes to improving the adsorption capacity. Besides, the possibility of tailoring the surface properties, such as surface charge density, functionality, reactivity and processability expands adsorbents for multiple pollutants [71]. Compared to other inorganic nanoparticles, the nanosized cellulose adsorbent exhibits many advantages, including sustainability, cost effectiveness, a high aspect ratio, high adsorbent capacity, and the possibility for selective adsorption via appropriate surface functionalization. In addition, nanocellulose can be classified as a non-toxic material, 100% biodegradable and having no side effects on the environment, the use of nanocellulose eliminates the safety concerns generally encountered for mineral and carbon nanoparticles [71, 94]. However, nanocellulose production processing is still challenging now. This will be figured out with the development of nanotechnology. Therefore, nanocellulose has been the first choice for adsorbents.

2.1.4 Cellulose

2.1.4.1 Source of cellulose

Cellulose is the most abundant renewable raw material in the biosphere, this that can be derived from virtually inexhaustible biomass feedstocks with an estimated production 1,012 tons annually

by photosynthesis [99]. It accounts for about 45% of the dry weight of wood [100], and around 33% of non-woody plants [101], mainly including agricultural residues. Although plant-based lignocellulosic materials are generally regarded as a ubiquitous source of cellulose, other living species such as algae [102], as well as certain bacteria, such as *Alcaligenes, Acetobacter, Pseudomonas, Agrobacterium, Rhizobium, or Sarcina* [103-106] and a few marine animals, like tunicates [107] can also synthesize cellulose [108, 109]. **Fig. 2-4** exemplify graphically some of these sources.

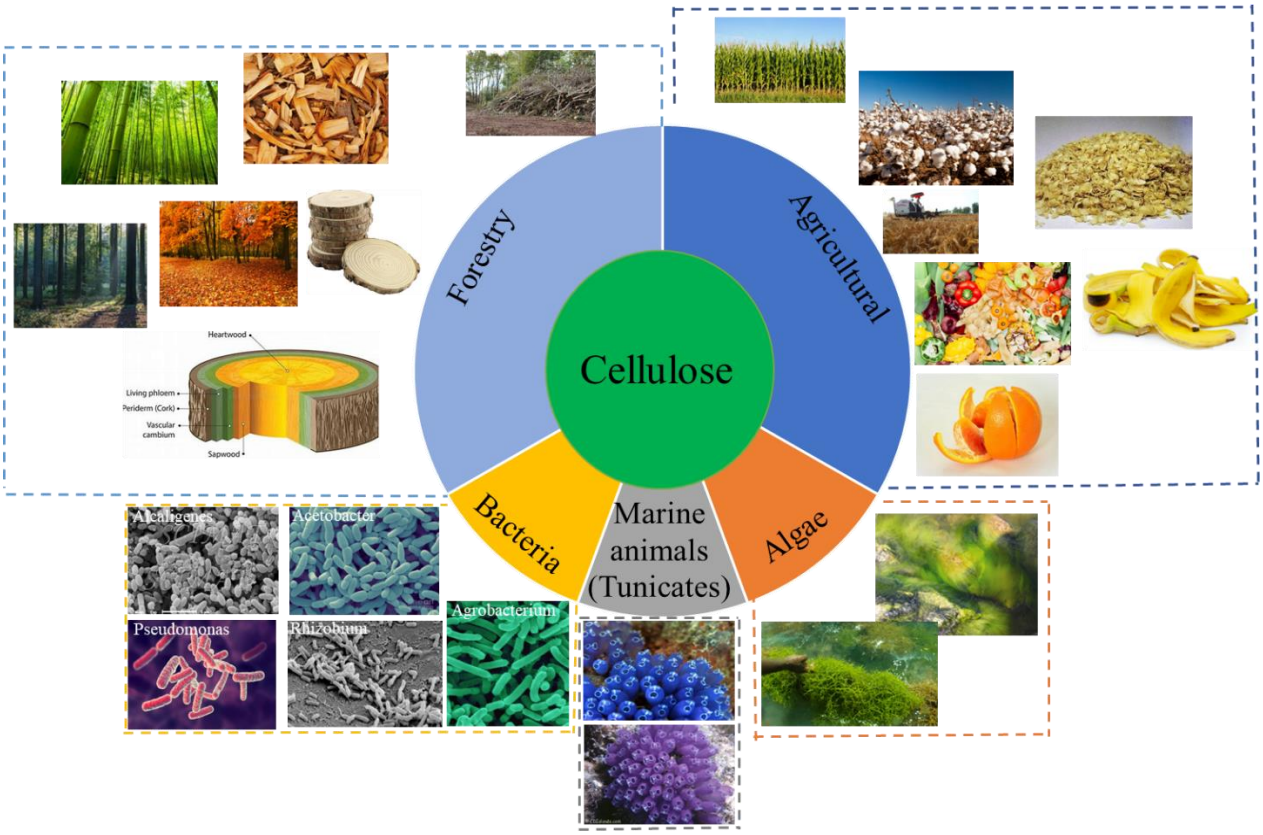

Figure 2-4. (A) Sources of cellulose. Some of pictures from the website or published papers (https://alchetron.com/Bacterial-cellulose#bacterial-cellulose-28bad1be-52ef-4be4-98ae-2adeb90c0a9-resize-750.jpeg) [102, 110].

2.1.4.2 Hierarchical structure of cellulose

In addition to its advantage as a potentially sustainable material, cellulose enables multiple functions and transformative applications that derive from its unique multidimensional structure

[111]. Cellulose fibers can be separated into fibrils with diameters ranging from less than 100 μm to around 2-4 nm [111-113]. Owing to this hierarchical structure (**Fig. 2-5**), microfibrillated cellulose (MFC, also known as cellulose nanofibril or CNFs) features substantial tunability in terms of its morphology and fibril size [114], which results in unique mechanical, optical, thermal, fluidic, and ionic properties that far surpass those of the parent cellulose fibers. MFC has attractive, tunable properties and is biocompatible, indicating the potential for practical implementation and commercialization [111]. The increased adoption of MFC is expected to facilitate the shift from petroleum to bio-based products in support of a more sustainable circular economy [111]. Recent research studies are focused intensely on cellulose at the nano-scale due to the consideration that it is an eco-friendly material, with special properties to be used as a versatile material with diverse applications, more details will be discussed in the section 2.5.

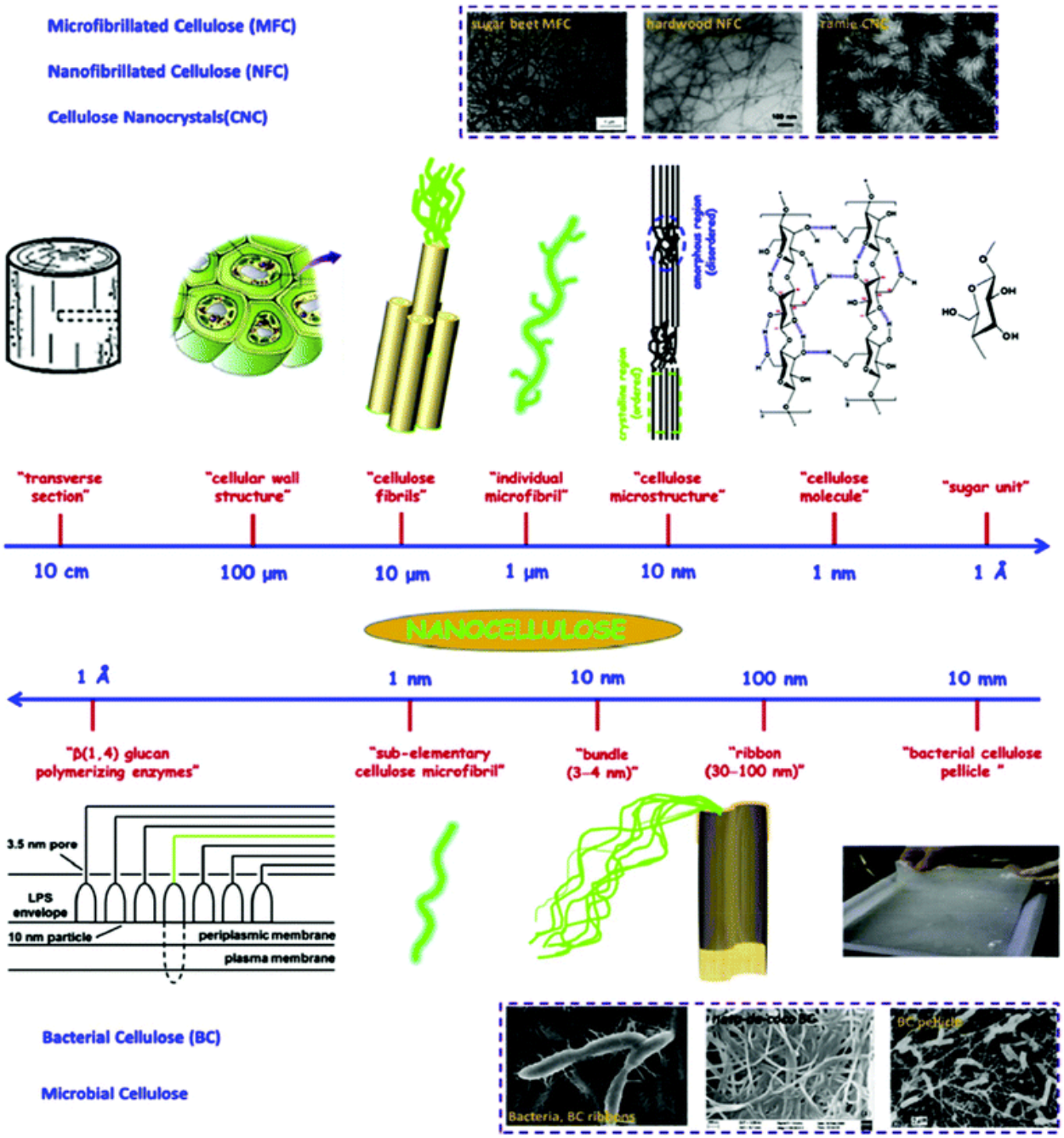

Figure 2-5. Hierarchical structure of cellulose [115].

2.1.4.3 Molecular structure of cellulose

The molecular structure of cellulose is composed of D-glucose units linked by β (1, 4) glycosidic linkage (**Fig. 2-6**). Three hydroxy groups with different reactivities are present on each glucose unit at the C2, C3, and C6 positions [116]. On the cellulose molecular chains, rich hydroxyl groups

can contribute to the formation of abundant intra- and inter-molecular hydrogen bonds, which in turn enable the creation of highly ordered, three-dimensional crystalline structures [111]. The dense packing of molecular chains originating from the presence of hydrophilic hydroxy groups and hydrophobic axial C-H planes, gives an amphiphilic character to nanocellulose. What's more, these hydroxy groups can be functionalized or cross-linked with other polymers to modify the mechanical and chemical properties, which make cellulose available to meet the needs of different applications [111].

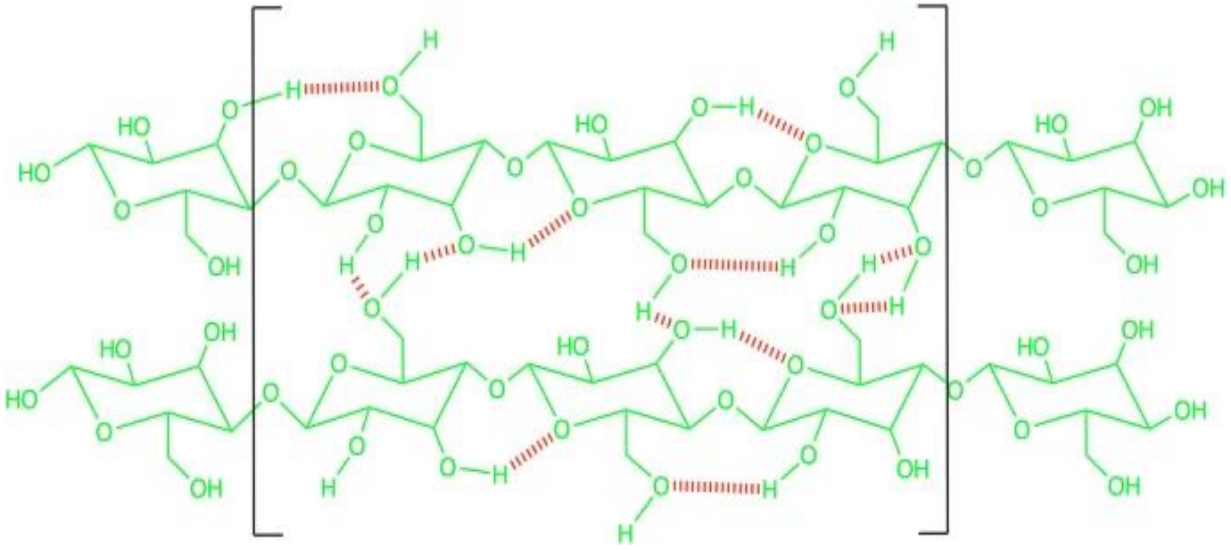

Figure 2-6. Molecular structure of cellulose [111].

2.1.5 Nanocellulose

Nanocellulose is defined as a cellulosic material having at least one dimension of 1–100 nm and can be isolated from natural cellulose fibrils [99, 117, 118]. Nanocellulose have attracted rapidly growing interest from both academic and industrial researchers due to their unique nanostructure and impressive physicochemical properties such as high tensile strength (up to 10 GPa) and elastic modulus (up to 220 GPa), high specific surface area (up to several hundreds of m^2/g), low density (1.6 g/cm3), reactive surfaces combined with biodegradability and renewability [119]. Based on sources, size, morphologies, properties, and preparation techniques, nanocellulose is mainly

divided into three categories: cellulose nanofibrils (CNFs), cellulose nanocrystals (CNCs), and bacterial nanocellulose (BNC) [99, 118-120]. At present, most of the CNFs and CNCs are isolated from lignocellulosic biomass (**Fig. 2-7 (A))**, as they are the most sustainable sources of cellulosic biomass. **Fig. 2-7 (B)** shows the relationship between different types of nanocellulose and the corresponding micrographs; **Fig. 2-7 (C**) shows the characteristics of different types of nanocellulose.

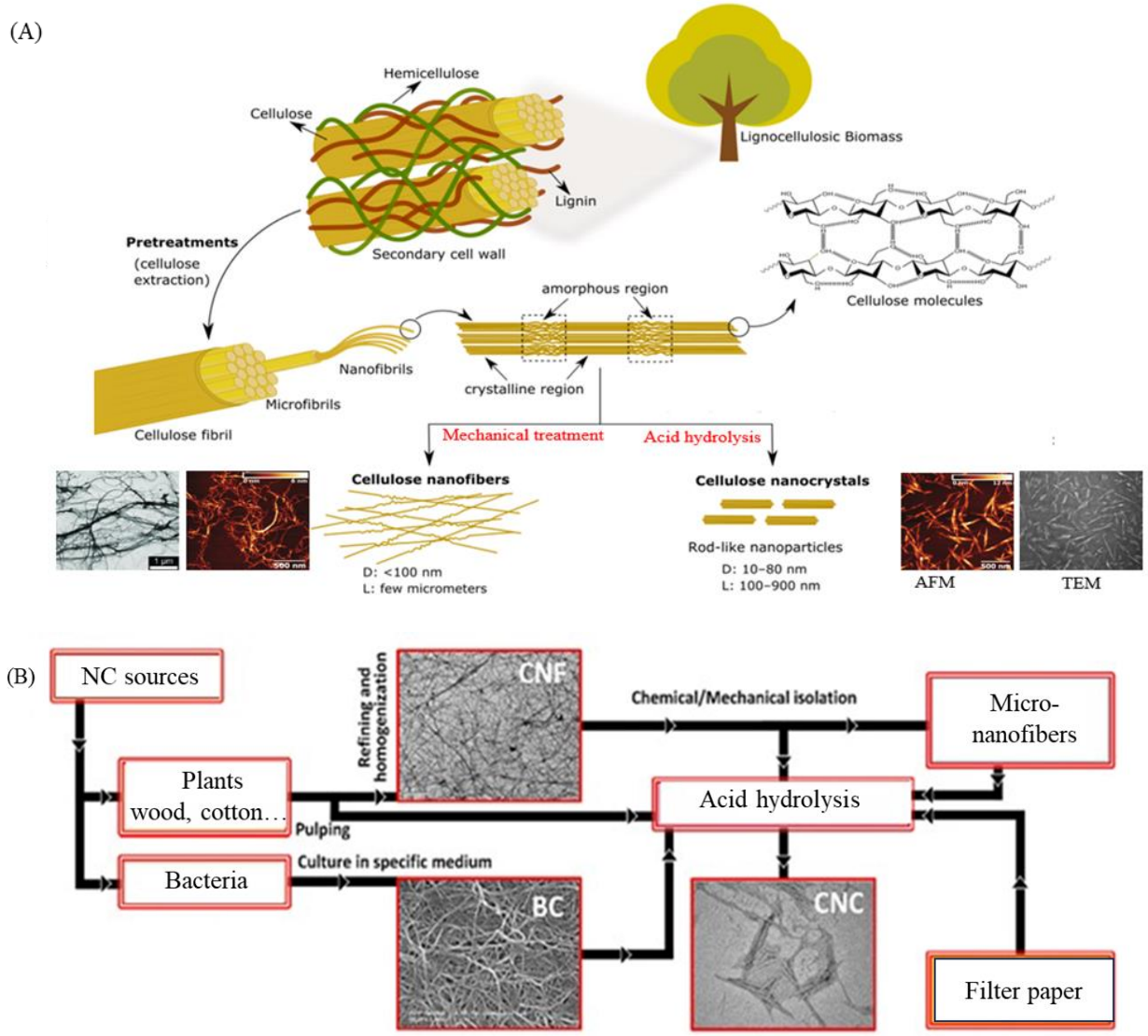

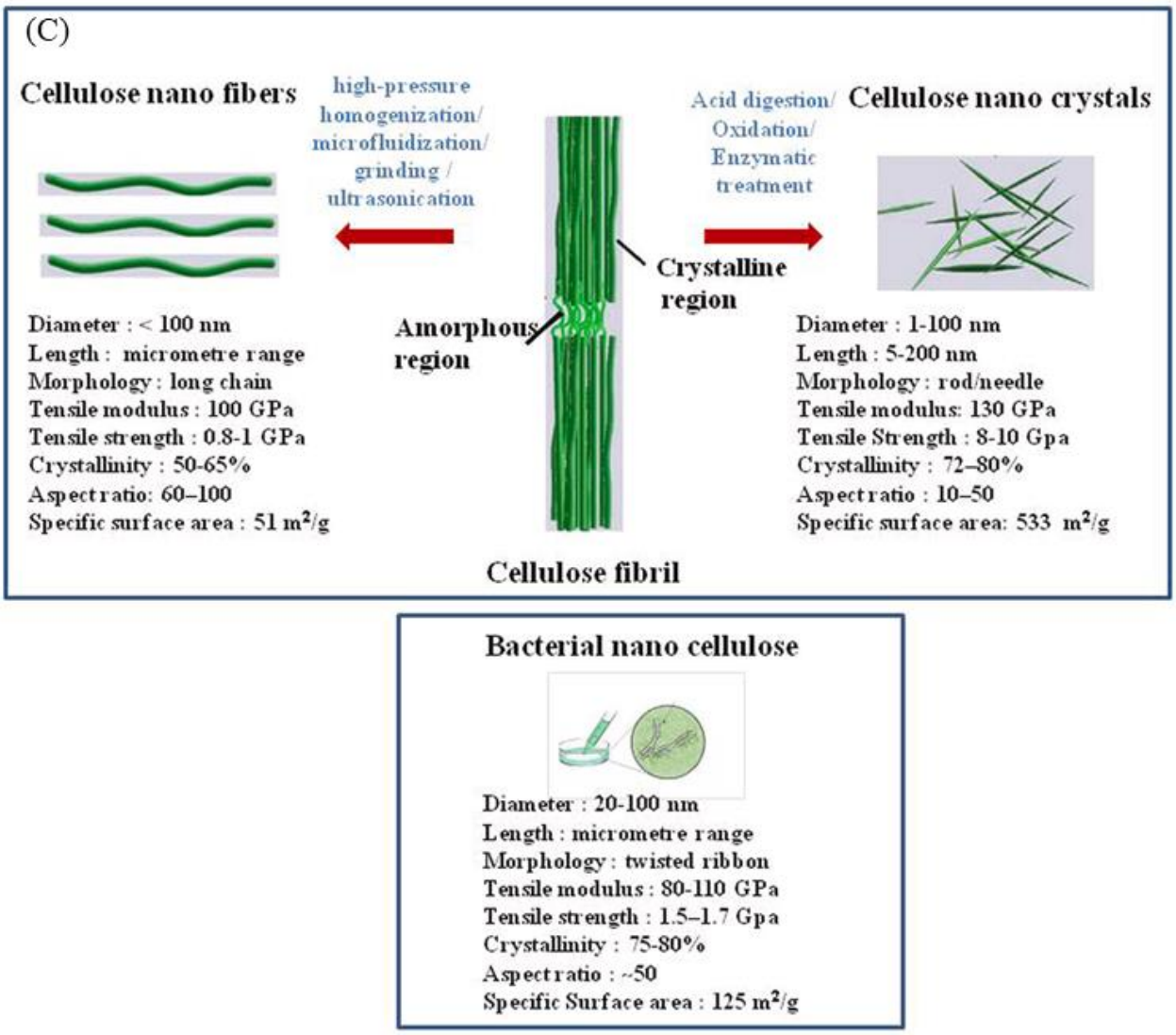

Figure 2-7. (A) Nanocellulose isolation processing from lignocellulosic materials. (B) Relationship between different types of NCs and the corresponding micrographs [118]. (C) Characteristics of different types of nanocellulose [121].

2.1.5.1 Cellulose nanofibers (CNFs)

CNFs, also named as nanofibrillated cellulose (NFC), are thin flexible fibrils with diameters <100 nm and lengths 50-500 nm or few micrometers, which are comprised of both crystalline and amorphous regions of cellulose [71, 118, 122, 123]. The quality of CNFs is very much dependent on the cellulose source and the extraction methods. However, CNFs are easily produced in high yields and present both crystalline and amorphous regions, which unlike CNCs, give a rigid and

complex network composition [118, 124, 125]. Their production process involved mainly intensive mechanical disintegration to break down the fiber's cell walls releasing elementary cellulose nanofibrils. such as high-pressure homogenization, micro fluidization, high-intensity mechanical grinding using a Masuko grinder, ball milling, and ultrasonication [122, 126-128].

Homogenization, including using homogenizers and microfluidizers, and grinding are the most common techniques used for mechanical production of CNF (**Fig. 2-8 (A)**). These techniques are the most efficient for delamination of fiber cell wall and CNF isolation, as well as are suitable for upscaling, which are for industrial production of CNF nowadays [126]. However, both of them are very energy intensive (12-70 MWh/t) [129]. Another issue is clogging when processing long cellulose fibers mainly due to the fact that long cellulose fibers tend to form entanglements [126, 130]. Meanwhile, other methods are studied in order to reduce energy consumption and find more beneficial solutions for CNF production, including enzymatic hydrolysis [131, 132], TEMPO-mediated oxidation [133, 134], sulfonation [135, 136], carboxymethylation [137-139], quaternization [140, 141], and others [126]. Among them, TEMPO mediated oxidation can selectively oxidize the cellulose C_6 hydroxyls to carboxylates introducing a large amount of negative carboxyl groups on the cellulose (**Fig.2-8 (B)**) [142]. Another strategy is introducing positive quaternary trimethylammonium groups on the surface of cellulose fiber to increase the electrostatic repulsion and enhance the fibrillation efficiency. Moreover, the introduced cationic groups endowed the final CNFs with antibacterial properties, which could be applied in food packaging and biomedical applications (**Fig.2-8 (C)**) [143]. Nevertheless, the above methods still face several drawbacks such as high cost of enzymes and chemicals, time-consuming process, difficulty to recover chemicals and environmental issues. Therefore, it is of critical importance to

develop a more cost-effective, sustainable and environmentally benign pretreatment methodology for the preparation of high-quality CNFs [130].

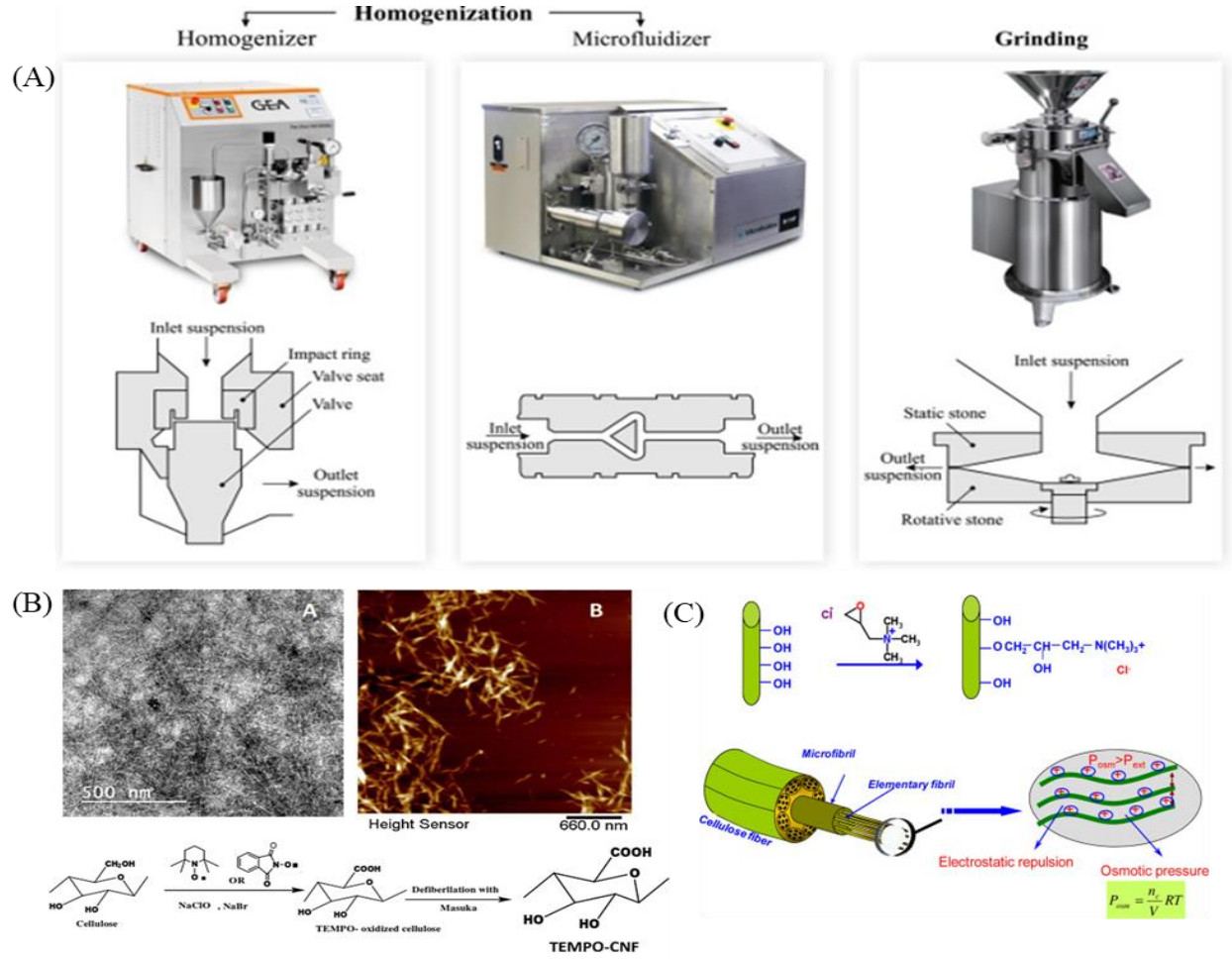

Figure 2-8. (A) Schematic diagrams of most widely used mechanical approaches and the corresponding instruments for CNFs production schematic diagrams [126]. (B) Systematic diagram of preparation of CNFs by surface carboxylation using TEMPO oxidation [144]. (C) Schematic illustration of how the fibers quaternization enhanced the fibrillation process [143].

2.1.5.2 Cellulose nanocrystals (CNCs)

CNCs, also termed nanocrystalline cellulose (NCC) or cellulose nanowhiskers (CNW), are rigid rod-like crystalline fibrils with 10–80 nm in diameter and 5–200 nm in length [99, 123].

Several methods have been developed for extracting CNCs from cellulose. The most used method for preparation of CNCs is using inorganic acid to selectively dissolve amorphous domains and release cellulose crystallites (**Fig. 2-9 (A)**). Sulfuric acid is the most commonly used acid for

producing sulfonated CNCs, which not only effectively isolates the crystalline regions by dissolving amorphous parts but also provides sulfate half-ester groups on the surface of CNCs, resulting in high colloidal stability for CNC dispersion in water owing to electrostatic repulsion [145, 146]. Some other inorganic acids such as hydrochloric acid [147], phosphoric acid [148], hydrobromic acid [149, 150], and nitric acid [151], have been used for the preparation of CNCs as well [152]. Strong acid hydrolysis is a simple and time-saving method. However, certain issues such as harsh corrosion of equipment, severe environmental pollution, large water usage, and low production yield need to be well addressed [130]. Enzymatic hydrolysis, Subcritical water hydrolysis are also used to produce CNCs (**Fig. 2-9 (B)**) [153]. Enzymatic hydrolysis has the benefit of not requiring harsh conditions such as highly concentrated acids. However, it is often not desirable due to the extended time that is required for the process to properly occur [153]. An alternate method for hydrolysis has been explored using subcritical water (**Fig. 2-9 (C)**), which has the advantage of not requiring harsh conditions as found in acid hydrolysis and also being a relatively quick process unlike enzymatic hydrolysis [154]. Besides, some sustainable and environmentally friendly methods based on the replacement by recyclable chemicals have been invented recently to address the above drawbacks, such as solid acid (e.g. phosphotungstic acid) hydrolysis [155, 156], organic acid (e.g. formic acid, oxalic acid) hydrolysis [157-159], and ionic liquid [160, 161] or deep eutectic solvents treatment [162, 163].

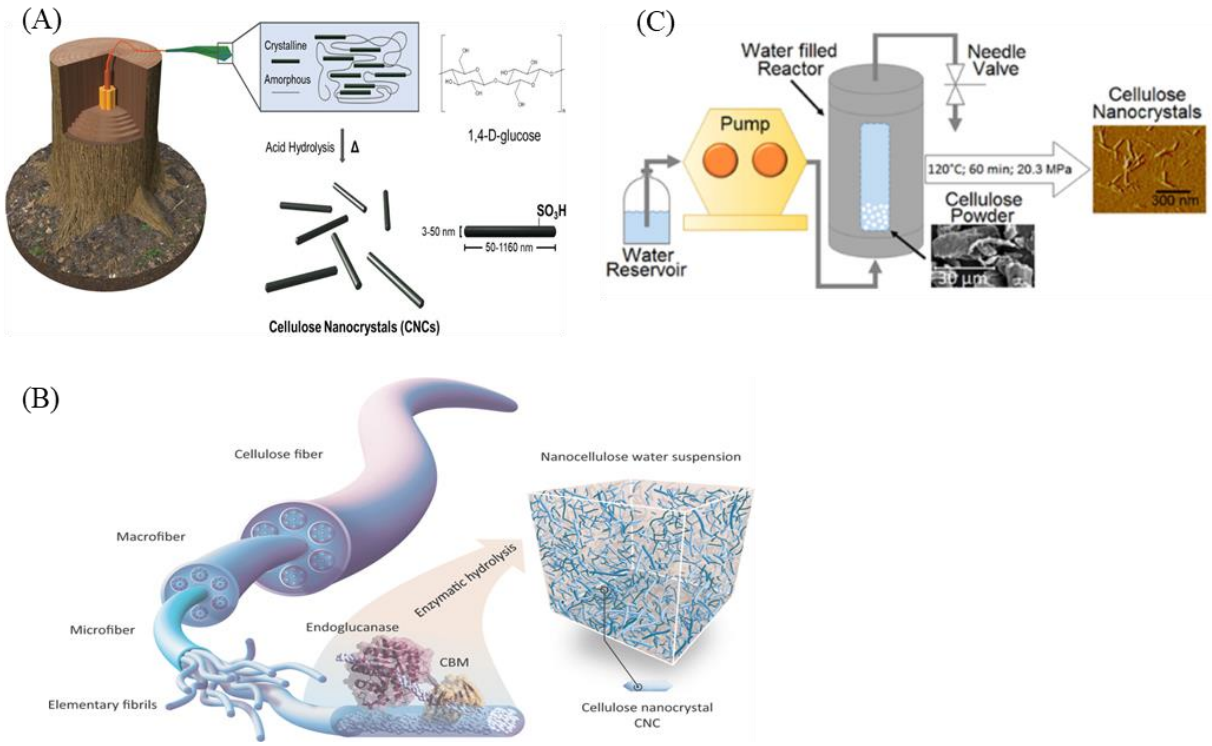

Figure 2-9. (A) Preparation of CNCs from wood: Wood pulp can be hydrolyzed with sulfuric acid to selectively remove amorphous regions, leaving behind crystalline cellulose nanorods [164]. (B) Illustration of cellulose enzymatic hydrolysis for CNCs [164]. (C) Schematic showing methodology for subcritical water hydrolysis [153].

2.1.5.3 Bacterial nanocellulose (BNC)

Bacterial nanocellulose (BNC) is a type of nanocellulose that has a high length-to-width ratio (approximately 100 nm in width and 100 um length) composed of nanofibrils of 2-4 nm width [165]. Besides, functional groups such as carbonyl and carboxyl are generally absent in BNC and exhibit pure cellulose without lignin and other foreign substances. BNC demonstrated a very extensive polymer chain (up to 8000) and crystallinity up to 90 % [105, 166].

BNC is generally created through the microbial fermentation process, **Fig. 2-10** [105]. The bacteria used for secretion extracellularly are some known genera such as *Alcaligenes, Acetobacter, Pseudomonas, Agrobacterium, Rhizobium, or Sarcina* [103-105]. Overall, NFC are known for possessing both long length and high aspect ratio but suffers from low crystallinity while CNC has

a shorter length and low aspect ratio but possesses good crystallinity and chemical stability. Conversely, BNC has high purity and crystallinity, which leads to superior mechanical strength and stability [105]. BNC may well have applications in numerous fields, including food, paper, pharmaceuticals, nonwoven cloth, waste treatment, textile industry, refineries, and broadcasting, due to its unique properties, such as high density, purity, and degree of crystallinity, good shape retention, and higher surface area and water-binding capacity [167-170]. However, the major challenges faced for the applications of bacterial cellulose are its up-scale production, the high cost of the media and the low productivity at industrial scale [171].

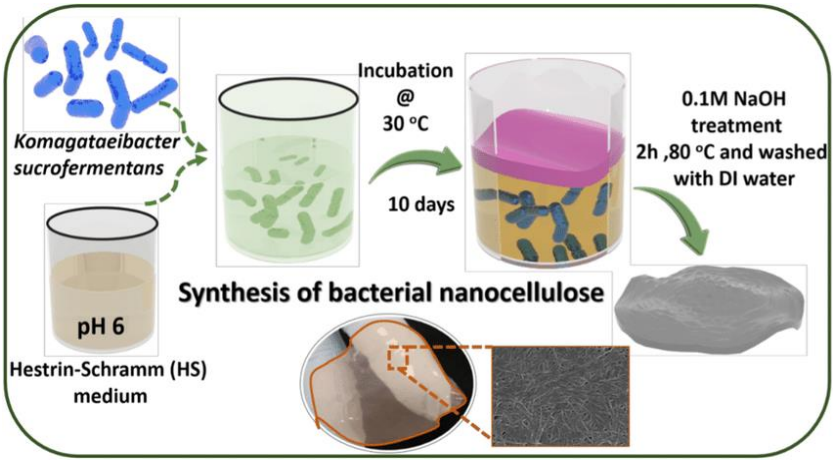

Figure 2-10. Bacterial nano-cellulose production from *K. sucrofermentans* [172].

2.1.6 Application nanocellulose in water remediation

Due to their valuable characteristics described in the previous section (2.1.5), like excellent resistance, chemical inertness, renewability, transparent appearance, stiffness, biocompatibility, high specific area, biodegradability, low thermal expansion coefficient, stable structure, low density, high surface area-to-volume ratio and capacity for hydrogen bonding interactions [171], nanocellulose is appealing for applications in biomedical engineering [173, 174], electronics [175,

176], textile [177], energy [178, 179], [117], contamination removal systems [180] and others, see **Fig. 2-11**.

Figure 2-11. Main applications of nanocellulose [171].

Some major nanocellulose attributes contribute to their use as adsorbent for water remediation is highly attractive, such as the high specific area of the nanoscale-cellulose materials results in an enhanced adsorption capacity, the high aspect ratio enhances the mechanical strength of the adsorbent, the high crystalline degree enhances the chemical resistance of the adsorbent [71]. However, the adsorption capacity of native nanocellulose remains relatively low due to the low activity ability of hydroxyl groups [48, 181]. Besides, nanocellulose are hydrophilic in nature because of the presence of abundant -OH groups in their structure. This makes it difficult to be dispersed evenly in nonpolar solvents and inadequate interfacial adhesion with hydrophobic matrixes so that nanocellulose materials are susceptible to aggregation which diminishes the surface area available for adsorption processes [20, 21]. Those limitations discourage the direct

use of nanocellulose in adsorbents. Therefore, it is of utmost necessity to modify the nanocellulose to overcome their incompatibility and poor interfacial interactions, as well as enhance adsorption performance [21, 48, 118].

2.1.7 Current nanocellulose modification strategies for improving adsorption

Surface modification is a key step to promote the adsorption of a specific class of pollutant and enhance the adsorption capacity [71, 108, 182]. The modification of nanocellulose is often dictated by the target absorbed species, the mechanism of action between the adsorbent and contaminant needs to be considered [48]. Normally, the negatively charged adsorbent will effectively absorb the positively charged heavy metals and dyes. Meanwhile, considering the hydrophobic and oleophilic characteristic of oils or solvents, the hydrophobic groups are commonly introduced to nanocellulose by using chemical or physical methods to improve their oil adsorption capacity [48]. Illustration of the possible modification according to the pollutant class is given in **Fig. 2-12** [71, 183]. These modifications can be achieved by 3 categories: 1) chemical surface modification, 2) grafting with polymers, and 3) formation of nanocomposites [108, 184].

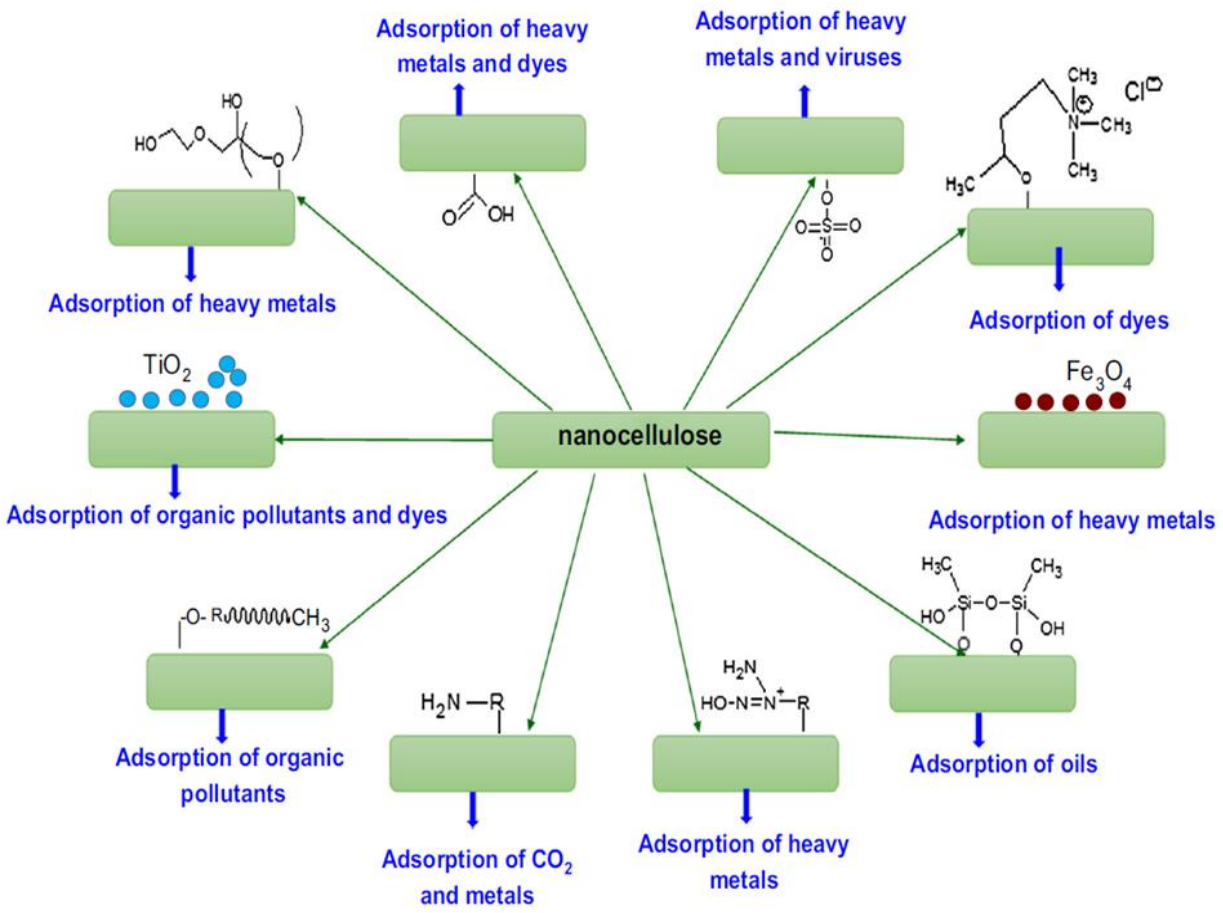

Figure 2-12. Surface modification strategies of nanocellulose according to the pollutant class [71].

2.1.7.1 Surface functionalization

Nanocellulose surfaces can be functionalized by multiple methods, such as silylation, carboxylation, acetylation, sulfonation, phosphorylation, and amidation [21, 48, 108, 185], by which the corresponding functional groups were introduced onto the nanocellulose surface. The reaction activity or adsorption capacity towards a specific contaminant is highly dependent on the concentration of corresponding functional groups [21, 186]. Silylation modification introduced silyl groups onto the surface of nanocellulose to improve compatibility with non-polar matrices and can be used to absorb oil spills or non-polar solvents or molecules [186]. It has also been

demonstrated that carboxyl, sulfonate, and phosphonate groups, when present on nanocellulose can exhibit selective uptake of contaminants, such as metal ions, dyes and microbes for water purification [187, 188]. Amidation has been well explored as a tool to tailor the surface of nanocellulose where amide linkage is formed by a reaction between amine and carboxylic moieties [189]. Therefore, the carboxy groups should be first introduced before carrying out amidation. Most of the amidation reactions are conducted on pre-oxidized nanocellulose through TEMPO-mediated oxidation [190]. Amino group can be pronated at acid pH range, usually used for cationic ions [191] or anionis dyes remove [192], but also can adsorption some cationic dyes [193] and emerging contaminants [32, 194].

2.1.7.2 Grafting with polymer

The hydroxy groups of nanocellulose can act as chemical handles [108]. Due to this uniqueness, nanocellulose also can be grafted with polymers, such as polyvinyl alcohol, poly lactic acid, polyvinyl acetate, polymethyl methacrylate, polyvinyl chloride, and many more synthetic polymers to yield better performance [21]. Surface grafting of polymer chains is considered an effective and versatile method for surface modification because interfacial properties can be tuned depending on the nature of the grafted polymers [108, 195]. Polymer grafting can be classified into two approaches: “grafting onto” and “grafting from” (**Fig. 2-13 (a) and (b)**) [108]. The grafting-onto approach relies on covalently attaching of a coupling agent (linker) and a polymer with a reactive-end group onto the surface of the nanocellulose. This approach is popular due to its simplicity, although the number of grafted functional groups that can be obtained from this approach is limited. In the grafting-from approach, a variety of specific groups on polymers are connected to the main chain of cellulose mainly by free radical polymerisation, ring-opening polymerisation to enable nanocellulose to adsorb different pollutants [184]. This method enables

production of polymer grafts with higher densities than those achieved with grafting-onto approach; however, the resulting polymers are difficult to characterize [108, 196]. Anyway, carboxylated polymers, aminated polymers, sulfhydrylated polymers and so on grafting of nanocellulose for metals and dyes adsorption [184].

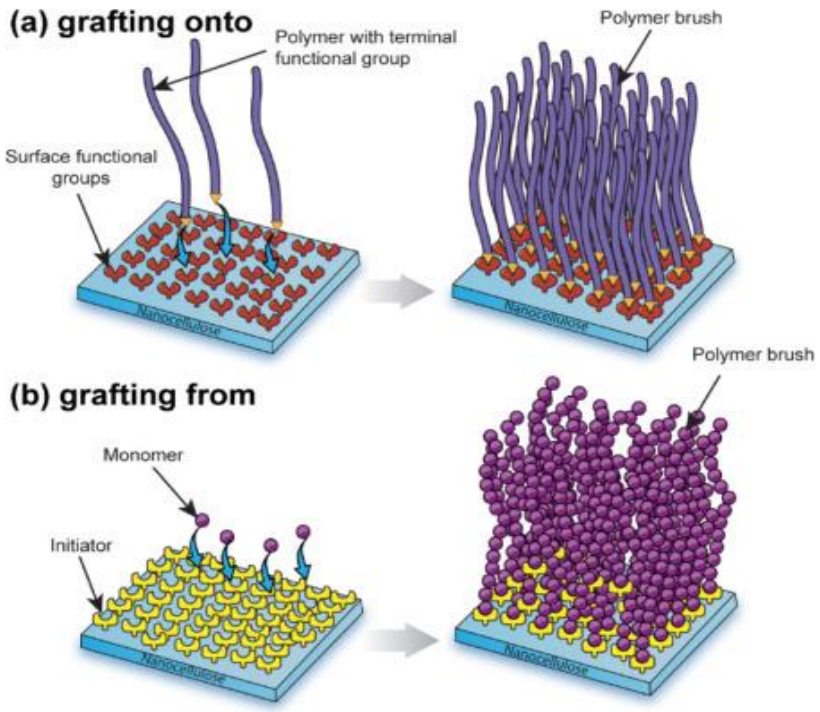

Figure 2-13. Schematic illustration of two grafting approaches – "grafting onto" (a) and "grafting from" (b) [108].

2.1.7.3 Formation of composites by non-covalent surface modification

The synthesis of nanomaterial composites is another method for obtaining nanocellulose-based adsorbents for water treatment. Nanocellulose composite adsorbents imainly nclude cellulose/metal nanocomposites, cellulose/organic polymer nanocomposites, cellulose/biomacromolecule nanocomposites, cellulose/inorganic nonmetallic nanocomposites, etc [184, 197, 198]. As an alternative to the covalent grafting of functional groups or long polymeric chains to the nanocellulose surface, non-covalent cross-linking is the simplest way to modify the nanocellulose surface [199, 200]. Non-covalent surface modifications are typically

achieved via non-covalent adsorption of surfactants or oppositely charged molecules onto the surface of the nanocellulose [108, 199, 200]. These interactions essentially are a number of reversible associations, such as electrostatic interactions, hydrophobic interactions, hydrogen bonds, or van der Waals force. The reversible non-covalent bonds can better recover from the adverse effects that result from the rupturing and dissipation of the energy in the network during the unloading process than covalent bonds [108]. Importantly, the reversible non-covalent bonds make it possible for the regeneration of adsorbents by desorption. Additionally, non-covalent physical assembly avoids the use of reagents that are harmful to the environment commonly used for covalent cross-linking interactions [201]. However, it is noteworthy that non-covalent interactions in most cases are not as strong as covalent interactions, making them more likely to break and possibly rearrange under stress [202].

2.1.8 Structure of novel nanocellulose-based adsorbents

The structure of nanocellulose-based adsorbent mainly exists in powders, hydrogels, and aerogels. The main drawbacks of powders are poor separability for reusing. 3-D hydrogels and aerogels are more popular in latest years because they can overcome the problems from powders.

2.1.8.1 Hydrogels

Hydrogels are 3D polymeric networks capable of absorbing and accommodating a large volume of water in their interstitial assemblies [21, 203, 204]. Great interest has been directed toward hydrogel applications since its discovery in the 1960s by Wichterle and Lim [205]. This is a result of its versatility enabling its usage for various applications such as biomedical devices [206-208], soft electronics [209-211], sensors [212, 213], actuators [214, 215], and adsorbents [204, 205, 208, 216]. Nanocellulose hydrogels are formed as a result of chemical or physical crosslinking **Fig. 2-14 (A)** [21, 217]. Chemical crosslinking refers to the addition of a specific crosslinker such as

citric acid or glutaraldehyde to the solution [116, 218, 219], which can react with the nanocellulose and form irreversible covalent bonds between the cellulose chains. TEMPO-oxidized CNFs were crosslinked by 1,2,3,4-butanetetracarboxylic acid (BTCA) as a chemical crosslinker to assist the formation of a crosslinking network structure by esterification reactions between the hydroxyl and carboxylic acid groups of CNFs and BTCA, respectively (**Fig. 2-14 (B)**) [117]. Physical interactions such as hydrogen bonds, van der Waals forces, and hydrophobic interactions, electrostatic interactions, and ionic interactions allow hydrogel formation by self-assembly. For example, carboxylic CNFs can undergo chelation with some multivalent metal ions via ionic gelation to form a hydrogel (**Fig. 2-14 (C)**) [116]. A stable, three-dimensional network structure could be created by the physical crosslinking of hydrogen bonds within and between molecules since its chain contains many hydroxyl groups, which greatly simplifies the aerogel manufacturing process [180]. Although physical crosslinked hydrogels are not strong and could dissociate, they are usually favored in adsorption processes for their non-toxic nature as they do not require additional chemicals and available adsorption sites. Recently, a lot of work focus on forming hydrogels by physical self-assembly [220-222].

However, most reported hydrogels are constrained by their poor mechanical performances, low adsorption capacity, or slow diffusion kinetics [216, 223, 224]. Incorporating adsorptive powders such as graphene [225], titanium dioxide, metal or metal oxide [226], and more recently biochar [227] into a tough hydrogel matrix is an effective way to improve the mechanical property of hydrogel while simultaneously enhancing its adsorption capacity [228]. However, this does not resolve the inherent slow diffusion kinetics problem of the bulk hydrogels [216]. Introducing pores into the hydrogel matrix is a valid way to accelerate solvent transport by invoking the capillary force [216, 229]. Enormous attempts have been taken to synthesize porous hydrogels through

mechanical frothing [230], gas foaming [231], porogen leaching [232], and freeze drying [216, 233]. However, most previously synthesized porous gels are very brittle and weak because of the existence of a large number of pores in the gels [216, 234]. Therefore, it is still beyond reach to develop a facile yet general technique to synthesize porous hydrogels with robust mechanical properties and excellent adsorption performances for water treatment [216].

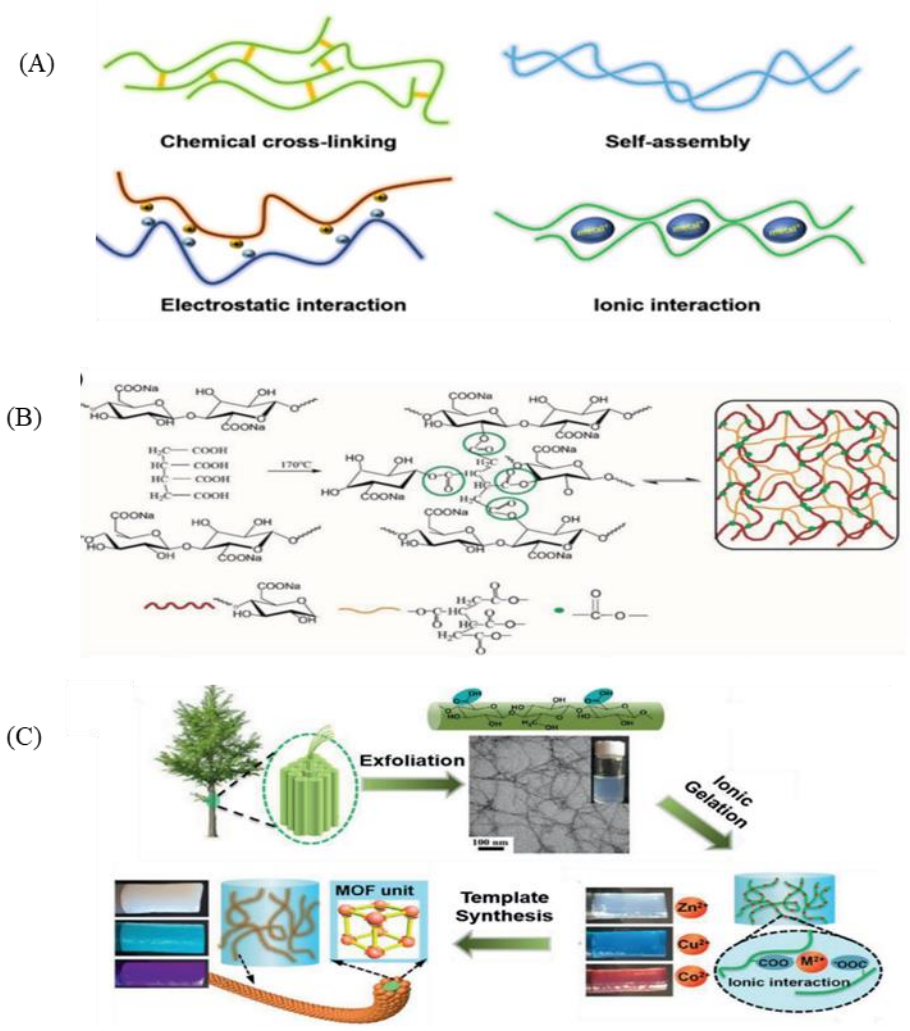

Figure 2-14. (A) The gelation behavior of nanocellulose by chemical crosslinking and physical crosslinking. (B) The mechanism of the gel formation by chemical crosslinking between CNFs and BTCA. (C) The gelation process of nanocellulose with physical crosslinking [116].

2.1.8.2 Aerogels

Once an hydrogel is formed, the solvent could be removed to obtain an aerogel [180]. Aerogels are 3D materials fabricated by substituting the solvent in hydrogels with air while maintaining the network structure [21]. The primary difficulty during the synthesis of aerogel is the elimination of solvent without collapsing the network structure. The drying method of wet gel is a fundamental factor in determining aerogel morphology and performance [180]. Atmospheric pressure drying (APD), freeze-drying (FD) and supercritical drying using CO_2 (SCD) are current techniques exploited in cellulose aerogel preparation. APD is a simple and easy-to-operate method. In APD, initially through the solvent exchange method, a low surface tension solvent is introduced in the hydrogel. This solvent is then dried at ambient pressure conditions [235]. However, during evaporation of the liquid from the gel pores, it produces capillary stresses at the liquid-vapor interface which results in shrinkage and reduction in porosity of the aerogel [236]. FD also known as lyophilization, involves freezing solvents in the gel using refrigerator/dry ice/liquid nitrogen at temperatures of −20,−78,−196 °C respectively [237]. The temperature, rate, and direction of freezing of the gel can control the rate of crystallization of ice and its growth direction, which can alter the overall pore structure and surface area of the aerogel [238]. The disadvantage of FD is that during crystal growth, cracks are formed and shrinkage happens to the cryogel structure [239]. Besides, it is an energy intensive process that consumes a lot of energy. To avoid pore structure damage and shrinking of aerogels as in FD and APD, SCD can be used. The SCD is carried out at the critical pressure and temperature of the solvent. The main advantage of this process is that capillary forces are avoided, due to the free movement of molecules at the critical state [239]. A better aerogel structure can be obtained without any apparent collapse of the pore structures and any pore damage as depicted in **Fig. 2-15**. The requirement of high temperature, pressure, time

consumption, and cost are the main limitations of the SCD method [180, 236]. Based on the pore structure integrity retained and density after removal of the solvents, the aerogels are named aerogel (SCD), xerogel (APD), or cryogel (FD), as shown in **Fig. 2-15**.

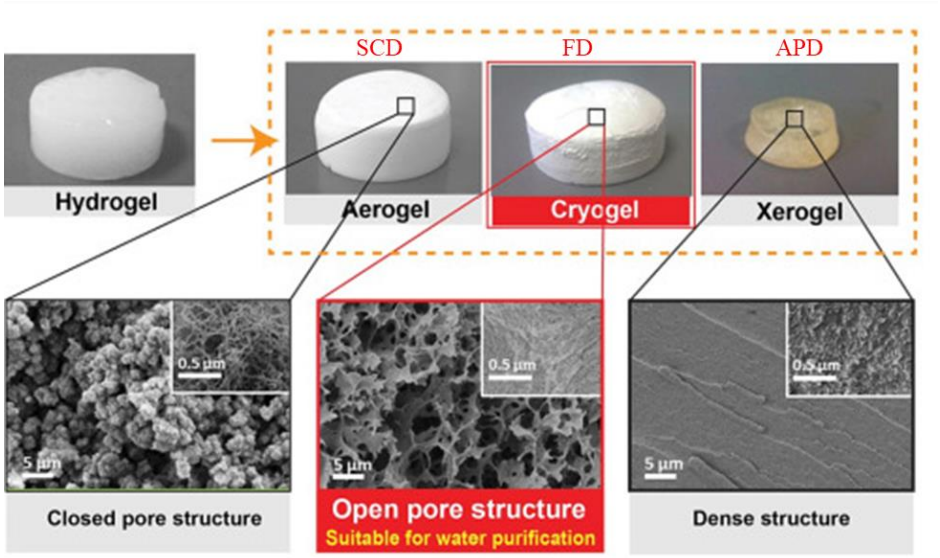

Figure 2-15. Cellulose hydrogel, aerogel, cryogel and xerogel forms (after dried by SCD, FD and APD, respectively) and their SEM images [180].

2.1.9 Current challenges of nanocellulose-based adsorbent in water remediation

Nanocellulose holds great promise as a new class of novel adsorbent for water remediation. However, before considering nanocellulose for real water treatment, many shortcomings need to be dissolved. Key challenges for future growth and integration of nanocellulose as a new class of sustainable adsorbent for water purification and environmental remediation are:

2.1.9.1 Limited adsorption capability

The adsorption capacity of nanocellulose remains relatively low due to the low activity of hydroxyl groups. A lot of modifications have increased the adsorption capability for different pollutants as talked in 2.1.7 section. For example, as shown in **Fig. 1-12 (A),** CNCs, TEMPO-modified CNFs, and phosphorylated cellulose nanocrystals show significantly increase in adsorption capability

compared to unmodified cellulose and CNFs due to because of sulfonic acid group, carboxyl group and phosphate group were introduced on the nanocellulose surface [21, 48, 184]. Moreover, if we consider that the inexpensive adsorbents are generally effective in the removal of pollutants with limits at the milligram per liter level, then nanocellulose-based adsorbents, with an outstanding capacity for removing hazardous contaminants with levels on the order of microgram per liter, should be environmentally and economically beneficial [71]. Therefore, further enhancement of the adsorption capacity and expansion of the range of pollutant species to be absorbed through target chemical modification of the nanocellulose surface is still needed.

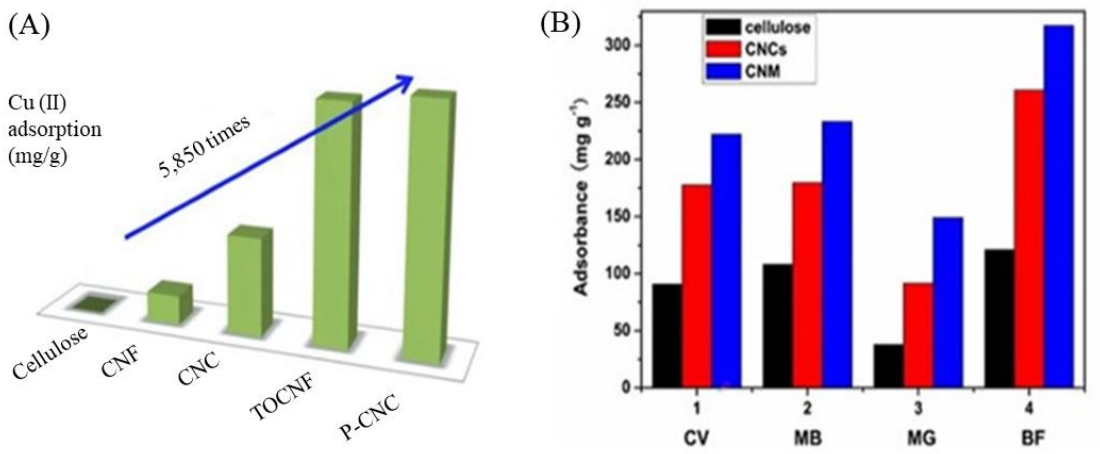

Figure 2-16. (A) Adsorption capacities for Cu(II) of various forms of cellulose: cellulose, cellulose nanofibrils (CNF), cellulose nanocrystals (CNC), TEMPO-oxidized cellulose nanofibrils (TOCNF) and phosphorylated cellulose nanocrystals (P-CNC) [183]. (B) Adsorption of different cationic dyes by cellulose, CNCs, and carboxyl functionalized nanocellulose, adsorbents (CNM) [184].

2.1.9.2 Multiple pollutants removal

Contaminants in real water are typically very complicated, with various types of contaminants usually coexisting [240]. The co-removal of multiple types of coexisting pollutants might be possible if multiple adsorption sites are available on the adsorbent [241]. However, no published work has tackled this aspect because the important challenge faced by the researchers is the simultaneous removal of a multitude of contaminants in a single stage. For this, the aerogel's

properties must be tuned in terms of porosity and functional groups present to perform simultaneous adsorption. Besides, how to test each pollutant's concentration change in mix solution is also a big issue [21, 180].

2.1.9.3 Regeneration of adsorbents

Most of the work so far has emphasized the usefulness of nanocellulose as an adsorbent since it significantly affects the operational cost [242]. However, the reuse and regeneration of nanocellulose-derived materials, and recovery of the contaminants at the end of each cycle are complex processes. Desorption involves the recovery of adsorbents by stripping them from the adsorbed species and then reusing them [21]. Cellulose-based adsorbents used for heavy metal ion and dye elimination are typically desorbed by acidic treatments (HCl, H_2SO_4, and HNO_3) or alkaline treatments (NaOH, $NaHCO_3$, Na_2CO_3 and KOH) if the adsorption process occurs due to the electrostatic attractions. However, it is very hard to desorb when adsorption process occurs due to the covalent bonding because it is irreversible. Anyway, this makes their long-term application economically feasible, especially in the case of functionalized nanocellulose adsorbents, given the higher cost involved in comparison with conventional adsorbents.

2.1.10 Merits of PEI modified nanocellulose adsorbents for current challenges

Compare with others, introducing amine group show great potential for adsorption more types of water pollutnasts, including metal ions, toxic dyes, some emerging contaminants and also can be used for carbon cauture. Branched polyethyleneimine (PEI), containing primary, secondary, and tertiary amino groups on its molecular chain, is an ideal water-soluble polymeric amine [23-25]. These active amino groups can be crosslinked by carboxyl, aldehyde, or epoxy groups to fabricate hydrogels, membranes, and fibers polymers to develop bio-sorbents for treating wastewater. Moreover, the charged amine groups in PEI can be protonated and deprotonated via adjusting the

pH to enable the adsorption and desorption of contaminants, thus realizing the regeneration of the adsorbent [11]. For example, Liuting et al. fabricated the amino functionalized 3D multi-wall perforated CNF-based polyethyleneimine (PEI) aerogels to remove Cu (II) efficiently, showing a maximum adsorption capacity of 485.44 mg/g. Desorption performance of this aerogel was determined using ethylenediaminetetraacetic acid (EDTA)-2Na, which was found that 4 cycles without signicant degradation [243]. Besides, CNM-PEI based composites also shoe super adsorption capability for anionic [192], cationic dyes [193], emerging contaminants [32, 194] and oil spills [244]. Therefore, PEI and nanocellulose composites show a great promising in water remediation [11, 23, 26], more details will be show in the 2.2 section (A literature review based on cellulose-PEI composites for water remediation, a version of this was published in *International Journal of Biological Macromolecules 232* (2023) 123342).

2.2 Literature Review - Comparison between nanocellulose-polyethyleneimine composites synthesis methods towards multiple water pollutants removal: A review

2.2.1 Abstract

Nanocellulose/polyethyleneimine composites have attracted growing attention due to their versatility as new materials for application in different fields. Water remediation is one of the traditional applications of these composites and their investigation as adsorbents for single water pollutants is well established. However, most water resources such as rivers, lakes, and even oceans contain complex mixtures of pollutants. Despite several recently published reviews on water purification technology, they only focused on these material as single pollutant removers and hardly mentioned their capacity for simultaneously recover multiple pollutants. Therefore, there is still a gap in the archived literature considering nanocellulose/polyethyleneimine

composites targeting water remediation with multiple water pollutants. In this review, methods for synthesizing such composites are classified and compared according to the mechanism of reactions, such as chemical crosslinking and physical adsorption, while outlining advantages and limitations. Then, the water pollutants mainly targeted by those composites are discussed in detail to expound the relationship between the synthesis method and the type and adsorption capacity. Finally, the last section presents challenges and opportunities of these nanocellulose/polyethyleneimine composites as emerging sorbents for sustainable multiple water pollutants purification technologies. This review aims to lay out the bases for future developments of these composites for multiple water pollutants.

2.2.2 Introduction

The combination of cellulose nanomaterials or cellulose nanofiber matrices (CNMs) with polyethyleneimine (PEI) has led to the production of a wide range of composites, which have found ample application in different fields, such as paper making [245-248], wastewater treatment [194, 249-251], drug release [252-255], sensing [256-258], heterogeneous catalysis [259], and others [189]. The potential utility of these composites has attracted significant interest from the scientific community. The number of publications in this field has progressively increased in the last 20 years (**Fig. 2-1**), with most of them (58.3%) dedicated to sorbent systems for water remediation [189].

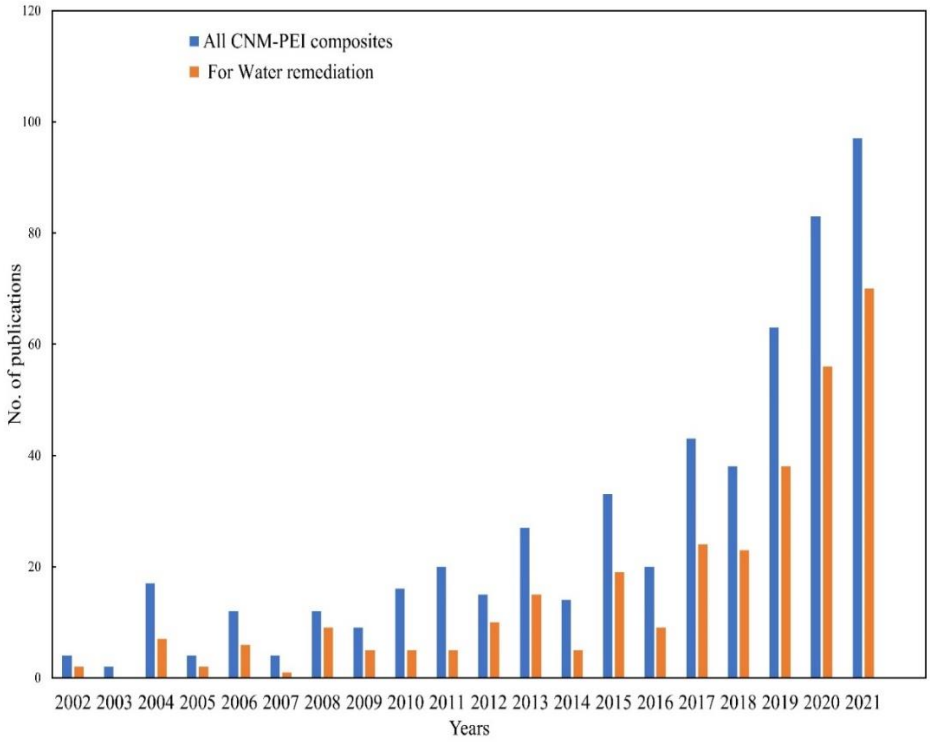

Figure 2-17. The number of publications describing CNM-PEI composites and their utility for water remediation during the past 20 years. The data obtained from Web of Science based on the search function: (polyethyleneimine OR PEI) AND (cellulose OR nanocellulose OR cellulose nanofiber (CNF) OR cellulose nanocrystal (CNC)) for All CNM-PEI composites; (polyethyleneimine OR PEI) AND (cellulose OR nanocellulose OR cellulose nanofiber (CNF) OR cellulose nanocrystal (CNC)) AND (water OR water remediation OR water treatment OR removal).

Being active in this research topic, we found that most research focused on using cellulose or nanocellulose/polyethyleneimine composites to target singular water pollutants. However, most water resources such as rivers, lakes, and even oceans contain complex mixtures of pollutants, including dyes, spilled oils, organic solvents, and heavy metals [240]. A paradigm shift from single pollutants to multiple pollutants control is crucial to tackle real-world water purification challenges [260, 261].

The synthesis method of the nanocellulose/polyethyleneimine composites largely determines the type and ability of contaminants that these composites can remove. Therefore, it is essential to review the methods for synthesizing such composites, and how they work towards removing

different types of pollutants to lay out the bases for future development of these composites for multiple water pollutants. In this review, the aim was to study the reported adsorption capabilities of the CNM-PEI composites from a single contaminant, finding the most common ones that can be used as comparison in the transformation route to multiple contaminant removal. Likewise, to close the gap in the exploration between the relationship of synthesis methods and the type and capacity of adsorbed pollutants.

2.2.3 Current synthetic strategies of CNM-PEI composites

When the different reported cellulose–PEI composites are compared, it can be noted that they were formed mainly by following two formation mechanisms: chemical crosslinking and physical adsorption. These are summarized in the scheme presented in **Fig.2-2**. The first approach, chemical crosslinking, can be subdivided into two types: with or without additional agents. These methods are largely dependent on whether the cellulose or CNMs have been pre-functionalized or not. Starting from cellulose sources without pre-functionalization often requires the use of proper crosslinkers to obtain stable and resistant composites. On the contrary, when operating in the presence of pre-functionalized cellulose, the formation of covalent bonds between the two building blocks by direct crosslinking is possible under proper and controlled reaction conditions [189]. Thus, a strong covalent bond can be obtained by heating [190] or by using condensation agents [194], without requiring additional molecules to act as bridges between the materials [189]. The second alternative is the direct assembly of the polymers by physical crosslinking between them. To achieve this, interacting forces such as hydrogen bonding, electrostatic forces, van der Waals forces, chain entanglements, and ionic & hydrophobic interactions dominate. Thus, allowing to maintain surface functional groups available as active point on the materials. Following, a detailed comparison between each method and the resulting composites was done.

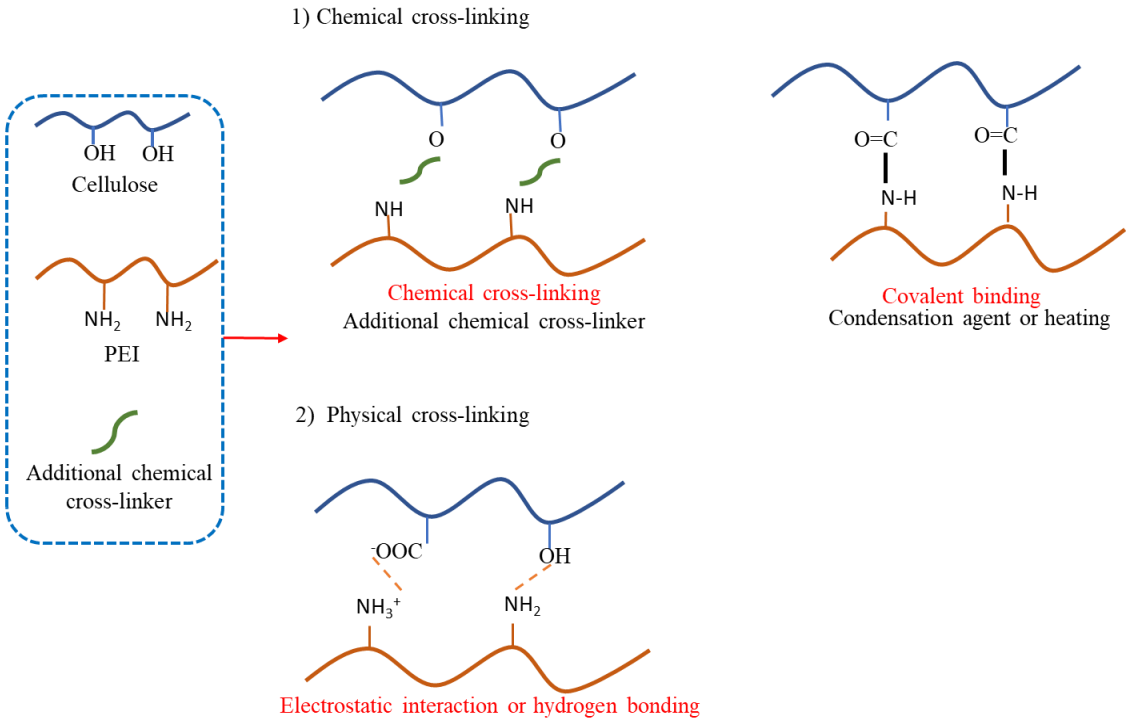

Figure 2-18. The synthesis strategies of CNM-PEI composites and reaction mechanism.

2.2.3.1 Chemical crosslinking

2.2.3.1.1 Using additional chemical crosslinker

CNM-PEI composites can be synthesized by several chemical crosslinkers, such as glutaraldehyde (GAL) [193, 262], epichlorohydrin (EPI) [192, 263], γ-(2,3-epoxypropoxy) propyltrimethoxysilane (GPTMS) [264], Tri-functional trimethylolpropane-tris-(2-methyl-1-aziridine) propionate (TMPTAP) [243], among others. For this formation pathway, a common feature is that the chemical crosslinker combines CNM and PEI together to form a complex through chemical bonds. The crosslinking agent may increase the complexes mechanical properties or help to form a porous structure. Moreover, some of them can introduce functional groups, increasing the trapping of the water pollutants. Meanwhile, when these crosslinkers are introduced into the composites, their toxicity must also be considered. Therefore, the reaction

mechanism, functionality of each crosslinker in CNM-PEI composites, and its toxicity will be discussed in detail.

The most frequently used crosslinkers are glutaraldehyde (GAL) and epichlorohydrin (EPI) because their use is operationally simple, and the reaction conditions are mild. For the GAL processing, the reaction can be conducted in one pot by simply stirring the reagents in polar solvents at room temperature [193, 262]. The use of GAL involves the crosslinking between PEI and cellulose through the formation of a Schiff base and a hemiacetal (**Fig.2-3 (A)**).

When using EPI as the crosslinker, heating (60-90 °C) was not necessary but can improve reactions. Alkaline condition was required to open the epoxide ring and promote ether formation to crosslink the cellulose and PEI as shown in **Fig. 2-3 (B)** [263, 265]. However, the CNM-PEI composites synthesized by these two methods exist in the form of powders, which have poor separability and recyclability [243]. To solve this problem, the latest research synthesized aerogels by a combination of freeze-drying and GAL crosslinking, in which an aerogel was formed by freeze-drying and then crosslinked by the GAL [266]. Besides, it still cannot be ignored that both GAL and EPI have been reported to be highly toxic for humans and animals [189, 267-269]. As alternatives, recent research suggested the use of new crosslinkers, such as GPTMS [264] and TMPTAP [243] instead of GAL and EPI to synthesize CNM-PEI aerogels.

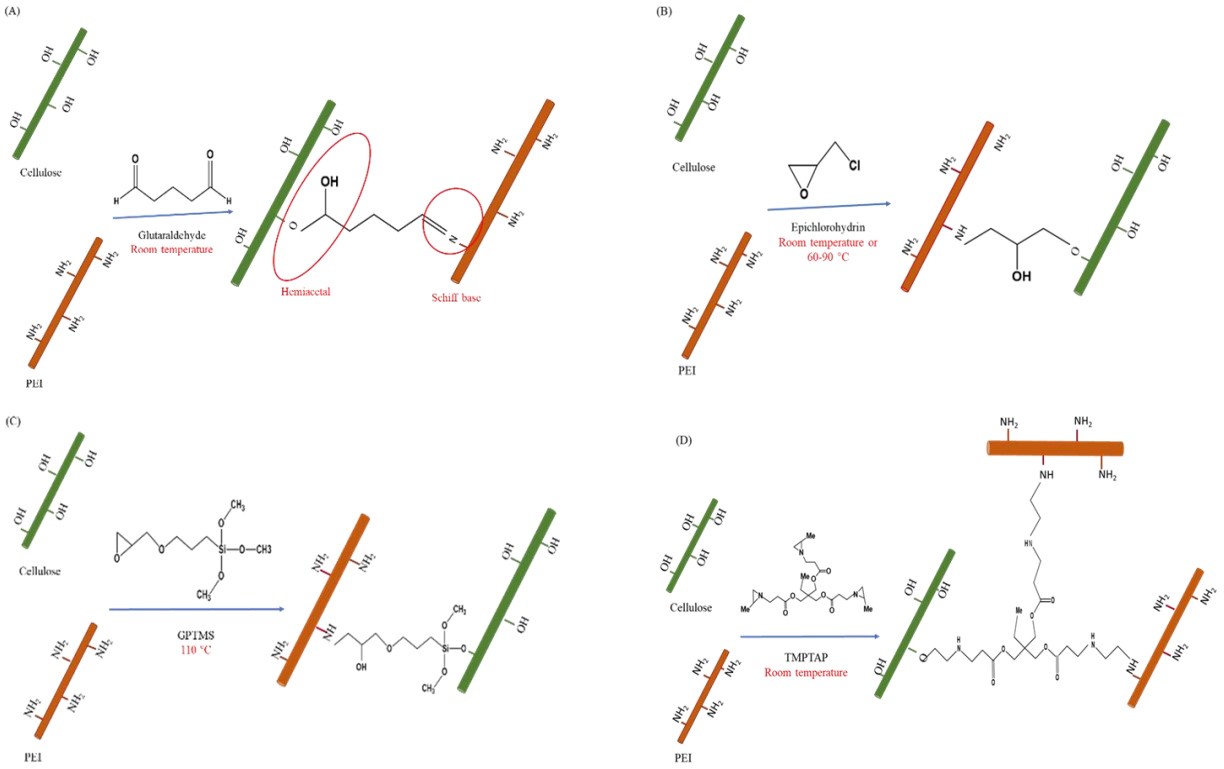

Figure 2-19. Reaction mechanism of different chemical crosslinkers.

For the GPTMS crosslinking process, condensation between the trimethoxy silane and cellulose hydroxyl groups results in covalent linkage (**Fig. 2-3 (C)**). This reaction started by the PEI being added into the mixture of cellulose and the crosslinker, the epoxide group on the end of GPTMS reacted sequentially with the amine groups on PEI, yielding robust networks [264, 270, 271]. The obtained mixture was introduced to liquid nitrogen via a syringe pump at a controlled rate to form uniform spherical beads. Afterward, these frozen beads were subjected to freeze-drying at −45°C to produce the aerogel beads [270, 271]. No toxicity was observed in cellular studies of the GPTMS-containing paste after 7 days, which showed GPTMS as superior to GAL and EPI [272]. Another crosslinker reported in literature was TMPTAP (Fig.3 D). This is a relatively safe skeleton tri-functional aziridine reagent, which is also an important intermediate for synthesizing massive nitrogen-containing biologically active compounds [273]. There, TCNF spontaneously reacted

with TMPTAP via a ring-opening reaction in an aqueous solution at room temperature and then crosslinked PEI into the composite. One of the advantages of this method is that TMPTAP acted not only as a crosslinker but also introduced many amino and oxygen-containing groups into the composite, thus increasing the adsorption ability for water pollutants [243]. All the synthetic processes involving chemical crosslinkers mentioned above can be operated under mild conditions. However, GPTMS and TMPTAP are relatively safer than GAL and EPI. In addition, TMPTAP was then superior to GAL, EPI, and GPTMS when it comes to introduction of additional functional groups to increase their trapping ability for water pollutants. Thus, TMPTAP seems as the ideal chemical crosslinking agent for the synthesis of CNM-PEI composites.

2.2.3.1.2 Direct covalent bonding between TCNF and PEI

As seen in the previous section, a lot of the current methods for synthesizing CNMs-PEI composites involved additional chemical crosslinking agents that can react under mild conditions. However, secondary pollution or toxicity caused by chemical crosslinking agents demonstrated to be an issue that could emerge and should be prevented. To avoid these problems, some research focuses on seeking a way to directly promote the crosslinking of covalent bonds between nanocellulose and PEI without adding additional chemical crosslinking agents. However, the reactivity of hydroxyl groups on nanocellulose is not compatible with the amino groups in PEI to form stable, covalent complexes without chemical crosslinkers. Therefore, nanocellulose needs to be pre-functionalized to introduce the functional group that can covalently bond with the amino group [189]. The most popular pre-functionalized methods were TEMPO-mediated or sodium periodate oxidization. These can introduce carboxyl and aldehyde groups into nanocellulose, respectively. Both functional groups can be covalently bound with the PEI amino

groups by amide or Schiff base reaction under proper conditions. At present, heating and adding condensation agents to promote the combination of CNMs and PEI have been reported.

By heating

The addition of heat into solutions containing anionic cellulose and PEI allows for the materials to break the energetic barrier to promote the condensation of the functional moieties and forming covalent bonds. This mechanism has been used to form TCNF and PEI composites with a sponge-like structure, good mechanical stability, and a shape-memory capability in water [190]. The composite formation was carried out in a multistep process. First freeze-drying was done to form a foam, followed by heating in an oven over a temperature ramp of 60 to 102°C, over 8 h followed by heating at 102 °C for 2 h, thus forming amide bonds between the two components during the thermal treatment [190] (Fig.4 A). Interestingly, a later study found that their mechanical properties can be further enhanced by the introduction of a natural crosslinker, citric acid [274]. This approach made it possible to obtain cellulose nano sponges (CNS) due to their inner nanostructure and nano porosity [189, 275, 276]. However, the problem with this method is that the synthesis of TCNF/PEI nano sponges needs a combination of freeze-drying and heating over 100 °C, both of which are energy-intensive processes [189, 275, 276].

By condensation agents-EDC

CNM/PEI composites could also be formed by using condensation agents, such as EDC (N-ethyl-N′-(3-(dimethylamino) propyl) carbodiimide) (**Fig. 2-4 (A)**), which promotes amide bond formation between the amines of PEI and the carboxyl groups of TEMPO-oxidized cellulose, instead of thermal treatment in the absence of additional chemical crosslinkers [194]. The advantage of this synthetic route relies on the possibility of operating at room temperature [189,

194]. The disadvantage is that the EDC needs to be removed by a dialysis process after crosslinking, which is a time tedious process.

By Schiff base reaction

Another alternative is the formation of the composite through Schiff base reaction. The CNF were pre-functionalized by sodium periodate oxidation to introduce aldehyde groups. Then a cryogel was prepared by freeze-induced chemical crosslinking between the aldehyde groups and hydroxyl groups on CNF. Finally, the cryogels were added to the PEI solution to functionalize to form the CNF-PEI composites cryogels by a Schiff base reaction (**Fig. 2-4 (B)**). The CNF/PEI hybrid aerogels exhibited good structural stability and shape recovery in water. Moreover, the squeeze-deformed CNF cryogel was recovered to its original shape upon contact with water [277]. The results of this study have made a breakthrough in improving the mechanical properties of CNF-PEI composites without heating, freeze drying and other conditions.

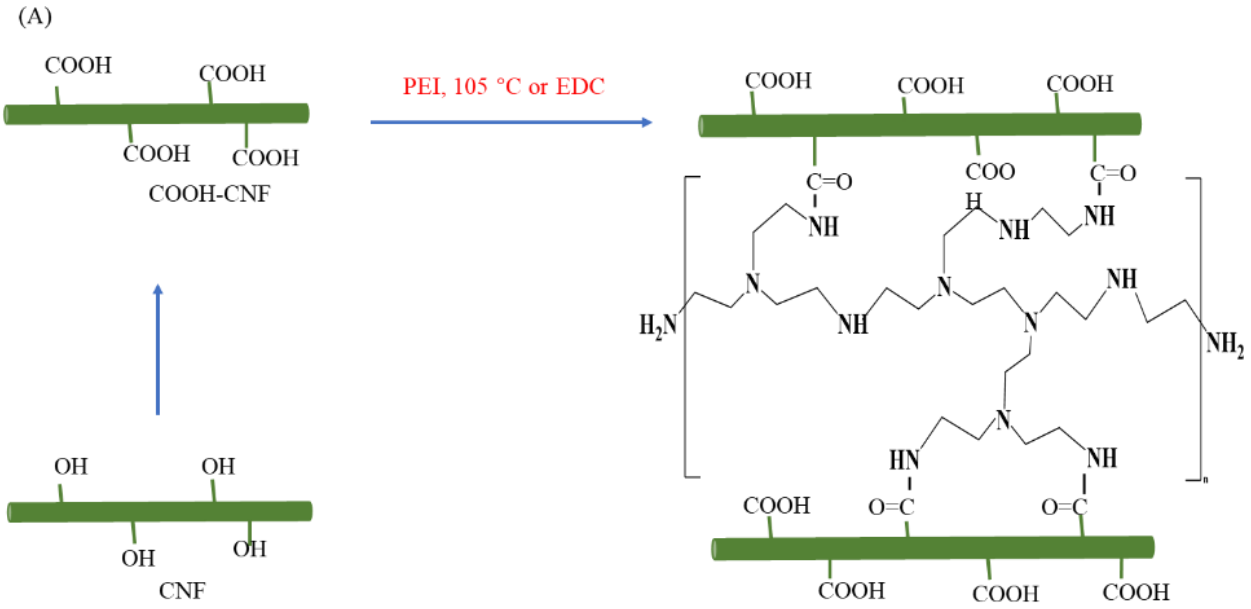

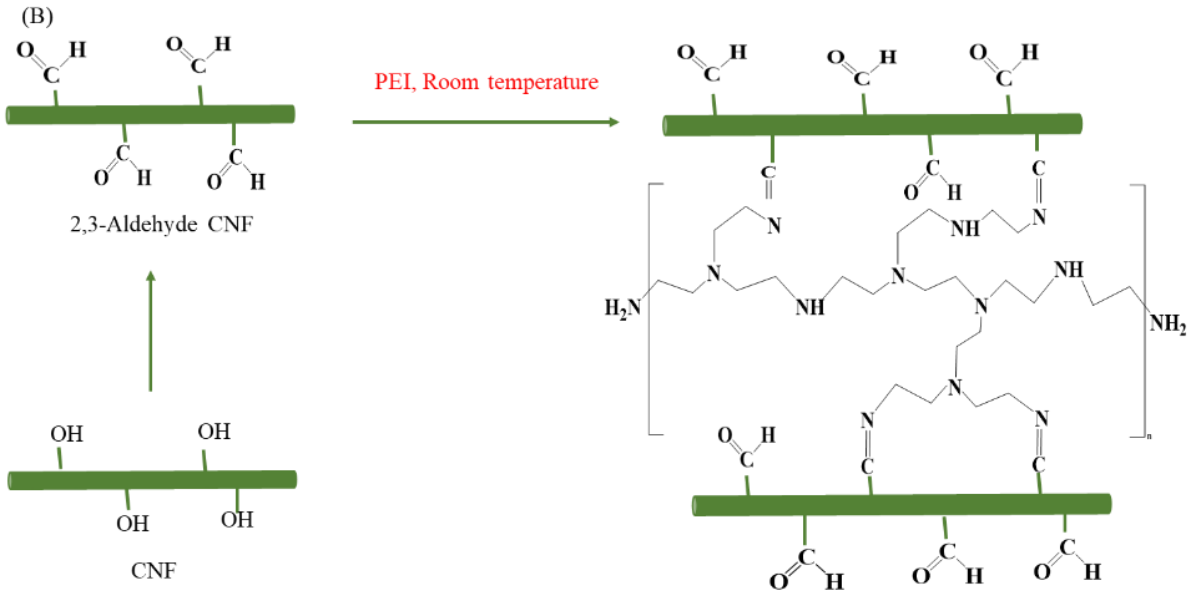

Figure 2-20. Reaction mechanism by covalent bonding.

2.2.3.2 Physical adsorption

The downside of the chemical crosslinking strategies is the problem of using toxic reagents, the chemical residues produced, and the extra cost added with new reactants [278]. Condensations promoted by high temperature are energy intensive processes. An alternative strategy involves physical crosslinking strategies that are governed by non-covalent interactions such as electrostatic interactions, hydrogen bonding, hydrophobic association, or chain winding [279]. In addition, the technology of physical crosslinking is much simpler (**Fig. 2-5**). Li and co-workers made a shape memory aerogel from TCNF and PEI via electrostatic combination without additional chemical crosslinking. These aerogels were generated by maintaining the total concentration of TCNF and PEI at 12 mg/mL at pH 10 for 4 h at room temperature followed by freeze-drying for 3 days at −91 °C. The CNF/PEI hybrid aerogels exhibited good structural stability and shape recovery in water [181]. In our research, a TCNF/PEI hydrogel was also formed by combination cationic chelating and physical adsorption. The TCNF was chelated by zinc ions to form a preliminary hydrogel

which was then put into the PEI solution to functionalize at room temperature, resulting in TCNF/PEI hydrogel composites (unpublished). These studies have confirmed that a physical adsorption method is also a good option for the synthesis of CNF-PEI composites for water remediation.

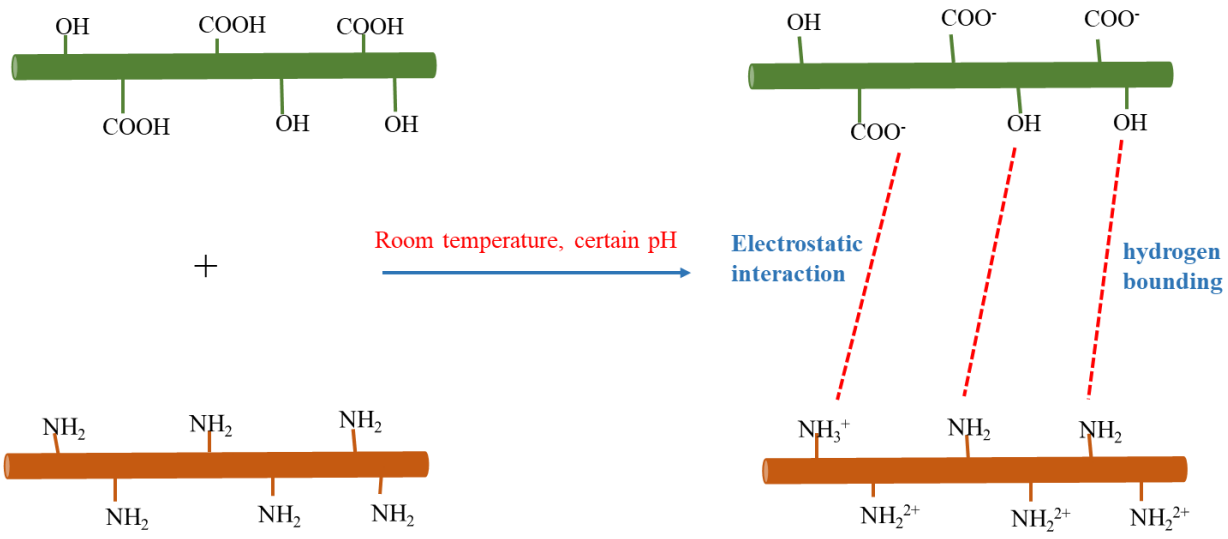

Figure 2-21. The synthesis of CNM-PEI composites by physical adsorption.

2.2.4 Possible interfacial interactions with CNM-PEI composites

It is very important to comprehensively understand the underlying mechanisms of adsorption to fully exploit the utility of CNM-PEI for water remediation. Due to the abundant amino groups added to the surface with PEI, as well as the presence of residual carboxyl and aldehyde groups, electrostatic interactions are prevalent. Moreover, the high density of hydroxyl groups on the cellulose backbone would allow hydration and the formation of hydrogen bonding between molecules in the media and exposed surfaces, as well as other van der Waals interactions. Likewise, cellulose structures are known to adsorb molecules into the hydrophobic crystalline face as their main entropic strategy to decrease the free energy in water systems [280]. The

understanding of adsorption mechanism is helpful to design optimal composites targeting more types and amounts of pollutants. Therefore, this section focuses on the adsorption mechanism of the different types of water pollutants onto CNM-PEI composites.

2.2.4.1 Metal ions

Taking Cu (II) as a model for divalent ions, previous studies showed that the adsorption capacity of CNM-PEI could be attributed to a large amount of amino functional groups (primary amine, secondary amine, and tertiary amine groups) and oxygen-containing functional groups (hydroxyl and carbonyl groups) available. These moieties provided abundant electrostatically charged sites for the adsorption of cations like Cu (II) [243]. Based on this, if the chemical crosslinker is rich in the amine group and oxygen-containing functional groups, it will increase the adsorption capacity for the ions.

Thus, one can roughly predict the order of metal ion adsorption capacity of CNM-PEI composites obtained by various synthetic methods according to the content of oxygen or amino groups introduced by chemical crosslinkers. The order is: TMPTAP>GPTMS>GA, EPI > covalent bonding by heating and EDC, physical adsorption> covalent bonding by Schiff base reaction if the same moles of chemical crosslinker were added with same moles of CNF and PEI. However, considerations on porosity, surface area, and structure need to be made to confirm this.

2.2.4.2 Toxic dyes or other organic chemicals

Most of the research focused on the removal of toxic dyes by adsorption onto CNM-PEI composites [192, 248]. PEI with abundant amine groups were immobilized on the surface of TCNF/PEI hydrogel. When TCNF/PEI hydrogels were put into aqueous solution whose pKa is lower than the pKa of PEI, amine groups on hydrogels would translate to positively charged amine groups [193]. These positively charged amine groups could form the cation-π interactions, which

are electrostatic attraction between positively charged cations and negatively charged electron-rich π systems [281]. Besides, positively charged amine group could also produce strong electrostatic attraction towards the negatively charged anionic dye molecules [192]. Furthermore, hydrogen bounding, hydrophobic interaction, and Van der Waals forces all could exist between the hydrogels and methyl blue dyes [281]. Finally, it cannot be ignored that the multilayer adsorption caused by π–π stacking is also a pathway of interaction between dye molecules having rich π systems [282].

In general, cation-π interactions show higher strength than hydrogen bonding, and in some cases, even charge–charge interactions, which are arguably one of the strongest noncovalent interactions in aqueous solutions [282-284]. However, according to other research, the strong electrostatic attraction between PEI and methyl blue dyes is prevalent, being the main reason PEI functionalized cellulose composites absorbed the methyl blue dyes [193]. More research is needed to determine which role is dominant among those.

For the cationic or non-ionic organic chemicals without π-systems, the adsorption is limited to these pollutants' capacity to form electrostatic attraction, van der Waals interaction or hydrogen bonding with the hydroxyl groups and other polarizable functionalities. Another important consideration is that the conditions of the system will also determine the pollutants adsorption onto cellulosic materials since the system's free energy needs to be decreased. Thus, the presence of salt and the exchange of water molecules for molecules on the surface would also favor the adsorption of the molecules, even when other phenomena are not driving it. For example, coupling hydrophobic molecules onto hydrophobic faces and points in the CNM-PEI composites will liberate water and cosolvents, increasing the entropy of the overall system.

2.2.5 Applications of CNM-PEI composites for water remediation

Nowadays, the research of CNM-PEI composites in the field of water remediation focuses mostly on heavy metal ions and organic dyes; with only some studies focusing on removing the emerging contaminants (ECs) that have been recently detected in natural environments. Different aspects of the composite, such as processing, conformation, and experimental conditions, determine the availability and reactivity of the active sites, modulating the removal efficiency [189]. All these aspects are mainly determined by the synthesis method. Therefore, it is necessary to compare the synthesis methods and the types and amounts of pollutants adsorbed. Understanding this will help select the method that can be used to synthesize CNM-PEI composites capable of targeting multiple types and higher amounts of pollutants.

2.2.5.1 Removal of metal ions

A general overview of cellulose–PEI composites achieved by different methods for removing heavy metals is provided in **Table 2-3**. Regardless of their methods of preparation, cellulose-PEI composite materials are well-suited for the adsorption of metal ions due to the large amount of charged moieties on the surface of the particles, as well as their capacity to chelate metal ions. The most tested metal ions include Cu (II), Pb (II), Cd (II), Ni (II) [191], Cr (VI) [285], As (III), As (V) [286], Fe (III), Cr (III) [287], and Zn (II) [288, 289]. Among all the metal ions of interest, Cu (II) has been widely taken as a reference in adsorption studies since it is well adsorbed, and the sorption is easy to detect by a simple UV analysis [189].

While comparing the adsorption capacity of such complexes, differences have been noted depending on the method of synthesis. TMPTAP crosslinked TEMPO-oxidized CNF and PEI aerogels had the highest adsorption capacity with up to 485.44 mg/g (Table 1) [243]. This difference is due to TMPTAP acting not only as a crosslinker but also introducing amino and oxygen-containing groups, which all can chelate Cu (II) ions, thus increasing the adsorption

capacity of the material. Based on **Table 2-3**, the order of the maximum adsorption capacity of CNM-PEI composites obtained by the various synthetic methods for Cu (II) is TMPTAP> GAL, EPI > covalent bonding by heating > physical adsorption> GPTMS> covalent bonding by Schiff Base reaction. This order is like the order we predicted only according to the content of carboxyl or amino groups introduced by synthetic process in the adsorption mechanism section except for the GPTMS.

It was also found that the composites that presented the highest adsorption capacity for Cu (II) ions, were also more likely to be highly adsorbent to other ions (Table 1). PEI-functionalized A4 paper has the higher adsorption capacity for Cu (II) (435mg/g) and Cd (II) (370 mg/g) as compared to TEMPO-oxidized cellulose-PEI sponges [288, 289]. Likewise, TEMPO-oxidized CNF/PEI aerogel performed better than the PEI- dialdehyde bacterial cellulose composites for the adsorption of Cu (II) and for Pb (II) with 357.44 mg/g and 141 mg/g, respectively [181, 290]. Therefore, the adsorption capacity order of this kind of material to other ions can be roughly judged according to the adsorption capacity order of copper ions.

Table 2-3. Cellulose–PEI composites are used for removal of metal ions.

Composites	Synthesis strategies		Metals ions and their maximum adsorption capacity (mg/g)	Reference
TEMPO-CNF/PEI aerogels	Crosslinker	TMPTAP	Cu (II) 485.44	[243]
PEI-functionalized A4 paper		GAL	Cu (II) 435, Cd (II) 370, Ni (II) 208， Cr (VI) 68	[291]
PEI-carboxymethyl cellulose nanofibrils aerogel			Cu (II) 380.03	[292]
PEI-CNF aerogel			Cu (II) 135.1	[265]
PEI-TEMPO oxidized cellulose hydrogels			Cu (II) 109.89, Pb (II) 279.32	[293]
PEI-nanowood			Cu (II) 93	[294]
PEI-modified TCNF powders			Cu (II) 53	[262]
PEI-modified microcrystalline cellulose			Cd (II) 217, Pb (II) 357	[295]
PEI-cellulose aerogel beads			Cr (VI) 229	[285]

PEI functionalized coffee cellulose membranes			As (III) 13, As (V) 46	[286]
Cellulose/PEI powder		EPI	Cu (II) 285.7	[263]
Porous spherical PEI-cellulose powders			Fe (III) 377.19, Cr (III) 83.98	[287]
Hyperbranched PEI modified cellulose fiber powders			As (III) 54.13, As(V) 99.35	[296]
Cellulose aerogel beads		GPTMS	Cu (II) 163.40	[270]
Cellulose nanofiber (CNF)-supported cryogel			Cu (II) 138	[297]
PEI modified cellulose-based adsorbent		GMA	Cu (II) 102	[298]
PEI coated bacterial cellulose nanofiber membranes		GDE	Cu (II) 90.01, Pb (II) 130	[299]
PEI -TEMPO oxidized cellulose sponges	Covalent bounding between carboxyl and amine group	Heating	Cu (II) 194, Cr (III) 94, Cd (II) 84, Zn (II) 125	[288]
TEMPO oxidized cellulose-PEI cellulose sponges			Cu (II) 89.6	[190]
PEI -TEMPO oxidized cellulose sponges			Zn (II) 100	[289]
PEI-TEMPO oxidized wood aerogel		EDC	Cu (II) 59.8	[182]
TEMPO-Oxidized cellulose nanocrystal-PEI powders			Cr (VI) 358.42	[264]
PEI- dialdehyde bacterial cellulose	Covalent bounding between aldehyde and amine group	Schiff base	Cu (II) 148, Pb (II) 141 mg/g	[290]
TEMPO-NFC/PEI aerogel	Physical adsorption	/	Cu (II) 175.44, Pb (II) 357.44	[181]

Moreover, in a closer view, the TMPTAP crosslinked TEMPO-oxidized CNF and PEI aerogels had the highest adsorption capability compared with other materials, as shown in **Table 2-4**. Most CNM-PEI composites showed higher adsorption capability than other materials, which indicates that CNM-PEI composites have excellent performance for metal ions.

Table 2-4. Comparison of the adsorption capacities of TEMPO-oxidized CNF/PEI crosslinked by TMPTAP with other types of materials for Cu (II).

Composites	Maximum adsorption capacity for Cu (II) (mg/g)	Reference
TEMPO-CNF/PEI aerogels crosslinked by TMPTAP	485.44	[243]
Magnetic tubular carbon nanofibers	375.93	[300]
Electrospun polyacrylonitrile-based lace nanostructures	354	[301]
Chitosan derivative	192.31	[302]
Graphene oxide/polyethyleneimine sponge	150.9	[303]
Graphene oxide functionalized chitosan-magnetite nanocomposite	111.11	[304]
Solid carbon nanoonions via catalytic co-pyrolysis of lignin and polyethylene	100	[305]

2.2.5.2 Removal organic dyes

Water pollution caused by synthetic dyes has received considerable attention since such dyes are extensively utilized in diverse industries such as textile, food, paper, drugs, leather, amongst others [306]. Nowadays, over 100,000 dyes are commercially available [189]. Most of these dyes feature toxic, nonbiodegradable, and carcinogenic features which cause adverse effects on human health and ecosystems [306]. During the washing process, a certain fraction of dyestuffs unavoidably ends up in the wastewater discharged into the environment.

Cellulose–PEI composites have also been used to remove these toxic dyes. A general overview of cellulose–PEI composites for the removal of toxic dyes is provided in **Table 2-5**. The removal efficacy has been demonstrated for both cationic and anionic dyes but most of the research focuses on the anionic examples. PEI-modified cellulose aerogels crosslinked by GAL showed high adsorption capacity for anionic Rose Bengal, methyl orange, and methyl blue reaching 1290, 1226, and 1200 mg/g, respectively [192]. The strong adsorption performance of cellulose-PEI

composites for anionic dyes was mainly ascribed to an electrostatic interaction between the cationic charges of the amino groups of PEI and the negative charges of anionic dyes, with a sorption efficiency depending on the charge present both on the surface of the composite and the contaminant dye [189]. Conversely, the adsorption capacity of cellulose-PEI composites for cationic dyes is lower than that of anionic dyes. It shows enormous difference for different cationic dyes, the adsorption capability up to 970 mg/g for Cationic Basic Yellow, but just has 6 mg/g, for methylene blue. The reason is not very clear. Further research is needed to be able to explain this behavior.

Unlike the research on metal ions, where most studies choose copper ions for reference, making it easier to compare different methods and materials, the use of standard reference dyes is not common. Thus, it is more difficult to compare the adsorption capacity of materials arising from different synthetic tactics. For methyl orange, the adsorption capacity of CNF/PEI aerogel crosslinked by EPI was up to 1226 mg/g [192], which was higher than that achieved with PEI-MFC aerogel (500 mg/g) which was generated by covalent bonding between aldehyde and amine group by Schiff base reaction [277]. In addition, the adsorption capacity of PEI modified cellulose-based bio-adsorbent crosslinked by GAL for the cationic dye bright yellow was 571.43 mg/g [193], which was also higher than that of an Aldehyde-CNF/PEI (160 mg/g) obtained by Schiff base reaction [307]. This difference might be because GAL or EPI not only functioned as a crosslinking agent but also introduced additional charged oxygen atoms, which can form hydrogen bonding with oxygen and nitrogen atoms in methyl orange.

Table 2-5. Cellulose–PEI composites are used for removal of different toxic dyes.

Composites	Synthesis strategies		Metals ions and their maximum adsorption ability (mg/g)	Reference
PEI-modified cellulose aerogels	Crosslinker	GAL	Anionic Rose Bengal, 1290 Anionic Methyl Blue, 1200 Anionic Alizarin Red, 360 Anionic Acid Orange 7, 280 Anionic Ponceau S, 220	[192]
PEI modified cellulose-based bioadsorbent			Anionic Reactive Yellow, 971	[193]
Oxidized cellulose membranes modified with PEI			Anionic Xilenol Orange, 241	[308]
CNF/PEI aerogel		EPI	Anionic Methyl orange,1226	[281]
Aldehyde-CNF/PEI cryogels or powders	Covalent bounding between aldehyde and amine group	Schiff base reaction	Anionic Brilliant Blue, 1000 Anionic Congo Red, 990 Anionic Reactive Red, 950 Anionic Eosin Y, 215	[307]
PEI-MFC aerogel			Anionic Methyl orange, 500	[277]
PEI modified cellulose-based bioadsorbent	Crosslinker	GAL	Cationic bright yellow 571.43	[193]
Oxidized cellulose membranes modified with PEI			Cationic Methylene blue, 144	[308]
PEI-modified cellulose aerogels			Cationic Methylene blue 6.0	[192]
Aldehyde-CNF/PEI powder	Covalent bounding between aldehyde and amine group	Schiff base reaction	Cationic Basic Yellow, 970 Cationic Bright Yellow, 160	[307]

When compared with other materials (as shown in **Table 2-6**), the adsorption capability of CNM-PEI composites for anionic Rose Bengal, methyl orange, and methyl blue and cationic basic yellow

was among the highest. Demonstrating that these composites also presented excellent adsorption performance for toxic dyes.

Table 2-6. Comparison of the maximum adsorption capacity of CNM-PEI composites for Rose Bengal, methyl orange, and methyl blue dyes with other materials.

Dyes		Absorbents	Shape	Maximum adsorption ability (mg/g)	References
Rose 60engal (-)	Other materials	Chitosan/PVA	Powder	44.4	[309]
		Kappa-carrageenan/tamarind kernel powder	Hydrogel	168.1	[310]
		Polyethyleneimine-functionalized cellulose beads	Beads	467.9	[311]
		Dextran hydrogel	Hydrogel	1700	[312]
	CNM-PEI composites	PEI-modified cellulose aerogels	Aerogels	1310	[192]
Methyl orange (-)	Other materials	Chitosan/polyvinyl Alcohol/zeolite electrospun composite	Membrane	153	[313]
		Chitosan microspheres	Microspheres	207	[314]
		Amino-functionalized three-dimensional graphene	3D-networks	270.3	[315]
		Functionalized carbon nanotube	Powder	310.2	[316]
		3D hierarchical GO-NiFe LDH	Sandwich-like structure	438	[317]
	CNM-PEI composites	PEI-modified cellulose aerogels	Aerogels	1226	[28]
Methyl blue (-)	Other materials	Cellulose membrane prepared from corn stalk	Membrane	8.8	[318]
		BaFe12O19 ferrite particles	Powder	223.9	[319]
		Poly (methacrylic acid-*co*-2-(dimethylamino) ethyl methacrylate) and carboxylated cellulose nanofibrils	Aerogel	598.8	[10]
		Diethylenetriamine-functionalized hollow polymer particles	Powder	1341	[320]
		B-Cyclodextrin functionalized SBA-15	Powder	1790.9	[321]
	CNM-PEI composites	PEI-modified cellulose aerogels	Aerogels	1333	[28]

Basic yellow (+)	Others	Fe@graphite core–shell nanocomposite	Nanocomposite	52.4	[322]
		Graphene oxide-Polyethylenimine-Polyvinyl alcohol	Hydrogel beads	862.1	[323]
	CNM-PEI composites	Aldehyde-CNF/PEI	Powder	970	[307]

2.2.5.3 Emerging contaminants (ECs)

ECs are a large and relatively new group of compounds and can potentially cause deleterious effects in aquatic and human life at environmentally relevant concentrations which are becoming a growing concern [324]. At present, just counted studies focusing on using the CNM-PEI composites for removal emerging contaminants [32, 194]. *P*-nitrophenol (*p*NPh) is an important industrial precursor in the synthesis of different drugs, fungicides, and dyes. It has been found that TEMPO-Oxidized cellulose-PEI prepared by the direct amination of the TCNF carboxylic groups with PEI by heating, and without using a supplementary crosslinker, can be used to adsorb the *p*NPh, as well as other Ecs like 2,4,5-trichlorophenol and amoxicillin. Their adsorption capacity reached 1630, 205 and 556 mg/g, which are higher or like that of other materials (**Table 2-7**). Interestingly, Swasy and her collaborators found that PEI-functionalized cellulose nanocrystals can potentially serve as a new and viable remediation technique based on their ability to effectively degrade various pesticides such as malathion, deltamethrin, and permethrin with 100%, 95%, and 78% degradation in water, respectively [194]. Therefore, the CNM-PEI composites also have an immense potential for removing and eliminating emerging contaminants. More attention should be paid to the removal of the emerging contaminants by CNM-PEI composites.

Table 2-7. Compare CNM-PEI composites with other materials for emerging contaminants adsorption capability.

Contaminants	Composites	Maximum adsorption capability (mg/g)	Reference
2,4,5-Trichlorophenol (tCPh)	Hypercrosslinked magnetic polymer	152.6	[325]
	Microporous activated carbon by $FeCl_3$ activation	184.9	[326]
	Nanographite oxide	268.5	[327]
	TEMPO-oxidized cellulose -PEI	1630	[32]
	Macroporous polymers foams (MPFs)	167.7	[328]
	Organo-acid-activated bentonite	244.6	[329]
	TEMPO-oxidized cellulose -PEI	205	[32]
Amoxicillin	CoFe2O4-modified biochar derived from banana pseudostem	99.99	[330]
	Mesoporous Fe3O4/SiO2/CTAB–SiO2	362.7	[331]
	TEMPO-oxidized cellulose -PEI	556	[32]

2.2.5.4 Oil spills

Furthermore, it is possible to apply CNM-PEI composite for the cleaning of oil spills [244]**.** CNC-PEI aerogel crosslinked by Di-epoxide and then coated by graphene were used to selectively absorb organic solvents with a weight ratio ranging from 25 to 58 g/g. Therefore, CNM-PEI based composite also showed satisfactory performance to clean oil spills.

2.2.6. Challenges and opportunities of CNM-PEI composites for multiple water pollutants

Although CNM-PEI composite sorbents demonstrated satisfactory sorption capabilities to remove different classes of contaminants, ranging from heavy metals, organic dyes, some emerging contaminants, and oil spills; most of these studies focused on the removal of a single water pollutant under an ideal model system condition. Realizing that this ideal condition may not exist

because polluted water systems are often contaminated with a wider array of pollutants, an urgent call for a multipollutant modeling approach aimed to target simultaneous uptake of coexisting water pollutants is needed. In particular, the performance efficiency for simultaneous uptake of coexisting water pollutants from different pollutant classes using CNM-PEI sorbents has rarely been reported in the literature and can be considered as one of the major gaps in adsorption studies. A shift of current conventional single-pollutant modeling toward a multipollutant approach should be undertaken for a more inclusive coverage of water pollutant assessment using emerging CNM-PEI sorbents. It cannot be guessed what would happen in complicated multiple pollutants system, including metal ions, dyes, and oil spills. The big challenge may be how to test the amount change of each single pollutant in a mixed system with multiple pollutants.

2.2.7 Conclusions

Different strategies have been used to synthesize the CNM-PEI composites as adsorbents for water remediation due to their superior adsorption performance compared with other materials. In this review, synthesis mechanism, processing, adsorption capability, toxic properties, and recyclability of CNM-PEI composites were compared.

By doing this, we found that TAMPT seems to be an ideal chemical crosslinking agent due to easy processing, high adsorption capability and non-toxic properties. TMPTAP acted not only as a crosslinker but also introduced many amino and oxygen-containing groups into the composite, thus increasing the adsorption ability for water pollutants. Based on this, the incorporation of chemical crosslinker has the capability to introduce more functional groups, appears to confer higher contaminant removal performances. Likewise, the accessibility of a high number of amino groups on PEI, the presence of hydroxyl, carbonyl, and carboxylic groups on cellulose fibers and

nanofibers, also opens the possibility of introducing other functional groups. Besides, physical adsorption also shows great potential to prepare CNM-PEI composites due to its comparable adsorption capability and no extra cost paid for crosslinkers. Moreover, CNM-PEI based composites demonstrated to be capable of adsorbing metals, dyes, emerging contaminants, and oils. Therefore, there is enough knowledge developed to transition CNM-PEI composites into a multipollutant modeling approach aimed targeting simultaneous uptake of coexisting water pollutants.

The current problem is that CNM-PEI composites are usually in powder form which has poor separating capacity and recyclability. Freeze-drying can help to transfer powders to aerogels, but increased energy consumption needs to be accounted for. How to generate stable 3-D structure adsorbents under mild conditions is still the goal of future efforts.

The comprehensive understanding presented herein opens the way for the fabrication of more sophisticated and functionalized systems, which would be capable of providing higher contaminant removal performances, even in multipollutant systems. Moreover, the origin of the CNM can be varied, making these biomass-based materials candidates for sustainable solutions for a wider range of uses.

2.3. Research objective and hypothesis

2.3.1 Overarching objective

The aim of this work was to synthesis CNM-PEI composites hydrogels *via* self-assembling mechanism for water remediation.

2.3.2 Specific objectives

Chapter 3:

i) To synthesize stable TCNF/PEI hydrogels by combination cationic chelation and physical adsorption.

ii) To characterize the formed hydrogels to learn their chemical and morphology properties.

iii) To explore the effect of concentration and pH of PEI solutions on the composite and performance of formed TCNF/PEI hydrogels.

iv) To investigate the adsorption efficiency of hydrogels for the capture of methyl blue dyes and Cu (II) ions from water.

Chapter 4:

i) To explore the impact of pH in the adsorption of methyl blue onto TCNF/PEI hydrogels.

ii) To elucidate the active interaction mechanism of TCNF/PEI hydrogels and methyl blue.

Chapter 5:

i) To integrate GO onto the TCNF/PEI hydrogel formulations.

ii) To explore the effect of GO content on the stability, surface properties, physical and chemical properties, and adsorption capability of multiple pollutants.

Chapter 6:

i) To explore the effect of enzyme hydrolysis by endoglucanase FiberCare® on the particle size change of TCNFs

ii) To study the effect of particle size decease on the surface properties and adsorption behavior of nanocellulose

2.3.3 Hypotheses

i) Stable TCNF/PEI composite hydrogels can be formed by combination cationic chelation of the carboxyl groups and PEI immobilization onto the surface of cellulose due to the hydrogen bonding.

ii) The TCNF/GO/PEI composite hydrogels can be formed by combination cationic chelation and physical adsorption due to carboxyl group in the GO can be chelated by cationic ions, and the hydrogen bonding between oxygen-containing groups in GO and amine group in PEI.

iii) Addition of GO in the TCNF/PEI hydrogels will promote multiple water pollutants adsorption due to multiple functional sites and high surface area of GO.

iv) The decrease of particle size will significantly increase the adsorption capability of toxic dyes due to the surface area increase.

Chapter 3. Valorized soybean hulls as TEMPO-oxidized cellulose nanofiber and polyethylenimine composite hydrogels and their potential removal of water pollutants

Note: this chapter was published as a peer-review article as "Nan, Y., Gomez-Maldonado, D., Iglesias, M. C., Whitehead, D. C., & Peresin, M. S. (2023). Valorized soybean hulls as TEMPO-oxidized cellulose nanofibril and polyethylenimine composite hydrogels and their potential removal of water pollutants. *Cellulose, 0123456789*. ttps://doi.org/10.1007/s10570-023-05086-y"

3.1 Abstract

Cellulose nanomaterials (CNM) and polyethylenimine (PEI) composites have attracted growing attention due to their multifunctional characteristics, which have been applied in different fields. In this work, soybean hulls were valorized into carboxyl cellulose nanofibers (TCNFs) and composited into hydrogels with PEI by combining them with cationic chelating and physical adsorption strategies. Cellulose nanofibrils (CNFs) were produced from soybean hulls prior to oxidation by a TEMPO mediated reaction to obtain TCNFs; then drops of zinc chloride were added to 1.5 % aqueous TCNF dispersions, which were left for 24 h to form TCNF hydrogels. Finally, the hydrogels were functionalized using different concentration of PEI solutions over a range of pH values. Elemental analysis results showed that 20% aq. PEI at pH 11.6 is the optimum condition to synthesize the TCNF/PEI hydrogels. Additionally, the adsorption efficiency for the removal of anionic methyl blue dyes and Cu (II) ions from water was tested, reaching 82.6 % and 69.8 %, respectively, after 24 h. These results demonstrate the great potential of TCNF/PEI hydrogels as adsorbent materials for water remediation.

3.2 Introduction

Cellulose nanomaterials/polyethylenimine (CNM-PEI) composites have attracted growing attention due to their multifunctional characteristics. Extensive research has been devoted to the design and development of new materials for different applications, such as paper making [332], wastewater treatment [249, 263, 333, 334], drug release [252, 253, 335], sensing [336, 337], heterogeneous catalysis [189, 259, 338], and of particular interest to this group for water remediation.

Current research mainly focuses on synthesizing adsorbents derived from CNM-PEI composites by chemical crosslinking [189, 190, 339]. The most frequently used crosslinking agents are glutaraldehyde (GAL) and epichlorohydrin (EPI), both of which have been reported to be highly toxic to humans and animals, causing second-hand contamination within water systems and the environment [192, 267, 340, 341]. Similarly, γ-(2,3-epoxypropoxy) propyltrimethoxysilane (GPTMS) and tri-functional trimethylolpropane-tris-(2-methyl-1-aziridine) propionate (TMPTAP) [342] have been used to synthesize CNM-PEI composites in recent years [270].

Considering the second-hand pollution issue caused by chemical crosslinkers, some research focuses on seeking a way to directly promote the crosslinking between nanocellulose and PEI without the need for additional chemical agents. The intermolecular interactions between the hydroxyl groups on the nanocellulose and the PEI amino groups are rather weak, which makes the formation of stable complexes by electrostatic interactions between these two motifs challenging. Therefore, pre-functionalization of the nanocellulose is preferred in order to either strengthen the intermolecular interactions that facilitate composite formation, or to provide appropriate functional groups that can be leveraged for covalent bonding to the PEI amino groups [189]. The most popular pre-functionalized strategy is TEMPO-mediated oxidization, which can selectively introduce a

carboxyl group on the C-6 carbinol of the glucose residues in nanocellulose [343, 344]. This group can then be used for covalent bond formation with the PEI amines via an amide linkage or facilitate the formation of ionic interactions (*i.e.* ammonium carboxylate formation) under appropriate conditions [189].

At present, heating and adding condensation agents to promote the combination of TCNFs and PEI has been the most studied method [189]. However, these processes require temperature and dialysis, making the overall procedure energy-and time-consuming. Another challenge for the use of CNM-PEI as an adsorbent is that most CNM-PEI composites exist in the form of a powder or aerogel. Their main drawbacks are that powders have poor separability and recyclability, while aerogels need high energy demand to generate absorbents. Hydrogels are an alternative material that seems to overcome the shortcomings of powders and aerogels.

Regarding the raw material utilized to produce the composites, soybean hulls are an appealing alternative as a cellulose source. In the U.S., over 96 million tons of soybeans are produced annually [345]. Approximately 6-10% of the crop is a fibrous byproduct denominated soybean hull, which is traditionally used as cattle feed [345, 346]. Previous work has demonstrated that soybean hulls can be valorized as bionanomaterial [345]. Soybean hulls contain variable amounts of cellulose (29–51%), hemicelluloses (10–25%), lignin (1–4%), pectins (4–8%), proteins (11–15%), soy oils (<2.5%) along with other minor extractives [347]. These components are easily extracted, and their properties are suitable for producing different materials. Nanofibrils of cellulose generated from soybean hulls exhibit high surface area, colloidal stability, and favorable polyanionic characteristics [348].

This work aims to address the design of stable hydrogels from soybean hulls and PEI. The hypothesis is that CNM-PEI composites can be synthesized by combing cationic chelation and physical adsorption. The novelty of this work relies on utilizing an agricultural by-product – soybean hulls – as a readily available raw material to produce hydrogels. To this end, TEMPO-oxidized CNFs from soybean hulls were chelated using zinc chloride at room temperature to form TCNF hydrogels, then immersed into a PEI solution to further functionalization by physical adsorption. In order to increase the amount of the absorbed PEI in the TCNF hydrogel system, the effect of concentration and pH of PEI solutions was also investigated. In addition, the adsorption efficiency of the hydrogels for the capture of methyl blue dyes and Cu (II) ions from water was tested to explore the potential application of this new material for water remediation. Schematic illustration of the preparation TCNF/PEI hydrogels form soybean hull and PEI in **Fig. 3-1.**

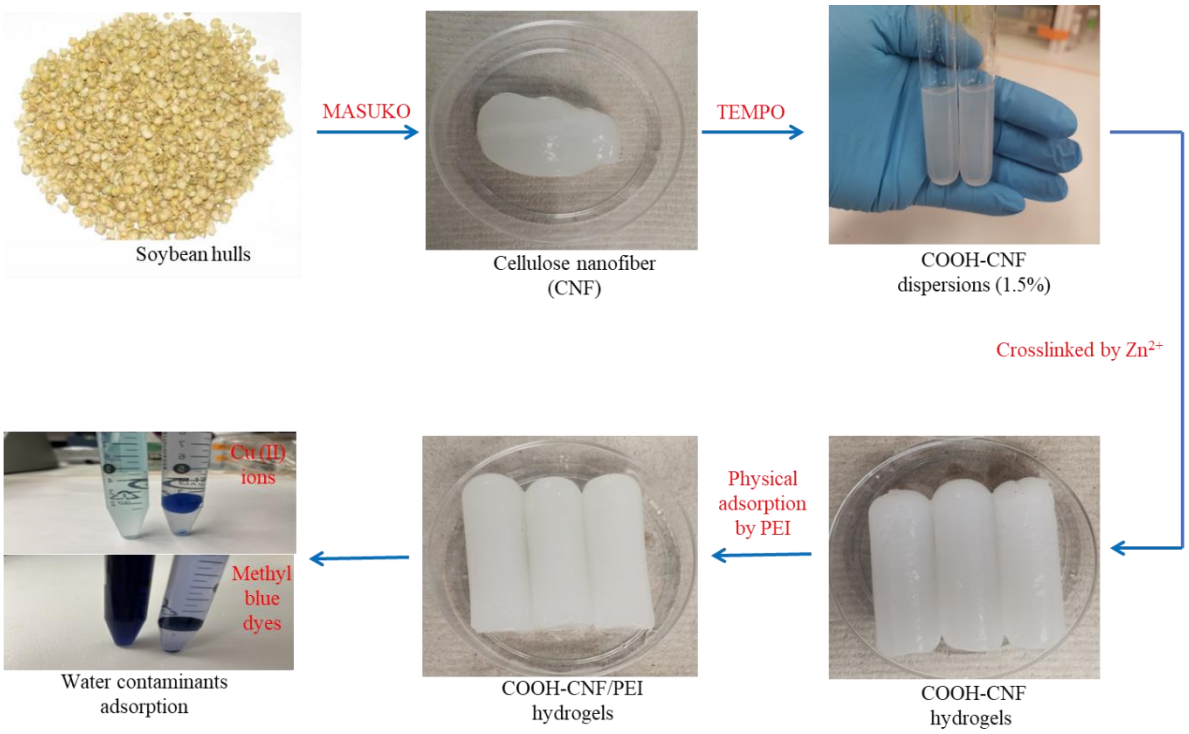

Figure 3-1. Schematic illustration of the preparation TCNF/PEI hydrogels form soybean hull and PEI.

3.3 Materials and methods

3.3.1 Materials

CNF from bleached soybean hull fibers was produced at the Forest Products Development Center (Auburn, AL) by mechanical processing on a Masuko supermasscolloider (MKZA10-15J, Masuko Sangyo Co., Fiber, Japan). For the preparation of the CNFs, bleached hulls were diluted to a 2% wt. suspension. The washing was done first by lowering the suspension pH to 3 with a 1 M HCl solution. After 30 min, hulls were rinsed with DI water until pH increased to 4.5–5. Then, $NaHCO_3$ was added to obtain a 0.001 M concentration and pH was adjusted to 9 with 1 M NaOH for 30 min. Finally, washings were performed until no changes in conductivity were measurable. The washed hulls were then processed by Masuko super mass colloider (MKZA-10-15 J) with 12 passes, obtaining a final consistency of 2.12% wt. at a pH of 5.8. Polyethylenimine (branched, Mw = 25,000 g/mol) was purchased from Sigma-Aldrich. (2,2,6,6-Tetramethylpiperidin-1-yl) oxyl (TEMPO), methyl blue anionic (MB) dye was purchased from VWR, and the anhydrous copper (II) sulfate (98%) from Alfa Aesar.

3.3.2 TEMPO oxidation of CNF

TEMPO mediated oxidation of CNFs (TCNFs) was adapted from studies previously reported [27]. Briefly, 5 g of CNFs (dry mass basis) were suspended in 500 mL of distilled water containing TEMPO 0.08 g (0.1 mmol/g CNF) and NaBr 0.5 g (1 mmol/g CNF), and the pH was adjusted to 10 by addition of 0.5 M aq. NaOH. Then 30 mL of 12.5% aq. NaClO solution was added slowly to the CNF slurry (1.65 mL/10 min, total 3 h) and the reaction mixture was maintained at pH 10.5 at room temperature by adding aq. 0.5 M NaOH simultaneously. Furthermore, the oxidized CNFs were precipitated by adding ethanol (1500 mL) and then centrifuged at 3800 rpm. Finally, the

oxidized CNFs were washed thoroughly with distilled water and filtered using a 0.20 µm cellulose acetate filter paper.

3.3.3 TCNFs hydrogel formation and functionalization with PEI

TCNF hydrogels were prepared by the dropwise addition of a 20 % wt. aq. $ZnCl_2$ solution along the walls of the glass tube into a 1.5% wt. aq. TCNF dispersion. The final zinc ion concentration was controlled to be 0.1 mol/L (0.35 mL of 20% $ZnCl_2$ solution). Then, the mixture was allowed to stand for 24 h without stirring to enable the formation of the nanocellulose hydrogels. Afterward, unbound Zn^{2+} ions were removed by rinsing the resulting hydrogels with 150 mL distilled water three times [349].

Next, TCNF hydrogels were immersed in an aq. PEI solution at room temperature for 24 h to functionalize. The effects of pH (5-12) and concentration (2%, 5%, 10%, 20% and 40%) of PEI on the amount of PEI adsorbed in TCNF hydrogel was investigated. Finally, the functionalized hydrogels were first placed into a 150 mL anhydrous ethanol solution for 2 h and then washed with 150 mL distilled water for about 5 times until the pH of the cleaning water remained neutral.

3.3.4 Characterization

3.3.4.1 Fourier transform infrared spectroscopy (FTIR)

Samples were freeze-dried at –50 °C for 48 h and then analyzed using a PerkinElmer Spotlight 400 FT-IR Imaging System (Massachusetts). An attenuated total reflectance (ATR) accessory with diamond/ZnSe crystal was used for collecting 64 scans with 4 cm^{-1} resolution. Data was processed with Spectrum 6 Spectroscopy Software (PerkinElmer).

3.3.4.2 Atomic force microscopy (AFM)

Surface characterization of the CNFs and TCNFs were performed using Tosca 400 equipment from Anton-Paar (Gratz, Austria). Surfaces were prepared by spin-coating (2 × 2 cm^2, with 150 µL

of 0.01% liquid samples at 3000 rpm for 30 s). Height images were obtained by tapping mode with a NanoWorld (Neuchâtel, Switzerland) ARROW-NCR-20 silicon SPM-sensor cantilever with a resonance frequency of 285 kHz and constant force of 42 N/m; scan sizes were 5×5 μm^2. Processing of the images was done with Gwyddion software 2.49 (SourceForge) and roughness calculations were done with ProfilmOnline (KLA Corporation, Milpitas, CA, U.S.).

3.3.4.3 Carboxyl group titration

The carboxyl content of oxidized cellulose samples was determined by conductometric titrations. The method was modified on the basis of previous studies [350]. Briefly, 30 mg (dry basis) of TCNF samples were suspended into 7.5 mL of 0.01 M HCl solution and adjusted to a pH of 2. After 2 h of stirring, the suspensions were titrated with 0.01 M NaOH.

3.3.4.4 Dynamic light scattering (DLS)

The Zeta potential for 0.1 % TCNF and PEI solutions were tested on a pH range from 2 to 12. All measurements were done in a Litesizer from Anton-Paar (Gratz, Austria). For all samples, twelve repetitions were done and averaged.

3.3.4.5 Elemental analysis

Elemental analysis was performed on each sample using an elemental analyzer (Elementar vario MICRO, Ronkonkoma, NY, USA). 2 mg of freeze-dried sample were used for the test, and measurements were performed by triplicate.

3.3.4.6. Scanning electron microscopy (SEM)

Freeze-dried samples were set onto aluminum studs and sputtered with gold for 90 s in an EMS ×550 Sputter Coating Device from Science Services (Munich, Germany). Images with magnifications of ×50, ×100, and ×1000 were recorded in a Zeiss Evo 50VP SEM (Oberkochen, Germany).

3.3.5 Quartz Crystal Microbalance with Dissipation Monitoring (QCM-D)

All the experiments were performed on a Q-Sense analyzer (Biolin Scientific. Västra Frölunda, Sweden). These measurements were performed on gold sensors that were purchased from Biolin Scientific (Västra Frölunda, Sweden). Analyte solutions at a concentration of 0.1% were prepared and flowed onto the sensors at 100 µL/min at 25 °C, according to previous works (Gomez-Maldonado et al., 2021).

3.3.6 Adsorption tests of Methyl blue and Cu (II) ions

The adsorption efficiency of the hydrogels for methyl blue dyes and Cu (II) ions was tested. The hydrogels were cut into a 3.5 mm long cylinder (0.0186 g dry basis) and then placed into 10 mL of 200 mg/L methyl blue buffer solutions with pH 5.7 and left without any shaking; aliquots were taken after different time intervals (3, 6, 12, 24 h) and the methyl blue dye concentrations in the supernatant were calculated by UV spectrophotometer at 596 nm. Hydrogel cylinders of the same size were also put into 10 mL of 320 mg/L Cu (II) solutions for 24 h. The remaining Cu (II) ions in solution after hydrogel treatment were quantified by ICP-MS.

3.4 Results and discussion

3.4.1 Characterization of CNFs and TCNFs from soybean hulls

In order to confirm that the carboxyl group was successfully introduced to the CNFs, a FTIR analysis was carried out. The FTIR spectra of CNFs and TCNFs are shown in **Fig. 3-2 (A)**. The characteristic bands for CNFs and TCNFs are observed at 3334 cm^{-1} and 2904 cm^{-1} which relate to O-H stretching and asymmetric C-H stretching, respectively. The band at 1723 cm^{-1} indicates a carboxyl stretching which is only observed in the TCNF spectra, suggesting the formation of carboxylate after TEMPO mediated oxidation [351, 352]. This was further confirmed by titration measurement where the carboxyl group content in the TCNFs was 1.8-2.0 mmol/g CNF [353]. The

morphology of the fibers was assessed by AFM measurements, and the images of CNFs and TCNFs are shown in **Fig. 3-2 (B)** and **(C)**. After oxidation, the root means square height (RSq) and arithmetic mean height (RSa) of the fiber decreased by 64% and 54.5%, which could be related to the decrease in fiber particle size. As can be observed in **Fig. 3-2 (B)** and **(C)**, the CNF sample presents longer fibers compared with TCNFs where the particles are clearly smaller, indicating a reduction in particle size after TEMPO-mediated oxidation [349].

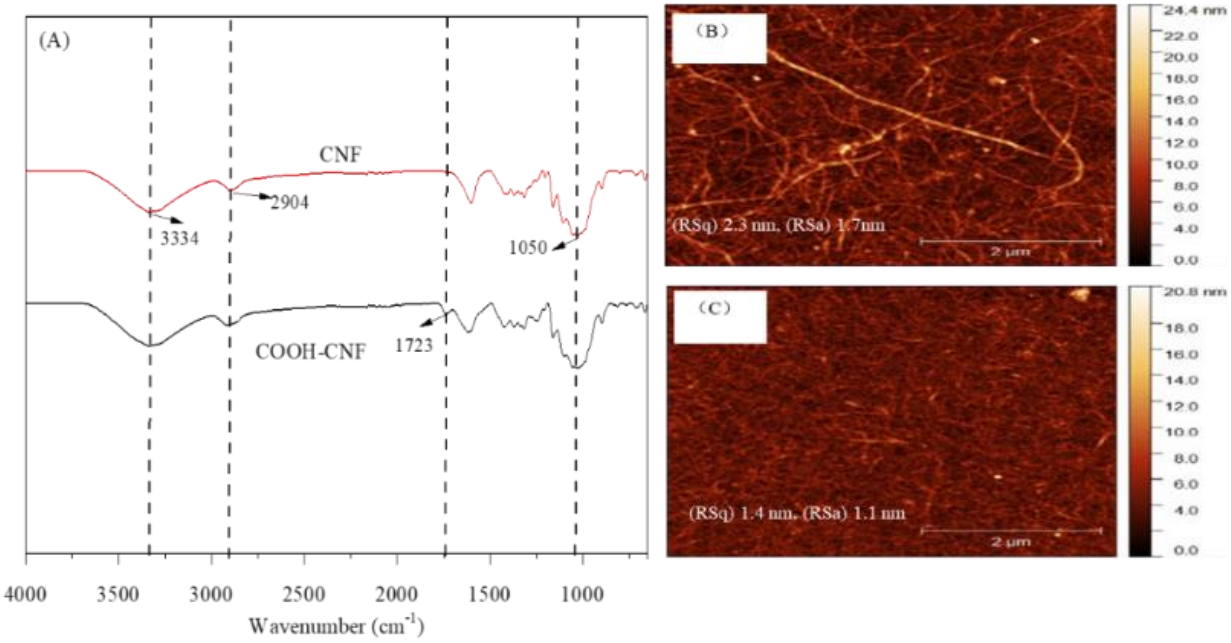

Figure 3-2. (A) FTIR spectra of CNFs and TCNFs, (B) (C) AFM images of CNFs and TCNFs.

3.4.2 Synthesis of hydrogels

To overcome the issues caused by chemical crosslinking, heating, and the use of condensation agents, a hydrogel absorbent was produced by combining cationic chelating and physical crosslinking. To achieve this strategy, TEMPO-oxidized CNF suspensions were chelated by zinc chloride at room temperature to form TCNF hydrogels (**Fig. 3-3 (B)**), then placed into PEI solutions to further functionalize by hydrogen bonding and electrostatic interactions based on rich

hydroxyl groups on the surface of the CNFs (**Fig. 3-3 (C)**). The results showed that the hydrogels become opaque and appear to be more rigid after functionalization by PEI, which is an indicator of successful adsorption of PEI into the TCNF hydrogels.

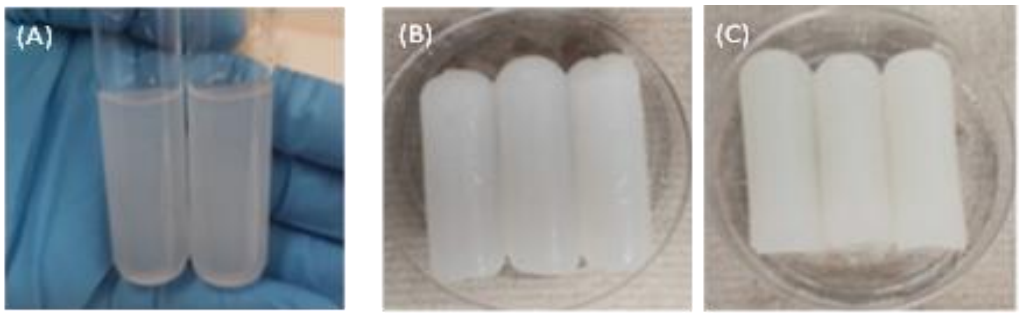

Figure 3-3. Images of TCNF dispersions (A), TCNF hydrogels (B)and TCNF/PEI hydrogels (C).

3.4.3 Optimization on PEI adsorption conditions

The concentration and pH of the PEI solutions utilized to functionalize the hydrogels can impact their composition and performance. The first study was performed by varying the pH of PEI solutions using a reference concentration of 20% [342]. Elemental analysis was utilized to confirm the presence of PEI in the TCNF hydrogel system (**Fig.3-4. (A) and (D)**). The nitrogen content increased from 6.6% to 9.0% as the pH of the solution was increased from 5.1 to 11.7 (**Fig. 3-4. (A)**), indicating that more PEI is absorbed in the hydrogel when the pH increased. It is important to emphasize that PEI can be adsorbed in the hydrogel system by means of hydrogen bonding, electrostatic interaction, and pore trapping [240]. At pH values higher than 10, electrostatic repulsions occur as evidenced by zeta potential values (**Fig. 3-4 (B) and (C)**), causing PEI to desorb from the system. However, results show that the nitrogen content still increases when the pH exceeds 10 compared to what was found elsewhere [354]. A possible explanation for this is that the amount of PEI absorbed due to hydrogen bonding and pore trapping overcomes the

desorption caused by the electrostatic repulsion at conditions of pH above 10 (**Fig. 3-4 (B) and (C)**).

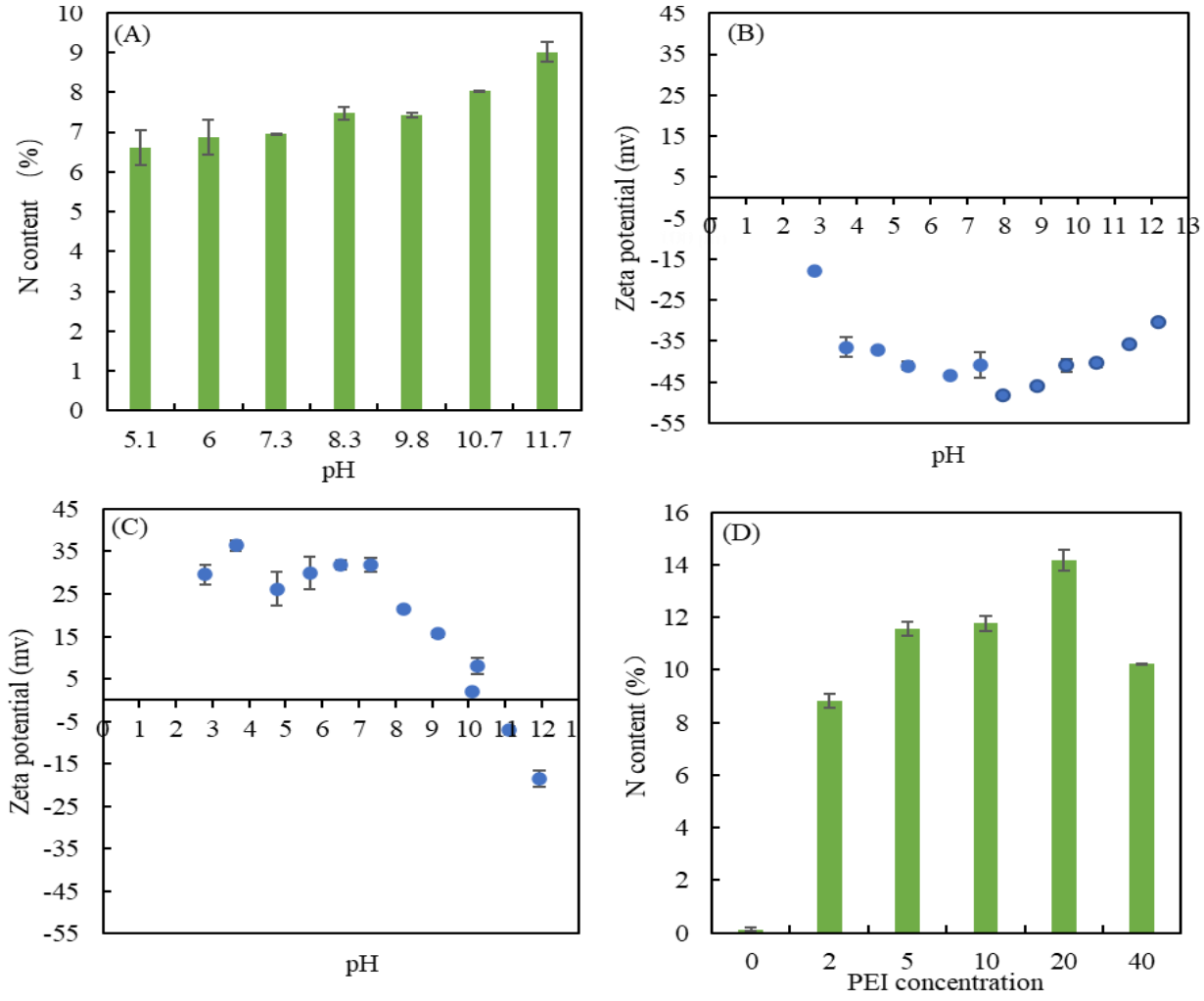

Figure 3-4. (A) The effect of pH on the N content in TCNF/PEI hydrogels; the DLS analysis for the zeta potential of (B) TCNFs and (C) PEI; and (D) the effect of concentration of PEI on the the N content in the TCNF/PEI hydrogels.

Further testing was done maintaining the adsorption pH at 11.65, where the adsorption of PEI was highest, while varying the PEI concentrations from 2% to 40%. Here, the nitrogen content increased with increasing concentration of PEI up to 20%, and then began to decline at higher PEI concentrations (**Fig. 3-5 (D)**) as demonstrated by elemental analysis. This may be caused by the volume reduction of TCNF/PEI hydrogel, as shown in **Fig. 3-5 (F)**, leading to a decrease in surface

area and pore size, which may be related to PEI immobilization. Thus, the best conditions for hydrogel synthesis were defined as pH 11.65 and 20% PEI concentration, resulting in 14.2% nitrogen content. A high nitrogen content in the hydrogel composite is essential for the adsorption ability of anionic dyes and copper ions, as will be discussed in the following section.

Figure 3-5. Image demonstrating the physical changes of TCNFs/PEI hydrogels with different PEI solutions.

3.4.4 Characterization of hydrogels

FTIR was used to probe the nature of the interactions of the PEI molecules attached to the TCNF hydrogel. The FTIR spectra of unmodified TCNF hydrogels, PEI, and TCNF/PEI hydrogels are presented in **Fig. 3-6 (A)**. The band at 1723 cm^{-1} corresponding to carboxyl groups was observed in the free TCNF spectra but cannot be found in the TCNF hydrogel or the TCNF/PEI hydrogels. This can be explained as complete chelation of the carboxyl group by zinc chloride, which should shift the asymmetric carboxyl stretching frequency to lower wavenumbers, thus obscuring it in the broader bands around 1600 cm^{-1} originating from cellulose and PEI [355]. For PEI, the absorption at 2936 and 2817 cm^{-1}, 1670 cm^{-1}, and 1050 cm^{-1} were the characteristic bands of -CH_2- stretching vibrations [356], amino groups, and C-C skeleton vibration, respectively [192]. Meanwhile, the absorbance band near 1599 cm^{-1} and 1459 cm^{-1} are the N–H bending vibration of primary amines in PEI [356, 357]. The absorption at 2936, 2817, and 1599 cm^{-1} were also found in the TCNF/PEI hydrogels, which proves the successful introduction of PEI to TCNF/PEI hydrogels. Moreover, no new bands were observed in the TCNF/PEI hydrogels indicating that PEI

functionalized hydrogel was physically blended and no chemical bonding occurred. Moreover, there is no notable change in the characteristic bands of PEI when the pH increases (**Fig. 3-6 (B)**). However, when varying the PEI concentration from 2 to 40%, there is a slight difference in the N-H band at 1599 cm^{-1} (**Fig. 3-6 (C)**). The value was the highest at 20% PEI concentration. This could be related to the higher PEI adsorption in the hydrogel at 20% PEI concentration, which agrees with the elemental analysis results.

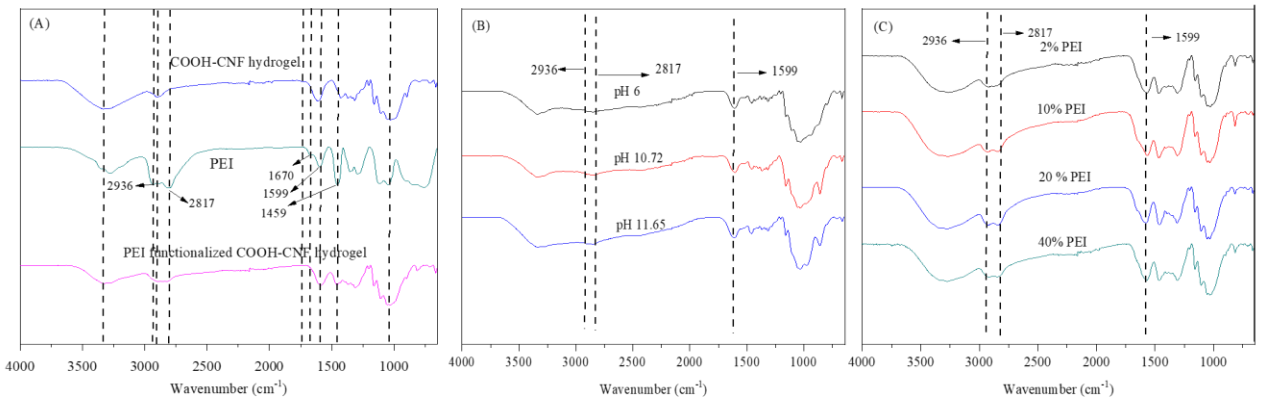

Figure 3-6. FTIR analysis for (A) TCNF hydrogels, PEI and TCNF-PEI hydrogels, (B) TEMPO CNF-PEI hydrogel in PEI solutions with different pH, and (C) different concentrations.

Morphological characteristics of the hydrogels were studied by SEM. As shown in **Fig. 3-7 (A), (B), and (C)**, TCNF hydrogels possessed a denser structure, compared with TCNF/PEI hydrogels in **Fig.3-7 (D), (E), and (F)** which showed an open and microporous structure. A similar phenomenon was reported by Li et al. (2018), where CNF-PEI composite aerogels possess an open and macroporous honeycomb structure [352]. While increasing surface area, the creation of pores within the sorbent network allows liquid to diffuse and fill the pores, which provides favorable interactions for the use of these materials for water contaminant removal [240]. Key features of the pore structure including pore type, size, and volume determine the access and entrapment of the pollutants within the pores of the adsorbents [240, 358].

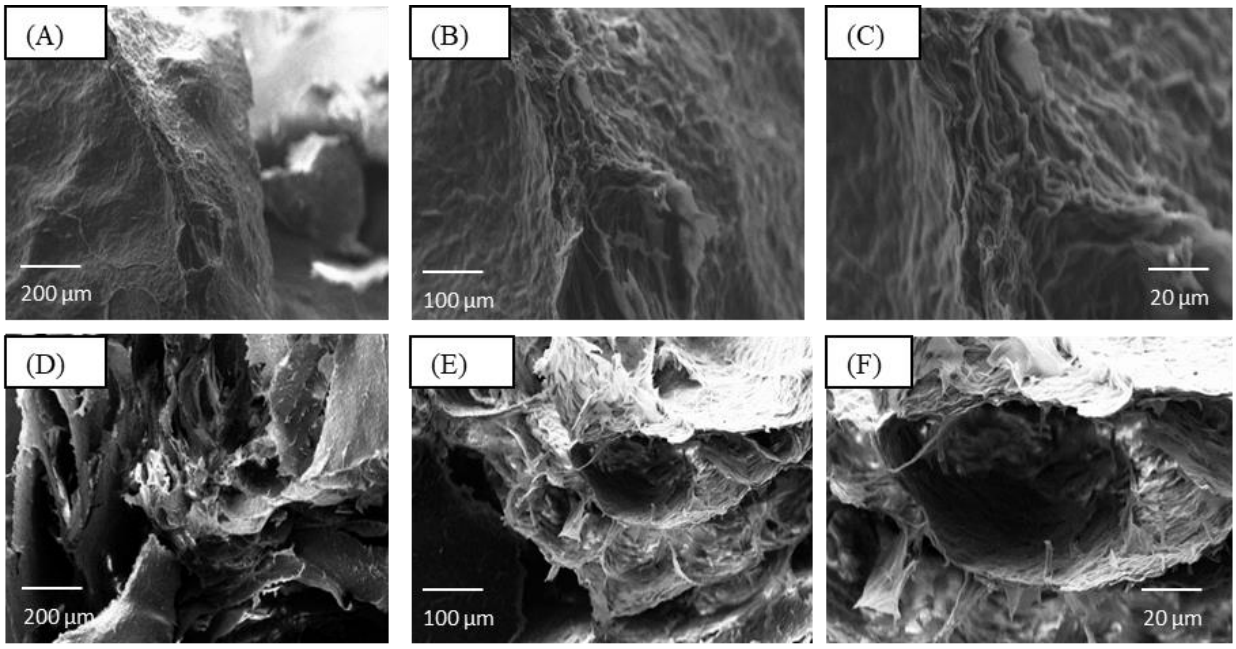

Figure 3-7. SEM image of TCNF hydrogels ((A), (B) and (C)) and TCNF/20%PEI hydrogels ((D), (E) and (F)) at different magnification times.

3.4.5 QCM-D analysis

To better understand the interaction between TCNFs and PEI, the adsorption phenomena was simulated on the surface of model films and followed by QCM-D at optimum conditions of pH and PEI concentration (**Fig. 3-8** and **Table 1**). The chemicals used to synthesize the hydrogel flowed through the QCM-D sessor in the same order that was used to prepare the hydrogels. The frequency and dissipation change are shown in **Fig. 3-8** and **Table 1**. A frequency shift of –38.44 Hz was noted for the formation of the TCNF film on the surface with a 3.56 ppm shift in dissipation, confirming the deposition of a viscous TCNF film on the surface of the sensor, which was stable after pure water was flowed on top. When an aqueous solution of $ZnCl_2$ was added, an increase in frequency of 1.22 Hz was observed as well as a dissipation drop of –1.02 ppm. The negative shift in dissipation confirms chelation at the surface of the film [359], and the shift in frequency can be linked to water being released from the film after crosslinking. The change of pH from neutral to a more alkaline value (pH 11.65) induced swelling of the CNF film as more sodium ions were

present in the media allowing for the weakening of the H-bonding [360] as indicated by frequency decreasing (–11.63) and dissipation increasing (2.82). Finally, PEI was irreversibly adsorbed onto the surface of the crosslinked TCNF model film as demonstrated by a negative frequency shift of –27.16 Hz, that remaind attached after rinsing.

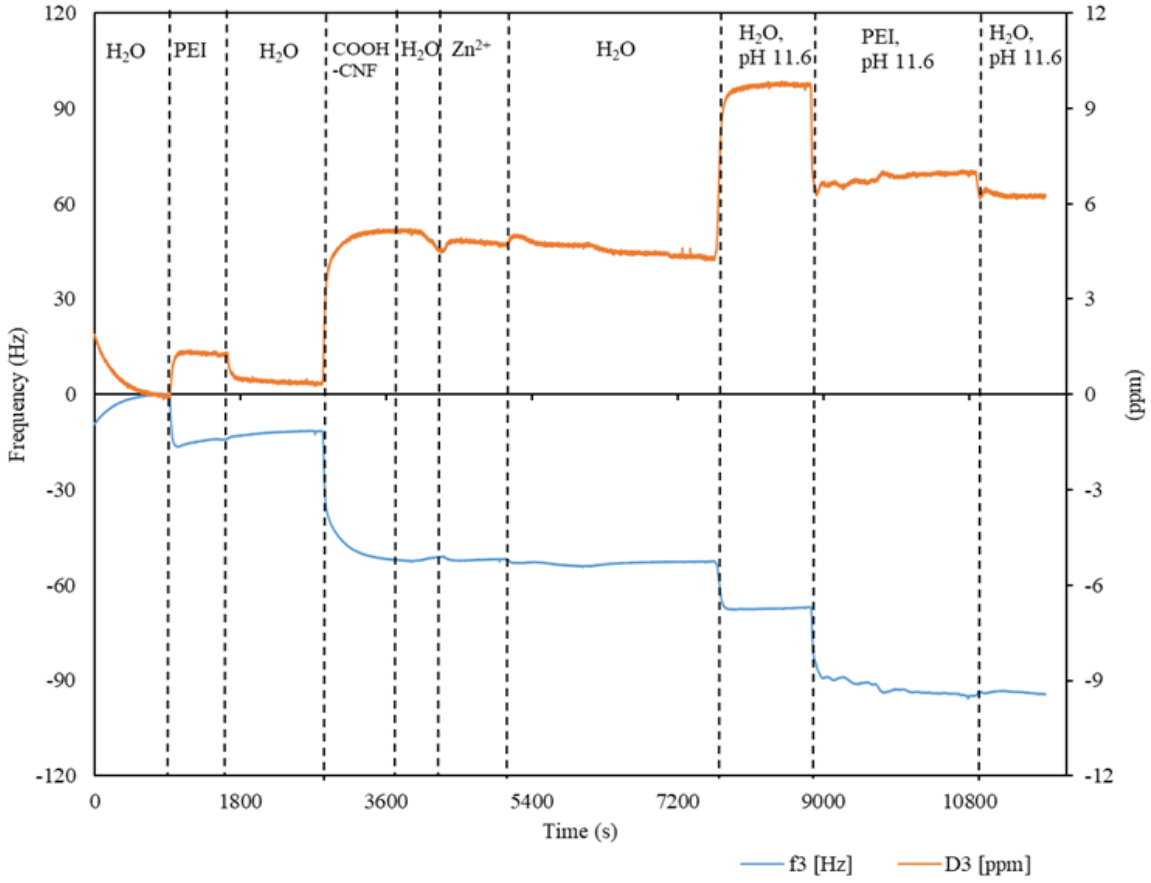

Figure 3-8. QCM-D sensogram of the analysis of the interaction between the components generating the TCNF/PEI composite hydrogels in thin model films.

Table 3- 1. Data extracted from the QCM-D sensograms.

Step	Δ F (Hz)	Δ D (ppm)
PEI	–11.36	0.44
TCNFs	–38.44	3.56

Zinc	1.22	–1.02
pH change	–11.63	2.82
PEI with pH 11.65	–27.16	–3.47

3.4.6 Hydrogel adsorption tests

For the cellulose-PEI composites, most research focuses on adsorption of anionic dyes and metal ions, usually methyl blue and Cu (II) [189]. Based on this, adsorption testing was done to quantify the removal ability of the hydrogels prepared in this study.

First, the effect of N content on the adsorption efficiency of methyl blue dye was tested to confirm the hypothesis that more PEI would result in a higher adsorption efficiency. As expected, the adsorption efficiency increased with the increase of the N content (**Fig. 3-9 (B)**).

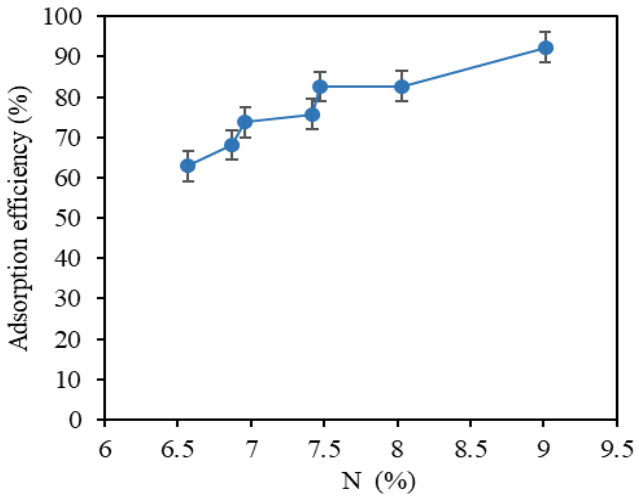

Figure 3-9. The effect of N content (A) and different cationic ions (B) used for formation hydrogel on the adsorption efficiency of TCNF/PEI hydrogel for the methyl blue dyes at initial 200 mg/L and pH 5.7 for 48 h.

Based on the previous results, testing was done at 24 h adsorption under the optimal conditions (pH 5.7) for the methyl blue and Cu (II) ions adsorption. Results showed that the adsorption efficiency reached 82.6% and 69.8 %, respectively (**Fig. 3-10**).

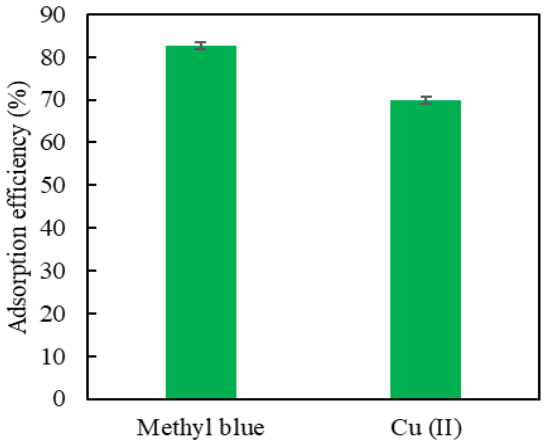

Figure 3- 10. The adsorption efficiency of TCNF/PEI hydrogels for methyl blue and Cu (II) at pH of 5.7 after 24 h.

3.5 Conclusion

In this work, a TCNF/PEI hydrogel originating from valorized soybean hulls was successfully synthesized by a combination of cationic chelation and physical adsorption. In order to increase the quantity of PEI on the surface, the effect of concentration and pH of the PEI solution on the N content of the composite was explored by elemental analysis. The results showed that the best conditions to introduce the highest nitrogen content (14.2%) in the TCNF/PEI hydrogel were the combination of a 20% solution of PEI with a pH of 11.65. The adsorption efficiency of TCNF/PEI hydrogels for the removal of methyl blue dye and Cu (II) from water were explored. The results showed that the adsorption efficiency for the methyl blue dyes and Cu (II) were 82.6 % and 69.8%, respectively, after 24 h at pH 5.7. The results suggest that these hydrogel composites originating from soybean hulls have potential uses in water remediation applications.

Chapter 4. Cellulose-polyethylenimine hydrogels for removal of anionic dyes

4.1 Abstract

Cellulose-polyethylenimine (PEI) composite has been widely used in water remediation. However, most of them are synthesized by chemical cross-linkers, which usually cause second pullulation and extra cost. In order to address these issues, a stable TEMPO-oxidized cellulose nanofibril (TCNF) and PEI composite hydrogel (TCNF/PEI) was synthesized by self-assembly mechanisms of cationic chelation and physical adsorption. These hydrogels were used to remove methyl blue ionic dyes from aqueous solutions. Interactions of the hydrogels and methyl blue dyes were found to be highly pH-dependent, resulting in dye removal by both adsorption and precipitation phenomena. Over the pH of 3.7–5.7, most of the dyes were removed by adsorption with a maximum adsorption obtained at pH value 4.7. Adsorption kinetics and isothermal data were fitted to a pseudo-second-order kinetic model and Langmuir model indicating that chemical adsorption on a homogeneous surface is the predominant mechanism of dye removal. The maximum adsorption predicted by the Langmuir adsorption isotherm model was 3,125 mg/g, which is higher than most cellulose-based materials. Up to four regeneration cycles were done with adsorption efficiencies is still higher than 82%. Furthermore, these hydrogels promoted rapid precipitation of methyl blue at acidic pH values 2.7, where a total of 98.4 mg/g (91.5%) of methyl blue was quickly removed from an initial 200 mg/L solution after 6 h. For the second cycling, the flocculation efficiency decreased to 24%. Removed methyl blue molecules were unaltered and did not present any chemical modification based on the XRD and FTIR analysis. Based on this finding, the TCNF/PEI hydrogels show great potential for the anionic dyes' removal and recovery from industrial wastewater.

4.2 Introduction

Nanocellulose displays high surface area, and high strength, as well as tunable surface chemistry, which makes it interesting for its use in water remediation [361-363]. However, adsorption capacity of pure nanocellulose materials is relatively low and the scaffold generated can easily disintegrated in water, which has limited their commercial incursion [17-19]. Despite this, numerous methods have been developed to functionalize nanocellulose to improve its functionally for wastewater treatment such as grafting [364], carboxylation [365], crosslinking [366], and composite formation[367, 368]. From the different possible chemical moieties that exist, amine groups are one of the most effective groups to remove contaminants from wastewater as they not only can remove cationic metal ions by chelating, but also can adsorb anions by electrostatic interaction [366, 367]. Moreover, amino groups are pH sensitive and can be protonated and deprotonated, allowing the pollutants to be absorbed and desorbed to permit the recycling of the adsorbents [369].

Recently, extensive research has been devoted to the use of polyethylenimine (PEI) to functionalize CNFs for water remediation, attributing to its great number of primary, secondary, and tertiary amines [19, 370, 371]. This combination has resulted in super adsorption performance for different water pollutants and these composites are easy to regenerate [243]. For example, Liuting et al. fabricated CNF- PEI based aerogels to remove Cu (II), showing a highest maximum adsorption capacity (485.44 mg/g), as well as being able to adsorb other ions. Furthermore, it was easy to regenerate maintaing adsorption capability without signicant degradation after 4 cycles [243]. Besides, cellulose nanomaterials (CNM)-PEI based composites also show super adsorption capability for anionic [28] and cationic dyes [193], emerging contaminants [32, 194] and oil spills [244].

Nevertheless, most studies focused on synthesizing PEI-nanocellulose composites by chemical crosslinking, either using crosslinking agents or high temperature heating, promoting covalent bond formation between the PEI amines and residual hydroxyls (*i.e.* from unmodified cellulose) or carboxyl groups on oxidized cellulose [27, 32, 189]. Despite the use of a sustainable polymer such as cellulose, most used chemical crosslinking agents are toxic, i.e., glutaraldehyde (GAL) and epichlorohydrin (EPI), and posing a risk of secondary contamination of water sources [28-31, 189] . Although avoiding chemical crosslinkers, heat mediated crosslinking strategies require a pretreatment by freeze-drying, followed by heating at high temperature (over 100 °C), making it a highly energy intensive process [32-35]. Moreover, most CNM-PEI composite adsorbents are available in powders form, which present poor separability and recyclability, thus making wastewater remediation a costly endeavor [243]. 3-D hydrogels and aerogels have become more popular in latest years because they can overcome the problems from powders. Compared with hydrogels, the formation of aerogels usually requires freeze-drying, as part of the manufacturing process, again consuming a high amount of energy, which is not economical.

Here, we pursued the generation of a stable 3-D hydrogel by cationic chelation and physical adsorption to avoid issues caused by using chemical cross-linkers. It was found that the resulting hydrogels demonstrated a great potential in removal of methyl blue dye from water. This work describes an extensive study about the effect of pH on the mechanisms of removal of methyl blue dye using PEI-CNF hydrogels. Interestingly, the results show that the formed hydrogels can remove methyl blue dyes by precipitation in addition to the traditionally reported adsorption as a function. This findings can open a way to design nanocellulose based 3-D hydrogel adsorbents-flocculants for water treatment. The Schematic illustration as shown in **Fig. 4-1.**

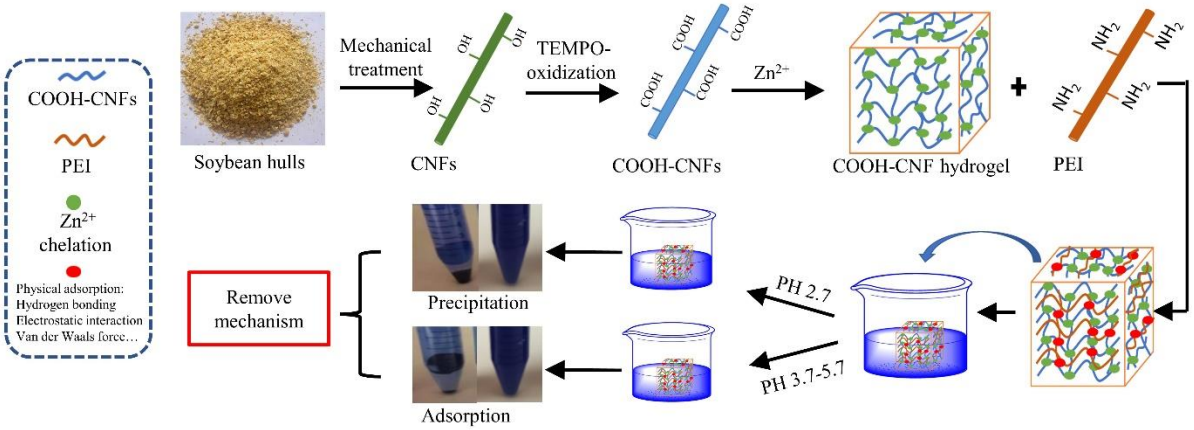

Figure 4-1. Schematic illustration of COOH-CN synthesis and its mechanism for removal of methyl blue.

4.3 Materials and methods

4.3.1 Materials

Briefly, CNFs were isolated from soybean hulls by mechanical processing on a Masuko supermasscolloider. Polyethylenimine (branched, Mw=25,000 g/mol) was purchased from Sigma-Aldrich. (2,2,6,6-Tetramethylpiperidin-1-yl) oxyl (TEMPO) and methyl blue anionic (MB) dye were bought from VWR.

4.3.2 TEMPO oxidation of CNF

TEMPO-mediated oxidation of CNFs (TCNFs) was conducted based on our previous study [366]. Briefly, 5 g of CNFs (dry mass basis) were diluted to 500 mL with distilled water containing 0.08 g of TEMPO (0.1 mmol/g CNF) and 0.5 g of NaBr (1 mmol/g CNF). The pH was adjusted to 10 using 0.5 M aq. NaOH. Then, 30 mL of a 12.5% NaOCl solution was added slowly to the CNF slurry (1.65 mL/10 min, total 3 h) while maintaining the pH at 10.5 at room temperature by adding 0.5 M aq. NaOH simultaneously. Next, the oxidized CNFs were precipitated by adding ethanol (1500 mL) and centrifuged at 3800 rpm. Finally, the oxidized CNF slurry was washed thoroughly with distilled water and filtered with 0.20 µm cellulose acetate filter paper.

4.3.3 TCNF Hydrogel formation and functionalization with PEI

TCNF hydrogels were prepared by the dropwise addition of a $ZnCl_2$ water solution (20 %, w/w) along the walls of a glass tube into the TCNF dispersion (1.5 % w/w) according to our previous research [366]. The final concentration of zinc ions was controlled to 0.1 mol/L (0.35 mL of 20% $ZnCl_2$ solution) in the mixture. The mixture was then allowed to stand for 24 h without stirring to enable formation of the nanocellulose hydrogels. Then, the unbound Zn^{2+} was removed by rinsing the resulting hydrogels with distilled water.[349] For PEI functionalization, the TCNF hydrogels were placed inside a 20% aq. PEI solution with pH 11.56 at room temperature for 24 h.

4.3.4 Methyl blue removal

4.3.4.1 The effect of pH on TCNF-PEI interaction with methyl blue dyes

The effect of different pH (2.7, 3.7, 4.7, 5.7, 6.7, 7.7) on the removal capability of PEI functionalized hydrogels for methyl blue dye was tested over time. Hydrogels were cut into 3.5 mm long cylinders (0.0186 g dry basis) and placed into 10 mL of a solution containing 200 mg/L methyl blue buffer solutions. To better control the pH of these experiments, phosphate buffer (0.05 M) was used instead of water, as the PEI functionalized hydrogel would change the pH of methyl blue dye water solution (from 5 to 10, data shown in the **Fig.S1**; The buffer solution PH changes after adsorption as shown in **Fig. S2**. All pH values mentioned in the text are initial methyl blue in buffer solution). Methyl blue dye concentrations in the supernatant were quantified by UV spectroscopy at 596 nm at different times.

4.3.4.2 Adsorption

4.3.4.2.1 Adsorption capability

The adsorption capacity was calculated according to the following equations:

$$q_{t=}\frac{C_0-C_t}{\mathrm{m}}V \quad (1)$$

$$q_{e=}\frac{C_0-C_e}{\mathrm{m}}V \quad (2)$$

where C_0 (mg/L) and C_t (mg/L) are the initial concentration and concentrations at time t, respectively; q_t (mg/g) is the adsorption capacity at time t; V (L) represents the solution volume of methyl blue, and m (g) represents the dry mass of the hydrogel adsorbent; C_e (mg/L) are equilibrium concentrations; q_e (mg/g) is the adsorption capacity at equilibrium.

4.3.4.2.2 Adsorption kinetics

A 0.0186 g sample of hydrogel was added to 10 mL of a 200 mg/L methyl blue solution at pH 5.7 and 25 ℃, until the adsorption reached equilibrium. Aliquots were taken at set time periods to obtain the dye concentration remining in solution. The adsorption data was then fitted to the pseudo-first and pseudo-second order kinetic model as well to the and intra-particle diffusion model, using the equations presented below:

$$Ln(q_{e-}q_t) = Lnq_e + k_1\mathrm{t} \quad (3)$$

$$\frac{t}{q_t} = \frac{t}{k_2 q_e^2} + \frac{t}{q_e} \quad (4)$$

$$q_t = K_{id}t^{0.5} + \mathrm{c} \quad (5)$$

where k_1 and k_2 are the rate constants for the pseudo-first order adsorption and pseudo-second order adsorption kinetic models, respectively. K_{id} is the rate constant (g mg^{-1} min^{-1}) of intra-particle diffusion kinetics, and c is the intercept.

4.3.4.2.3 Adsorption isotherms

A 0.0186 g sample of TCNF/PEI hydrogels was immersed in 10 mL methyl blue dye solution with a concentration between 20 to 70000 mg/L to study the adsorption isotherms. The adsorption experiments were carried out at 25 ℃ at an initial pH of 5.7 after 120 h. The adsorption values were fitted into linear (equation 6) and non-linear (equation 7) Langmuir isotherm models.

Likewise, the data was fitted into linear (equation 8) and non-linear (equation 9) Freundlich isotherm models to describe its behavior [28, 372, 373]. The equations used are described below:

$$\frac{C_e}{q_e} = \frac{C_e}{q_m} + \frac{1}{K_L q_m} \quad (6)$$

$$q_e = \frac{q_m K_L C_e}{1 + K_L C_e} \quad (7)$$

$$R_L = \frac{1}{1 + K_L C_0} \quad (8)$$

where q_m (mg g^{-1}) is the maximum adsorption capacity estimated by the Langmuir model, and K_L (L mg^{-1}) is Langmuir constant which is related to the adsorption intensity [28, 373]. RL is the separation factor, which values indicate the adsorption to be unfavorable when $R_L > 1$, linear when $R_L = 1$, favorable when $0 < R_L < 1$, and irreversible when $R_L = 0$. $C_{0_\circ}$ refers to the initial concentration of the adsorbate in (mg/L)

$$Lnq_e = LnK_F + \frac{LnC_e}{\mathrm{n}} \quad (9)$$

$$q_e = K_F c_e^{1/n} \quad (10)$$

K_F are constants of the Freundlich equations; 1/n in the Freundlich model represents an empirical parameter, which is related to the energetic heterogeneity of the adsorbent surface and determines either the favorable or unfavorable curve. When 1/n is greater than zero ($0 < 1/n < 1$) the adsorption is deemed favorable, when 1/n is greater than 1, the adsorption process is unfavorable, and it is irreversible when 1/n = 1.

4.3.4.3 Precipitation

The effect of concentration on precipitation was investigated by immersing 0.0186 g of TCNF/PEI hydrogels into different concentrations (50, 100, 200 and 400 mg/L) of methyl blue buffer solution. Then methyl blue dye concentrations in the supernatant were quantified after 6 h and 24 h by UV spectroscopy.

4.3.4.4 Regeneration studies of TCNF-PEI hydrogels

0.0186 g sample of TCNF/PEI hydrogels were put in 200 mg/L methyl blue solution to finish adsorption at pH 5.7 after 120 h and precipitation at pH 2.7 after 6 h, respectively. Then hydrogels were taken out and immersed in 1 M sodium hydroxyl for 24 h to stimulate desorption of the methyl blue or other ions, then washed by DI water until neutral PH. This procedure was repeated 4 times and the adsorption and precipitation capability for each cycle was calculated.

4.4 Results and discussion

4.4.1 Chemical and morphological properties of the hydrogels

The TCNF/PEI hydrogel synthesis and characterization has been discussed in detail in our previous publication [366]. In brief, the PEI was successfully absorbed on the TCNF hydrogels based on the FTIR and elemental analysis resulting in hydrogels with a N content up to 14.8%. Most importantly, the structure of TCNF/PEI hydrogels became a porous honeycomb structure after functionalization with PEI, which is conducive to the adsorption of the water pollutants, especially in the case of macromolecular organic dye pollutants.

4.4.2 Stability of methyl blue dye solution at different pH

It is well established that pH is a key factor affecting the adsorption performance of adsorbents [374]. However, several articles have mentioned that methyl blue solutions are not stable at different pH conditions without providing a detailed explanation about why or under which conditions [375, 376]. Thus, herein the stability of methyl blue and the linear relationship between absorbance and concentration were explored while varying the pH of the solution.

As shown in the **Fig.4-2 (A)**, the absorbance of methyl blue buffer solution decreased from 1.557 to 0.005 as the pH was increased from 2.7 to 8.7 at the same initial concentration (20 mg/L); however, the absorbance did not change over time at each pH value (**Fig.4-2 (B)**). The linear

relationship between the concentration and absorbance of methyl blue buffer solution under different pH conditions (**Fig.4-2 (C)**) was also explored. A high correlation ($R^2 > 0.99$) was found at each pH value. Here, we observed the solution color become lighter at higher pH conditions, but it becomes stable over time at each pH value. Thus, a linear relationship between the concentration and methyl blue buffer solution absorbance under each pH condition can be established, and it can be used to calculate the methyl blue concentration upon adsorption.

It worth noting that that when the pH value was increased to 8.7, the absorbance value of the 100 mg/L MB solution was less than 0.05, which falls below the detection limit for UV-Vis. Xie et al. (2021) also showed that methyl blue was stable in aqueous solution with a pH value of 5.0–8.0 [376]. However, Li et al. (2021) and Shu et al. (2015) carried out their adsorption for methyl blue water solution at pH 2-10 and showed contradictory results to the Xie study [375, 377]. We suspected that the different results might be caused by the ionic content of the media. To confirm this, the color changes of methyl blue aqueous solutions at different pH values were also examined, and we confirmed that aqueous solutions of methyl blue were almost colorless at pH 10, as shown in **Fig.4-2 (D)**. Therefore, in this work, we limited our pH range to 2.7-7.

.

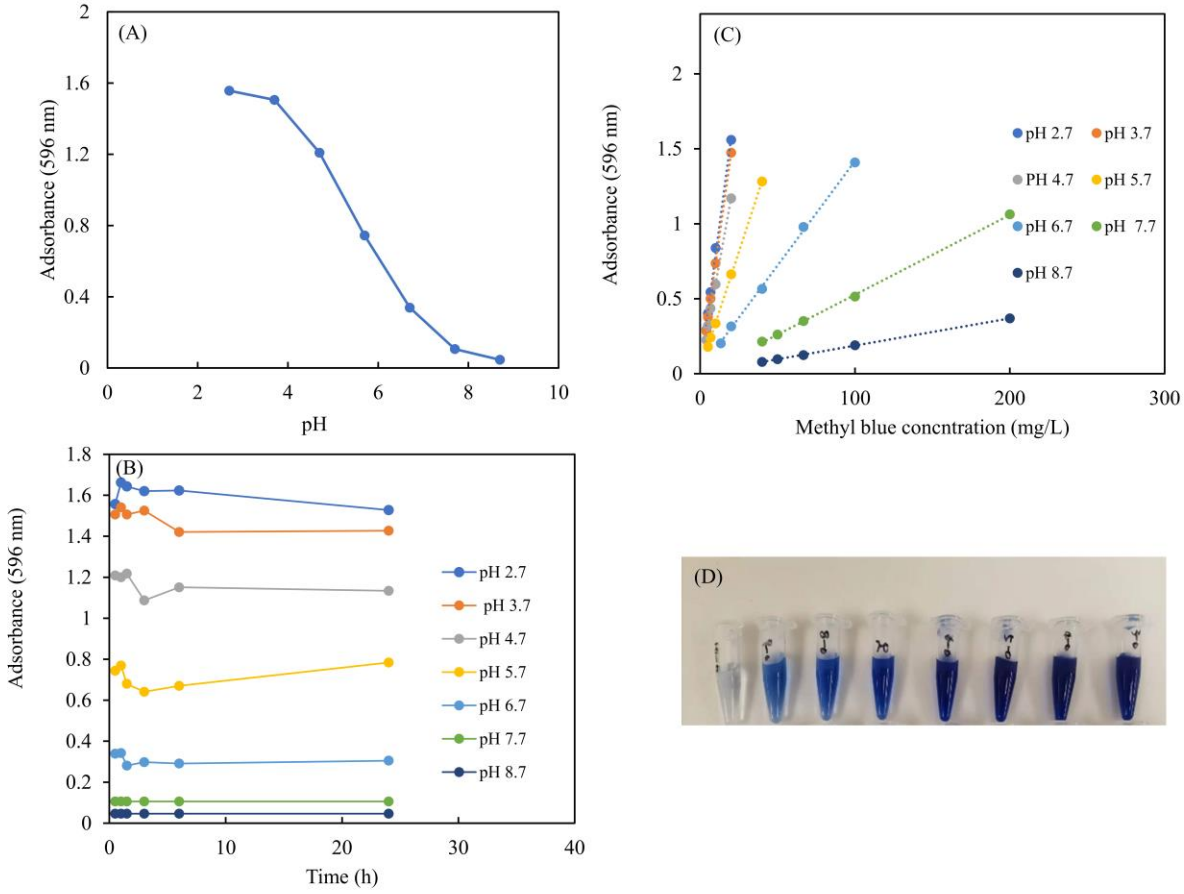

Figure 4-2. Dependence of absorbance of methyl blue solutions at **(A)** different pH values, and (B) over time. linear relationship between methyl blue concentration and absorbance at different pH values (C); and Color change of methyl blue aqueous solution (200 mg/L) at different pH (from left to right is 10-3) (D).

4.4.3 Adsorption and precipitation of methyl blue dyes on a function of pH

The effect of pH of methyl blue buffer solutions on the removal performance of TCNF and TCNF/PEI hydrogels was investigated. It was found that the maximum removal efficiency of methyl blue by TCNF hydrogels was less than 14.4% over the tested pH range of 2.7 to 7.7 after 48 h using 200 mg/L as initial concentration (**Fig.4-3 (A)**). However, the removal efficiency increased to more than 82.6% after the TCNF hydrogels were functionalized with PEI (**Fig. 4-3 (B)**). Interestingly, the TCNF/PEI hydrogels were able to remove methyl blue dye by adsorption

and precipitation, depending on pH. When the pH was 2.7, 91.2% of methyl blue dye was quickly removed mainly by precipitation after 6 h. The removal efficiency slowly increased to 94.9 % over 48 h. Meanwhile, at pH values between 3.7 and 5.7, most of the dye was removed by adsorption, with a maximum adsorption efficiency obtained of 88.34% at a pH of 4.7 after 48 h. When the pH was between 6.7 to 7.7, the methyl blue was removed by both mechanisms, and we are unable to distinguish which was the dominant mechanism of removal. The different modes of dye removal (i.e. precipitation vs. adsorption) are easily distinguishable based on the formation of a blue precipitate at the bottom of the tube after contact with the TCNF/PEI hydrogels (**Fig. 4-3 (E)**) or the depth of color of the hydrogels surface after adsorption (**Fig. 4-3 (F)**). As pH value of 2.7, a stronger blue precipitation was observed, while the hydrogel surface resulted in a lighter color. Conversely, little blue precipitation was produced at pH 3.7-5.7, with a more visible coloration on the hydrogel surface. Based on these results, pH 5.7 was selected for further studies on the adsorption behavior of the TCNF/PEI hydrogels, which aligns with the pKa (pKa of methyl blue is 5) of methyl blue solutions.

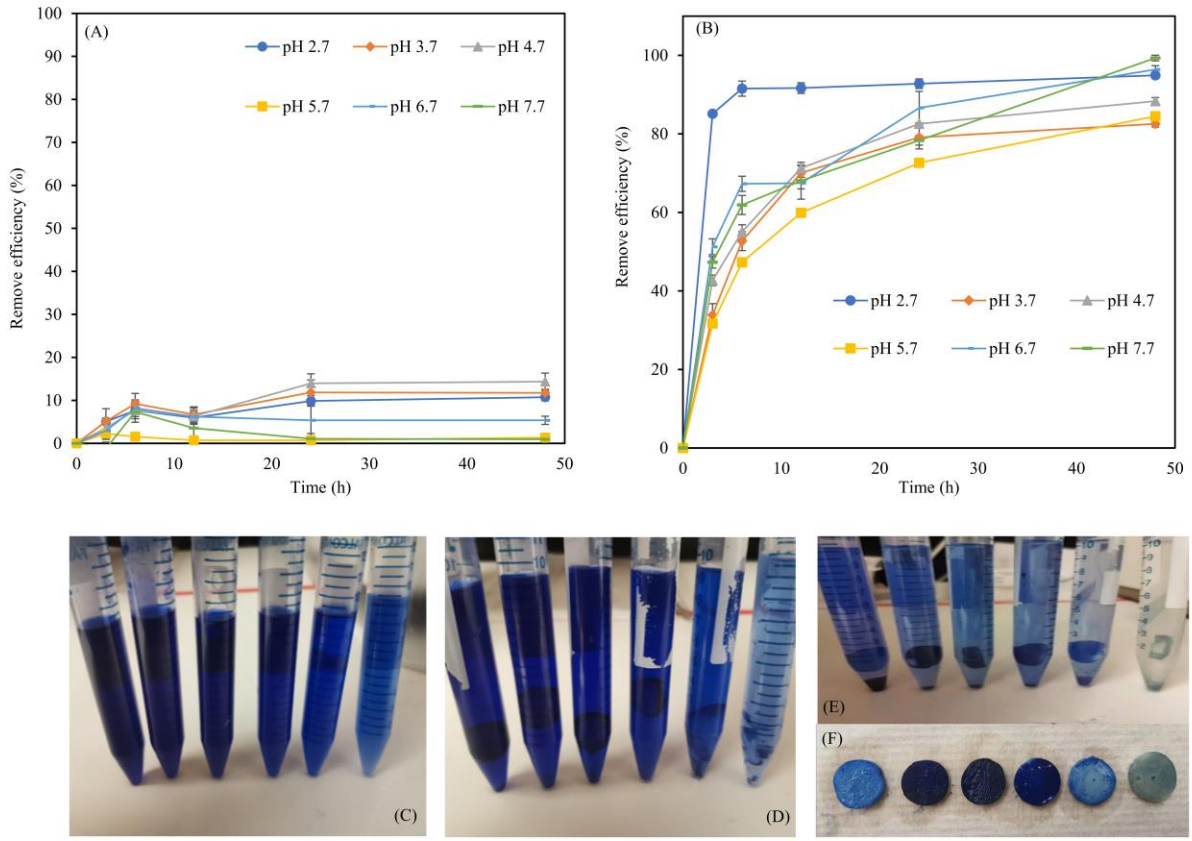

Figure 4-3. Removal capability and efficiency of methyl blue dyes by (A) TCNF hydrogels and (B) TEMPO CNF-PEI hydrogels at different pH values (2.7-7.7 from left to right) over time, each pH point has three repeats. The pH change of methyl blue dyes buffer solution (C) before and (D) after TCNF hydrogels or TCNF/PEI hydrogel adsorption (E). Surface color changes of the hydrogels after adsorption (F).

4.4.4 Adsorption studies

4.4.4.1 Adsorption kinetics

The absorption kinetics of TCNF/PEI hydrogels at different initial methyl blue concentrations are shown in **Fig. 3.** All adsorption curves presented a fast increase during the first 6 h, disregarding the initial concentration present in the solution (**Fig. 4-4 (A) and (B)**). The dyes werecompletely adsorbed when the initial concentration is 20 and 50 mg/L after 24 h. However, when the initial concentration was higher than 50 mg/L it did not reach equilibrium until after 120 h.

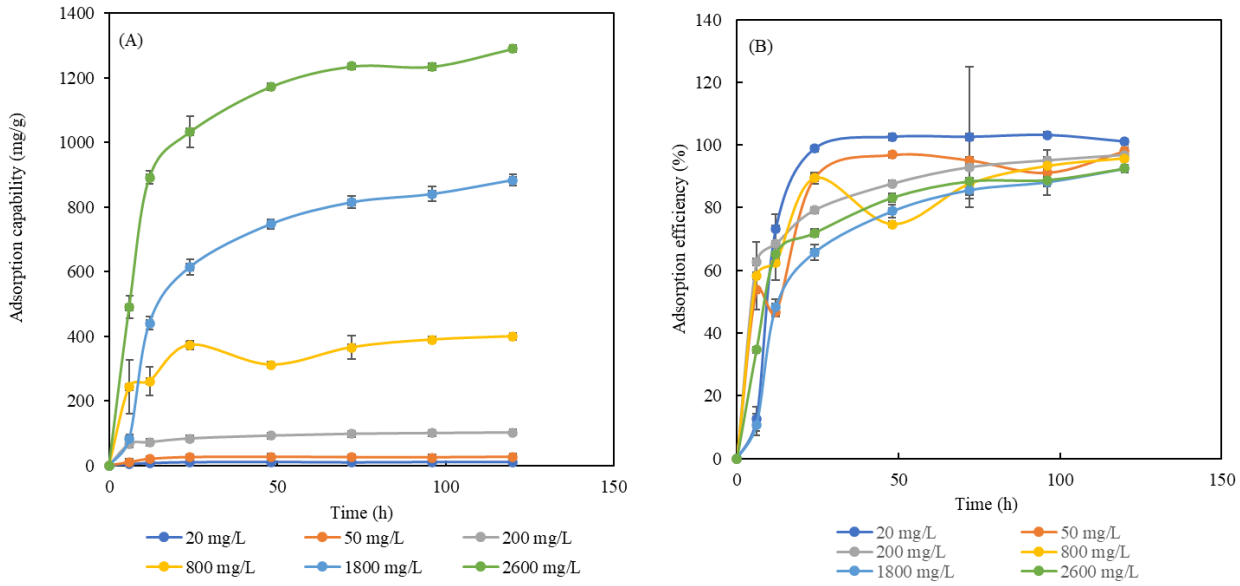

Figure 4-4. Plots of the absorption kinetics of TCNF/PEI hydrogels at different initial methyl blue concentrations with pH 5.7.

To investigate the adsorption behavior and mechanism, the adsorption data was fitted to pseudo-first and pseudo-second order models as shown in **Fig. 4-5 (A)**. The fitting parameters are shown in Table 4-1. The R^2 value of the pseudo-second order model (R^2=0.9745) was higher than that of the pseudo-first order model (R2=0.9591), suggesting that chemisorption was the predominant mechanism of the removal process of dyes [378, 379]. This result agreed with previous studies, which found that chemical adsorption is the predominant mechanism between the PEI modified cellulose aerogels crosslinked by glutaraldehyde [28].

To further examine the diffusion mechanism in the methyl blue dye adsorption process, an intra-particle diffusion model was evaluated. As shown in **Fig. 4-5 (B)**, the plots of q_t versus $t^{0.5}$ yielded three linear regions, which are assigned to three stages of diffusion of methyl blue dye: (1) external diffusion from bulk solution to the surface of the hydrogel, (2) internal diffusion from the surface to the inner section of the hydrogel once the surface sites are saturated, (3) slow diffusion until the

surface became saturated [380]. The slopes of the three stages were calculated from the intraparticle diffusion model and are summarized in **Table 4-1**. It is evident that Kid,1 > Kid,2 > Kid,3, suggesting the adsorption rate in the first stage was fastest. Supporting the previous discussion on external surface adsorption process, which being faster than intra-particle diffusion process.

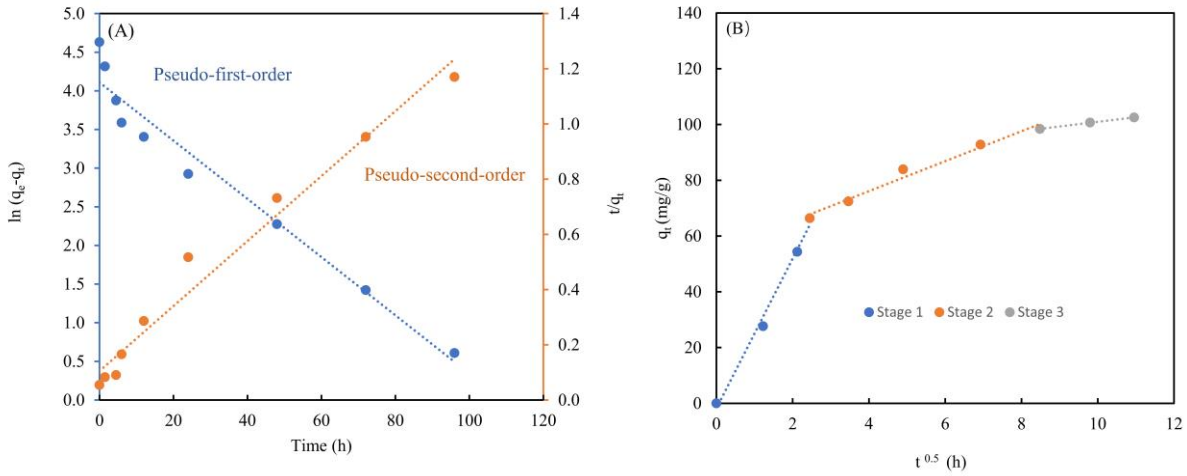

Figure 4-5. Model data of the kinetics fitted to (A) pseudo- first- order and Pseudo- second- order models; and (B) intra-particle diffusion model.

Table 4-1. Parameters extracted from the pseudo- first- order, pseudo- second- order, and Intra-particle diffusion models for adsorption kinetics.

Kinetic parameters	TCNF/PEI hydrogel
$q_{e,exp}$ (mg/g)	102.5
Pseudo-first-order model	
qe (mg/g)	60.9
K_1 (mg/(g*h))	–0.0377
R^2	0.9591
Pseudo-second-order model	
qe (mg/g)	84.74576
K_2 (mg/(g*h))	0.001327
R^2	0.9745
Intraparticle diffusion model	
$k_{i,1}$ (mg/(g*h))	26.9
c_1	–1.8

R_1^2	0.9918
$k_{i,2}$ (mg/(g*h))	5.4
c_2	54.6
R_2^2	0.9785
$k_{i,3}$ (mg/(g*h))	1.7
c_3	84.2
R_3^2	0.9992

4.4.4.2 Adsorption isotherm

Adsorption isotherm analyses were carried out to examine the maximum adsorption capacity and interaction behaviors between the adsorbent and methyl blue dye. The adsorption data were fitted into the Langmuir and Freundlich linear and non-linear models as shown in **Fig. 4-6**. The parameters obtained from the fittings are summarized in **Table 4-2**. Compared with the non-linear model, the correlation coefficient R^2 of linear Langmuir (0.99829) and Freundlich (0.8955) models were higher than that of the non-linear Langmuir model (0.9311) and Freundlich (0.8377) models. For both linear and non-linear adsorption models, R^2 of Langmuir models were higher than those of Freundlich models, suggesting that the adsorption process occurred on the homogeneous surface. [381]. The adsorption isotherm model agreed with results from a cellulose-PEI aerogel crosslinked by glutaraldehyde [28], confirming that the availability of amino groups is the determinant factor in adsorption mechanism instead of the type of crosslinker needed in the hydrogels synthesis.

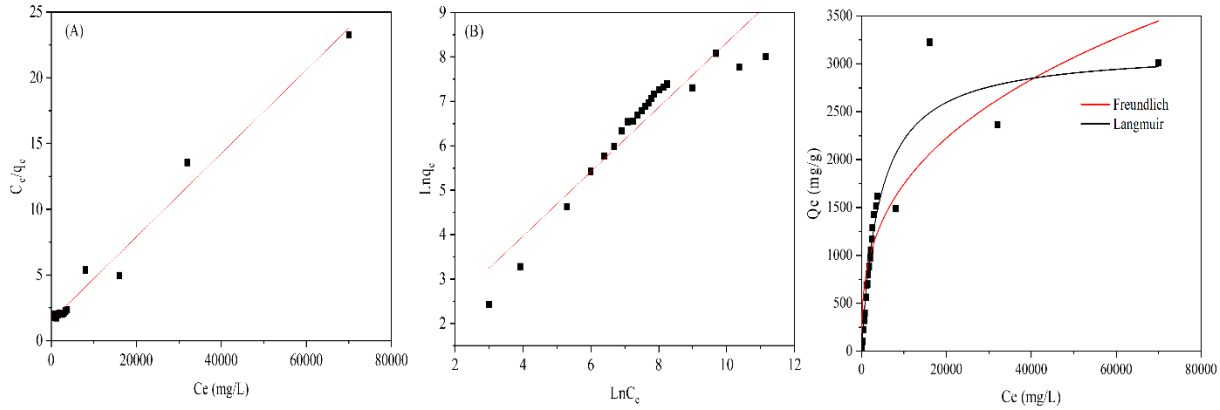

Figure 4-6. Adsorption data fitted to (A) linear Langmuir isothermal model, (B) linear Freundlich model, (C) non-linear Langmuir and Freundlich isothermal model.

Table 4-2. Langmuir and Freundlich constants of TCNF/PEI hydrogels adsorption of methyl blue.

Adsorption isotherm		Model parameters	Statistics parameter
Linear model	Langmuir	Q_m=3125.0 mg/g, K_L=0.00021, R_L =0.06-0.99	R^2=0.9829
	Freundlich	K_F=2.9084, n=1.3789	R^2=0.8955
Non-linear model	Langmuir	Q_m=3151.6 mg/g, K_L=0.00023	R^2=0.9311
	Freundlich	K_F=69.6226, n=2.8586	R^2=0.8377

Langmuir fitting can predict the maximum adsorption capability of an adsorbent when forming a monolayer adsorption [380]. Q_m of the linear Langmuir isotherm (3125.0 mg/g) was closer to the experimental value (3010.5 mg/g) than that of non-linear Langmuir isotherm (3151.6 mg/g), further indicating the better fitting to the linear Langmuir isotherm (as shown in **Table 4-3**). Throughout the archived literature, there are several adsorbents that have been evaluated to remove methyl blue dye from wastewater. The maximum adsorption capacity measured for the TCNF-PEI hydrogels developed herein (3125 mg/g) is higher than most other materials, showing significantly superior performance. With the additional advantage of being produced from a low-cost and sustainable source. Interestingly, the maximum adsorption capability of the TCNF/PEI hydrogels in this work was more than two times higher than that of PEI-modified cellulose aerogels synthesized by glutaraldehyde crosslinking in the previous study. The reason for this notable increase might be due to the high PEI content immobilized in the TCNF/PEI hydrogels (i.e. 14.8 %

of N content based on the element analysis from our previous research) [366]. However, homogeneous monolayer adsorption was dominant for both of them based on the adsorption isotherm models, which means synthesis strategies didn't change the adsorption mechanism.

Table 4-3. Comparison with other results.

Absorbents		Shape	Adsorption ability (mg/g)	References
Cellulose based	Epoxy chloropropane and diethylenetriamine modified cellulose membrane prepared from corn stalk	Membrane	9.06	[382]
	Poly(methacrylic acid-*co*-2-(dimethylamino) ethyl methacrylate) and carboxylated cellulose nanofibrils	Aerogel	598.8	[383]
	PEI-modified cellulose aerogels	Aerogel	1333	[28]
	TCNF/PEI	Hydrogel	3125	This work
Other materials	BaFe12O19 ferrite particles	Powder	223.86	[384]
	Diethylenetriamine-functionalized hollow polymer particles	Powder	1341	[385]
	β-Cyclodextrin functionalized SBA-15	powder	1790.9	[375]
	Polyaspartate−montmorillonite composite withquaternary phosphonium salt (Mt/IPS2)	Aerogel	7958	[386]
	Macroscopic yttrium oxide aerogel monoliths	Powder	8080	[387]

4.4.4.3 Adsorption mechanisms

As explained throughout this manuscript, PEI with abundant amine groups was immobilized on the surface of TCNF/PEI hydrogels through physical adsorption. When TCNF/PEI hydrogels were placed into aqueous solution, amine groups on hydrogels would translate to positively charged

amine groups. This positively charged amine group could promote cation-π interactions, which are electrostatic attraction between positively charged cations and negatively charged electron-rich π systems [388], producing strong electrostatic attraction towards the negatively charged anionic dye molecules [28] (**Fig. 4-7**). The other electrostatic attraction exists between positively charged amine group of hydrogel and natively charged sulfate group of dyes [184]. Additionally, hydrogen bonding, hydrophobic interactions, and Van der Waals forces can also promote adsorption of methyl blue dye on the hydrogels [184].

Furthermore, it cannot be ignored that the multilayer adsorption caused by π–π stacking could also exist [389]. In general, these interactions typically show higher strength than hydrogen bonding, and in some cases, are even stronger than charge–charge interactions, which are arguably one of the strongest noncovalent interactions in aqueous solutions [389-391]. However, according to this and other research [392], the strong electrostatic attraction between PEI and methyl blue dye, which is the main interaction between PEI functionalized cellulose composites and methyl blue dye, is the most probable adsorption mechanism.

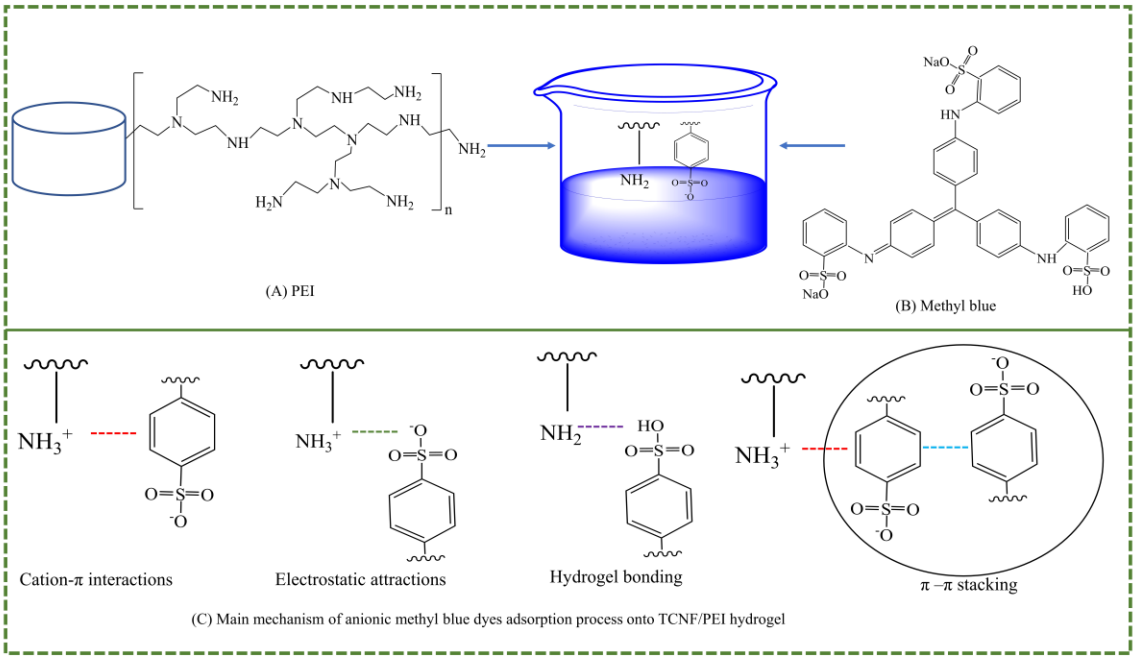

Figure 4-7. Schematic of the structures of PEI and methyl blue, as well as the probable mechanisms of adsorption processes between the anionic methyl blue dyes onto TCNF/PEI hydrogels.

4.4.5 Precipitation

4.4.5.1 The effect of concentration on precipitation

The effect of methyl blue concentration on the precipitation performance was tested, as shown in **Fig. 4-8**. The precipitation capability increased with the increase of methyl blue concentration until the concentration values of 200 mg/L, after which it started to decrease due to the charge neutralization mechanism caused by electrostatic absorption among cationic amine groups on the hydrogel and anionic groups on the methyl blue surface [393, 394]. The higher methyl blue concentration, the more anionic sites available to flocculate through the above mechanisms. Thus, precipitation efficiency increases with the increase of methyl blue concentration. However, when the methyl blue concentration is above the hydrogel maximum flocculation capability, the precipitation efficiency decreases.

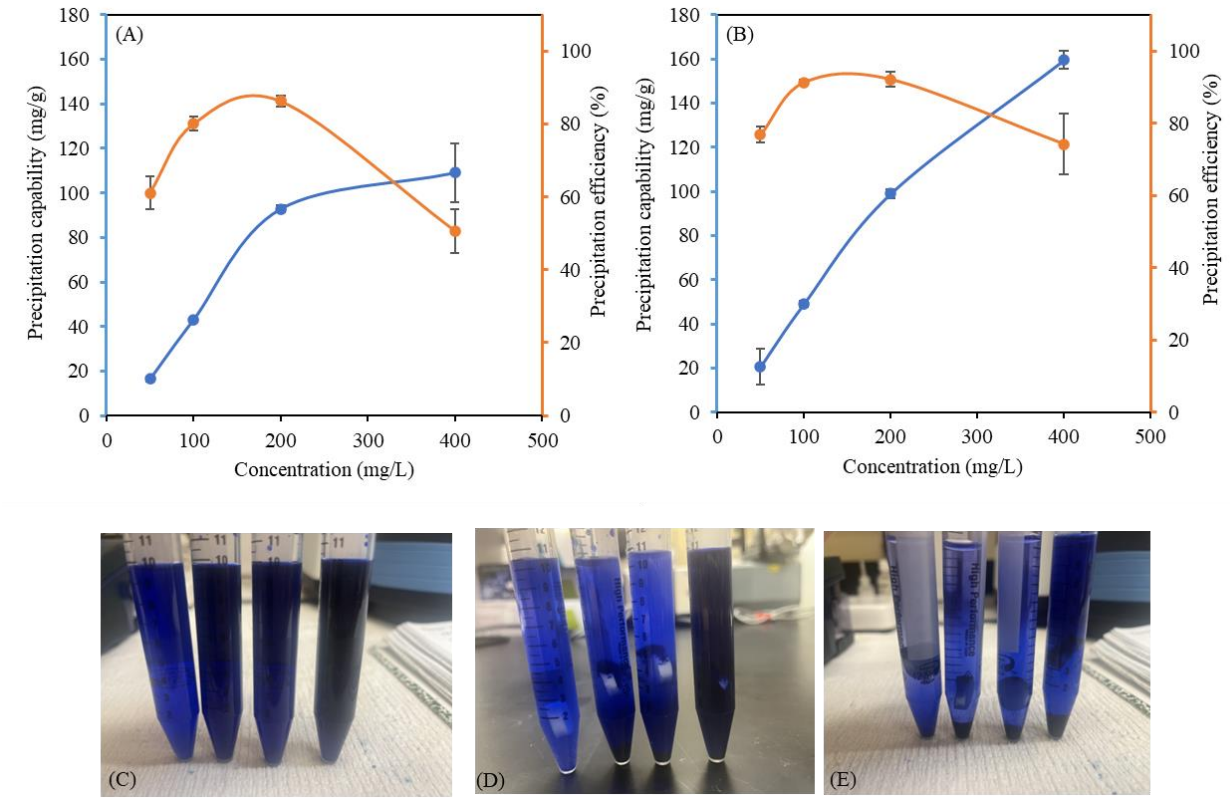

Figure 4-8. The precipitation performance changes with various methyl blue concentrations after (A) 6 h and (B) 24 h. Each test has three repeats. 200 mg/L methyl blue in buffer solution before adsorption (C), after adsorption 6 h (D) and 24 h (E).

4.4.5.2 Precipitation mechanism

As mentioned above, PEI-CNF hydrogels also promoted the precipitation of more than 90% of the methyl blue dye under 2.7 pH buffer conditions. An explanation for this was sustained on the hypothesis that the zinc ions or PEI were released from the hydrogel and consequently coagulated the dye. To confirm this, zinc chloride and PEI were separately added in excess into methyl blue dye buffer solutions and checked after 48 h. There was no precipitation found in the tubes where the PEI was added (**Fig. 4-9 (A) and (B)**), while blue precipitate occurred when zinc chloride was added at pH 2.7 and white precipitate occurred at 3.7-7.7. From this result, it could be inferred that zinc chloride can precipitate methyl blue dyes at pH 2.7. However, only 20-34% of the methyl blue was precipitated by a 10 times higher concentration of the zinc ions than that of zinc ions used

in the synthesis of the hydrogels. In the adsorption test, 90% of methyl blue dyes were removed by precipitation promoted by the TCNF/PEI hydrogels at pH 2.7. A similar observation was made in previous research where precipitation of the dye anions was induced by soluble Ca^{2+} and Mg^{2+} in alkaline white mud suspensions [395]. Although both cations were responsible for the methyl blue precipitate, the pH conditions were opposite ours, suggesting a different mechanism causing the methyl blue precipitation. Therefore, the leaching of zinc ions might not be the dominant cause of methyl blue precipitation and there should be the hydrogels serve as an efficient flocculant makes the methyl blue dyes flocculate and precipitate [393, 394]. The precipitation mechanism could be mainly attributed to the charge neutralization mechanism caused by electrostatic absorption among cationic amine groups on the hydrogel and anionic groups on the methyl blue surface [393, 394].

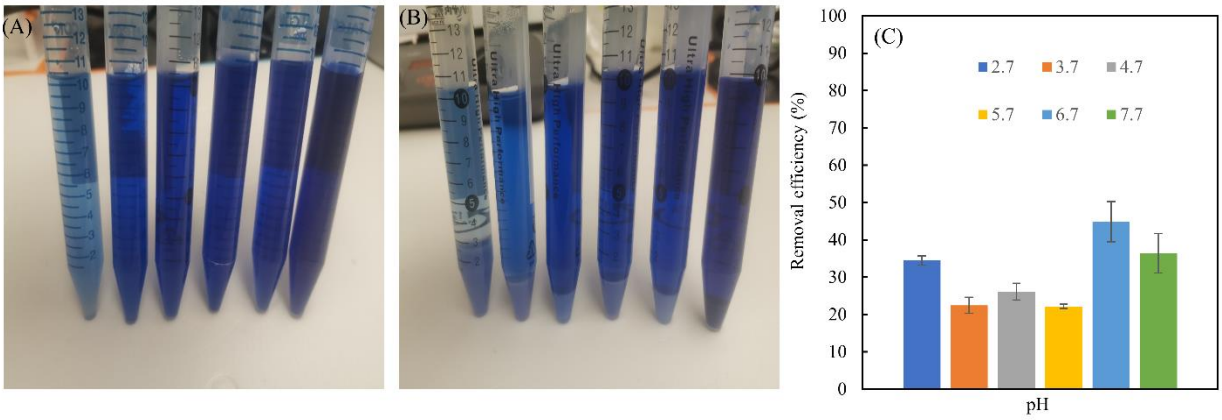

Figure 4-9. The investigation of precipitation of methyl blue by PEI (A) and zinc chloride (B) at pH from 7.7 to 2.7 (from left to right); (C) methyl blue removal efficiency by zinc chloride at pH 2.7-7.7.

To better understand the composition of the precipitates and identify if $ZnCl_2$ or PEI were in there, characterization by FTIR and XRD were done (**Fig. 4-10 (A) and (B)**). It can be observed that adsorption bands and diffraction peaks corresponding to methyl blue were found in precipitated methyl blue. The band at 1161 and 1337 cm^{-1} can be assigned to the strong characteristic

adsorption band of the S=O of MB [386, 396]. 1600, 1571 and 1084 cm^{-1} are the C=C peaks of aromatic rings [397]. The 1496 cm^{-1} is C=N stretching. 1146 and 995 cm^{-1} are C-N stretching [386, 398]. These results suggest that the structure of re-precipitated methyl blue dyes did not change, and that this method can be used to remove and recover methyl blue dye from industry wastewater. The XRD analysis agrees with the FTIR showing a pattern with the main peaks of the methyl blue (**Fig. 9 B)**.

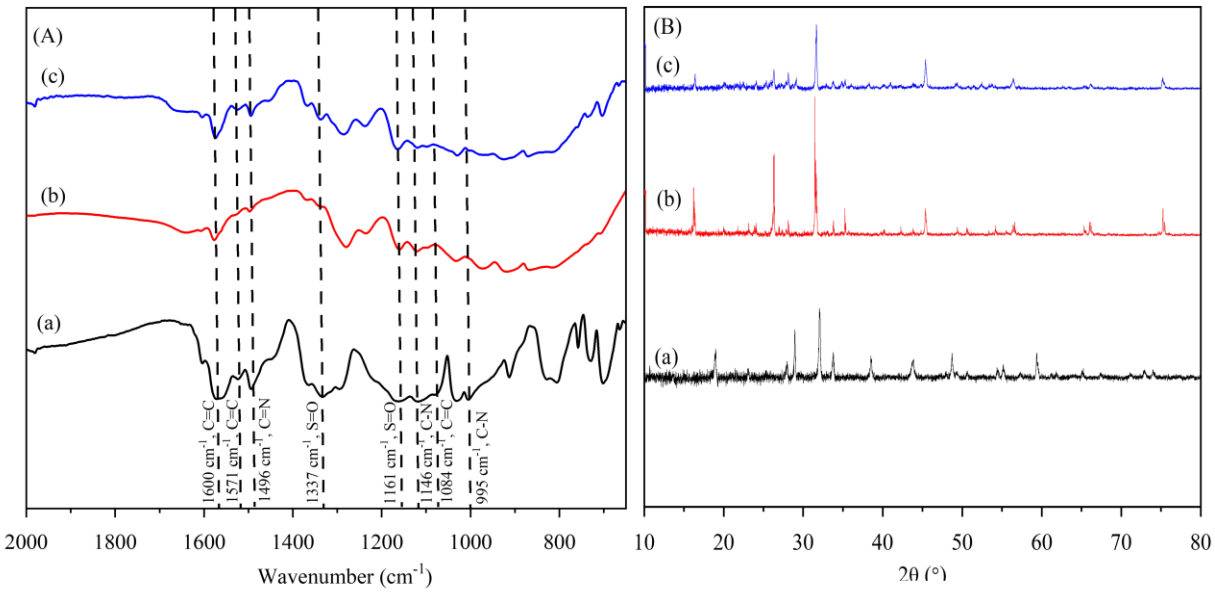

Figure 4-10. The FTIR (A) and XRD (B) analysis of (a) pure methyl blue, (b) methyl blue dissolved in 0.5 M buffer solution at pH 5.7, then freeze dried and (c) methyl blue precipitated by TCNF/PEI hydrogels in 0.5 M buffer solution at pH 5.7 after 48 h then removed hydrogel and freeze dried.

4.4.6 Regeneration

To address the issue of economical and sustainable viability of the adsorption process, we evaluated the TCNF/PEI hydrogels recyclability and reusability [399]. Here, the adsorption mechanism is mainly driven by electrostatic interaction, so the dyes can be desorbed from the adsorbent by drastically changing the pH of the solution. To this end, sodium hydroxide solution 1 M was used for desorption of dyes. After 4 cycles, the adsorption efficiency was still higher than

82 %, indicating that the hydrogels have the capability of being recycled multiple times (**Fig. 4-11 (A)**).

The flocculation recyclability of hydrogels was also tested, as shown in Fig. 10 (B). It was observed that the flocculation efficiency decreased to 24% after 2 cycles. This is probably due to the hydrogel local charges being neutralized by coupling ions from the buffer solution.

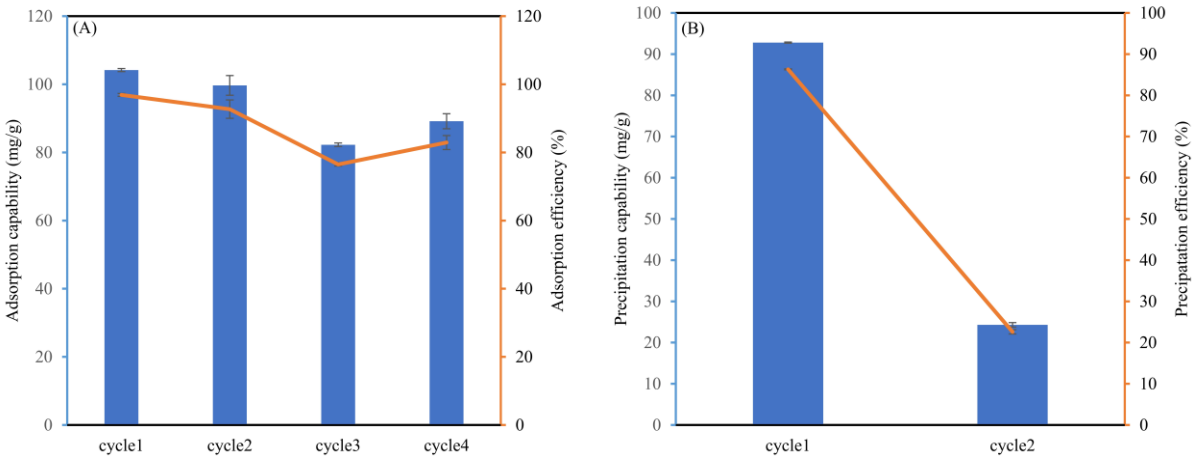

Figure 4-11. Generation test of TCNF/PEI hydrogel in the 200 mg/L methyl blue solution with pH 5.7 for adsorption (A) and flocculation (B).

4.5 Conclusion

This study provides a promising strategy for the development of efficient, sustainable, and cost-effective adsorbents and flocculants for the removal of methyl blue dye from aqueous solutions. The synthesised TCNF/PEI hydrogels exhibited excellent adsorption capability and flocculation capability, as a function of pH, which was mainly attributed to electrostatic interaction. The physical adsorption was also supported by hydrogen bonding, hydrophobic interaction, Van der Waals force, and π-π stacking. The adsorbent showed great reclcling ability, withadsorption efficiency still above 82% after 4 cycles. Importantly, in strong acidic conditions, these hydrogels also promoted the rapid precipitation of methyl blue dye, while flocculation efficiency decreased to 24% after 2 cycles. The structure of re-precipitated methyl blue dyes did not change during the

precipitation process, indicating the possibility of recovering and reusing the dyes in related industries. This study open a pathway to design nanocellulose-based 3-D hydrogel adsorbents-flocculants for water treatment.

Chapter 5. Polyethyleneimine functionalized graphene oxide and cellulose nanofibril composite hydrogels for removal of water pollutants

5.1 Abstract

Nanocellulose-based adsorbent has been widely studied for single water pollutants. However, most water sources like wells, rivers, lakes, and even oceans are drowning in a complex mixture of pollutants, such as metals, dyes, organic compounds, and spilled oils. Therefore, developing efficient technologies to remove multiple pollutants from water sources is necessary. Here, a stable TEMPO-CNF (TCNF)/graphene oxide (GO)/polyethylenimine (PEI) composite hydrogel was synthesized by combining cationic chelation and physical adsorption instead of extra chemical crosslinkers. Their chemical, morphology, surface properties as well as thermal stability were characterized with AIT-FTIR, Raman, elemental analyzer, SEM, IGC-SEA and TGA techniques, and the adsorption behavior for methyl blue (–) was systematically investigated in terms of the optimal GO content, pH effect, kinetics, and isotherm models. Besides, the adsorption capability for methylene blue (+), Cu (II), and soybean oils was also tested. The results indicated that a negative relation between GO content and surface energy was found, but a positive correlation between GO content and the amount of immobilized PEI or surface area was found in the TCNF/GO/PEI hydrogel. Moreover, adding GO did not change the main adsorption isotherm model and adsorption mechanism but increased the external diffusion rate of the intraparticle diffusion model. Based on the Langmuir adsorption model, the maximum adsorption capability for the methyl blue increased from 3125 to 3962 mg/g when 0.2% of GO was added at maximum methyl blue solubility (70,000 mg/L). The adsorption capability for Cu (II) ions and soybean oils increased from 205.3 to 218.5 and 2.1 to 7.2 mg/g, respectively. This work not only provides a

simple and cost-effective synthetic route to TCNF/GO/PEI hydrogels, but also offers valuable clues for the removal of multiple water pollutants.

5.2 Introduction

Cellulose nanomaterial and polyethylenimine (CNM-PEI) composites are widely applied in different fields such as paper making [245, 332], wastewater treatment [400-404], drug release [405-408], sensing [409, 410], heterogeneous catalysis [411-413], and others. Among all, water remediation has attracted most of the attention due to its excellent adsorption capability for water pollutants compared with other materials [16, 414]. The adsorption of CNM-PEI composites on specific and single classes of water pollutants, such as heavy metal ions [401, 415], toxic dyes, and other organic chemicals has been studied in depth, which show super adsorption performance and good regeneration ability. Furthermore, the use of CNM-PEI composite coated by graphene was also demonstrated efficacy for cleaning of oil spills [416]**.** Therefore, CNM-PEI based composites have shown a great potential to absorb various single water pollutants existing in the water body [417]. However, most water resources such as rivers, lakes, and even oceans are polluted by a complex mixture of multiple pollutants, such as toxic metals, plastics, manufactured chemicals, petroleum, urban and industrial wastes, pesticides, fertilizers, pharmaceutical chemicals, agricultural runoff, and sewage [22, 418, 419]. Therefore, a paradigm shift from single pollutant to multipollutant control is crucial for realizing its industrial application [40, 420]. The design of CNM-PEI composite adsorbents for multiple pollutants may be the key to solving this challenge. Considering the hydrophilic properties of both cellulose and PEI, it is necessary to introduce other substances with adsorption capability for the hydrophobic molecules, solvents, and oils to widen their application scale.

Conferring adsorptive powders, such as graphene [225], titanium dioxide, metal or metal oxide [226], and more recently biochar [227], into a tough hydrogel matrix is an effective way to enhance its adsorption capacity [228]. Recently GO has been reported as a novel material for the removal of contaminants from water resources [22, 421]. Owing to its high surface area of about 2600 m^2/g, GO is an excellent material for the removal of oil, organic compounds, and metal ions from aqueous solutions [22]. Moreover, GO has abundant of oxygen-containing functional groups such as carboxyl, epoxy, keto, etc., which are active site to further increase the adsorption capability for water pollutants [422], while presenting good mechanical and chemical stability. Thus, combining it with other nanomaterials can further improve their dimensional stability, which is important for water resistance applications [421, 423]. Various research studies have reported the ability of graphene oxide as an excellent adsorbent for wastewater treatment [22, 421, 424]. However, a major drawback of using GO as a neat material is the difficult separation from the aqueous medium, since GO disperses in water [22]. To overcome this shortcoming, the GO needs to be crosslinked with polymers to arrest the leaching of GO into water.

There are two methods to introduce other polymers into nanocellulose: covalent or non-covalent bonding. As an alternative to the covalent bonding of functional groups or long polymeric chains to the nanocellulose surface, non-covalent interaction is the simplest way to synthesis composites [199, 200]. These interactions essentially are a number of reversible associations, such as ionic interestion, electrostatic interactions, hydrophobic interactions, hydrogen bonds, or van der Waals force [108, 199, 200]. The reversible non-covalent bonds can better recover from the adverse effects that result from the rupturing and dissipation of the energy in the network during the unloading process than covalent bonds [108]. Importantly, the reversible non-covalent bonds make it possible to regenerate adsorbents by desorption. Additionally, non-covalent physical assembly

avoids the use of reagents that are harmful to the environment commonly used for covalent cross-linking interactions [201].

The aim of this work was to introduce GO into CNM-PEI composites by physical interactions to design a new 3-D CNM/GO/PEI composite hydrogel to target multiple water pollutants. Here, it was hypothesized that a stable CNM/GO/PEI composite hydrogel can be synthesized by the combination of cationic chelation and physical adsorption. Moreover, an increase in the diversity and ability of contaminant adsorption would exist by introducing GO into CNM/PEI composites, partially attributed to high surface area and oxygen functional groups on the GO. To this end, TCNFs from soybean hulls and GO were combined by cationic chelating to form the TCNF/GO hydrogels and further functionalized in PEI solution by TCNF physical adsorption to form the TCNF/GO/PEI hydrogel. To test the adsorption capability of resulting TCNF/GO/PEI hydrogels for multiple water pollutants, the methyl anionic dyes, methylene blue cationic dyes, Cu (II) ions, and soybean oils were regarded as references, the show in the **Fig. 5-1**. By doing this, soybean hulls were successfully valorized to a valuable TCNF/GO/PEI hydrogel by an easy and cost-effective way and can be applied for the removal of various water pollutants.

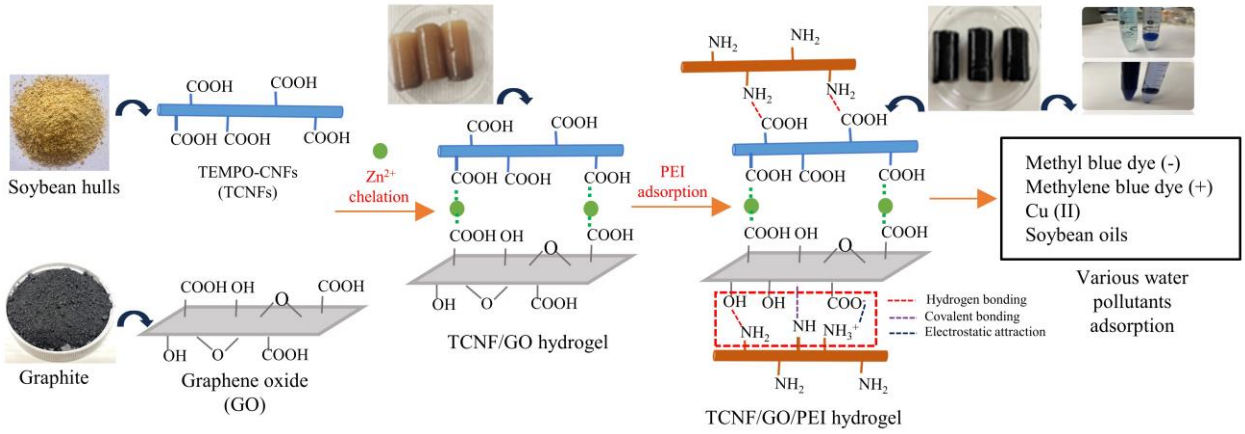

Figure 5-1. Schematic illustration of COOH-CN synthesis and its mechanism for removal of methyl blue.

5.3 Materials and methods

5.3.1 Materials

CNFs, TCNFs and GO were prepared at the Sustainable Bio-Based Materials Laboratory, Auburn University (Auburn, AL), details were provided in the supplemental data. Polyethylenimine (CAS number 9002-98-6, branched, Mw = 25,000 g/mol) was purchased from Sigma-Aldrich. (2,2,6,6-Tetramethylpiperidin-1-yl) oxyl (TEMPO) and methyl blue anionic (MB) dye were purchased from VWR. Graphene flake (99.8%) and anhydrous copper (II) sulfate (98%) from Alfa Aesar. The soybean oil was supplied by Archer Daniels Midland company.

5.3.1.1 Preparation bleached pulp from soybean hulls

Soybean hull is hydrolyzed with 0.1 N HCl solution at 1:20 w/w (fiber to liquor ratio), at 90 ± 5 °C for 1h using a magnetic stirrer at 190rpm. Afterward, the sample is filtered without cooling using a Whatman #4 qualitative paper. Fibers are retained in the funnel and filter paper. Wash profusely with DI water to neutral.

100 g fibers (dry base) from previous extraction were added in 2.5L of DI water with 56 g of $NaClO_2$ (80% from Alfa-Aesar) and 15 mL of glacial acetic acid (99.9% Fisher-scientific). 5 Doses of $NaClO_2$ and glacial acetic acid were added to complete the bleaching step at 1 h intervals.

5.3.1.2 Preparation of CNFs

Briefly, the bleached pulp from soybean hulls was diluted to 2 wt.% suspension and then washed to low the pH to 3 with a 1 M HCl solution; after 30 min, washings of the pulp with DI water until pH increased to 4.5. Then, $NaHCO_3$ was added to obtain a 0.001 M concentration, and pH was adjusted to 9 with 1 M NaOH. After 30 min, washings with water exchanges were performed until the conductivity of DI water was obtained. Finally, the washed pulp was processed with Masuko

super mass collider (MKZA-10-15 J) for 12 passes, with a final consistency of 2.12 wt.% at pH 5.8.

5.3.1.3 preparation of TCNFs

TCNFs were produced by TEMPO-mediated oxidation based on our previous study [366]. Briefly, 5 g of CNF (dry mass basis) was dispersed in 500 mL of distilled water with TEMPO 0.08 g (0.1 mmol/g CNF) and NaBr 0.5 g (1 mmol/g CNF), and the pH was adjusted to 10 by addition of 0.5 M aq. NaOH. Then 30 mL of 12.5% aq. NaClO solution was added slowly to the CNF slurry (1.66 mL/10 min, total 3 h) and the reaction mixture was maintained at pH 10.5 at room temperature by adding aq. 0.5 M NaOH simultaneously. Next, the oxidized CNFs were precipitated by adding ethanol (1500 mL) and then centrifuged at 3800 rpm. Finally, the oxidized CNFs were washed thoroughly with distilled water and filtered using a 0.20 µm cellulose acetate filter paper.

5.3.1.4 Preparation of GO

GO was prepared by the oxidation of graphite flake (according to Hummers method with a slight modification. Briefly, 3 g of graphene flake (325 mesh) and 18 g of potassium permanganate were added in a 1 L flat-bottomed flask, slowly adding the acid mix with 360 mL of 98 wt.% H_2SO_4 and 40 mL of 85 wt.% H_3PO_4. Then, the reaction system was put in an oil bath at 50 ºC and stirred at 500 rpm for 30 h. After that, the reaction solution was poured into a beaker with ice (formed by 500 mL DI water) and followed by a slow addition of 15 mL H_2O_2 (30%) with a syringe (turning the color of the solution from dark brown to yellow) and stirred at 500 rpm for 20 h. Finally, the solid part was washed sequentially by DI water, hydrochloric acid (36-38%), and ethanol by centrifuging at 6000 rpm to remove the metals and manganese chloride.

5.3.2 Synthesis and functionalization of TCNF/GO hydrogels

TCNF/GO hydrogels were prepared by dropwise addition of a 20 wt.% aq. $ZnCl_2$ solution along the walls of the glass tube into a 1.5 wt.% aq. TCNFs dispersion with 0 wt.%, 0.05, 0.1 and 0.2 wt.% of GO (all wt.% based on the total suspension mass). The final zinc ion concentration was controlled to be 0.1 mol/L. Then, the mixture was allowed to stand for 24 h at rest to enable the formation of the hydrogels. Afterward, the resulting hydrogel rinsed with 150 mL distilled water three times to remove unbound Zn^{2+} ions. Next, TCNF/GO hydrogels were immersed in an aq. PEI solution with pH 11.6 at room temperature for 24 h to functionalize. Finally, unfunctionalized hydrogel were named TCNF, TCNF/0.05%GO, TCNF/0.1%GO and TCNF/0.2%GO. While the functionalized hydrogels, named TCNF/PEI, TCNF/0.1% GO/PEI, and TCNF/ 0.2% GO/PEI hydrogels, respectively. They were first placed into 150 mL anhydrous ethanol solution for 2 h and then washed with 150 mL distilled water for about 5 times until the pH of the cleaning water remained neutral.

5.3.3 Materials characterization

5.3.3.1 Attenuated Total Reflectance-Fourier Transform Infrared spectroscopy (ATR-FTIR)

In order to confirm that GO and PEI were successfully introduced into the hydrogels, ATR-FTIR was used to test their corresponding functional groups in the hydrogels. Samples were freeze-dried at –50 °C for 48 h and then analyzed using a PerkinElmer Spotlight 400 FT-IR Imaging System (Massachusetts). An attenuated total reflectance (ATR) accessory with diamond/ZnSe crystal was used for collecting 64 scans with 4 cm^{-1} resolution. Data was processed with Spectrum 6 Spectroscopy Software (PerkinElmer).

5.3.3.2 Raman spectroscopy

To further confirm the GO existed in the TCNF/GO and TCNF/GO/PEI hydrogels, Raman spectroscopic analysis was carried out by DXR Raman Spectroscopy (Thermo Scientific). A

532 nm (50.0 mW power) wavelength laser was used in the Raman spectrometer to analyze the sample. The data acquisition has been carried out in a range of 500-3500 cm^{-1} by OMNIC software.

5.3.3.3 Elemental analysis

In order to investigate the effect of GO content on the chemical composition of TCNF/GO/PEI hydrogels, elemental analysis was carried out to test the C, N and H content. 2 mg of freeze-dried sample were used for elemental analysis by an elemental analyzer (Elementar vario MICRO, Ronkonkoma, NY, USA). Each sample has three replicates.

5.3.3.4 Scanning Electron Microscopy (SEM)

SEM was used to observe the morphological properties. Freeze-dried samples were set onto aluminum studs and sputtered with gold for 90 s in an EMS ×550 Sputter Coating Device from Science Services (Munich, Germany). Images with magnifications of ×100 were recorded in a Zeiss Evo 50VP SEM (Oberkochen, Germany).

5.3.3.5 Inverse Gas Chromatography-Surface Energy Analyzer (IGC-SEA)

Surface energy analyses and Brunauer–Emmett–Teller (BET) surface area measurements were conducted using IGC-SEA (Surface Measurement Systems, UK). Each sample (20 – 50 mg) was packed into a 4 mm chromatographic column and conditioned under a nitrogen gas flow for 2 h. The dispersive components of the surface energy were measured using n-alkanes probes, including octane, nonane, decane, and undecane. The acid-base components of the surface energy were determined using ethyl acetate and dichloromethane as probes. All measurements were carried out under controlled conditions (30 °C, 0% RH). The BET specific surface areas (SBET) were determined by calculating the isotherm of octane with a pressure ratio (P/P0) ranging between 0.05 and 0.35.

5.3.3.6 Thermogravimetric Analysis (TGA)

Thermogravimetric analysis was utilized for the investigation of thermal stability of the hydrogels using a Q-500 thermogravimetric analyzer from TA instruments Inc. Sample weight of the materials were maintained between a range of 10-15 mg and were placed on a platinum plate. The temperature range was from ambient conditions upward to 600°C with a scan speed of 5°C /min; samples were continuously run under a nitrogen atmosphere with a purge flow rate of 60mL/min.

5.3.4 Adsorption behaviors

5.3.4.1 Effect of GO content and retention time

Hydrogels containing 0, 0.1 and 0.2 % of GO were cut into a 3.5 mm long cylinder (0.0186 g dry basis) and then submerged into 10 mL of 200 mg/L methyl blue buffer solutions with different pH 2.7-7.7 and left at rest. To better control the pH of these experiments, phosphate buffer (0.05 M) was used instead of water. Aliquots were taken after 24 h to test the methyl blue left in the solutions by UV-Vis spectrophotometer at $\lambda = 596$ nm.

5.3.4.2 Adsorption kinetics

0.0186 g of absorbent hydrogel was added to 10 mL 200 mg/L methyl blue solution at pH 5.7 and 25 ℃, until the adsorption reached an equilibrium. Aliquots were taken at set time periods to obtain the concentration remaining in the solution. The adsorption capacities were calculated with the following equations:

$$q_{t=}\frac{C_0-C_t}{\mathrm{m}}V \quad (1)$$

$$q_{e=}\frac{C_0-C_e}{\mathrm{m}}V \quad (2)$$

where C_0 (mg/L) and C_t (mg/L) are the initial and concentrations after t time, respectively; q_t (mg/g) is the adsorption capacity at time t; V (L) represents the solution volume of methyl blue, and m (g)

represents the dry mass of the hydrogel adsorbent; Ce (mg/L) are equilibrium concentrations; q_e (mg/g) is the adsorption capacity at equilibrium.

The adsorption data were then fitted to the pseudo-first-order kinetic model, pseudo-second-order kinetic model, and intra- particle diffusion model, using the equations presented below:

$$Ln(q_{e-}q_t) = Lnq_e + k_1\mathrm{t} \quad (3)$$

$$\frac{t}{q_t} = \frac{t}{k_2 q_e^2} + \frac{t}{q_e} \quad (4)$$

$$q_t = K_{id}t^{0.5} + \mathrm{c} \quad (5)$$

where k_1 and k_2 are the rate constants for the pseudo-first order adsorption and pseudo second order adsorption kinetic models, respectively. K_{id} is the rate constant (g mg^{-1} min^{-1}) of intra-particle diffusion kinetics, c is intercept.

5.3.4.3 Adsorption isotherms

0.0186 g absorbents were immersed in 10 mL methyl blue dye solutions with concentration from 20 to 70000 mg/L to study the adsorption isotherm. The adsorption experiments were carried out at 25 ℃ at an initial pH of 5.7 after 120 h. The adsorption values were fitted into linear (equation 6) and non-linear (equation 7) Langmuir isotherm models. Additionally, the data was fitted into linear (equation 9) and non-linear (equation 10) Freundlich isotherm models to describe its behavior. The equations used are described below:

$$\frac{C_e}{q_e} = \frac{C_e}{q_m} + \frac{1}{K_L q_m} \quad (6)$$

$$q_e = \frac{q_m K_L C_e}{1+K_L C_e} \quad (7)$$

$$R_L = \frac{1}{1+K_L C_0} \quad (8)$$

where q_m (mg g^{-1}) is the maximum adsorption capacity estimated by the Langmuir model, and K_L (L mg^{-1}) is Langmuir constant which is related to the adsorption intensity (Guo et al., 2018; Wang

et al., 2020). *RL* is the separation factor, which values indicate the adsorption to be unfavorable when $R_L > 1$, linear when $R_L = 1$, favorable when $0 < R_L < 1$, and irreversible when $R_L = 0$. $C_{0_\circ}$ refers to the initial concentration of the adsorbate in (mg/L)

$$Lnq_e = LnK_F + \frac{LnC_e}{\mathrm{n}} \quad (9)$$

$$q_e = K_F c_e^{1/n} \quad (10)$$

K_F are constants of the Freundlich equations; 1/n in the Freundlich model represents an empirical parameter, which is related to the energetic heterogeneity of the adsorbent surface and determines either the favorable or unfavorable curve. When 1/n is greater than zero ($0 < 1/n < 1$) the adsorption is favorable, when 1/n is greater than 1, the adsorption process is unfavorable, and it is irreversible when 1/n = 1.

5.3.4.4 Adsorption capability for various pollutants

The adsorption capability of the hydrogels for methylene blue (+) dyes, Cu (II) ions and soybean oils was also tested. The hydrogels 0.0186 g dry basis were put into 10 mL of 200 mg/L methylene blue buffer solutions with pH 5.7 left at rest and samples were taken after different time intervals (3, 6, 12, 24 h). Methylene blue concentrations in the supernatant were calculated by UV spectrophotometer at 664 nm, respectively. Hydrogel cylinders of the same size were also put into 10 mL of 320 mg/L Cu (II) solutions for 24 h. The remaining Cu (II) ions in solution after hydrogel treatment were quantified by Inductively Coupled Plasma-Mass Spectrometry (ICP-MS). Finally, the same size of hydrogels was put in the 5 g (W1) of pure soybean oil after 30 min, then removed hydrogels and tested the weight of oil left in the container (W_2). The soybean oil adsorption efficiency was calculated based on the following (equation 11):

$$\textit{Soybean oil adsorption efficiency (\%)} = \frac{w1-w2}{w1} \times 100 \quad (11)$$

5.4 Results and discussion

5.4.1 The effect of GO concentration on the stability of TCNF/GO hydrogels

Carboxyl group in TCNF can be chelated by cationic to form stable hydrogels [366, 425]. Here, GO was introduced into the TCNF dispersions (**Fig. 5-2 (A)**) and chelated by Zn^{2+} to form TCNF/GO hydrogels. The interaction promoting the hydrogel formation was based on the existence of similar carboxyl groups in GO that resulted in a stable TCNF/GO hydrogel when the GO concentration was less than 0.2 % (**Fig. 5-2. (B)**). However, a higher concentration of GO resulted in a collapse of structure. After PEI functionalization, the color of TCNF/GO hydrogel changed from brown to black likely induced by the GO reduction to graphene [426], which will be further confirmed by the FTIR in the following section. Another visible change was that the material seemed stiffer after PEI functionalization due to the crosslinking by the PEI.

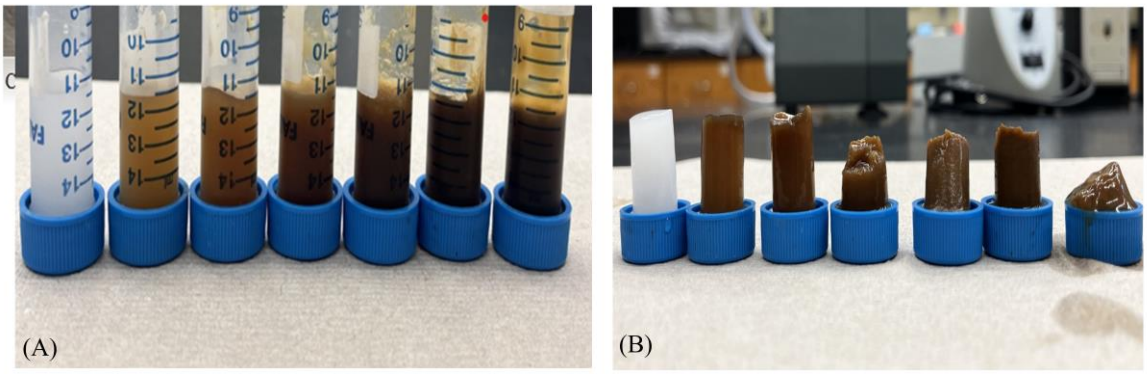

Figure 5-2. Images of TCNF/GO dispersions and TCNF/GO hydrogels with different concentration of GO (from left to right: 0% GO, 0.1% GO, 0.2% GO, 0.5% GO, 1.0% GO, 1.5% GO with 1.5 % TCNF, 1.5 % GO without TCNF) chelated by cationic ions.

5.4.2 Characterization of the hydrogels

5.4.2.1 Chemical properties

FTIR was used to identify the functional chemical group in PEI, GO, and corresponding hydrogels (**Fig. 5-3**). For the GO (**Fig. 5-3 (A)**), the band at around 3400 cm^{-1} is related to O–H stretching

vibration, 2917 cm^{-1} is symmetric stretching vibration of C–H, 1723 cm^{-1} is C=O stretching vibration in carboxyl group and the band at 1624 cm^{-1} corresponds to the skeletal stretching of C=O alkene group, C–O–C bending vibrations at 1417 cm^{-1} [427, 428], 1226, 1050 and 987 cm^{-1} are C-OH stretching/bending vibrations. Besides, C–C and C–O are around 913 and 857 cm^{-1} [429]. High intensity of major bands in GO revealed that large amounts of oxygen-containing groups are present after the oxidation process [430-432]. For PEI (**Fig. 5-3 (B))**, the signals at 2936 and 2817 cm^{-1} were the characteristic bands of -CH_2 stretching vibrations, while the bands at 1670 cm^{-1} and 1050 cm^{-1} correlated to the -NH_2 stretching vibrations, and C–C skeleton vibration, respectively [433]. Besides, the band near 1599 cm^{-1} and 1459 cm^{-1} are the N–H bending vibration of primary amines in PEI; 1350, 1278, 1126, and 1041 cm^{-1} are C-N stretching vibrations [434]. After PEI functionalization, some of GO characteristic peaks (1417, 1226, 987, 913 and 1050 cm^{-1}) were visible in the TCNF/0.1%GO and TCNF/0.2%GO hydrogel spectra, which means GO was successfully introduced into the hydrogels (**Fig. 5-3 (A)**). However, these signal bands become weakened. Besides, some of GO signal bands (1723, 1624, 913 cm^{-1}) disappeared after PEI functionalization. The weakened or disappearing bands for oxide-containing groups in TCNF/GO/PEI hydrogels indicate that reductive PEI could partially reduce GO to graphene (**Fig. 5-3 (B))** [426]. All PEI characteristic bands were observed in PEI functionalized hydrogels, proving the successful introduction of PEI to TCNF/PEI hydrogels.

To further make sure GO or graphene exists in the TCNF/GO and TCNF/GO/PEI hydrogels, all samples were tested by Raman spectroscopy, as shown in **Fig. 5-3 (C)**. GO, TCNF/GO, and TCNF/GO/PEI hydrogels show peaks at ∼1315 cm^{-1} (D band) and ∼1594 cm^{-1} (G band) corresponding to sp^3 disordered carbon and sp^2 hybridized carbon, respectively [429, 435]. In comparison with GO, the D and G bands did not shift in hydrogels, but several changes occured

in the D and G peaks of the TCNF/GO and TCNF/GO/PEI hydrogels. Both D and G bands in TCNF/GO and TCNF/GO/PEI hydrogels become broader than those of GO. Besides, the D and G bands become narrower when GO increase from 0.1% to 0.2%. However, both D and G bands in TCNF/GO/PEI hydrogels became narrower after PEI functionalization compared with TCNF/GO hydrogels. To explain this, the intensity ratio of the D and G bands (I_D/I_G) has been used to find out the sp^2 domain size and partially ordered crystal structure of carbon, respectively. The ratio of I_D/I_G of GO is 1.41, it decreased to 1.22 and 0.97 in the TCNF/0.1%GO and TCNF/0.2%GO, respectively. It definitely proves that TCNF has repaired the structural defects on the surface of GO, thus reducing the I_D/I_G [436]. It seems 1.5% of TCNF can repair more than 0.2% of GO, because TCNF/0.2%GO hydrogel has a higher shift of I_D/I_G ratio. However, the I_D/I_G ratio increased to 1.23 and 1.38 after PEI functionalization. This indicates that PEI functionalization can increase the amount of graphite edges due to the reduction of GO [437].

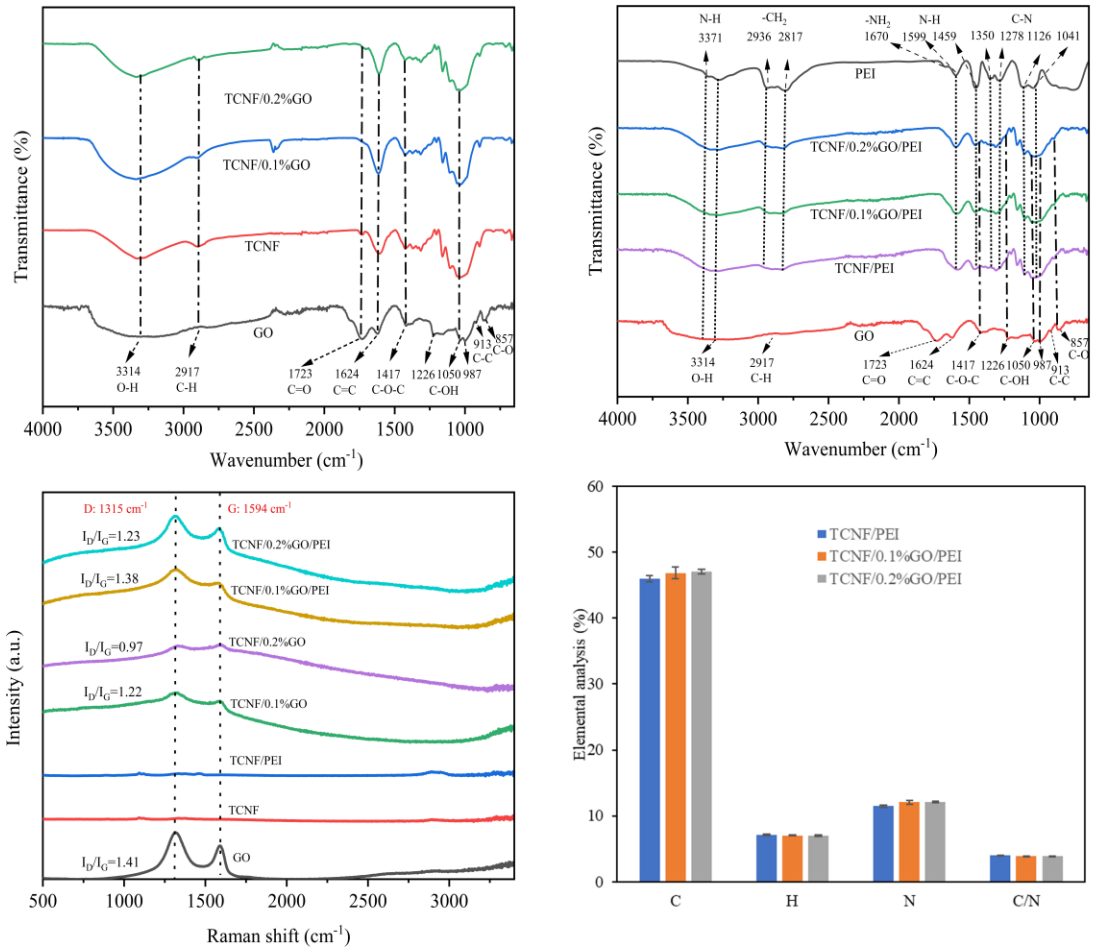

Figure 5-3. FTIR (A) and (B), Raman (C) and elemental (D) analysis of all studied samples.

To explore the effect of GO content on the amount of PEI adsorbed on the TCNF/GO hydrogels, elemental analysis was done to test the N content in the PEI functionalized these hydrogels. The results showed that the N content increased with the increase of GO content (**Fig. 5-3(D)**). The N content increased from 11.5 % to 12.1% when the GO content increased from 0% to 0.2%, which can be attributed to oxygen-containing group on the GO can combine PEI by covalent bonding, hydrogen bonding and electrostatic attraction force [438]. The N content was related to the adsorption capability of these hydrogels for water pollutants, the higher N content, the higher

adsorption capability [366]. However, for all hydrogels, the values for carbon and hydrogen are lower than expected, which could be explained by surface adsorption of water [439].

5.4.2.2 Morphology characterization

Morphologies were observed by SEM (**Fig. 5-4**). The TCNF hydrogel presented a dense structure (**Fig. 5-4 (A)**), while TCNF/0.1% GO hydrogels and TCNF/PEI hydrogels showed a microporous scaly structure (**Fig. 5-4 (B) and (D)**), but TCNF/0.1% GO hydrogels look fluffier, while hydrogel structure became cross-linked when GO content increased to 0.2%, looked more organized (**Fig. 5-4 (C)**). The structure of TCNF/0.1% GO/PEI and TCNF/0.2% GO/PEI look more compact and more tightly (**Fig. 5-4 (E) and (F)**) compared with their unmodified analogs. Generally, a more porous structure would have a higher surface area, which translates to higher adsorption capabilities for the water pollutants [440]. To confirm this, the surface area of those materials was tested (see next section).

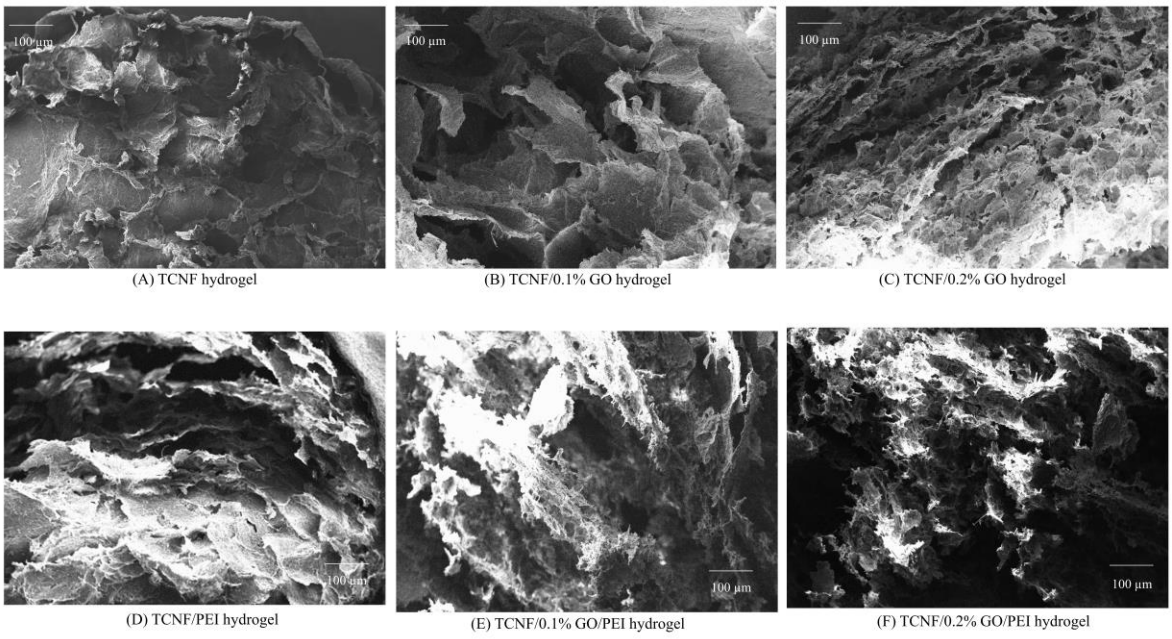

Figure 5-4. SEM images of TCNF/PEI hydrogels with different concentration of GO at 100x.

5.4.2.3 Surface area and surface energy

SEM images in **Fig. 5-5** demonstrated changes in morphology caused by GO and PEI functionalization. Here, BET surface area measurements were used to quantify the changes in morphology relative to an unmodified control. As shown in **Fig. 5-5**, compared with TCNF hydrogel (5 m^2/g), the surface area of TCNF/GO hydrogels increased with the increase of GO content, up to 5.76 m^2/g when GO content increased to 0.1%, then decreased to 3.74 m^2/g when the GO content was increased to 0.2%. This indicated that low GO content (≤0.1%) can help to increase the surface area of TCNF hydrogels. However, the surface area of TCNF/PEI hydrogel decreased to 2.82 m^2/g. It means PEI functionalization caused a significant decrease in surface area. Interestingly, it was found that the surface area of TCNF/GO/PEI hydrogel increased from 2.82 to 4.78 m^2/g when GO content increased from 0% to 0.2%, which means adding GO in the TCNF/PEI hydrogels can help prevent surface area loss of TCNF hydrogel directly functionalized by PEI.

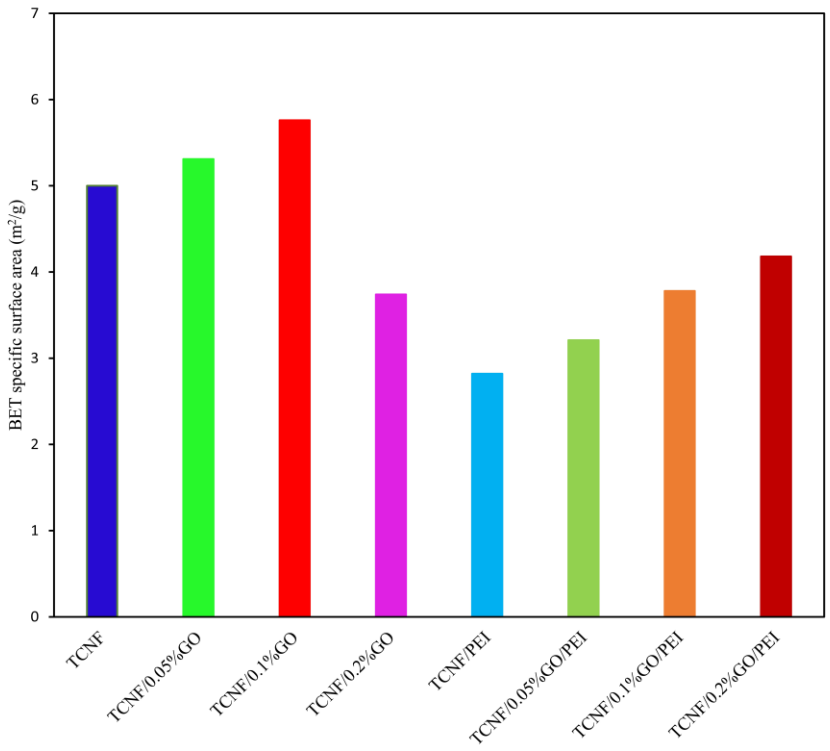

Figure 5-5. Surface area of all prepared hydrogels tested by IGC-SEA.

IGC-SEA was utilized to investigate the impact of surface modification and composite formation on the surface energy of the hydrogels, and how these changes in energy profiles may influence the final adsorption properties and mechanism of the composites. **Fig. 5-6 (A)**, **(B)** and **(C)** show the dispersive surface energy (γ_S^D), specific (acid-base) surface energy (γ_S^{AB}) and total surface energy (γ_S^{Tot}) of the studied hydrogels as a function of surface coverage for probe gases. Here, "n" represents the amount of gas adsorbed, and "nm" is the monolayer capacity of the powders, respectively. The γ_S^{Tot} of solid surfaces is composed of γ_S^D, and γ_S^{AB} components. The result revealed that γ_S^D contributes a significant portion of the total surface energy for all the samples tested [441, 442]. Moreover, these values decrease significantly with increasing surface coverage at lower coverage levels, indicating that the samples are energetically heterogeneous. This heterogeneity is further confirmed by the distribution of γ_S^{Tot} (**Fig. 5-6 (D)**). However, the decreasing trend was not significant when the surface coverage was larger than 0.05. γ_S^{Tot} has the

same change trend with γ_S^D in spite of γ_S^{AB} continuing to be slightly decreasing when the surface coverage was larger than 0.05, which was due to γ_S^D was the dominant component of γ_S^{Tot}. These changes in surface energy align with previous literature examples for cellulosic materials, where higher surface energies at lower coverages result from the preferential binding of probe molecules to higher-energy surface sites under dilute conditions [443, 444].

Compared with TCNF hydrogels, all functionalized hydrogels with GO or PEI presented higher γ_S^D and γ_S^{AB} at the most of surface coverage points (**Fig. 5-6 (A) and (B)**), which means all these modifications increased the surface energy of TCNF hydrogels. The γ_S^{Tot} of TCNF/GO hydrogels increased from 49.4 (TCNF hydrogels) to 78.4 mJ/m^2 when the GO content was 0.05%, then decreased to 56.1 mJ/m^2 when the GO continued to being increased to 0.2% at lowest surface coverage (**Fig. 5-6 (C)**). When these hydrogels were further functionalized by PEI, TCNF/PEI hydrogel showed highest γ_S^{Tot} 144.9 mJ/m^2, while γ_S^{Tot} of TCNF/GO/PEI hydrogels decreased to 70.0 mJ/m^2 when the GO content increased to 0.2%. This result indicates that low levels of GO (less than 0.1%) functionalization can enhance the surface energy of TCNF hydrogel, which is consistent with the changes observed in surface area after functionalization with GO. The presence of PEI on the surface significantly increases the surface energy of TCNF hydrogels, contrary to the change in surface area after PEI functionalization. However, the addition of GO to TCNF hydrogels followed by PEI functionalization leads to a decrease in surface energy, also contradicting the change in surface area. Therefore, it appears that there is no clear relationship between surface area and surface energy, contrary to previous research findings [445].

Meanwhile, compared to TCNF hydrogel, all functionalized hydrogels showed a broader distribution profile of total surface energy (**Fig. 5-6 (D)**), which indicated that they had a large

surface heterogeneity due to their complex physical structure (more porous) and chemical composition (new functional groups were introduced into the TCNF hydrogel). Among them, COOH-PEI hydrogel displays the broadest distribution profile and the highest γ_S^{Tot}. It is worth noting that the order of the distribution profiles of all the hydrogels, from broadest to narrowest, coincides with the order of their surface energy, from highest to lowest. Hence, a higher surface energy corresponds to a larger surface heterogeneity [445, 446].

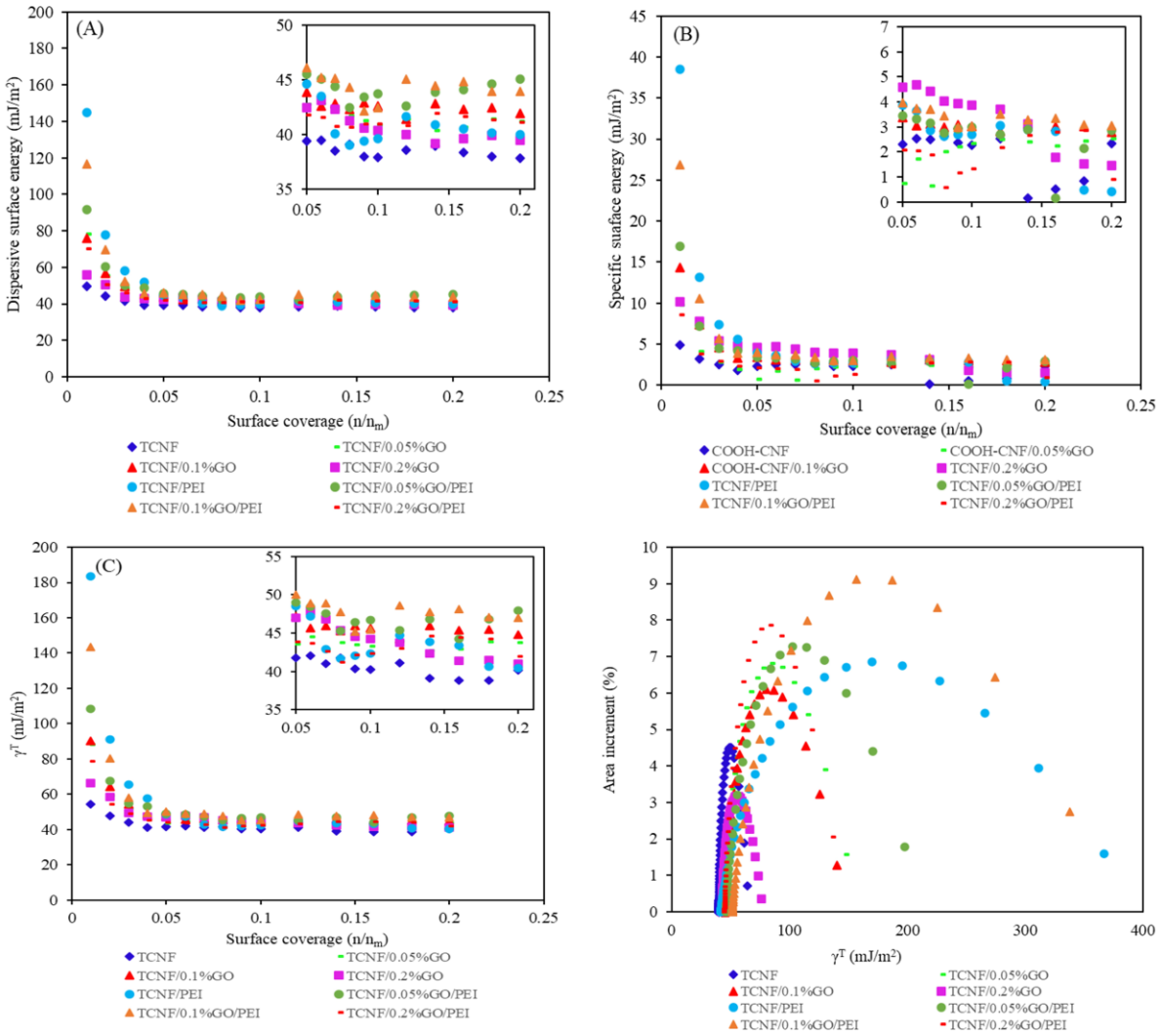

Figure 5-6. Surface energy (A): γ^D, dispersive energy, (B): γ^{AB}, specific energy, (C): γ^T, total energy (γ^T=: γ^D+ γ^{AB}), (D): distribution of γ^T tested by IGC-ESA.

5.4.2.4 Thermal stability

Fig. 5-7 (A) and **(B)** shows the thermogravimetric (TG) and first derivative thermogravimetric (DTG) curves of all tested hydrogels, respectively. As shown in Fig**. 5-7 (A),** the mass loss of all samples when temperature ≤ 100 °C is caused by volatilization of water molecules physically absorbed onto the samples. The main mass loss of GO is around 170 °C. This is due to thermal decomposition of oxygen-containing groups in graphite oxide to CO, CO_2, and H_2O [447]. However, the main mass loss temperature of GO is around 200 °C based on other research [447, 448], the different was probably induced by the producing process of GO. Pure PEI degraded nearly completely at around 320-420°C, which is similar with previous study [448]. TCNF hydrogel mainly decayed at 230-335 °C, which is decomposition of hydroxyl and carboxyl groups [144]. Correspondingly, the initial decomposition temperature (T_0), the decomposition temperature at 10% weight loss ($T_{10\%}$) and maximum decomposition temperature (T_{max}) are summarized in **Table 1**. The order of T_0, $T_{10\%}$, and T_{max} was constant in the order of GO < TCNF hydrogel < PEI, which means PEI had the highest and GO had the smallest thermal stability. The GO functionalized TCNF hydrogels showed lower T_0, $T_{10\%}$, and T_{max} than pristine TCNF hydrogel, while PEI functionalized TCNF hydrogels have lower T_0, $T_{10\%}$, but higher T_{max} than pristine TCNF hydrogel. This indicated that GO functionalization decreased the thermal stability of TCNF hydrogel, while PEI functionalization can increase the thermal stability of TCNF hydrogel. Besides, the residues of GO or PEI functionalized hydrogels were also lower than that of TCNF hydrogels because of the GO and PEI decomposition [449]. Therefore, the char-forming performance of TCNF hydrogel didn't improve after adding GO, PEI, and both GO and PEI, respectively.

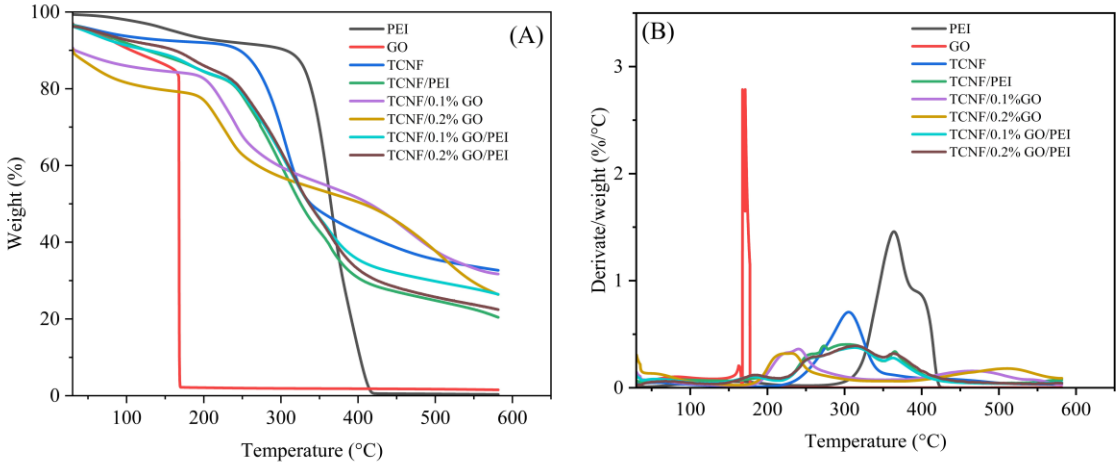

Figure 5-7. TG (A) and DTG (B) curves of PMS and CNFs.

Table 5- 1. Summary of thermal decomposition parameters of PMS and CNFs samples.

Aerogels	T_0 (°C)	$T_{10\%}$ (°C)	T_{max} (°C)	Residues (%)
GO	167	167	168	0.3
PEI	325	341	364	1.5
TCNF	258	284	304	32.7
TCNF/0.1% GO	201	232	241	31.7
TCNF/0.2% GO	198	227	237	26.6
TCNF/PEI	233	268	313	20.4
TCNF/0.1% GO/PEI	231	267	313	26.6
TCNF/0.2% GO/PEI	222	263	313	22.5

Note: T_0, T10%, Tmax represent the start decomposition temperature, the decomposition temperature at 10% weight loss, and maximum decomposition temperature, respectively.

5.4.3 Adsorption

5.4.3.1 Effect of GO addition

Testing was conducted to investigate the impact of GO addition on the adsorption performance of the corresponding hydrogel for methyl blue, an anionic dye. The adsorption process was examined within a pH range of 3.7-7.7 and measured after a 24-hour period. As depicted in **Fig. 5-8**, the adsorption capacity of TCNF hydrogels increased after GO addition. In comparison to the TCNF hydrogel (7.9 mg/g), the adsorption capacity of the GO-modified CNF hydrogel showed an

increase with higher GO content, reaching a maximum of 42.3 mg/g at a GO content of 0.1% and a pH of 5.7. However, when the GO content continued to increase to 0.2%, the adsorption capacity decreased to 36.9 mg/g. These results align with the changes observed in surface area and surface energy (γ_S^D, γ_S^{AB} and γ_S^{Tot}) based on variations in GO content.

5.4.3.2 Effect of further PEI functionalization

Further modification of the TCNF and TCNF/GO hydrogels through physical adsorption of PEI led to a sharp increase in adsorption capacity. The adsorption capacity of TCNF/PEI hydrogel ranged from 64.6 to 79.1 mg/g within the pH range of 3.7-7.7. The adsorption capacity of TCNF/GO/PEI further increased with higher GO content, reaching 86.9-96.3 mg/g across the tested pH range. This increase can be attributed to the combined effect of surface area and surface energy. Although the surface energy decreased with increasing GO content for TCNF/GO/PEI hydrogel, the surface area increased. Consequently, GO-functionalized hydrogels exhibited lower adsorption capacity compared to PEI-functionalized ones due to the presence of electrostatic attraction between the PEI-modified hydrogel and methyl blue, as indicated by the higher total surface energy of the PEI-modified hydrogel mentioned earlier.

Furthermore, electrostatic attraction or repulsion, which depends primarily on pH, influenced the adsorption capacity when the GO content was below 0.2% for both TCNF/GO and TCNF/GO/PEI hydrogels [28, 388]. Conversely, the adsorption capacity of TCNF/0.2%GO/PEI hydrogel remained similar across all pH conditions. This suggests that when the GO content is below 0.2%, the adsorption capacity is pH-dependent, whereas with a GO content of 0.2%, the adsorption capacity becomes independent of pH. This finding indicates a different adsorption mechanism, prompting further investigation through adsorption kinetics and adsorption isotherm modeling to clarify this difference.

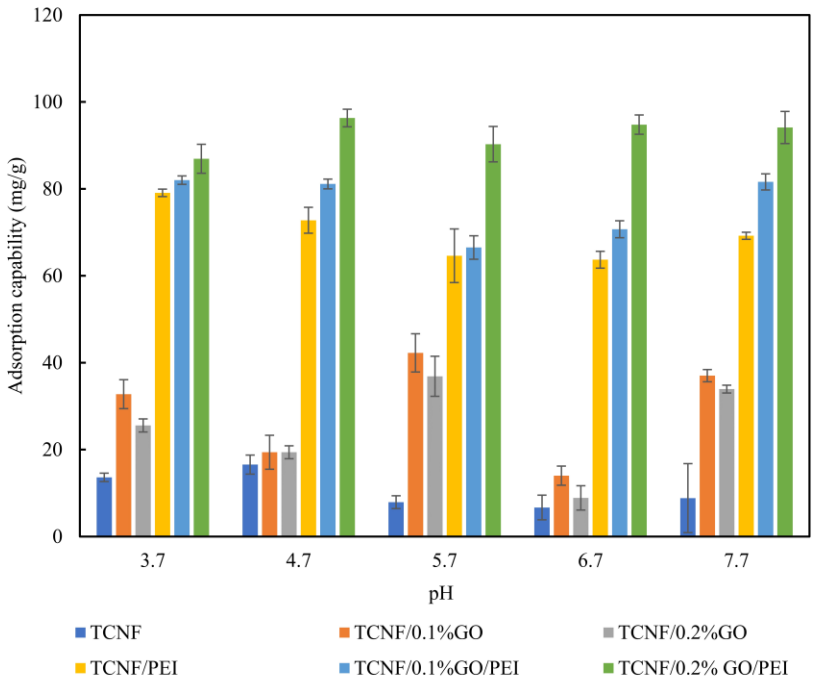

Figure 5-8. The effect of GO and PEI modification on the adsorption capability of corresponding hydrogels.

5.4.3.3 Adsorption kinetics

The adsorption capability and kinetics were evaluated using an initial concentration of 200 mg/L using 0.0186 g of material (**Fig. 5-9 (A)**). The results showed that the adsorption capability of TCNF/0.2%GO/PEI hydrogel reached 82.2 mg/g after just 12 h, while TCNF/PEI hydrogel needed 24 h to get to 85.9 mg/g. The time was cut in half for the TCNF/0.2%GO/PEI hydrogel to get almost the same adsorption capability as the TCNF/PEI hydrogel. However, the adsorption capability became similar after 48 h, up to 92.8 and 94.2 mg/g, respectively. This indicates that the addition of GO leads to an increase in the initial adsorption rate. This was further explored by adsorption kinetics modeling. The adsorption reached equilibrium after 120 h, with an adsorption capability of 102.5 mg/g and the adsorption efficiency was 96.8%, which meant almost all methyl blue dyes were adsorbed at initial concentration of 200 mg/L.

The adsorption kinetics were modeled to learn more about the adsorption behavior. The data was fitted to pseudo-first and pseudo-second-order models (**Fig. 5-9 (B), (C)**). For both the TCNF/PEI and TCNF/0.2% GO/PEI hydrogels, the R^2 of pseudo-second-order models were 0.9745 for both, which were higher than that of pseudo-first order models (0.9591 and 0.9211). This meant that the adsorption kinetic model was more fitted to pseudo-second-order models. To further reveal the diffusion mechanism in the methyl blue dye adsorption process, the intra-particle diffusion model was tested. As shown in **Fig. 5-9 (D)**, the plots of q_t versus $t^{0.5}$ yielded three linear regions, which are assigned to three stages of diffusion of methyl blue dyes: (1) external diffusion from the bulk solution to the surface of the hydrogel, (2) internal diffusion from the surface to the inner section of the hydrogel once the surface sites are saturated, (3) slow diffusion until the surface became saturated [450]. The slopes of the three stages were calculated from the intraparticle diffusion model and summarized in Table 2. It is evident that Kid,1 > Kid,2 > Kid,3, suggesting the adsorption rate in the first stage was faster than the other stages. This indicates the external surface adsorption process was faster than the intra-particle diffusion process. Compared with TCNF/PEI hydrogels (Kid,1=26.9; Kid,2=5.4; Kid,3=1.7), TCNF/0.2% GO/PEI (Kid,1=29.6; Kid,2 =3.7; Kid,3=1.6) has higher Kid,1 but lower Kid,2 and almost similar Kid,3. This was likely caused by the higher PEI content in the TCNF/0.2% GO/PEI, as observed on elemental analysis, which provided higher adsorption site on the hydrogel surface so that obtaining higher adsorption rate and higher adsorption capability on the hydrogel surface during the first stage. Besides, the surface area also increased after adding 0.2% of GO (TCNF/0.2%GO/PEI) compared with without GO (TCNF/PEI). Nevertheless, the higher surface adsorption capability made the holes crowded according to SEM observation, so the diffusion rate from the surface to the inner section of the hydrogel became slower, likewise, the Kid,2 was lower. After those two stages, the adsorption

almost reached adsorption equilibrium, and the adsorption capability changed slightly, leading to a similar Kid,3.

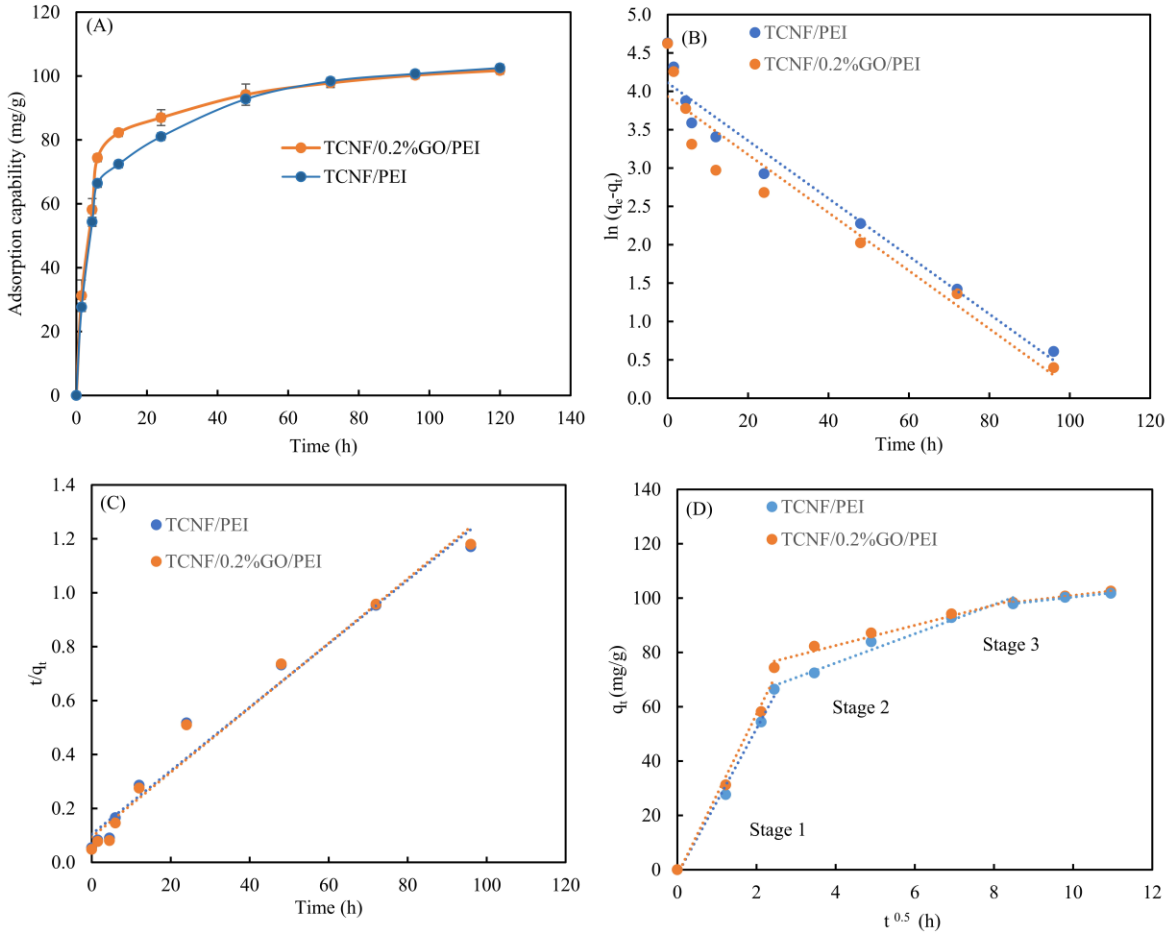

Figure 5-9. The Pseudo- first order (A), Pseudo- second order (B) and Intra-particle diffusion model (C) for adsorption kinetics of TEMPO-CNF/PEI hydrogel and TEMPO-CNF/0.2%GO/PEI hydrogel.

Table 5- 2. Parameters of Pseudo- first-order, Pseudo- second- order and Intra-particle diffusion model for adsorption kinetics.

Kinetic parameters	TCNF/PEI hydrogel	TCNF/0.2% GO/PEI hydrogel
$q_{e,\ exp}$ (mg/g)	102.5	101.7
Pseudo-first order		
qe (mg/g)	60.9284	50.9885
K_1 (mg/(g*h))	-0.0377	-0.0378
R^2	0.9591	0.9211
Pseudo-second order		
qe (mg/g)	84.7458	84.7458

K_2 (mg/(g*h))	0.0013	0.0013
R^2	0.9745	0.9745
Intraparticle diffusion model		
$k_{i,1}$ (mg/(g*h))	26.9	29.6
c_1	-1.8	-1.9
R_1^2	0.9918	0.9890
$k_{i,2}$ (mg/(g*h))	5.4	3.7
c_2	54.6	67.7
R_2^2	0.9785	0.9637
$k_{i,3}$ (mg/(g*h))	1.7	1.6
c_3	84.2	84.5
R_3^2	0.9992	0.9902

5.4.3.4 Adsorption isotherms

To obtain adsorption isotherms, dye concentrations were varied (**Fig. 5-10**). It was found that the adsorption capability of TCNF/PEI and TCNF/0.2% GO/PEI hydrogel had the same trend at the beginning, in which the adsorption capability increased linearly with the increase of methyl blue concentration, obtaining up to 1617 mg/g when methyl blue concentration was 3000 mg/L. After that concentration, the adsorption capability increased slowly for both, with TCNF/0.2% GO/PEI hydrogels showing higher adsorption capability than TCNF/PEI, up to 3551.8 and 3010.5 mg/g, respectively, at the maximum dye solubility (70 000 mg/L).

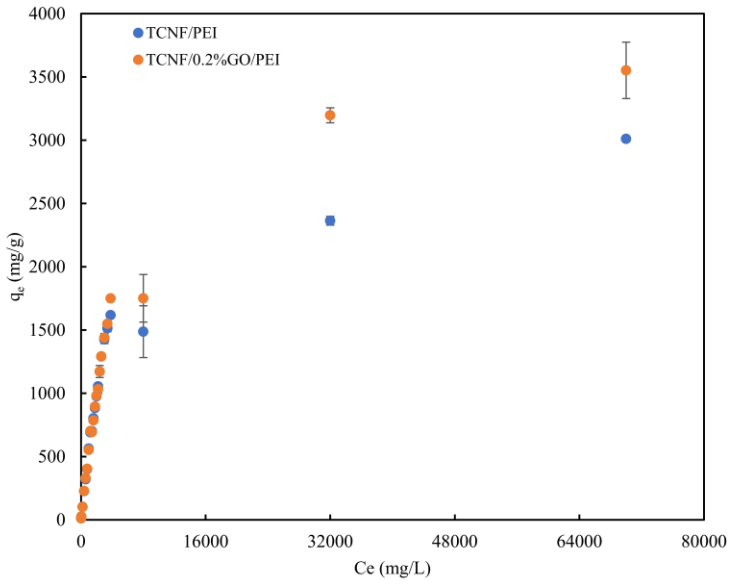

Figure 5-10. The adsorption efficiency change of TEMPO-CNF/0.2GO/PEI hydrogel over time.

The adsorption data were fitted into the linear and non-linear Langmuir and Freundlich models to determine mechanisms and model maximum capacities (**Fig. 5-11**). The parameters obtained from the fittings are summarized in **Table 5-3**. Compared with the non-linear model, the correlation coefficient R^2 values of linear Langmuir (0.9829, 0.9914; **Fig. 5-11 (A)**) and Freundlich (0.8955, 0.9192; **Fig. 5-11 (B)**) models were higher than that of the non-linear Langmuir model (0.9311, 0.9647; Fig. **5-11(C)**) and Freundlich (0.8377, 0.8972; **Fig. 5-11 (D)**) models for TCNF/PEI and TCNF/0.2% GO/PEI hydrogels, respectively. The R^2 of Langmuir models were higher than those of Freundlich models, suggesting that the homogenous monolayer adsorption was predominant [381]. The adsorption isotherm model agreed with the cellulose-PEI aerogel crosslinked by glutaraldehyde [28]. These similar results confirmed that the availability of amino groups was the determinant factor in the adsorption mechanism rather than the crosslinking process utilized.

Based on the above, linear Langmuir is the best to describe the adsorption behavior. The maximum adsorption capability predicted by the linear Langmuir model for TCNF/PEI and TCNF/0.2%

GO/PEI hydrogels were 3125.0 and 3846.2 mg/g, respectively. Confirming that adding GO can increase the maximum adsorption capability of TCNF/PEI hydrogels.

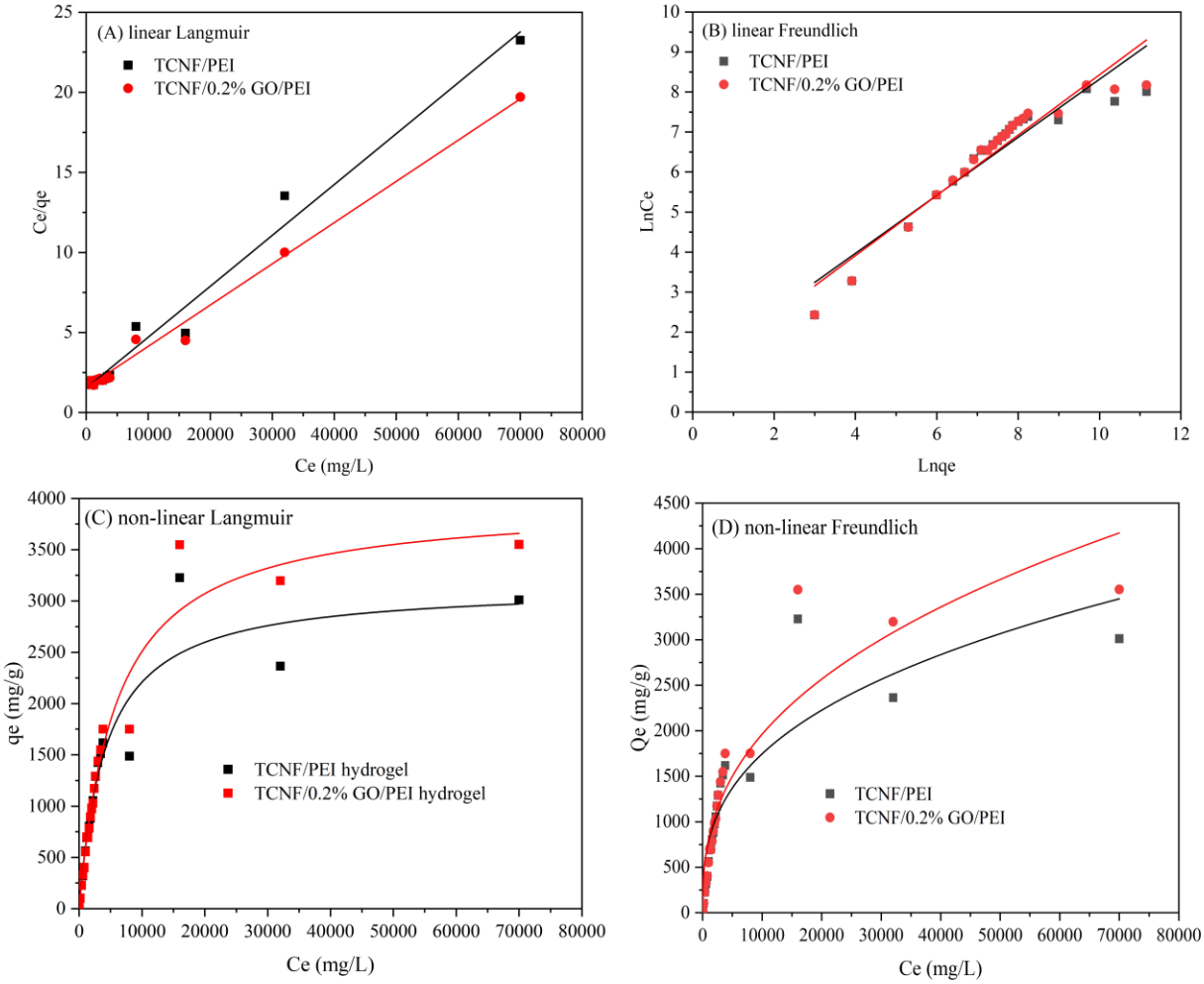

Figure 5-11. Adsorption data fitted to linear and non-linear Langmuir and Freundlich isotherm model.

Table 5-3. Langmuir and Freundlich constants of TEMPO-CNF/PEI and TEMPO-CNF/0.2% GO/PEI hydrogel for methyl blue adsorption.

Hydrogels	Adsorption isotherm		Equation	Model parameters	Statistics parameter
TCNF/PEI hydrogel	Linear model	Langmuir	$C_e/q_e = C_e/q_m + 1/(K_L * q_m)$	q_m=3125.0 mg/g, K_L=0.00021	R^2=0.9829
		Freundlich	$Lnq_e = LnK_F + (LnC_e)/n$	K_F=2.9084, n=1.3789	R^2=0.8955
	Non-linear model	Langmuir	$q_e = (q_m * K_L * C_e)/(1 + K_L * C_e)$	q_m=3151.6 mg/g, K_L=0.00023	R^2=0.9311
		Freundlich	$q_e = (q_m * K_L * C_e)/(1 + K_L * C_e)$	K_F=69.6226, n=2.8586	R^2=0.8377

TCNF/0.2%GO / PEI hydrogel	Linear model	Langmuir	$C_e/q_e = C_e/q_m + 1/(K_L * q_m)$	q_m=3846.2 mg/g, K_L=0.00017	R^2=0.9914
		Freundlich	$Lnq_e = LnK_F + (LnC_e)/n$	K_F=1.0937, n=1.1141	R^2=0.9192
	Non-linear model	Langmuir	$q_e = (q_m * K_L * C_e)/(1 + K_L * C_e)$	q_m=3962.2mg/g, K_L=0.00017	R^2=0.9647
		Freundlich	$q_e = (q_m * K_L * C_e)/(1 + K_L * C_e)$	K_F=55.0140, n=2.5773	R^2=0.8792

5.4.3.5 Adsorption for various pollutants

The adsorption capability for methylene blue (+), Cu (II) and soybean oil were tested to transfer those materials for various species of water pollutants. It was found that the adsorption capability for methylene blue (+) dyes did not change (**Fig. 5-12 (A)**). This result could be expected as the main driving mechanism would be the electrostatic interaction between carboxyl groups that are being occluded by the positively charged PEI on the surface.

Meanwhile, the adsorption capability for Cu (II) ions and soybean oil increased from 205.3 to 218.5 and 2.1 to 7.2 mg/g, respectively (**Fig. 5-12 (B) and (C)**). The increase in copper ion capturing is most likely due to higher PEI content that helps coordinate with the ions, while the soybean oil capturing would be driven by the interaction with the hydrophobic faces of the GO reduced into graphene after PEI functionalization.

Overall, these results confirmed that TCNF/GO/PEI hydrogel has a great potential for the removal of multiple pollutants from water resources.

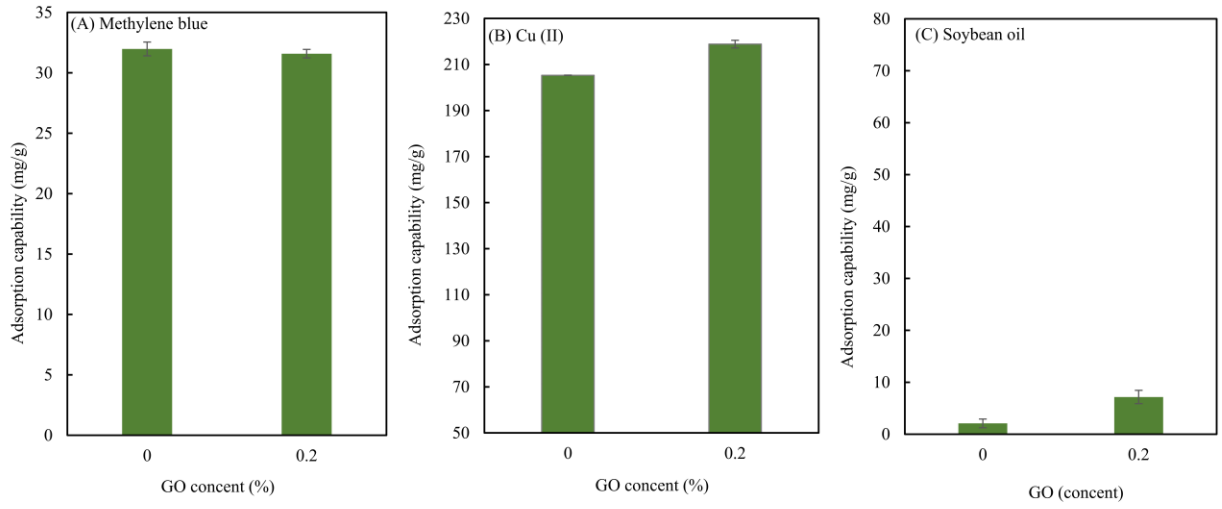

Figure 5-12. Adsorption capability (A, B and C) and efficiency (D, E and F) of TEMPO-CNF/PEI and TEMPO-CNF/0.2% GO/PEI hydrogel for Methylene blue (+) dyes at initial concentration of 200 mg/L with pH 5.7 after 24 h, Cu (II) ions and soybean oils, respectively.

5.4.4 Regeneration of TCNF/PEI hydrogel

5.5 Conclusion

A facile and cost-effective route to prepare TCNF/GO/PEI composite hydrogels was developed and reported herein. Compared with TCNF/ PEI hydrogel, TCNF/GO/PEI hydrogel presented lower surface energy, but higher surface area and the surface area increased with the increase of GO content. Besides, adding GO did not change the adsorption isotherm model and adsorption mechanism but increased the external diffusion rate of the Intra-particle diffusion model. Importantly, the adsorption capability of optimized TCNF/GO/PEI hydrogel for methyl blue (–) dye, Cu (II), soybean oils increased except for methylene blue (+) dye after addition of GO. These results indicate that TCNF/GO/PEI hydrogel has a great potential for the removal of multiple pollutants from water resources.

Chapter 6. The effect of nanocellulose particle size on its surface properties and adsorption behavior of toxic dyes

6.1 Abstract

With the development of nanocellulose-based adsorbents, effects related to particle size on the adsorption capability have been noted. However, no systematic research has been done, including the impact of surface properties. In this work, endoglucanase FiberCare® was used to decrease particle size in a controlled way, without changing the carboxyl group content for TEMPO-oxidized cellulose nanofibers (TCNFs). The obtained fibers were used to explore the effect of particle size on fibers' assembly and adsorption behavior of their formed hydrogel for toxic dyes. The results showed that the average fiber length changed significantly (decreased from 32.6 nm to 23.6 nm) after 12 h hydrolysis by endoglucanase FiberCare®, after that the average fiber length did not present significantly change (from 23.6 to 21.0 nm from 12 h to 24 h hydrolysis). The content of the carboxyl group remained constant after all digestion. Conversely, the zeta potential increased less than 5 mV after the average fiber length changed this range. The adsorption capability of formed TCNF hydrogel for cationic methylene blue increased by 13.1 mg/g and TCNF/PEI hydrogel for methyl blue anionic dyes increased by 8.6 mg/g after 24 h. Once fitted, no change for the adsorption mechanism was observed, there was an increase in the adsorption rate of first stage based on data fitted to pseudo-second- order kinetic model, and intra-particle diffusion model. Moreover, it was found that the dominant adsorption mechanism for the dyes was electrostatic attraction, taking up more than 90%, all other mechanisms, like hydrogen bonding, Van der Waals forces, hydrophobic interaction, π–π stacking etc. only corresponded to less than 10 %, which herein were quantified first time by design adsorption of dyes of the same and

opposite charge as the adsorbent. This mechanistic and systematic study then presents a step forward to develop and design cellulose-based sorbents for the emerging dye contamination.

6.2 Introduction

Dyes are widely used in various field, such as in textiles [451, 452], paper making [453], printing [454], cosmetics [455], food [456] and among other industries. The demand for dyes in all those fields is increasing with the rapid development of industries and technologies, over 10, 000 types of dyes are manufactured and more than 700, 000 tonnes of dyes are produced annual worldwide [457]. It is disheartening to know that around 10% of dyes used are discharged into our environment and water resources [457]. Most of these dyes are complex organic compounds, such as aromatic compounds, amines and traces of heavy metals with high toxicity, nonbiodegradable, and even carcinogenic and mutagenic, which cause the serious threats to environment and human health [458]. Hence, it is necessary to develop efficient technologies to remove the dyes from water resources. Various methods including Fenton oxidation, catalysis, photo-degradation, membrane filtration, adsorption and others have been established to eliminate dyes from wastewater [459]. Among those, adsorption has proved as a favorable one since it is cost-effective, ease to operate, repeatable and competitive for low concentration contaminants [459, 460]. Presently, research is focusing on searching low-cost and environmentally friendly adsorbents.

Over the last two decades, nanotechnology has incursion in almost all branches of science and technology, thus, likewise nanomaterials have been prepared and used for the removal of water pollutant [461]. The most used nanomaterials include carbon nanotubes (CNTs) [462, 463], graphene-based nanomaterials [464, 465], nano metal oxides [466, 467], nano zerovalent iron [468], cellulose nanomaterials [118] among others. Cellulose has the advantages of nontoxicity, a high yield (1011–1012 t/y) [183], and a high content of hydroxyl groups which are conducive to

further modification [184, 198]. When minimized into nano scale by hydrolysis or homogenization treatment, the specific surface area of nanocellulose obtained of cellulose increased dramatically from 1-4 m^2/g [469] to between 50 and 200 m^2/g [470], which lead to the increase of adsorption capability. However, the adsorption capacity of nanocellulose itself remains relatively low and needs to be improved by further modification [108, 118, 255]. Various modifications of nanocellulose and their effect on the adsorption capability have been widely studied with the most used modification being TEMPO-mediated oxidization [471]. TEMPO-oxidized CNCs (2.1 mmol/g carboxyl group) have be used to adsorb the cationic methylene blue dyes in an aqueous solution with an adsorption capacity up to 769 mg/g, which was 6.5-fold that of non-carboxylated CNCs (118 mg/g) [472]. The maximum adsorption capacities of other carboxylated CNF or CNC for methylene blue were between 100–200 mg/g [473-475]. Different adsorption capacities can mainly be attributed to different carboxyl contents. Besides, it also attributes to the reduction of particle size caused by oxidization, which is ignored in previous research. The reason is the introduction of carboxyl group and particle size reduction always happened at same time for the TEMPO-oxidization. The effect of particle size on the surface properties and adsorption performance of dyes should be explored to deeply understand and perfect the theory.

To this end, this work aimed to get different particle size of TEMPO-CNFs but keep the carboxyl group content constant by using enzymatic hydrolysis with FiberCare®. Then, the effect of particle size on the surface properties and adsorption behavior of toxic dyes was investigated. Methylene blue and methyl blue were chosen as representative of cationic and anionic dyes, respectively.

6.3 Materials and methods

6.3.1 Materials

CNF from bleached soybean hull fibers was produced at the Forest Products Development Center (Auburn, AL) by mechanical processing on a Masuko supermasscolloider (MKZA10-15J, Masuko Sangyo Co., Fiber, Japan). Polyethylenimine (branched, Mw = 25,000 g/mol) was purchased from Sigma-Aldrich. (2,2,6,6-Tetramethylpiperidin-1-yl) oxyl (TEMPO), methyl blue anionic (MB) dye was purchased from VWR, and the anhydrous copper (II) sulfate (98%) from Alfa Aesar. A commercial endoglucanase, FiberCare®, was complimentarily provided by Novozymes North America (Franklinton, NC, United States). Protein content of FiberCare® was assayed at 7.53 mg/mL.

6.3.2 TEMPO oxidation of CNF

TEMPO mediated oxidation of CNFs (TCNFs) was adapted from studies previously reported [27]. Briefly, 5 g of CNFs (dry mass basis) were suspended in 500 mL of distilled water containing TEMPO 0.08 g (0.1 mmol/g CNF) and NaBr 0.5 g (1 mmol/g CNF), and the pH was adjusted to 10 by addition of 0.5 M aq. NaOH. Then 30 mL of 12.5% aq. NaClO solution was added slowly to the CNF slurry (1.65 mL/10 min, total 3 h) and the reaction mixture was maintained at pH 10.5 at room temperature by adding aq. 0.5 M NaOH simultaneously. Furthermore, the oxidized CNFs were precipitated by adding ethanol (1500 mL) and then centrifuged at 3800 rpm. Finally, the oxidized CNFs were washed thoroughly with distilled water and filtered using a 0.20 μm cellulose acetate filter paper.

6.3.3 Preparation of different particle size TEMPO-CNF

2% TEMPO-CNF prepared in the 6.3.3 section treated by endoglucanase (FiberCare® loading in 0.4 mg protein/g TEMPO-CNF) in acetate buffer solution at pH 4.8 for 0, 12 h and 24 h respectively. Then, boil them for 5 minutes in a water bath to stop the reaction.

6.3.4 TCNFs hydrogel formation and functionalization with PEI

TCNF hydrogels were prepared by the dropwise addition of a 20 % wt. aq. $ZnCl_2$ solution along the walls of the glass tube into a 1.5% wt. aq. TCNF dispersion. The final zinc ion concentration was controlled to be 0.1 mol/L (0.35 mL of 20% $ZnCl_2$ solution). Then, the mixture was allowed to stand for 24 h without stirring to enable the formation of the nanocellulose hydrogels. Afterward, unbound Zn^{2+} ions were removed by rinsing the resulting hydrogels with 150 mL distilled water three times (Lu et al., 2020).

6.3.5 Characterization

6.3.5.1 Atomic force microscopy (AFM)

Surface characterization of the CNFs and TCNFs was performed using Tosca 400 equipment from Anton-Paar (Gratz, Austria). Surfaces were prepared by spin-coating (1.5×1.5 cm^2, with 150 µL of 0.01% liquid samples at 3000 rpm for 30 s). Height images were obtained by tapping mode with a NanoWorld (Neuchâtel, Switzerland) ARROW-NCR-20 silicon SPM-sensor cantilever with a resonance frequency of 285 kHz and constant force of 42 N/m; scan sizes were 5×5 μm^2. Processing of the images was done with Gwyddion software 2.49 (SourceForge) and roughness calculations were done with ProfilmOnline (KLA Corporation, Milpitas, CA, U.S.).

6.3.5.2 Carboxyl group titration

The carboxyl content of oxidized cellulose samples was determined by conductometric titrations. The method was modified on the basis of previous studies (Saito et al., 2009). Briefly, 30 mg (dry basis) of TCNF samples were suspended into 7.5 mL of 0.01 M HCl solution and adjusted to a pH of 2. After 2 h of stirring, the suspensions were titrated with 0.01 M NaOH.

6.3.5.3 Dynamic light scattering (DLS)

The Zeta potential for 0.1 % TCNF and PEI solutions were tested on a pH range from 2 to 12. All measurements were done in a Litesizer from Anton-Paar (Gratz, Austria). For all samples, twelve

repetitions were done and averaged.

6.3.5.4 Elemental analysis

Elemental analysis was performed on each sample using an elemental analyzer (Elementar vario MICRO, Ronkonkoma, NY, USA). 2 mg of freeze-dried sample were used for the test, and measurements were performed by triplicate.

6.3.5.5. Scanning electron microscopy (SEM)

Freeze-dried samples were set onto aluminum studs and sputtered with gold for 90 s in an EMS ×550 Sputter Coating Device from Science Services (Munich, Germany). Images with magnifications of ×50, ×100, and ×1000 were recorded in a Zeiss Evo 50VP SEM (Oberkochen, Germany).

6.3.6 Adsorption

0.0186 g of absorbent hydrogel were added to 10 mL 200 mg/L methylene blue or methylene blue solution with different pH values 3.7-9.7, 3.7-7.7, respectively to test the adsorption capability after 24 h and find out the best pH value for adsorption. Besides, the same mass of adsorbent was put in 200 mg/L methylene blue or methyl blue solution with their best PH condition, asliquots were taken at set time periods to obtain the concentration remining in solution. The adsorption data were then fitted to the pseudo-first order kinetic model, pseudo-second order kinetic model, and intra-particle diffusion model, using the equations presented below:

$$Ln(q_{e-}q_t) = Lnq_e + k_1\mathrm{t} \quad (3)$$

$$\frac{t}{q_t} = \frac{t}{k_2 q_e^2} + \frac{t}{q_e} \quad (4)$$

$$q_t = K_{id}t^{0.5} + \mathrm{c} \quad (5)$$

where k_1 and k_2 are the rate constants for the pseudo-first order adsorption and pseudo-second order adsorption kinetic models, respectively. K_{id} is the rate constant (g mg^{-1} min^{-1}) of intra-particle diffusion kinetics, c is intercept.

6.4 Results and discussion

6.4.1 The particle size distribution

The change of particle size was tested by AFM, as shown in **Fig. 6-1**. The average fiber length decreased from 32.6 nm to 23.6 nm, 21.0 nm after hydrolysis 12 and 24 h, respectively, which is agree with the previous research [476]. Turkey HSD Test indicate that the difference of average fiber length is significant between 0 h and 12 h, 0 h and 24 h hydrolysis, but not significant between 12 h and 24 h hydrolysis. This means that after 12 h hydrolysis, the particle size did not further change.

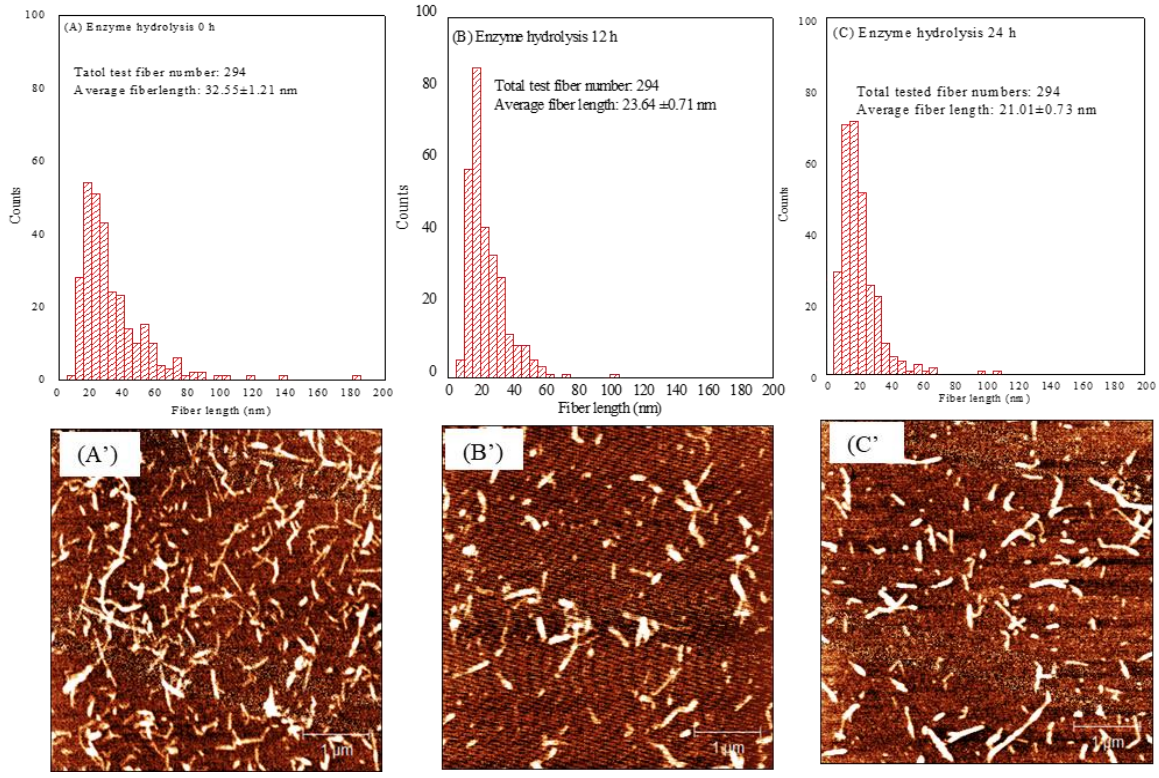

Figure 6-1. AFM analysis of the change of particle size after hydrolyzed by endoglucanase (FiberCare®) after (A) 0 h, (B) 12 h, and (C) 24.

Table 6-1. Average fiber length after hydrolysis 0 h, 12 h and 24 h, and the Turkey HSD test to compare the difference of Average fiber length change.

Treatment	Enzyme hydrolysis 0 h-A	Enzyme hydrolysis 12 h -B	Enzyme hydrolysis 24 h-C
Average fiber length (nm)	32.6±20.82	23.6±12.11	21.0±12.55
P-value	$P<0.05^{AB}$	$P=0.10^{BC}>0.05$	$P<0.05^{AC}$

6.4.2 The effect of particle size on surface properties of fibers

The change in carboxyl group content was tested after hydrolysis (in **Fig. 6-2** and **Table 6-1**). Results indicated that the carboxyl group did not change when the average fiber length decreased from 32.6 nm to 23.6 nm or 21.0 nm after hydrolysis 12 or 24 h. This is because enzymatic hydrolysis will not produce the new carboxyl group. This result is different from previous study, which found that the carboxyl group increased with the particle decrease (measured by DLS diameter) after passes through a pilot-scale homogenizer, which processing may produce some carboxyl group because of heating produced during the high pressure homogenizer processing [476].

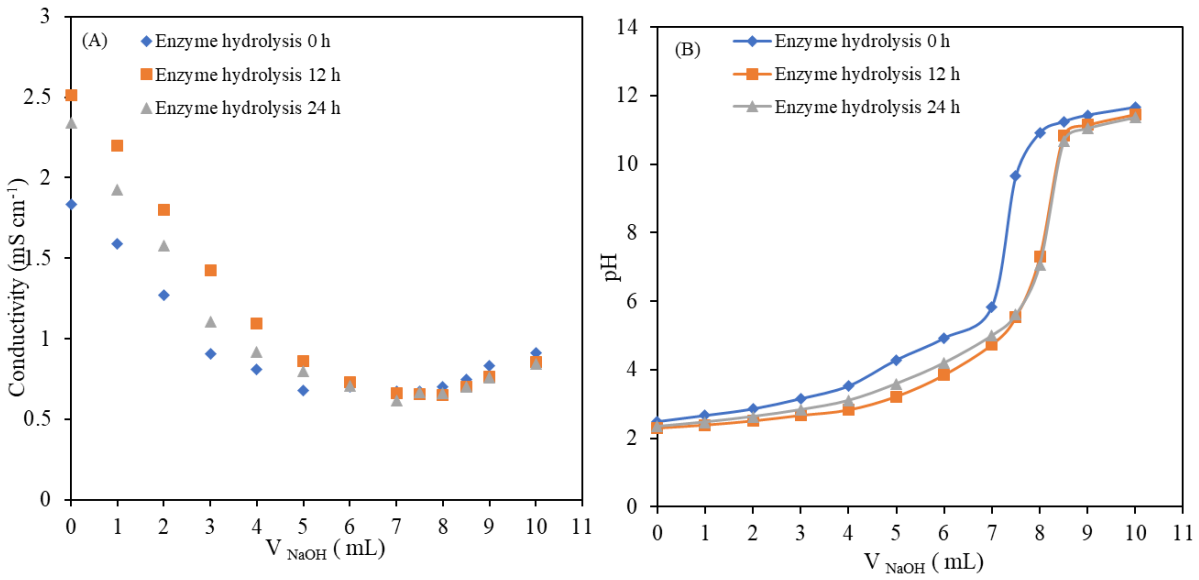

Figure 6-2. The carboxyl group test of samples after hydrolysis for 0-24 h by endoglucanase (FiberCare®).

Table 6-2. The carboxyl group test of samples after hydrolysis for 0-24 h by endoglucanase (FiberCare®).

Enzymatic hydrolysis	0 h	12 h	24 h
DO (%)	25.7	25.7	25.7
Carboxyl content (mmol/g)	1.5	1.5	1.5

The effect of particle size on the zeta potential was also tested (**Fig. 6-3**). The results showed that the zeta potential changes less than 5 mV (from -38.71 to –38.9 at pH 5.7, from -42.6 to -46.5 at pH 11.65) with the particle size change range after hydrolysis 12 and 24 h, respectively. This result is different from previous study, which found that the zeta potential increased more than 10 mV with the particles decrease (the zeta potential increase from -33.5 to -44.5 when DLS diameter decrease from 693 nm to 649 nm) [476]. This change may be due to the number of hydroxyl groups increase from particle size change is not enough to make the zeta potential change significantly in this work.

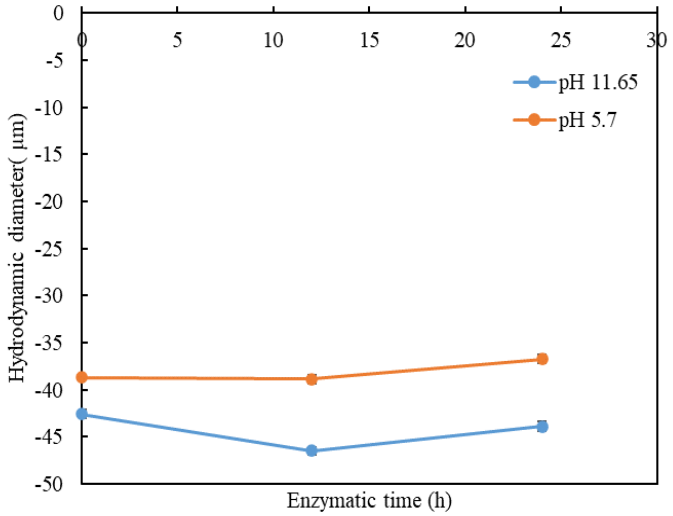

Figure 6-3. The zeta potential test of samples after hydrolysis for 0-24 h at pH 5.7 and 11.65 (the former is the pH of adsorption, and the latter is pH of PEI functionalization in the following section).

6.4.3 The effect of particle size on hydrogels surface properties

The carboxyl group was chelated by cationic zinc ions to form TCNF hydrogels, or these hydrogels were further functionalized by PEI for water remediation due to the fact that hydrogels are easy to separate, and reuse compared to nanoparticle-based powders. The Morphological properties of those hydrogels were observed by SEM, as shown in **Fig. 6-4**. Compared with TCNF hydrogel formed by non-enzymatic hydrolysis TCNFs, the hydrogels formed by TCNFs enzyme hydrolyzed after 12 h and 24 h looks more porous because the particle size decreases, which leads to an increase of surface area. There is no significant difference between 12 h and 24 h hydrolysis due to particle size change being not significant based on above. This was confirmed by surface area test in the following section.

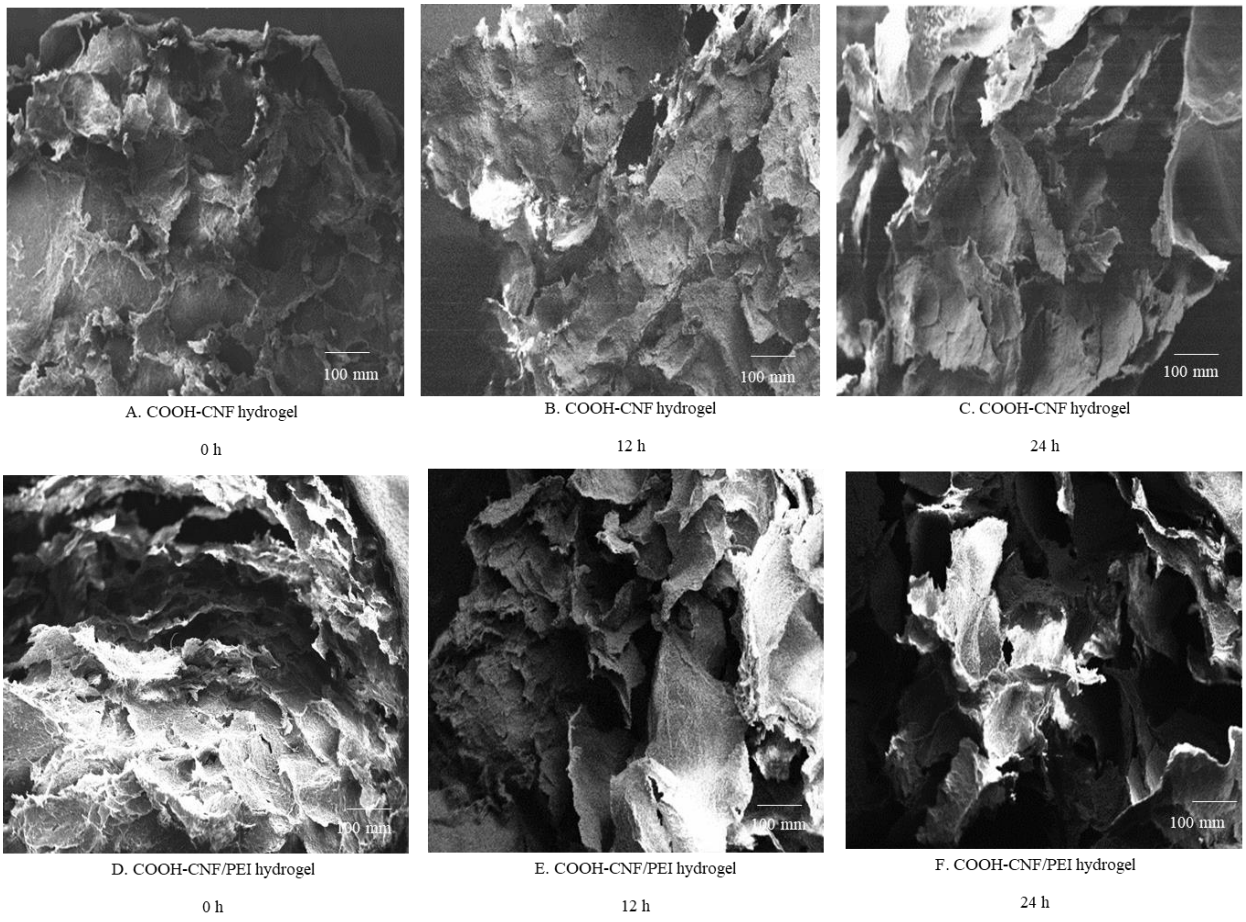

Figure 6-4. SEM images of hydrogel formed by different particle size of TCNF produced by enzymatic hydrolysis by endoglucanase (FiberCare®).

6.4.4 The effect of particle size on hydrogel adsorption behavior for toxic dyes

Carboxylate nanocellulose-based hydrogels usually used to adsorption methylene blue cationic dyes [473-475]. Here, the effect of particle size of TCNF on the adsorption capability of corresponding hydrogels at different pH values and adsorption kinetic of methylene dyes was investigated. As shown in **Fig. 6-5**, the adsorption capability increased significantly at all pH values, for example increased from 64.5 to 77.6 mg/g at pH 5.7 was measured (**Fig. 6-5 (A)**) (adsorption efficiency increased from 61.0 to 73.4%, **Fig. 6-5 (B)**) due to the average fiber length decreasing by 10 nm. After that, the adsorption capability and efficiency minimally increased as average fiber length did not change significantly. The best pH for methylene blue adsorption was 5.7.

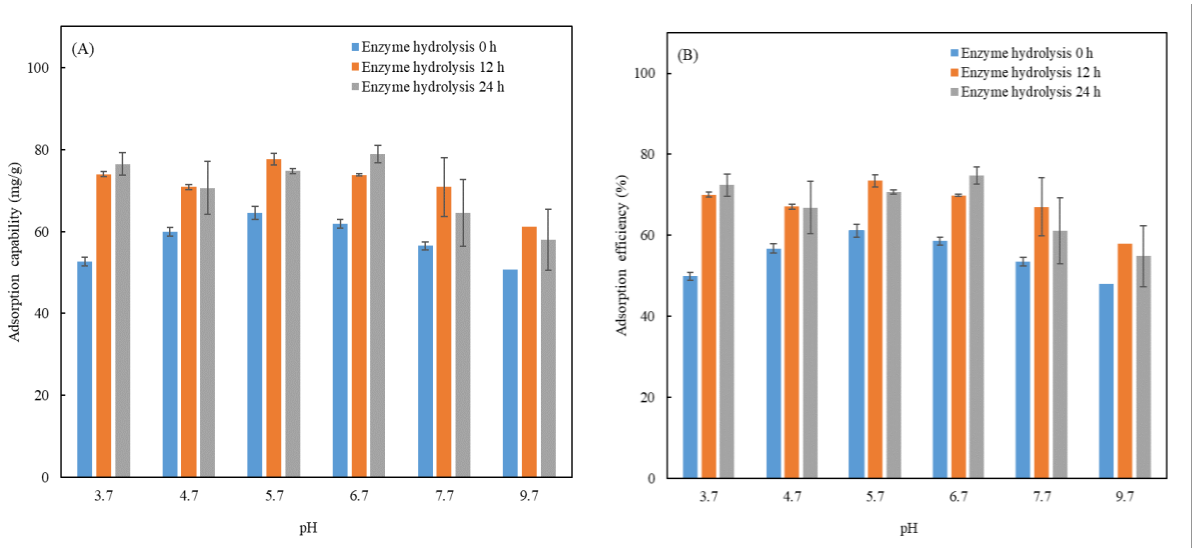

Figure 6-5. The effect of particle size on the adsorption capability (A) and adsorption efficiency (B) of TCNF hydrogels for methylene blue at different pH values after 24 h adsorption.

The adsorption kinetics was done at pH **5.7** with initial methylene blue concentration 200 mg/L **(Fig. 6-6 (A)**). The result showed that methylene blue adsorption equilibrium reached after 120 h and the hydrogels formed with the hydrolyzed for 12 or 24 h presented higher adsorption capability before adsorption equilibrium. Data were fitted to the pseudo-first-order and pseudo-second-order

model as well as intraparticle diffusion model **(Fig. 6-6 (B), (C) and (D)**). The fitting parameters are shown in **Table 6-3**. For all of the hydrogels formed by TCNFs with different particle size, the R^2 value of the pseudo-second-order model (R^2=0.9745) was higher than that of the pseudo-first order model (R2=0.9591), suggesting that chemisorption was the predominant mechanism of the removal process of dyes and the particle size did not change the adsorption mechanism. The slopes of the three stages were calculated from the intraparticle diffusion model and are summarized in **Table 6-3**. It is evident that Kid,1 > Kid,2 > Kid,3, suggesting the adsorption rate in the first stage was fastest. Supporting the previous discussion on external surface adsorption process, which being faster than intra-particle diffusion process. Interestingly, the TCNF hydrogels formed by smaller particle size has higher the Kid,1 (Kid,1 for hydrogels formed by TCNF with particle size 32.6 nm, 23.6 nm, and 21.0 nm), which indicates that decrease particle size leads to an increase in adsorption rate for external surface adsorption.

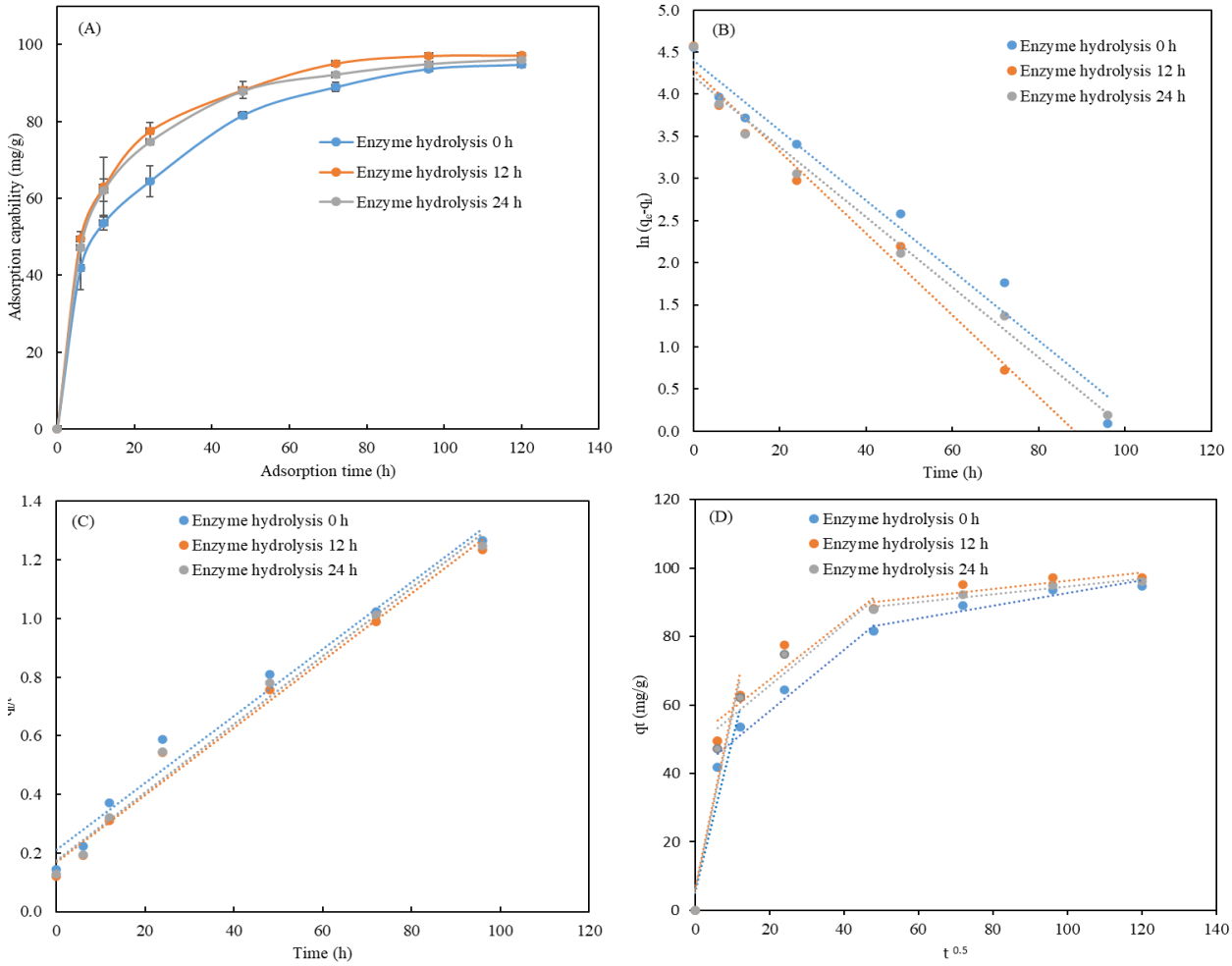

Figure 6-6. (A) The adsorption kinetic of TCNF hydrogel for methylene blue (+) dyes at pH 5.7 with initial methylene blue concentration is 200 mg/L. (B) Data fitted to pseudo-first-order kinetics model, (C) pseudo-second-order kinetics model, and (D) intraparticle diffusion model.

Table 6-3. Parameters extracted from the pseudo-first-order, pseudo-second-order, and Intra-particle diffusion models of TCNF hydrogel for methylene blue (+).

Kinetic parameters	Enzyme hydrolysis 0 h	Enzyme hydrolysis 12 h	Enzyme hydrolysis 24 h
$q_{e,exp}$ (mg/g)	94.8	97.2	96.1
Pseudo-first-order			
q_e,cal (mg/g)	81.4916	94.9452	67.5657
K_1 (mg/(g*h))	0.0416	0.0635	0.0418
R^2	0.9753	0.9774	0.9841
Pseudo-second-order			
q_e,cal (mg/g)	87.7193	86.95652	86.2069
K_2 (mg/(g*h))	0.00062	0.00078	0.00077
R^2	0.9782	0.9839	0.9839
Intraparticle diffusion model			
$k_{i,1}$ (mg/(g*h))	4.47	5.24	5.18
c_1	5.03	6.00	5.39
R_1^2	0.9047	0.9016	0.9172
$k_{i,2}$ (mg/(g*h))	0.89	0.86	0.89
c_2	40.3.	50.24	47.95
R_2^2	0.9637	0.8883	0.9049
$k_{i,3}$ (mg/(g*h))	0.184	0.1202	0.1141
c_3	74.33	84.338	83.162
R_3^2	0.9092	0.7754	0.9408

The effect of particle size of TCNF on the adsorption capability of corresponding hydrogels at different pH values and adsorption kinetic of methyl blue anionic dyes was also investigated, as shown in **Fig. 6-7**. The adsorption capability of difference particle size of TCNF hydrogels for the methyl blue dyes adsorption was less than 10 mg/g at the adsorption equilibrium point, which mainly from like hydrogen bonding, Van der Waals forces, hydrophobic interaction, π–π stacking etc. The adsorption capability from those interactions was so low and can almost be ignored.

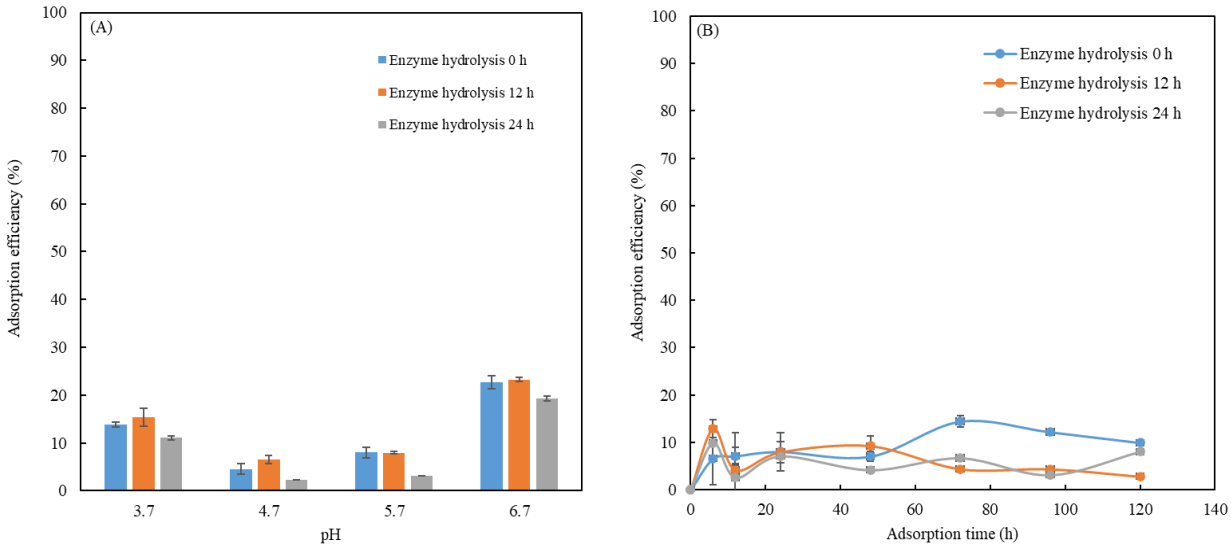

Figure 6-7. The effect of different particle sizes on adsorption capability of their TCNF hydrogel for methyl blue (-) dyes at different PH values (A) and with time change (B).

However, it has been reported that PEI functionalized nanocellulose based adsorbent has super adsorption capability for anionic dyes. In order to test the effect of different particle sizes on anionic dyes adsorption, TCNF hydrogels were further functionalized by PEI. Before test the methyl blue dyes adsorption, the effect of different particle sizes of TCNF on amount of PEI immobilization onto the TCNF surface were tested first, as shown in **Fig. 6-8.** The N content changed (from 13.72 % to 14.21% and 13.39%) after hydrolysis 12 h and 24 h with the average fiber length decreased from 32.6 nm to 23.6 nm and 21.0 nm.

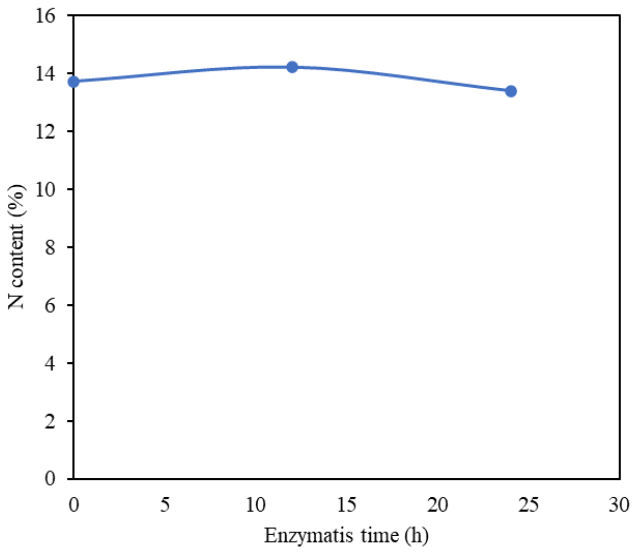

Figure 6-8. The effect of particle size on the PEI adsorption capability during the PEI functionalization processing (surface functionalization capability).

Then, adsorption kinetics were done at pH 5.7 with initial methyl blue concentration 200 mg/L (**Fig. 6-9 (A)**). The adsorption equilibrium reached after 120 h and TCNF/PEI hydrogels formed by TCNF hydrolyzed for 12 or 24 h presented higher adsorption capability before adsorption equilibrium. Data were fitted to the pseudo-first-order and pseudo-second-order model to predict the mechanism, as shown in **Fig. 6-9 (B) and (C)** and intraparticle diffusion model was also fitted to investigate the methylene diffusion rate in hydrogels **Fig. 6-9 (D)**. All the parameters were shown in **Table 6-4.** The R^2 value in the pseudo-second-order kinetics model was found to be higher than the pseudo-first-order kinetics model for all hydrogels independently of particle size. Besides, q_e,cal and q_e,exp values were found to be closer to each other in the pseudo-second-order kinetics model. As a result, the pseudo-second-order kinetics model is more suitable in adsorption studies for all hydrogels. Therefore, particle size was not a driving mechanism for the adsorption of methyl blue. These results were expected as the PEI content was similar between the hydrogels and results were similar to previous results.

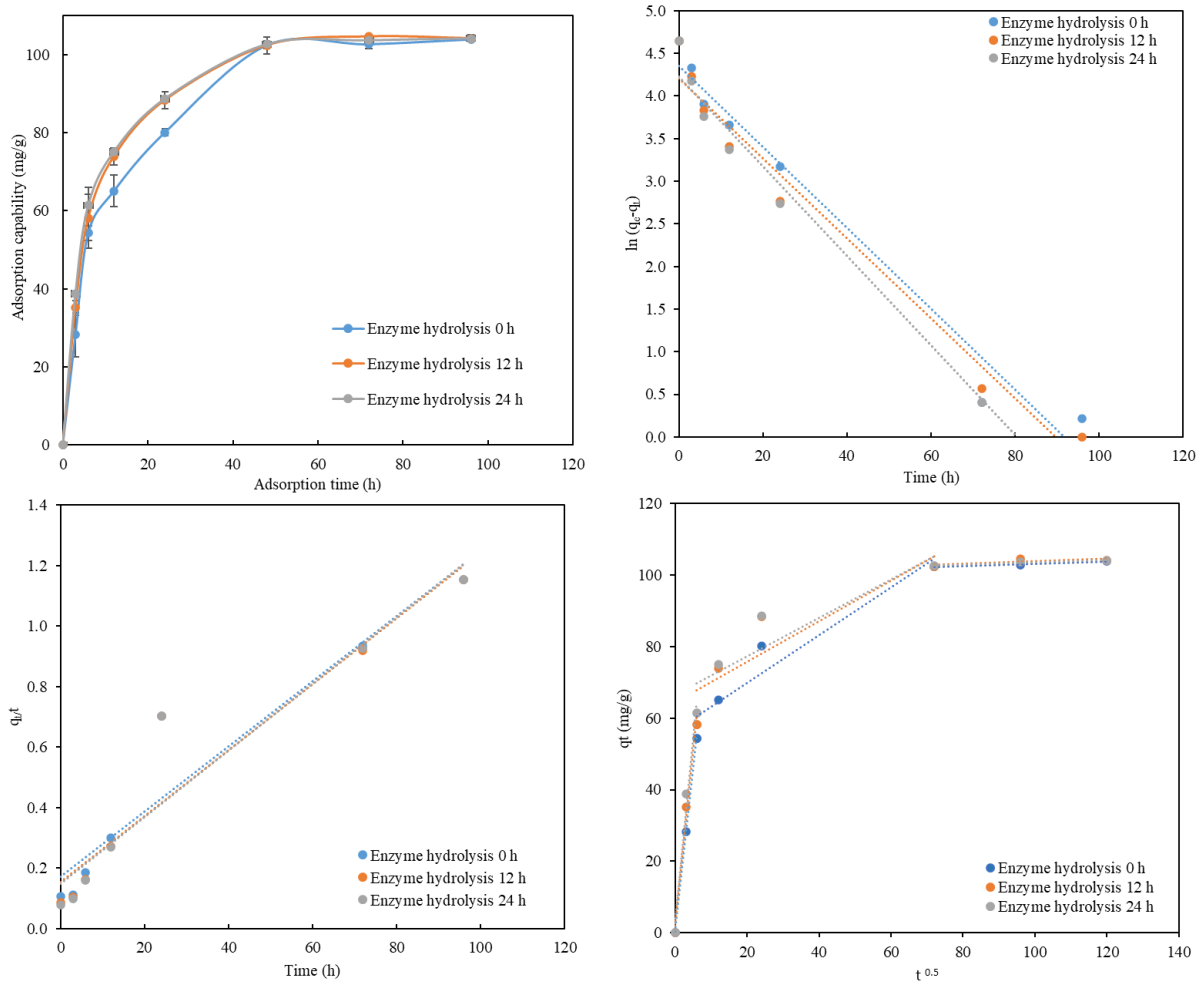

Figure 6-9. (A) The adsorption kinetic of TCNF/PEI hydrogel for methyl blue (-) dyes at pH 5.7 with initial methyl blue concentration is 200 mg/L. (B) pseudo-first-order kinetics model, (C) pseudo-second-order kinetics model, and (D) intraparticle diffusion model for methyl blue (-) adsorption.

Table 6-4. Parameters extracted from the pseudo- first- order, pseudo- second- order, and Intra-particle diffusion models of TCNF/PEI hydrogel for methyl blue (-) dyes adsorption.

Kinetic parameters	Enzyme hydrolysis 0 h	Enzyme hydrolysis 12h	Enzyme hydrolysis 24 h
$q_{e,exp}$ (mg/g)	104.0000	104.1000	104.1000
Pseudo-first-order			
qe (mg/g)	77.4088	67.2220	68.4908
K_1 (mg/(g*h))	0.0475	0.0470	0.0525
R^2	0.9706	0.9726	0.9863
Pseudo-second-order			
qe (mg/g)	92.5926	91.7431	90.9091
K_2 (mg/(g*h))	0.0007	0.0008	0.0008
R^2	0.9160	0.9113	0.9120
Intraparticle diffusion model			

$k_{i,1}$ (mg/(g*h))	9.0473	9.6918	10.2250
c_1	0.3718	2.0326	2.6894
R_1^2	0.9994	0.9856	0.9775
$k_{i,2}$ (mg/(g*h))	0.6694	0.5679	0.5373
c_2	56.3950	64.4670	66.5910
R_2^2	0.9929	0.8025	0.8234
$k_{i,3}$ (mg/(g*h))	0.0314	0.0369	0.0313
c_3	100.0300	100.1400	100.4300
R_3^2	0.8777	0.5650	0.9643

The effect of particle size of TCNF on the adsorption capability of corresponding TCNF/PEI hydrogels at different pH values and adsorption kinetic for methylene blue cationic dyes were also investigated, as shown in **Fig. 6-10**. The adsorption capability of all those TCNF/PEI hydrogels for the methylene blue dyes adsorption was less than 10 mg/g at the adsorption equilibrium point, which can almost be ignored because of the electrostatic repulsion force between the adsorbents and methyl blue dyes.

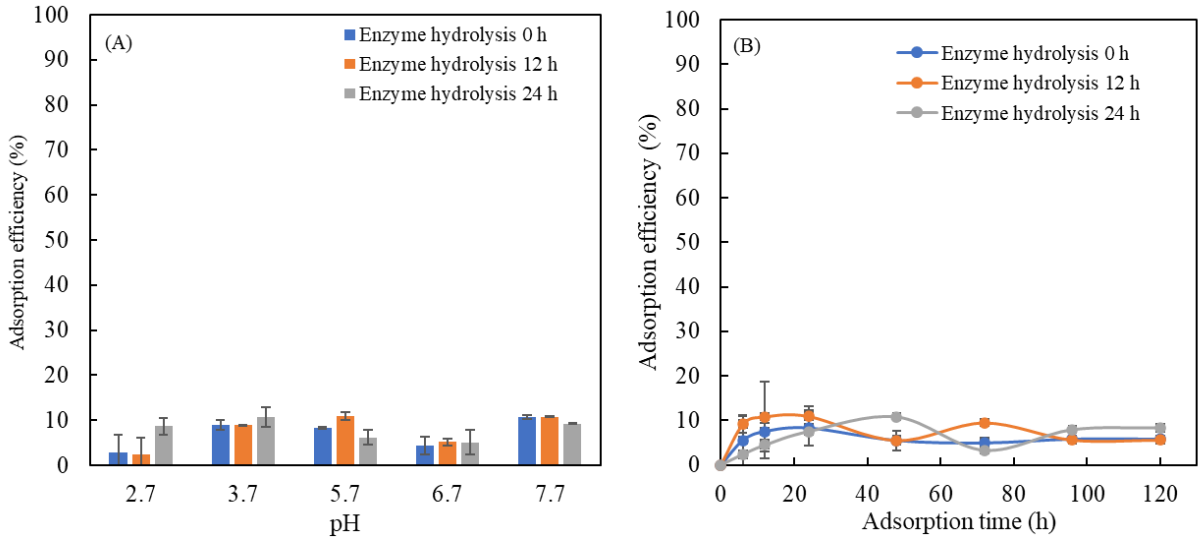

Figure 6-10. The effect of different particle size on adsorption capability of TCNF/PEI hydrogels for methylene blue (+) dyes at different PH values (A) and with time change (B).

6.4.5 Adsorption mechanism

Based on above, it was found that adsorption capability of TCNF hydrogels for methylene blue cationic dyes and TCNF/PEI hydrogel for methyl blue anionic dyes are much higher (94.8

and104.1 mg/g, respectively) than that of TCNF hydrogels for anionic methyl blue and TCNF/PEI hydrogel for methylene blue cationic dyes (less than 10 mg/g). This is due to the former the adsorption mainly caused by electrostatic attraction, the latter, the adsorption result from hydrogen bonding, van der Waals forces, hydrophobic interaction, π–π stacking etc. This is congruent with the dominant adsorption mechanism described for nanocellulose based adsorbents for toxic dyes [184, 477]. However, these studies did not give specific quantifications, which herein were quantified by design adsorption of dyes of the same and opposite charge as the adsorbent.

6.5 Conclusion

This work demonstrated that enzyme hydrolysis by endoglucanase FiberCare® is a viable alternative way to decrease the nanocellulose particle size without affecting surface charge. When the average fiber length decreases, their zeta potential and adsorption capability increased. What's more, the particle size decrease did not change the adsorption mechanism but increased the adsorption rate in the initial stage adsorption processing according to the adsorption kinetic model and intra-particle diffusion model. Moreover, the adsorption capability of the TCNF hydrogel and TCNF/PEI hydrogel for methyl blue and methylene blue with same charges with their surface, respectively were also tested, being less than 10 mg/g. Based on this, it was found that the dominant adsorption mechanism for the dyes is electrostatic attraction, taking up more than 90%, all other mechanisms, like hydrogen bonding, Van der Waals forces, hydrophobic interaction, π–π stacking etc. together just take up less than 10 %. This mechanistic and systematic study then presents a step forward to develop and design cellulose-based sorbents for the emerging dye contamination.

Chapter 7. Conclusions and future work

7.1 Conclusions

In summary, this dissertation successfully valorized soybean hulls into stable 3-D composites hydrogels by self-assembling mechanism for water remediation, solving the issues of second pollution and extra cost caused by traditional chemical cross-linkers strategy and powders adsorbents problems with poor separation and recyclability. In the following sections, the main findings and the future work of each project will be summarized separately.

In the first project, a stable TCNF/PEI composites hydrogel was synthesized by combination cationic chelation and physical adsorption. It was found that the concentration and pH of the PEI solutions utilized to functionalize the hydrogels can impact their composition and performance. The maximum N content was 14.8 % in synthesized TCNF/PEI hydrogels at the best functionalized conditions (the PEI concentration is 20% and pH 11.56). This hydrogel presented microporous structure and showed great potential for adsorption of methyl blue dyes and Cu (II) heavy metal ions (their adsorption efficiency got to 82.6% and 69.8%, respectively). Therefore, the first project provides a simple and cost-effective method to synthesis 3-D nanocellulose-based composites hydrogel as an adsorbent for water remediation.

In the second project, the interaction mechanisms between TCNF/PEI hydrogels and methyl blue dyes were investigated. It was found to be pH-dependent, resulting in dye removal by both adsorption and flocculation depending on pH of solution, which was mainly attributed to electrostatic interaction. Over the pH range of 3.7–5.7, most of the dyes were removed by adsorption. The maximum adsorption predicted by the Langmuir adsorption isotherm model was 3125 mg/g, which is higher than most of other materials. The adsorbent showed great reclcling

ability, withadsorption efficiency still above 82% after 4 cycles. Interestingly, these hydrogels also promoted the rapid precipitation of methyl blue dye in strong acidic conditions (pH 2.7). The structure of re-precipitated methyl blue dyes did not change during the precipitation process, indicating the possibility of recovering and reusing the dyes in related industries. Therefore, this project provides a promising strategy for the development of efficient, sustainable, and cost-effective nanocellulose-based adsorbents and flocculants for the removal and recovery of methyl blue dye from industries wastewater.

In the third project, GO was successfully introduced into TCNF/PEI hydrogel to form new stable TCNF/GO/PEI hydrogels by a combination of cationic chelation and physical adsorption to further increase the adsorption capability and target multiple water pollutants. A negative relation between GO content and surface energy was found, but a positive correlation between GO content and surface area was found. Moreover, adding GO increased the external diffusion rate and maximum adsorption capability. Based on the Langmuir adsorption model, the maximum adsorption capability for the methyl blue increased from 3125 to 3962 mg/g when 0.2% of GO was added at maximum methyl blue solubility (70,000 mg/L). The adsorption capability for Cu (II) ions and soybean oils increased from 205.3 to 218.5 mg/g and 2.1 to 7.2 mg/g, respectively. These results indicate that TCNF/GO/PEI hydrogel has great potential for the removal of multiple pollutants from water resources. This project not only provides a simple and cost-effective synthetic route to TCNF/GO/PEI hydrogels, but also offers valuable clues for the removal of multiple water pollutants.

In the last project, it was demonstrated that enzyme hydrolysis by endoglucanase FiberCare® is a good way to decrease the nanocellulose particle size without affecting the carboxyl group content

of TCNF. When the average fiber length decreases, their zeta potential and adsorption capability as well as the adsorption rate in the initial stage of adsorption processing increase. However, the particle size decrease did not change the adsorption mechanism. What's more, it was found that the dominant adsorption mechanism for the dyes is electrostatic attraction, taking up more than 90%, whereas, other mechanisms, such as hydrogen bonding, Van der Waals forces, hydrophobic interaction, π–π stacking etc. together just take up less than 10 %, which were quantified first time by design adsorption of dyes of the same and opposite charge as the adsorbent. This mechanistic and systematic study presents a step forward to develop and design cellulose-based sorbents for the emerging dye contamination.

7.2 Future work

Based on the findings, the following recommendations could be considered for future work.

1) It was found that low GO (<0.1%) content can increase the surface area of TCNF/PEI hydrogel, when the GO content continues to increase to 0.2%, the surface area decreases. However, the surface area of TCNG/GO/PEI hydrogel increased with the increase in GO content. The reason is not very clear. More concentration value should be tested and SEM analysis to observe the morphology property, which will be helpful to explain the reason.

2) The adsorption experiment was done in distilled water with single pollutants in this study. However, multiple pollutants usually exist in water resources. In order to facilitate large scale application and/or commercialization of this technology for simultaneous multiple pollutant adsorption, further adsorption should use real natural water samples and conditions instead of DI water to carry out all experiments.

3) In this dissertation, soybean hulls were used as the raw materials to extract CNFs and composited to nanocellulose-based hydrogels. In the future, other CNFs should also be tried to synthesize hydrogels to expand sources of raw materials and verify the generalizability of this study.

4) This dissertation highlighted the advantages of nanocellulose-based adsorbents for water remediation. Environmentally friendly and sustainability are the most important aspects. However, it was reported that PEI is potentially cytotoxic. Therefore, future work should focus on the pursuit of bio-based polymers that can replace PEI. Chitosan extracted from shells of shrimp and contains an abundance of amine group may be used to replace PEI to form the 3-D hydrogel by self-assembling mechanism for water remediation.

5) The adsorption capability of TCNF/GO/PEI hydrogel for oil spills is low. The future work should design a new cellulosed-based composite hydrogel or aerogels to improve the adsorption capability for multiple pollutants. Based on our preliminary test, TCNF aerogels synthesized by freezing and thawing method and freezing dry and then functionalized by gas deposited silane groups on the aerogel surface, which presented a great adsorption capability and regeneration capability for oil spills.

6) TCN/PEI and TCNF/GO/PEI hydrogels present pH sensitive in water and high adsorption capability for both anionic dyes and metal ions, which may be used for adsorption of other emerging pollutants or carbon capture or fertilizer release. Some preliminary studies have been done for carbon capture, which show great potential. More research will be done to expand their application scope.

References

[1] S.T. Weinman, E.K. Wujcik, A. Koh, M.R. Esfahani, H. Mokarizadeh, Polymer-Based Devices and Remediation Strategies for Emerging Contaminants in Water, ACS Applied Polymer Materials (3) (2021).

[2] M.B. Ahmed, J.L. Zhou, H.H. Ngo, W. Guo, N.S. Thomaidis, J. Xu, Progress in the biological and chemical treatment technologies for emerging contaminant removal from wastewater: A critical review, Journal of Hazardous Materials 323(pt.A) (2016) 274-298.

[3] Peng, Liu, Chuantao, Zhu, Aji, P., Mathew], Mechanically robust high flux graphene oxide - nanocellulose membranes for dye removal from water, Journal of Hazardous Materials (2019).

[4] D.R. Manenti, A.N. Módenes, P.A. Soares, F.R. Espinoza-Quiones, R.A.R. Boaventura, R. Bergamasco, V.J.P. Vilar, Assessment of a multistage system based on electrocoagulation, solar photo-Fenton and biological oxidation processes for real textile wastewater treatment, Chemical Engineering Journal 252(252) (2014) 120-130.

[5] A. Masmoudi, G. Zante, D. Trebouet, R. Barillon, M. Boltoeva, Solvent Extraction of Lithium Ions using Benzoyltrifluoroacetone in New Solvents, Separation and Purification Technology (2020).

[6] W.S. Koe, J.W. Lee, W.C. Chong, Y.L. Pang, L.C. Sim, An overview of photocatalytic degradation: photocatalysts, mechanisms, and development of photocatalytic membrane, Environmental Science and Pollution Research 27 (2020) 2522-2565.

[7] L. Jiang, Y. Zhang, M. Zhou, L. Liang, K. Li, Oxidation of Rhodamine B by persulfate activated with porous carbon aerogel through a non-radical mechanism, Journal of Hazardous Materials 358(SEP.15) (2018) 53.

[8] A.J. Auslin, A. Gnanaprakasam, V.M. Sivakumar, M. Thirumarimurugan, M. Ahamed, R.S. Azarudeen], Enhanced dye removal using polymeric nanocomposite through incorporation of Ag doped ZnO nanoparticles: Synthesis and characterization, Journal of Hazardous Materials (2019).

[9] I. Hussain, L. Yang, J. Qi, J. Li, L. Wang, Nitrogen-enriched carbon sheet for Methyl blue dye adsorption, Journal of Environmental Management 215(jun.1) (2018) 123.

[10] L. Yang, Y. Zhan, Y. Gong, E. Ren, S. Lin, Development of eco-friendly CO2-responsive cellulose nanofibril aerogels as "green" adsorbents for anionic dyes removal, Journal of Hazardous Materials 405 (2020) 124194.

[11] C. Zhu, Y. Xia, Y. Zai, Y. Dai, X. Liu, J. Bian, Y. Liu, J. Liu, G. Li, Adsorption and desorption behaviors of HPEI and thermoresponsive HPEI based gels on anionic and cationic dyes, Chemical Engineering Journal (2019).

[12] N. Mahfoudhi, S. Boufi, Nanocellulose as a novel nanostructured adsorbent for environmental remediation: a review, Cellulose 24(3) (2017) 1171-1197.

[13] H. Zhou, H. Zhu, X. Shi, L. Wang, S. Wang, Design of amphoteric bionic fibers by imitating spider silk for rapid and complete removal of low-level multiple heavy metal ions, Chemical Engineering Journal 412(20) (2021) 128670.

[14] L. Maiuolo, V. Algieri, F. Olivito, M.A. Tallarida, P. Costanzo, A. Jiritano, A.J.C. De Nino, Chronicle of Nanocelluloses (NCs) for Catalytic Applications: Key Advances, 11(1) (2021) 96.

[15] H. Kargarzadeh, I. Ahmad, S. Thomas, A. Dufresne, Handbook of Nanocellulose and Cellulose Nanocomposites, 2 Volume Set, 10.1002/9783527689972 (2017) 833-849.

[16] L. Riva, A. Fiorati, C. Punta, Synthesis and Application of Cellulose-Polyethyleneimine Composites and Nanocomposites: A Concise Review, Materials (Basel) 14(3) (2021).

[17] P. Lu, Y.L. Hsieh, Preparation and characterization of cellulose nanocrystals from rice straw, Carbohydr. Polym 87(1) (2012) 564-573.

[18] W. Zhang, Y. Zhang, C. Lu, Y. Deng, Aerogels from crosslinked cellulose nano/micro-fibrils and their fast shape recovery property in water, J. Mater. Chem. A 22(23) (2012) 11642-11650.

[19] J. Li, K. Zuo, W. Wu, Z. Xu, Y. Yi, Y. Jing, H. Dai, G. Fang, Shape memory aerogels from nanocellulose and polyethyleneimine as a novel adsorbent for removal of Cu(II) and Pb(II), Carbohydr Polym 196 (2018) 376-384.

[20] K. Missoum, M.N. Belgacem, J. Bras, Nanofibrillated cellulose surface modification: a review, Materials 6(5) (2013) 1745-1766.

[21] B. Aoudi, Y. Boluk, M.G. El-Din, Recent advances and future perspective on nanocellulose-based materials in diverse water treatment applications, Science of The Total Environment 843 (2022) 156903.

[22] P.L. Yap, M.J. Nine, K. Hassan, T.T. Tung, D.N.H. Tran, D. Losic, Graphene-Based Sorbents for Multipollutants Removal in Water: A Review of Recent Progress, Advanced Functional Materials 31(9) (2020).

[23] A. Fathima, S. Munirasu, Z. Jerina, B. Fawzi, A.H. Mohammad, Polyethylenimine modified graphene oxide hydrogel composite as an efficient adsorbent for heavy metal ions, Separation and Purification Technology 209 (2018) S1383586618312152-.

[24] Y. Chen, B. Pan, S. Zhang, H. Li, L. Lu, W.J.J.o.H.M. Zhang, Immobilization of polyethylenimine nanoclusters onto a cation exchange resin through self-crosslinking for selective Cu(II) removal, 190(1-3) (2011) 1037-1044.

[25] Shao, Zhengzhong, Huang, Yufang, Liu, Jie, Yao, Jinrong, Dihan, A.M.f.e. Chen %J Journal of Materials Chemistry, sustainability, Soy protein-based polyethylenimine hydrogel and its high selectivity for copper ion removal in wastewater treatment, 5(8) (2017) 4163-4171.

[26] L. Riva, A. Fiorati, C. Punta, materials Synthesis and Application of Cellulose-Polyethyleneimine Composites and Nanocomposites: A Concise Review, Materials 14(3) (2021) 473.

[27] X.Z. Tang, B. Yu, R.V. Hansen, X. Chen, X. Hu, J. Yang, Grafting Low Contents of Branched Polyethylenimine onto Carbon Fibers to Effectively Improve Their Interfacial Shear Strength with an Epoxy Matrix, Adv. Mater. Interfaces 2(12) (2015) 1-5.

[28] D.M. Guo, Q.D. An, L. Ran, Z.Y. Xiao, S.R. Zhai, Ultrahigh selective and efficient removal of anionic dyes by recyclable polyethylenimine-modified cellulose aerogels in batch and fixed-bed systems, Colloids Surf. A 555 (2018) 150-160.

[29] C. Zhang, J. Su, H. Zhu, J. Xiong, X. Liu, D. Li, Y. Chen, Y. Li, The removal of heavy metal ions from aqueous solutions by amine functionalized cellulose pretreated with microwave-H_2O_2, RSC Adv. 7 (2017) 34182-34191.

[30] E. Zeiger, B. Gollapudi, P. Spencer, Genetic toxicity and carcinogenicity studies of glutaraldehyde-a review, Mutat Res Rev Mutat Res 589(2) (2005) 136-151.

[31] P. Wexler, B.D. Anderson, ENCYCLOPEDIA OF TOXICOLOGY, 1 (2014).

[32] L. Melone, B. Rossi, N. Pastori, W. Panzeri, A. Mele, TEMPO-Oxidized Cellulose Cross-Linked with Branched Polyethyleneimine: Nanostructured Adsorbent Sponges for Water Remediation, ChemPlusChem 80(9) (2015) 1408-1415.

[33] L. Melone, A. Fiorati, G. Turco, A. Travan, E. Caneva, N. Pastori, M. Cametti, C. Punta, L. Melone, Mechanical and Drug Release Properties of Sponges from Cross-linked Cellulose Nanofibers, ChemPlusChem 82(6) (2017) 848-858.

[34] G. Paladini, V. Venuti, L. Almásy, L. Melone, V. Crupi, D. Majolino, N. Pastori, A. Fiorati, C. Punta, Cross-linked cellulose nano-sponges: a small angle neutron scattering (SANS) study, Cellulose 26(17) (2019) 9005-9019.

[35] G. Paladini, V. Venuti, V. Crupi, D. Majolino, C. Punta, FTIR-ATR analysis of the H-bond network of water in branched polyethyleneimine/TEMPO-oxidized cellulose nano-fiber xerogels, 27(15) (2020).

[36] L. Mo, H. Pang, Y. Tan, S. Zhang, J.J.C.E.J. Li, 3D multi-wall perforated nanocellulose-based polyethylenimine aerogels for ultrahigh efficient and reversible removal of Cu (II) ions from water, 378 (2019) 122157.

[37] Liu, Qiongzhen, Chen, Jiahui, Mei, Tao, He, Xiaowei, Zhong, A.M.f.e. Weibing %J Journal of Materials Chemistry, sustainability, A facile route to the production of polymeric nanofibrous aerogels for environmentally sustainable applications, (2018).

[38] H.J.C.E.J. Maleki, Recent advances in aerogels for environmental remediation applications: A review, 300 (2016) 98-118.

[39] P.L. Yap, M.J. Nine, K. Hassan, T.T. Tung, D.N. Tran, D.J.A.F.M. Losic, Graphene-based sorbents for multipollutants removal in water: a review of recent progress, 31(9) (2021) 2007356.

[40] M. Strokal, J.E. Spanier, C. Kroeze, A.A. Koelmans, M. Flörke, W. Franssen, N. Hofstra, S. Langan, T. Tang, M.T.J.C.o.i.e.s. van Vliet, Global multi-pollutant modelling of water quality: scientific challenges and future directions, 36 (2019) 116-125.

[41] R.P. Schwarzenbach, T. Egli, T.B. Hofstetter, U. Von Gunten, B. Wehrli, Global water pollution and human health, Annual review of environment and resources 35 (2010) 109-136.

[42] D.N. Chakkaravarthy, T. Balakrishnan, Water scarcity-challenging the future, International Journal of Agriculture, Environment and Biotechnology 12(3) (2019) 187-193.

[43] N. Martoredjo, Benny, D. Kusumajati, Increasing Environmental Awareness in Facing Water Scarcity Problems Through Education Based on Local Wisdom Values, International Conference on Energy Engineering and Environmental Engineering, Springer, 2022, pp. 177-185.

[44] R. Kumar, Emerging challenges of water scarcity in India: the way ahead, International Journal of Innovative Studies in Sociology and Humanities 4(4) (2019) 6-28.

[45] A. Ahamad, S. Madhav, A.K. Singh, A. Kumar, P. Singh, Types of water pollutants: Conventional and emerging, Sensors in water pollutants monitoring: Role of material (2020) 21-41.

[46] A. Azizullah, M.N.K. Khattak, P. Richter, D.-P. Häder, Water pollution in Pakistan and its impact on public health—a review, Environment international 37(2) (2011) 479-497.

[47] N. Akhtar, M.I. Syakir Ishak, S.A. Bhawani, K. Umar, Various natural and anthropogenic factors responsible for water quality degradation: A review, Water 13(19) (2021) 2660.

[48] M.N.F. Norrrahim, N.A.M. Kasim, V.F. Knight, M.S.M. Misenan, N. Janudin, N.A.A. Shah, N. Kasim, W.Y.W. Yusoff, S.A.M. Noor, S.H. Jamal, Nanocellulose: A bioadsorbent for chemical contaminant remediation, RSC advances 11(13) (2021) 7347-7368.

[49] S.A. Alrumman, A.F. El-kott, S. Keshk, Water pollution: Source and treatment, American Journal of Environmental Engineering 6(3) (2016) 88-98.

[50] M. Chaturvedi, A. Mishra, K. Sharma, G. Sharma, G. Saxena, A.K. Singh, Emerging contaminants in wastewater: sources of contamination, toxicity, and removal approaches, Emerging treatment technologies for waste management (2021) 103-132.

[51] P.R. Rout, T.C. Zhang, P. Bhunia, R.Y. Surampalli, Treatment technologies for emerging contaminants in wastewater treatment plants: A review, Science of the Total Environment 753 (2021) 141990.

[52] R. Kumar, M. Qureshi, D.K. Vishwakarma, N. Al-Ansari, A. Kuriqi, A. Elbeltagi, A. Saraswat, A review on emerging water contaminants and the application of sustainable removal technologies, Case Studies in Chemical and Environmental Engineering 6 (2022) 100219.

[53] G. Crini, E. Lichtfouse, Advantages and disadvantages of techniques used for wastewater treatment, Environmental Chemistry Letters 17 (2019) 145-155.

[54] A. Khazaie, M. Mazarji, B. Samali, D. Osborne, T. Minkina, S. Sushkova, S. Mandzhieva, A. Soldatov, A review on coagulation/flocculation in dewatering of coal slurry, Water 14(6) (2022) 918.

[55] B. Li, J. Zhao, W. Ge, W. Li, H. Yuan, Coagulation-flocculation performance and floc properties for microplastics removal by magnesium hydroxide and PAM, Journal of Environmental Chemical Engineering 10(2) (2022) 107263.

[56] J. Cevallos-Mendoza, C.G. Amorim, J.M. Rodríguez-Díaz, M.d.C.B. Montenegro, Removal of contaminants from water by membrane filtration: a review, Membranes 12(6) (2022) 570.

[57] H. Xiang, X. Min, C.-J. Tang, M. Sillanpää, F. Zhao, Recent advances in membrane filtration for heavy metal removal from wastewater: A mini review, Journal of Water Process Engineering 49 (2022) 103023.

[58] H.S. Jarusheh, A. Yusuf, F. Banat, M.A. Haija, G. Palmisano, Integrated photocatalytic technologies in water treatment using ferrites nanoparticles, Journal of Environmental Chemical Engineering (2022) 108204.

[59] A.H. Khan, N.A. Khan, S. Ahmed, A. Dhingra, C.P. Singh, S.U. Khan, A.A. Mohammadi, F. Changani, M. Yousefi, S. Alam, Application of advanced oxidation processes followed by different treatment technologies for hospital wastewater treatment, Journal of Cleaner Production 269 (2020) 122411.

[60] L. Goswami, R.V. Kumar, K. Pakshirajan, G. Pugazhenthi, A novel integrated biodegradation—microfiltration system for sustainable wastewater treatment and energy recovery, Journal of hazardous materials 365 (2019) 707-715.

[61] F. Mashkoor, A. Nasar, Magsorbents: Potential candidates in wastewater treatment technology–A review on the removal of methylene blue dye, Journal of magnetism and magnetic materials 500 (2020) 166408.

[62] M. Ksibi, Chemical oxidation with hydrogen peroxide for domestic wastewater treatment, Chemical Engineering Journal 119(2-3) (2006) 161-165.

[63] H. Ali, Biodegradation of synthetic dyes—a review, Water, Air, & Soil Pollution 213 (2010) 251-273.

[64] G.L. Dotto, G. McKay, Current scenario and challenges in adsorption for water treatment, Journal of environmental chemical engineering 8(4) (2020) 103988.

[65] R. Rashid, I. Shafiq, P. Akhter, M.J. Iqbal, M. Hussain, A state-of-the-art review on wastewater treatment techniques: the effectiveness of adsorption method, Environmental Science and Pollution Research 28 (2021) 9050-9066.

[66] J. Manchisi, E. Matinde, N.A. Rowson, M.J. Simmons, G.S. Simate, S. Ndlovu, B. Mwewa, Ironmaking and steelmaking slags as sustainable adsorbents for industrial effluents and wastewater treatment: a critical review of properties, performance, challenges and opportunities, Sustainability 12(5) (2020) 2118.

[67] C.Y. Teh, P.M. Budiman, K.P.Y. Shak, T.Y. Wu, Recent advancement of coagulation–flocculation and its application in wastewater treatment, Industrial & Engineering Chemistry Research 55(16) (2016) 4363-4389.

[68] Z. Yin, F. Yuan, M. Li, M. Xue, D. Zhou, Y. Chen, X. Liu, Y. Luo, Z. Hong, C. Xie, Self-cleaning, underwater writable, heat-insulated and photocatalytic cellulose membrane for high-efficient oil/water separation and removal of hazardous organic pollutants, Progress in Organic Coatings 157 (2021) 106311.

[69] I. Anil, S.T. Gunday, A. Bozkurt, O. Alagha, Design of crosslinked hydrogels comprising poly (Vinylphosphonic Acid) and bis [2-(Methacryloyloxy) Ethyl] phosphate as an efficient adsorbent for wastewater dye removal, Nanomaterials 10(1) (2020) 131.

[70] H. Sukmana, N. Bellahsen, F. Pantoja, C. Hodur, Adsorption and coagulation in wastewater treatment–Review, Progress in Agricultural Engineering Sciences 17(1) (2021) 49-68.

[71] N. Mahfoudhi, S. Boufi, Nanocellulose as a novel nanostructured adsorbent for environmental remediation: a review, Cellulose 24 (2017) 1171-1197.

[72] W.S. Chai, J.Y. Cheun, P.S. Kumar, M. Mubashir, Z. Majeed, F. Banat, S.H. Ho, P.L. Show, A review on conventional and novel materials towards heavy metal adsorption in wastewater treatment application, Journal of Cleaner Production 296 (2021).

[73] T.A. Saleh, Protocols for synthesis of nanomaterials, polymers, and green materials as adsorbents for water treatment technologies, Environmental Technology & Innovation 24 (2021).

[74] K. Gupta, P. Joshi, R. Gusain, O.P. Khatri, Recent advances in adsorptive removal of heavy metal and metalloid ions by metal oxide-based nanomaterials, Coordination Chemistry Reviews 445 (2021).

[75] R. Gusain, N. Kumar, S.S. Ray, Recent advances in carbon nanomaterial-based adsorbents for water purification, Coordination Chemistry Reviews 405 (2020).

[76] F. Ansari, L.A. Berglund, Toward Semistructural Cellulose Nanocomposites: The Need for Scalable Processing and Interface Tailoring, Biomacromolecules 19(7) (2018) 2341-2350.

[77] M. Nasrollahzadeh, M. Sajjadi, S. Iravani, R.S. Varma, Green-synthesized nanocatalysts and nanomaterials for water treatment: Current challenges and future perspectives, Journal of Hazardous Materials 401 (2021).

[78] F. Lu, D. Astruc, Nanocatalysts and other nanomaterials for water remediation from organic pollutants, Coordination Chemistry Reviews 408 (2020).

[79] M. Salman, S. Jahan, S. Kanwal, F. Mansoor, Recent advances in the application of silica nanostructures for highly improved water treatment: a review, Environmental Science and Pollution Research 26(21) (2019) 21065-21084.

[80] R.O.A. Rahman, A.M. El-Kamash, Y.T. Hung, Applications of Nano-Zeolite in Wastewater Treatment: An Overview, Water 14(2) (2022).

[81] J. Rivera-Utrilla, M. Sánchez-Polo, V. Gómez-Serrano, P. Álvarez, M. Alvim-Ferraz, J. Dias, Activated carbon modifications to enhance its water treatment applications. An overview, Journal of hazardous materials 187(1-3) (2011) 1-23.

[82] F. Farjadian, S. Abbaspour, M.A.A. Sadatlu, S. Mirkiani, A. Ghasemi, M. Hoseini-Ghahfarokhi, N. Mozaffari, M. Karimi, M.R. Hamblin, Recent developments in graphene and

graphene oxide: Properties, synthesis, and modifications: A review, ChemistrySelect 5(33) (2020) 10200-10219.

[83] S. Korkmaz, İ.A. Kariper, Graphene and graphene oxide based aerogels: Synthesis, characteristics and supercapacitor applications, Journal of Energy Storage 27 (2020) 101038.

[84] K. Thakur, B. Kandasubramanian, Graphene and graphene oxide-based composites for removal of organic pollutants: a review, Journal of Chemical & Engineering Data 64(3) (2019) 833-867.

[85] Z. Chen, K.O. Kirlikovali, P. Li, O.K. Farha, Reticular chemistry for highly porous metal–organic frameworks: The chemistry and applications, Accounts of chemical research 55(4) (2022) 579-591.

[86] S.A. Jadhav, H.B. Garud, A.H. Patil, G.D. Patil, C.R. Patil, T.D. Dongale, P.S. Patil, Recent advancements in silica nanoparticles based technologies for removal of dyes from water, Colloid and Interface Science Communications 30 (2019) 100181.

[87] R.K. Kankala, Y.H. Han, J. Na, C.H. Lee, Z. Sun, S.B. Wang, T. Kimura, Y.S. Ok, Y. Yamauchi, A.Z. Chen, Nanoarchitectured structure and surface biofunctionality of mesoporous silica nanoparticles, Advanced materials 32(23) (2020) 1907035.

[88] P.G. Jeelani, P. Mulay, R. Venkat, C. Ramalingam, Multifaceted application of silica nanoparticles. A review, Silicon 12 (2020) 1337-1354.

[89] R.O.A. Rahman, A.M. El-Kamash, Y.-T. Hung, Applications of nano-zeolite in wastewater treatment: An overview, Water 14(2) (2022) 137.

[90] Z. Zhou, Synthesis of Functionalized Nano Zeolite and Zeolitic Imidazolate Framework Crystals.

[91] S. Mintova, J. Grand, V. Valtchev, Nanosized zeolites: quo vadis?, Comptes Rendus Chimie 19(1-2) (2016) 183-191.

[92] A. Palčić, S. Moldovan, H. El Siblani, A. Vicente, V. Valtchev, Defect sites in zeolites: origin and healing, Advanced Science 9(4) (2022) 2104414.

[93] A.O. Ibrahim, K.A. Adegoke, R.O. Adegoke, Y.A. AbdulWahab, V.B. Oyelami, M.O. Adesina, Adsorptive removal of different pollutants using metal-organic framework adsorbents, Journal of Molecular Liquids 333 (2021) 115593.

[94] A. Bhatnagar, M. Sillanpää, A. Witek-Krowiak, Agricultural waste peels as versatile biomass for water purification–A review, Chemical engineering journal 270 (2015) 244-271.

[95] I. Petreanu, V.-C. Niculescu, S. Enache, C. Iacob, M. Teodorescu, Structural Characterization of Silica and Amino-Silica Nanoparticles by Fourier Transform Infrared (FTIR) and Raman Spectroscopy, Analytical Letters 56(2) (2023) 390-403.

[96] N. Abid, A.M. Khan, S. Shujait, K. Chaudhary, M. Ikram, M. Imran, J. Haider, M. Khan, Q. Khan, M. Maqbool, Synthesis of nanomaterials using various top-down and bottom-up approaches, influencing factors, advantages, and disadvantages: A review, Advances in Colloid and Interface Science 300 (2022) 102597.

[97] S. Velusamy, A. Roy, S. Sundaram, T. Kumar Mallick, A review on heavy metal ions and containing dyes removal through graphene oxide-based adsorption strategies for textile wastewater treatment, The Chemical Record 21(7) (2021) 1570-1610.

[98] I. Ahmed, S.H. Jhung, Applications of metal-organic frameworks in adsorption/separation processes via hydrogen bonding interactions, Chemical Engineering Journal 310 (2017) 197-215.

[99] P. Kaur, N. Sharma, M. Munagala, R. Rajkhowa, B. Aallardyce, Y. Shastri, R. Agrawal, Nanocellulose: resources, physio-chemical properties, current uses and future applications, Frontiers in Nanotechnology 3 (2021) 747329.

[100] X. Yang, L.A. Berglund, Structural and Ecofriendly Holocellulose Materials from Wood: Microscale Fibers and Nanoscale Fibrils, Advanced Materials 33(28) (2021).

[101] V.A. Barbash, O.V. Yashchenko, Preparation and application of nanocellulose from non-wood plants to improve the quality of paper and cardboard, Applied Nanoscience 10(8) (2020) 2705-2716.

[102] A. Mihranyan, Cellulose from cladophorales green algae: From environmental problem to high-tech composite materials, Journal of Applied Polymer Science 119(4) (2011) 2449-2460.

[103] H. El-Saied, A.H. Basta, R.H. Gobran, Research progress in friendly environmental technology for the production of cellulose products (bacterial cellulose and its application), Polymer-Plastics Technology and Engineering 43(3) (2004) 797-820.

[104] I. Siró, D. Plackett, Microfibrillated cellulose and new nanocomposite materials: a review, Cellulose 17 (2010) 459-494.

[105] P. Lokhande, P.P. Singh, D.-V.N. Vo, D. Kumar, K. Balasubramanian, A. Mubayi, A. Srivastava, A. Sharma, Bacterial nanocellulose: Green polymer materials for high performance energy storage applications, Journal of Environmental Chemical Engineering 10(5) (2022) 108176.

[106] U. Römling, M.Y. Galperin, Bacterial cellulose biosynthesis: diversity of operons, subunits, products, and functions, Trends in microbiology 23(9) (2015) 545-557.

[107] T. Saito, R. Kuramae, J. Wohlert, L.A. Berglund, A. Isogai, An ultrastrong nanofibrillar biomaterial: the strength of single cellulose nanofibrils revealed via sonication-induced fragmentation, Biomacromolecules 14(1) (2013) 248-253.

[108] M. Ghasemlou, F. Daver, E.P. Ivanova, Y. Habibi, B. Adhikari, Surface modifications of nanocellulose: From synthesis to high-performance nanocomposites, Progress in Polymer Science 119 (2021) 101418.

[109] L. Solhi, V. Guccini, K. Heise, I. Solala, E. Niinivaara, W. Xu, K. Mihhels, M. Kröger, Z. Meng, J. Wohlert, Understanding Nanocellulose–Water Interactions: Turning a Detriment into an Asset, Chemical reviews 123(5) (2023) 1925-2015.

[110] C. Jiang, M. Wu, F. Zhang, C. Liu, M. Sun, B. Li, All-Tunicate Cellulose Film with Good Light Management Properties for High-Efficiency Organic Solar Cells, Nanomaterials 13(7) (2023) 1221.

[111] T. Li, C. Chen, A.H. Brozena, J. Zhu, L. Xu, C. Driemeier, J. Dai, O.J. Rojas, A. Isogai, L. Wågberg, Developing fibrillated cellulose as a sustainable technological material, Nature 590(7844) (2021) 47-56.

[112] A. Paajanen, S. Ceccherini, T. Maloney, J.A. Ketoja, Chirality and bound water in the hierarchical cellulose structure, Cellulose 26 (2019) 5877-5892.

[113] V.A. Lovikka, L. Rautkari, T.C. Maloney, Changes in the hygroscopic behavior of cellulose due to variations in relative humidity, Cellulose 25 (2018) 87-104.

[114] A. Isogai, Development of completely dispersed cellulose nanofibers, Proceedings of the Japan Academy, Series B 94(4) (2018) 161-179.

[115] R. Mohammadinejad, S. Karimi, S. Iravani, R.S. Varma, Plant-derived nanostructures: types and applications, Green Chemistry 18(1) (2016) 20-52.

[116] Y. Chen, L. Zhang, Y. Yang, B. Pang, W. Xu, G. Duan, S. Jiang, K. Zhang, Recent progress on nanocellulose aerogels: Preparation, modification, composite fabrication, applications, Advanced Materials 33(11) (2021) 2005569.

[117] M.Y. Khalid, A. Al Rashid, Z.U. Arif, W. Ahmed, H. Arshad, Recent advances in nanocellulose-based different biomaterials: types, properties, and emerging applications, Journal of Materials Research and Technology 14 (2021) 2601-2623.

[118] A. Shahzad, M.W. Ullah, J. Ali, K. Aziz, M.A. Javed, Z. Shi, S. Manan, M. Ul-Islam, M. Nazar, G. Yang, The versatility of nanocellulose, modification strategies, and its current progress in wastewater treatment and environmental remediation, Science of The Total Environment 858 (2023) 159937.

[119] P. Phanthong, P. Reubroycharoen, X. Hao, G. Xu, A. Abudula, G. Guan, Nanocellulose: Extraction and application, Carbon Resources Conversion 1(1) (2018) 32-43.

[120] J.D.P. de Amorim, K.C. de Souza, C.R. Duarte, I. da Silva Duarte, F. de Assis Sales Ribeiro, G.S. Silva, P.M.A. de Farias, A. Stingl, A.F.S. Costa, G.M. Vinhas, Plant and bacterial nanocellulose: Production, properties and applications in medicine, food, cosmetics, electronics and engineering. A review, Environmental Chemistry Letters 18 (2020) 851-869.

[121] R. Reshmy, D. Thomas, E. Philip, S.A. Paul, A. Madhavan, R. Sindhu, P. Binod, A. Pugazhendhi, R. Sirohi, A. Tarafdar, Potential of nanocellulose for wastewater treatment, Chemosphere 281 (2021) 130738.

[122] S. Kalia, S. Boufi, A. Celli, S. Kango, Nanofibrillated cellulose: surface modification and potential applications, Colloid and Polymer Science 292 (2014) 5-31.

[123] A.W. Carpenter, C.-F. de Lannoy, M.R. Wiesner, Cellulose nanomaterials in water treatment technologies, Environmental science & technology 49(9) (2015) 5277-5287.

[124] A. Guo, Z. Sun, N. Sathitsuksanoh, H. Feng, A review on the application of nanocellulose in cementitious materials, Nanomaterials 10(12) (2020) 2476.

[125] N. Pandi, S.H. Sonawane, K.A. Kishore, Synthesis of cellulose nanocrystals (CNCs) from cotton using ultrasound-assisted acid hydrolysis, Ultrasonics sonochemistry 70 (2021) 105353.

[126] O. Nechyporchuk, M.N. Belgacem, J. Bras, Production of cellulose nanofibrils: A review of recent advances, Industrial Crops and Products 93 (2016) 2-25.

[127] H.A. Khalil, Y. Davoudpour, M.N. Islam, A. Mustapha, K. Sudesh, R. Dungani, M. Jawaid, Production and modification of nanofibrillated cellulose using various mechanical processes: a review, Carbohydrate polymers 99 (2014) 649-665.

[128] M. Jonoobi, R. Oladi, Y. Davoudpour, K. Oksman, A. Dufresne, Y. Hamzeh, R. Davoodi, Different preparation methods and properties of nanostructured cellulose from various natural resources and residues: a review, Cellulose 22 (2015) 935-969.

[129] Ø. Eriksen, K. Syverud, Ø. Gregersen, The use of microfibrillated cellulose produced from kraft pulp as strength enhancer in TMP paper, Nordic Pulp & Paper Research Journal 23(3) (2008) 299-304.

[130] H. Du, Sustainable Preparation of Cellulose Nanofibrils and Their Applications for Multifunctional Nanocomposites, (2021).

[131] O. Nechyporchuk, F. Pignon, M.N. Belgacem, Morphological properties of nanofibrillated cellulose produced using wet grinding as an ultimate fibrillation process, Journal of Materials Science 50 (2015) 531-541.

[132] M. Henriksson, G. Henriksson, L. Berglund, T. Lindström, An environmentally friendly method for enzyme-assisted preparation of microfibrillated cellulose (MFC) nanofibers, European polymer journal 43(8) (2007) 3434-3441.

[133] M. Bäckström, S. Bolivar, J. Paltakari, Effect of ionic form of fibrillation and the development of the fibre network strength during the refining of the kraft pulps, O´ Papel 73(7) (2012) 57-65.

[134] S. Coseri, G. Biliuta, B.C. Simionescu, K. Stana-Kleinschek, V. Ribitsch, V. Harabagiu, Oxidized cellulose—Survey of the most recent achievements, Carbohydrate polymers 93(1) (2013) 207-215.

[135] J.A. Sirvio, A. Kolehmainen, M. Visanko, H. Liimatainen, J. Niinimaki, O.E. Hormi, Strong, self-standing oxygen barrier films from nanocelluloses modified with regioselective oxidative treatments, ACS Applied Materials & Interfaces 6(16) (2014) 14384-14390.

[136] H. Liimatainen, M. Visanko, J. Sirviö, O. Hormi, J. Niinimäki, Sulfonated cellulose nanofibrils obtained from wood pulp through regioselective oxidative bisulfite pre-treatment, Cellulose 20 (2013) 741-749.

[137] T. Heinze, A. Koschella, Carboxymethyl ethers of cellulose and starch–a review, Macromolecular Symposia, Wiley Online Library, 2005, pp. 13-40.

[138] L. Wågberg, G. Decher, M. Norgren, T. Lindström, M. Ankerfors, K. Axnäs, The build-up of polyelectrolyte multilayers of microfibrillated cellulose and cationic polyelectrolytes, Langmuir 24(3) (2008) 784-795.

[139] I. Siró, D. Plackett, M. Hedenqvist, M. Ankerfors, T. Lindström, Highly transparent films from carboxymethylated microfibrillated cellulose: the effect of multiple homogenization steps on key properties, Journal of Applied Polymer Science 119(5) (2011) 2652-2660.

[140] Y. Song, Y. Sun, X. Zhang, J. Zhou, L. Zhang, Homogeneous quaternization of cellulose in NaOH/urea aqueous solutions as gene carriers, Biomacromolecules 9(8) (2008) 2259-2264.

[141] C. Aulin, E. Johansson, L. Wågberg, T. Lindström, Self-organized films from cellulose I nanofibrils using the layer-by-layer technique, Biomacromolecules 11(4) (2010) 872-882.

[142] C.J. Chirayil, L. Mathew, S. Thomas, REVIEW OF RECENT RESEARCH IN NANO CELLULOSE PREPARATION FROM DIFFERENT LIGNOCELLULOSIC FIBERS, Reviews on advanced materials science 37 (2014).

[143] A. Chaker, S. Boufi, Cationic nanofibrillar cellulose with high antibacterial properties, Carbohydrate polymers 131 (2015) 224-232.

[144] Z.A. Al-Ahmed, A.A. Hassan, S.M. El-Khouly, S.E. El-Shafey, TEMPO-oxidized cellulose nanofibers/TiO 2 nanocomposite as new adsorbent for Brilliant Blue dye removal, Polymer Bulletin 77 (2020) 6213-6226.

[145] B. Sun, M. Zhang, Q. Hou, R. Liu, T. Wu, C. Si, Further characterization of cellulose nanocrystal (CNC) preparation from sulfuric acid hydrolysis of cotton fibers, Cellulose 23 (2016) 439-450.

[146] S.L. Leong, S.I.X. Tiong, S.P. Siva, F. Ahamed, C.-H. Chan, C.L. Lee, I.M.L. Chew, Y.K. Ho, Morphological control of cellulose nanocrystals via sulfuric acid hydrolysis based on sustainability considerations: An overview of the governing factors and potential challenges, Journal of Environmental Chemical Engineering 10(4) (2022) 108145.

[147] M.A. Gallardo-Sánchez, T. Diaz-Vidal, A.B. Navarro-Hermosillo, E.B. Figueroa-Ochoa, R. Ramirez Casillas, J. Anzaldo Hernández, L.C. Rosales-Rivera, J.F.A. Soltero Martínez, S. García Enríquez, E.R. Macías-Balleza, Optimization of the obtaining of cellulose nanocrystals from agave Tequilana weber var. Azul Bagasse by acid hydrolysis, Nanomaterials 11(2) (2021) 520.

[148] O.M. Vanderfleet, D.A. Osorio, E.D. Cranston, Optimization of cellulose nanocrystal length and surface charge density through phosphoric acid hydrolysis, Philosophical Transactions of the Royal Society A: Mathematical, Physical and Engineering Sciences 376(2112) (2018) 20170041.

[149] O.M. Vanderfleet, E.D. Cranston, Production routes to tailor the performance of cellulose nanocrystals, Nature Reviews Materials 6(2) (2021) 124-144.

[150] H. Sadeghifar, I. Filpponen, S.P. Clarke, D.F. Brougham, D.S. Argyropoulos, Production of cellulose nanocrystals using hydrobromic acid and click reactions on their surface, Journal of materials science 46 (2011) 7344-7355.

[151] S.M. Mohomane, S.V. Motloung, L.F. Koao, T.E. Motaung, Effects of acid hydrolysis on the extraction of cellulose nanocrystals (CNCs): A review, Cellul. Chem. Technol 56 (2022) 691-703.

[152] P. Dhar, S.M. Bhasney, A. Kumar, V. Katiyar, Acid functionalized cellulose nanocrystals and its effect on mechanical, thermal, crystallization and surfaces properties of poly (lactic acid) bionanocomposites films: A comprehensive study, Polymer 101 (2016) 75-92.

[153] L. Thompson, J. Azadmanjiri, M. Nikzad, I. Sbarski, J. Wang, A. Yu, Cellulose nanocrystals: production, functionalization and advanced applications, Reviews on Advanced Materials Science 58(1) (2019) 1-16.

[154] L.P. Novo, J. Bras, A. García, N. Belgacem, A.A. da Silva Curvelo, A study of the production of cellulose nanocrystals through subcritical water hydrolysis, Industrial Crops and Products 93 (2016) 88-95.

[155] M.A. Torlopov, E.V. Udoratina, I.S. Martakov, P.A. Sitnikov, Cellulose nanocrystals prepared in H 3 PW 12 O 40-acetic acid system, Cellulose 24 (2017) 2153-2162.

[156] Y. Liu, H. Wang, G. Yu, Q. Yu, B. Li, X. Mu, A novel approach for the preparation of nanocrystalline cellulose by using phosphotungstic acid, Carbohydrate polymers 110 (2014) 415-422.

[157] H. Du, C. Liu, D. Wang, Y. Zhang, G. Yu, C. Si, B. Li, X. Mu, H. Peng, Sustainable preparation and characterization of thermally stable and functional cellulose nanocrystals and nanofibrils via formic acid hydrolysis, biomedical materials 2 (2017) 4.

[158] L. Chen, J. Zhu, C. Baez, P. Kitin, T. Elder, Highly thermal-stable and functional cellulose nanocrystals and nanofibrils produced using fully recyclable organic acids, Green Chemistry 18(13) (2016) 3835-3843.

[159] W. Xu, H. Grénman, J. Liu, D. Kronlund, B. Li, P. Backman, J. Peltonen, S. Willför, A. Sundberg, C. Xu, Mild Oxalic-Acid-Catalyzed Hydrolysis as a Novel Approach to Prepare Cellulose Nanocrystals, ChemNanoMat 3(2) (2017) 109-119.

[160] J. Miao, Y. Yu, Z. Jiang, L. Zhang, One-pot preparation of hydrophobic cellulose nanocrystals in an ionic liquid, Cellulose 23 (2016) 1209-1219.

[161] H. Abushammala, I. Krossing, M.-P. Laborie, Ionic liquid-mediated technology to produce cellulose nanocrystals directly from wood, Carbohydrate polymers 134 (2015) 609-616.

[162] J.A. Sirvio, M. Visanko, H. Liimatainen, Acidic deep eutectic solvents as hydrolytic media for cellulose nanocrystal production, Biomacromolecules 17(9) (2016) 3025-3032.

[163] Y. Liu, B. Guo, Q. Xia, J. Meng, W. Chen, S. Liu, Q. Wang, Y. Liu, J. Li, H. Yu, Efficient cleavage of strong hydrogen bonds in cotton by deep eutectic solvents and facile fabrication of cellulose nanocrystals in high yields, ACS Sustainable Chemistry & Engineering 5(9) (2017) 7623-7631.

[164] A. Tran, C.E. Boott, M.J. MacLachlan, Understanding the Self-Assembly of Cellulose Nanocrystals—Toward Chiral Photonic Materials, Advanced Materials 32(41) (2020) 1905876.

[165] F.G. Torres, S. Commeaux, O.P. Troncoso, Biocompatibility of bacterial cellulose based biomaterials, Journal of functional biomaterials 3(4) (2012) 864-878.

[166] M. Iguchi, S. Yamanaka, A. Budhiono, Bacterial cellulose—a masterpiece of nature's arts, Journal of materials science 35(2) (2000) 261-270.

[167] M.A. Akhlaghi, R. Bagherpour, H. Kalhori, Application of bacterial nanocellulose fibers as reinforcement in cement composites, Construction and Building Materials 241 (2020) 118061.

[168] K. Ludwicka, M. Kaczmarek, A. Białkowska, Bacterial nanocellulose—A biobased polymer for active and intelligent food packaging applications: Recent advances and developments, Polymers 12(10) (2020) 2209.

[169] H.M. Ávila, E.-M. Feldmann, M.M. Pleumeekers, L. Nimeskern, W. Kuo, W.C. de Jong, S. Schwarz, R. Müller, J. Hendriks, N. Rotter, Novel bilayer bacterial nanocellulose scaffold supports neocartilage formation in vitro and in vivo, Biomaterials 44 (2015) 122-133.

[170] R. Reshmy, E. Philip, D. Thomas, A. Madhavan, R. Sindhu, P. Binod, S. Varjani, M.K. Awasthi, A. Pandey, Bacterial nanocellulose: engineering, production, and applications, Bioengineered 12(2) (2021) 11463.

[171] S. Mateo, S. Peinado, F. Morillas-Gutiérrez, M.D. La Rubia, A.J. Moya, Nanocellulose from agricultural wastes: Products and applications—A review, Processes 9(9) (2021) 1594.

[172] A. Abraham, V.R. Jothi, J. Lee, S.-C. Yi, B.-I. Sang, Bacterial nanocellulose as a green and flexible electrode matrix for efficient hydrogen evolution reaction in alkaline conditions, Cellulose 27 (2020) 8135-8146.

[173] R. Rai, P. Dhar, Biomedical engineering aspects of nanocellulose: A review, Nanotechnology 33(36) (2022) 362001.

[174] S. Tortorella, V. Vetri Buratti, M. Maturi, L. Sambri, M. Comes Franchini, E. Locatelli, Surface-modified nanocellulose for application in biomedical engineering and nanomedicine: A review, International journal of nanomedicine (2020) 9909-9937.

[175] R. Sabo, A. Yermakov, C.T. Law, R. Elhajjar, Nanocellulose-enabled electronics, energy harvesting devices, smart materials and sensors: A review, J. Renew. Mater., 4 (5): 297-312. 4(5) (2016) 297-312.

[176] P. Nizam, D.A. Gopakumar, Y.B. Pottathara, D. Pasquini, A. Nzihou, S. Thomas, Nanocellulose-based composites: fundamentals and applications in electronics, Nanocellulose Based Composites for Electronics, Elsevier2021, pp. 15-29.

[177] M.A. Jenol, M. Norrrahim, N.M. Nurazzi, Nanocellulose nanocomposites in textiles, Industrial applications of nanocellulose and its nanocomposites, Elsevier2022, pp. 397-408.

[178] N. Muhd Julkapli, S. Bagheri, Nanocellulose as a green and sustainable emerging material in energy applications: a review, Polymers for Advanced Technologies 28(12) (2017) 1583-1594.

[179] K. Heise, E. Kontturi, Y. Allahverdiyeva, T. Tammelin, M.B. Linder, Nonappa, O. Ikkala, Nanocellulose: recent fundamental advances and emerging biological and biomimicking applications, Advanced Materials 33(3) (2021) 2004349.

[180] J. Paul, S.S. Ahankari, Nanocellulose-based aerogels for water purification: A review, Carbohydrate Polymers (2023) 120677.

[181] J. Li, K.M. Zuo, W.B. Wu, Z.Y. Xu, Y.G. Yi, Y. Jing, H.Q. Dai, G.G. Fang, Shape memory aerogels from nanocellulose and polyethyleneimine as a novel adsorbent for removal of Cu(II) and Pb(II), Carbohydrate Polymers 196 (2018) 376-384.

[182] J.W. Meng, H. Guan, X.J. Dai, X.Q. Wang, Amino-Functionalized Wood Aerogel for Efficient Removal of Copper Ions from Water, International Journal of Polymer Science 2021 (2021).

[183] K. Köse, M. Mavlan, J.P. Youngblood, Applications and impact of nanocellulose based adsorbents, Cellulose 27(6) (2020) 2967-2990.

[184] A. Qiao, M. Cui, R. Huang, G. Ding, W. Qi, Z. He, J.J. Klemeš, R. Su, Advances in nanocellulose-based materials as adsorbents of heavy metals and dyes, Carbohydr. Polym 272 (2021) 118471.

[185] D. Wang, A critical review of cellulose-based nanomaterials for water purification in industrial processes, Cellulose 26 (2019) 687-701.

[186] A. Singh, J.G. Vijayan, K.G. Moodley, Surface Functionalizations of Nanocellulose for Wastewater Treatment, Handbook of Nanocelluloses: Classification, Properties, Fabrication, and Emerging Applications, Springer2022, pp. 1-48.

[187] P. Liu, K. Oksman, A.P. Mathew, Surface adsorption and self-assembly of Cu (II) ions on TEMPO-oxidized cellulose nanofibers in aqueous media, Journal of colloid and interface science 464 (2016) 175-182.

[188] C. Zhu, I. Dobryden, J. Ryden, S. Öberg, A. Holmgren, A.P. Mathew, Adsorption behavior of cellulose and its derivatives toward Ag (I) in aqueous medium: an AFM, spectroscopic, and DFT study, Langmuir 31(45) (2015) 12390-12400.

[189] L. Riva, A. Fiorati, C. Punta, Synthesis and application of cellulose-polyethyleneimine composites and nanocomposites: A concise review, Materials 14(3) (2021) 473.

[190] L. Melone, B. Rossi, N. Pastori, W. Panzeri, A. Mele, C. Punta, TEMPO-oxidized cellulose cross-linked with branched polyethyleneimine: nanostructured adsorbent sponges for water remediation, ChemPlusChem 80(9) (2015) 1408-1415.

[191] C. Santhosh, V. Velmurugan, G. Jacob, S.K. Jeong, A.N. Grace, A. Bhatnagar, Role of nanomaterials in water treatment applications: A review, Chemical Engineering Journal 306 (2016) 1116-1137.

[192] D.-M. Guo, Q.-D. An, R. Li, Z.-Y. Xiao, S.-R. Zhai, Ultrahigh selective and efficient removal of anionic dyes by recyclable polyethylenimine-modified cellulose aerogels in batch and fixed-bed systems, Colloids and Surfaces A: Physicochemical and Engineering Aspects 555 (2018) 150-160.

[193] X. Chen, L. Liu, Z. Luo, J. Shen, Q. Ni, J. Yao, Facile preparation of a cellulose-based bioadsorbent modified by hPEI in heterogeneous system for high-efficiency removal of multiple types of dyes, React Funct Polym 125 (2018) 77-83.

[194] M.I. Swasy, B.R. Brummel, C. Narangoda, M.F. Attia, J.M. Hawk, F. Alexis, D.C. Whitehead, Degradation of pesticides using amine-functionalized cellulose nanocrystals, RSC advances 10(72) (2020) 44312-44322.

[195] G. Zhu, N. Lin, Surface chemistry of nanocellulose, Nanocellulose: from fundamentals to advanced materials (2019) 115-153.

[196] S.A. Kedzior, J.O. Zoppe, R.M. Berry, E.D. Cranston, Recent advances and an industrial perspective of cellulose nanocrystal functionalization through polymer grafting, Current Opinion in Solid State and Materials Science 23(2) (2019) 74-91.

[197] R.E. Abouzeid, R. Khiari, N. El-Wakil, A. Dufresne, Current state and new trends in the use of cellulose nanomaterials for wastewater treatment, Biomacromolecules 20(2) (2018) 573-597.

[198] A. Tshikovhi, S.B. Mishra, A.K. Mishra, Nanocellulose-based composites for the removal of contaminants from wastewater, International journal of biological macromolecules 152 (2020) 616-632.

[199] M. Mariano, F. Pilate, F.B. de Oliveira, F. Khelifa, P. Dubois, J.-M. Raquez, A. Dufresne, Preparation of cellulose nanocrystal-reinforced poly (lactic acid) nanocomposites through noncovalent modification with PLLA-based surfactants, Acs Omega 2(6) (2017) 2678-2688.

[200] B.L. Tardy, S. Yokota, M. Ago, W. Xiang, T. Kondo, R. Bordes, O.J. Rojas, Nanocellulose–surfactant interactions, Current Opinion in Colloid & Interface Science 29 (2017) 57-67.

[201] L. Liang, S. Bhagia, M. Li, C. Huang, A.J. Ragauskas, Cross-linked nanocellulosic materials and their applications, ChemSusChem 13(1) (2020) 78-87.

[202] I. Capron, O.J. Rojas, R. Bordes, Behavior of nanocelluloses at interfaces, Current Opinion in Colloid & Interface Science 29 (2017) 83-95.

[203] E.M. Ahmed, Hydrogel: Preparation, characterization, and applications: A review, Journal of advanced research 6(2) (2015) 105-121.

[204] P. Heidarian, A. Kaynak, M. Paulino, A. Zolfagharian, R.J. Varley, A.Z. Kouzani, Dynamic nanocellulose hydrogels: Recent advancements and future outlook, Carbohydrate Polymers 270 (2021) 118357.

[205] O. Wichterle, D. Lim, Hydrophilic gels for biological use, Nature 185(4706) (1960) 117-118.

[206] P. Heidarian, A.Z. Kouzani, A. Kaynak, M. Paulino, B. Nasri-Nasrabadi, Dynamic hydrogels and polymers as inks for three-dimensional printing, ACS Biomaterials Science & Engineering 5(6) (2019) 2688-2707.

[207] Y.S. Zhang, A. Khademhosseini, Advances in engineering hydrogels, Science 356(6337) (2017) eaaf3627.

[208] R. Curvello, V.S. Raghuwanshi, G. Garnier, Engineering nanocellulose hydrogels for biomedical applications, Advances in Colloid and Interface Science 267 (2019) 47-61.

[209] P. Heidarian, A.Z. Kouzani, A. Kaynak, M. Paulino, B. Nasri-Nasrabadi, R. Varley, Double dynamic cellulose nanocomposite hydrogels with environmentally adaptive self-healing and pH-tuning properties, Cellulose 27 (2020) 1407-1422.

[210] J. Kang, J.B.-H. Tok, Z. Bao, Self-healing soft electronics, Nature Electronics 2(4) (2019) 144-150.

[211] H. Liu, M. Li, S. Liu, P. Jia, X. Guo, S. Feng, T.J. Lu, H. Yang, F. Li, F. Xu, Spatially modulated stiffness on hydrogels for soft and stretchable integrated electronics, Materials Horizons 7(1) (2020) 203-213.

[212] Q. Chang, M.A. Darabi, Y. Liu, Y. He, W. Zhong, K. Mequanin, B. Li, F. Lu, M.M. Xing, Hydrogels from natural egg white with extraordinary stretchability, direct-writing 3D printability and self-healing for fabrication of electronic sensors and actuators, Journal of Materials Chemistry A 7(42) (2019) 24626-24640.

[213] O.Y. Kweon, S.K. Samanta, Y. Won, J.H. Yoo, J.H. Oh, Stretchable and self-healable conductive hydrogels for wearable multimodal touch sensors with thermoresponsive behavior, ACS applied materials & interfaces 11(29) (2019) 26134-26143.

[214] X. Le, W. Lu, J. Zhang, T. Chen, Recent progress in biomimetic anisotropic hydrogel actuators, Advanced science 6(5) (2019) 1801584.

[215] Y. Wang, Q. Chang, R. Zhan, K. Xu, Y. Wang, X. Zhang, B. Li, G. Luo, M. Xing, W. Zhong, Tough but self-healing and 3D printable hydrogels for E-skin, E-noses and laser controlled actuators, Journal of Materials Chemistry A 7(43) (2019) 24814-24829.

[216] Z. Wu, P. Zhang, H. Zhang, X. Li, Y. He, P. Qin, C. Yang, Tough porous nanocomposite hydrogel for water treatment, Journal of Hazardous Materials 421 (2022) 126754.

[217] D.M. Nascimento, Y.L. Nunes, M.C. Figueirêdo, H.M. de Azeredo, F.A. Aouada, J.P. Feitosa, M.F. Rosa, A. Dufresne, Nanocellulose nanocomposite hydrogels: technological and environmental issues, Green Chemistry 20(11) (2018) 2428-2448.

[218] A. Liu, L. Medina, L.A. Berglund, High-strength nanocomposite aerogels of ternary composition: poly (vinyl alcohol), clay, and cellulose nanofibrils, ACS applied materials & interfaces 9(7) (2017) 6453-6461.

[219] B. Wu, G. Zhu, A. Dufresne, N. Lin, Fluorescent aerogels based on chemical crosslinking between nanocellulose and carbon dots for optical sensor, ACS applied materials & interfaces 11(17) (2019) 16048-16058.

[220] X. Zhang, I. Elsayed, C. Navarathna, G.T. Schueneman, E.B. Hassan, Biohybrid hydrogel and aerogel from self-assembled nanocellulose and nanochitin as a high-efficiency adsorbent for water purification, ACS applied materials & interfaces 11(50) (2019) 46714-46725.

[221] F. Jiang, Y.-L. Hsieh, Super water absorbing and shape memory nanocellulose aerogels from TEMPO-oxidized cellulose nanofibrils via cyclic freezing–thawing, Journal of Materials Chemistry A 2(2) (2014) 350-359.

[222] D. Selianitis, M.-N. Efthymiou, E. Tsouko, A. Papagiannopoulos, A. Koutinas, S. Pispas, Nanocellulose production from different sources and their self-assembly in composite materials,

Handbook of Nanocelluloses: Classification, Properties, Fabrication, and Emerging Applications, Springer2022, pp. 1-32.

[223] Z.I. Kalcioglu, R. Mahmoodian, Y. Hu, Z. Suo, K.J. Van Vliet, From macro-to microscale poroelastic characterization of polymeric hydrogels via indentation, Soft Matter 8(12) (2012) 3393-3398.

[224] C.H. Yang, M.X. Wang, H. Haider, J.H. Yang, J.-Y. Sun, Y.M. Chen, J. Zhou, Z. Suo, Strengthening alginate/polyacrylamide hydrogels using various multivalent cations, ACS applied materials & interfaces 5(21) (2013) 10418-10422.

[225] C. Hou, Q. Zhang, Y. Li, H. Wang, P25–graphene hydrogels: Room-temperature synthesis and application for removal of methylene blue from aqueous solution, Journal of hazardous materials 205 (2012) 229-235.

[226] P. Thoniyot, M.J. Tan, A.A. Karim, D.J. Young, X.J. Loh, Nanoparticle–hydrogel composites: Concept, design, and applications of these promising, multi-functional materials, Advanced Science 2(1-2) (2015) 1400010.

[227] L. Weerasundara, B. Gabriele, A. Figoli, Y.-S. Ok, J. Bundschuh, Hydrogels: Novel materials for contaminant removal in water—A review, Critical Reviews in Environmental Science and Technology 51(17) (2021) 1970-2014.

[228] E. Makhado, S. Pandey, K.D. Modibane, M. Kang, M.J. Hato, Sequestration of methylene blue dye using sodium alginate poly (acrylic acid)@ ZnO hydrogel nanocomposite: kinetic, isotherm, and thermodynamic investigations, International Journal of Biological Macromolecules 162 (2020) 60-73.

[229] C.B. Godiya, L.A.M. Ruotolo, W. Cai, Functional biobased hydrogels for the removal of aqueous hazardous pollutants: current status, challenges, and future perspectives, Journal of Materials Chemistry A 8(41) (2020) 21585-21612.

[230] Z. Wu, X. Chen, B. Yuan, M.-L. Fu, A facile foaming-polymerization strategy to prepare 3D MnO2 modified biochar-based porous hydrogels for efficient removal of Cd (II) and Pb (II), Chemosphere 239 (2020) 124745.

[231] C. Colosi, M. Costantini, A. Barbetta, R. Pecci, R. Bedini, M. Dentini, Morphological comparison of PVA scaffolds obtained by gas foaming and microfluidic foaming techniques, Langmuir 29(1) (2013) 82-91.

[232] D. Wu, F. Xu, B. Sun, R. Fu, H. He, K. Matyjaszewski, Design and preparation of porous polymers, Chemical reviews 112(7) (2012) 3959-4015.

[233] H.T. Nguyen, N.H. Do, H.D. Lac, P.L. Nguyen, P.K. Le, Synthesis, properties, and applications of chitosan hydrogels as anti-inflammatory drug delivery system, Journal of Porous Materials 30(2) (2023) 655-670.

[234] B. Sun, Z. Wang, Q. He, W. Fan, S. Cai, Porous double network gels with high toughness, high stretchability and fast solvent-absorption, Soft matter 13(38) (2017) 6852-6857.

[235] L.E. Nita, A. Ghilan, A.G. Rusu, I. Neamtu, A.P. Chiriac, New trends in bio-based aerogels, Pharmaceutics 12(5) (2020) 449.

[236] L. Zuo, Y. Zhang, L. Zhang, Y.-E. Miao, W. Fan, T. Liu, Polymer/carbon-based hybrid aerogels: preparation, properties and applications, Materials 8(10) (2015) 6806-6848.

[237] P. Wu, B. Zhang, Z. Yu, H. Zou, P. Liu, Anisotropic polyimide aerogels fabricated by directional freezing, Journal of Applied Polymer Science 136(11) (2019) 47179.

[238] C. Simón-Herrero, S. Caminero-Huertas, A. Romero, J.L. Valverde, L. Sánchez-Silva, Effects of freeze-drying conditions on aerogel properties, Journal of Materials Science 51 (2016) 8977-8985.

[239] J.L. Gurav, I.-K. Jung, H.-H. Park, E.S. Kang, D.Y. Nadargi, Silica aerogel: synthesis and applications, Journal of Nanomaterials 2010 (2010) 1-11.

[240] P.L. Yap, M.J. Nine, K. Hassan, T.T. Tung, D.N. Tran, D. Losic, Graphene-based sorbents for multipollutants removal in water: a review of recent progress, Advanced Functional Materials 31(9) (2021) 2007356.

[241] K.V. Kumar, S. Gadipelli, B. Wood, K.A. Ramisetty, A.A. Stewart, C.A. Howard, D.J. Brett, F. Rodriguez-Reinoso, Characterization of the adsorption site energies and heterogeneous surfaces of porous materials, Journal of materials chemistry A 7(17) (2019) 10104-10137.

[242] J.N. Putro, A. Kurniawan, S. Ismadji, Y.-H. Ju, Nanocellulose based biosorbents for wastewater treatment: Study of isotherm, kinetic, thermodynamic and reusability, Environmental Nanotechnology, Monitoring & Management 8 (2017) 134-149.

[243] L. Mo, H. Pang, Y. Tan, S. Zhang, J. Li, 3D multi-wall perforated nanocellulose-based polyethylenimine aerogels for ultrahigh efficient and reversible removal of Cu (II) ions from water, Chem. Eng. J 378(15) (2019) 122157.

[244] S. Chatterjee, W. Ke, Y. Liao, Elastic nanocellulose/graphene aerogel with excellent shape retention and oil absorption selectivity, Taiwan Inst Chem Eng 111 (2020) 261-269.

[245] S. Wu, G. Li, W. Liu, D. Yu, G. Li, X. Liu, Z. Song, H. Wang, H. Liu, Fabrication of polyethyleneimine-paper composites with improved tribopositivity for triboelectric nanogenerators, Nano Energy 93 (2022) 106859.

[246] F. Xie, J. Bao, L. Zhuo, Y. Zhao, W. Dang, L. Si, C. Yao, M. Zhang, Z. Lu, Toward high-performance nanofibrillated cellulose/aramid fibrid paper-based composites via polyethyleneimine-assisted decoration of silica nanoparticle onto aramid fibrid, Carbohydrate polymers 245 (2020) 116610.

[247] H.-W. Chien, M.-Y. Tsai, C.-J. Kuo, C.-L. Lin, Well-dispersed silver nanoparticles on cellulose filter paper for bacterial removal, Nanomaterials 11(3) (2021) 595.

[248] W. Zhang, L. Wang, E. Mäkilä, S. Willför, C. Xu, Ultralight and porous cellulose nanofibers/polyethyleneimine composite aerogels with exceptional performance for selective anionic dye adsorption, Industrial Crops and Products 177 (2022) 114513.

[249] T. Luo, R. Wang, F. Chai, L. Jiang, P. Rao, L. Yan, X. Hu, W. Zhang, L. Wei, A. Khataee, Arsenite (III) removal via manganese-decoration on cellulose nanocrystal-grafted polyethyleneimine nanocomposite, Chemosphere 303 (2022) 134925.

[250] R. Si, C. Wu, D. Yu, Q. Ding, R. Li, Novel TEMPO-oxidized cellulose nanofiber/polyvinyl alcohol/polyethyleneimine nanoparticles for Cu 2+ removal in water, Cellulose 28 (2021) 10999-11011.

[251] L. Mo, Y. Tan, Y. Shen, S. Zhang, Highly compressible nanocellulose aerogels with a cellular structure for high-performance adsorption of Cu (II), Chemosphere 291 (2022) 132887.

[252] Q. Wang, M. Li, Z. Zheng, Y. Niu, X. Xue, C. Ao, W. Zhang, C. Lu, Polyethylenimine-functionalized nanofiber nonwovens electrospun from cotton cellulose for wound dressing with high drug loading and sustained release properties, Polymers 14(9) (2022) 1748.

[253] H. He, M. Cheng, Y. Liang, H. Zhu, Y. Sun, D. Dong, S. Wang, Intelligent cellulose nanofibers with excellent biocompatibility enable sustained antibacterial and drug release via a pH-responsive mechanism, Journal of agricultural and food chemistry 68(11) (2020) 3518-3527.

[254] X. Chen, X. Xu, W. Li, B. Sun, J. Yan, C. Chen, J. Liu, J. Qian, D. Sun, Effective drug carrier based on polyethylenimine-functionalized bacterial cellulose with controllable release properties, ACS Applied Bio Materials 1(1) (2018) 42-50.

[255] N. Li, Y. Wang, Y. Guo, Z. Ji, Z. Zhang, J. Yu, L. Zhang, Surface modified cellulose nanocrystalline hybrids actualizing efficient and precise delivery of doxorubicin into nucleus with: in vitro and in vivo evaluation, Journal of Applied Polymer Science 138(48) (2021) 51536.

[256] J. Wang, Y. Guo, G. Long, Y.L. Tang, Q. Tang, X.-T. Zu, J. Ma, B. Du, H. Torun, Y. Fu, Integrated sensing layer of bacterial cellulose and polyethyleneimine to achieve high sensitivity of ST-cut quartz surface acoustic wave formaldehyde gas sensor, Journal of hazardous materials 388 (2020) 121743.

[257] W. Hu, S. Chen, L. Liu, B. Ding, H. Wang, Formaldehyde sensors based on nanofibrous polyethyleneimine/bacterial cellulose membranes coated quartz crystal microbalance, Sensors and Actuators B: Chemical 157(2) (2011) 554-559.

[258] S. Danwittayakul, P. Muensri, Polyethyleneimine coated polyacrylonitrile cellulose membrane for colorimetric copper (II) determination, Journal of Water Chemistry and Technology 42 (2020) 22-29.

[259] L. Riva, C. Punta, A. Sacchetti, Co-Polymeric Nanosponges from Cellulose Biomass as Heterogeneous Catalysts for amine-catalyzed Organic Reactions, ChemCatChem 12(24) (2020) 6214-6222.

[260] M. Strokal, J.E. Spanier, C. Kroeze, A.A. Koelmans, M. Flörke, W. Franssen, N. Hofstra, S. Langan, T. Tang, M.T. van Vliet, Global multi-pollutant modelling of water quality: scientific challenges and future directions, Current opinion in environmental sustainability 36 (2019) 116-125.

[261] G.N. Hlongwane, P.T. Sekoai, M. Meyyappan, K. Moothi, Simultaneous removal of pollutants from water using nanoparticles: A shift from single pollutant control to multiple pollutant control, Science of The Total Environment 656 (2019) 808-833.

[262] N. Zhang, G.-L. Zang, C. Shi, H.-Q. Yu, G.-P. Sheng, A novel adsorbent TEMPO-mediated oxidized cellulose nanofibrils modified with PEI: Preparation, characterization, and application for Cu (II) removal, Journal of hazardous materials 316 (2016) 11-18.

[263] H. Ge, H. Huang, M. Xu, Q. Chen, Cellulose/poly (ethylene imine) composites as efficient and reusable adsorbents for heavy metal ions, Cellulose 23 (2016) 2527-2537.

[264] C. Liu, R.-N. Jin, X.-k. Ouyang, Y.-G. Wang, Adsorption behavior of carboxylated cellulose nanocrystal—polyethyleneimine composite for removal of Cr (VI) ions, Applied Surface Science 408 (2017) 77-87.

[265] F. Wahid, H. Bai, F.-P. Wang, Y.-Y. Xie, Y.-W. Zhang, L.-Q. Chu, S.-R. Jia, C. Zhong, Facile synthesis of bacterial cellulose and polyethyleneimine based hybrid hydrogels for antibacterial applications, Cellulose 27 (2020) 369-383.

[266] H.-J. Hong, G. Ban, H.S. Kim, H.S. Jeong, M.S. Park, Fabrication of cylindrical 3D cellulose nanofibril (CNF) aerogel for continuous removal of copper (Cu2+) from wastewater, Chemosphere 278 (2021) 130288.

[267] E. Zeiger, B. Gollapudi, P. Spencer, Genetic toxicity and carcinogenicity studies of glutaraldehyde—a review, Mutation Research/Reviews in Mutation Research 589(2) (2005) 136-151.

[268] W. Lawrence, M. Malik, J. Turner, J. Autian, Toxicity profile of epichlorohydrin, Journal of Pharmaceutical Sciences 61(11) (1972) 1712-1717.

[269] J. John, J. Quast, F. Murray, L. Calhoun, R. Staples, Inhalation toxicity of epichlorohydrin: effects on fertility in rats and rabbits, Toxicology and applied pharmacology 68(3) (1983) 415-423.

[270] M. Gan, G. Yang, Z. Wang, X. Sui, Y. Hou, Highly efficient oxidative desulfurization catalyzed by a polyoxometalate/carbonized cellulose nanofiber composite, Energy & Fuels 34(1) (2019) 778-786.

[271] C.X. Tang, P. Brodie, Y.Z. Li, N.J. Grishkewich, M. Brunsting, K.C. Tam, Shape recoverable and mechanically robust cellulose aerogel beads for efficient removal of copper ions, Chemical Engineering Journal 392 (2020).

[272] M. Sohrabi, B.E. Yekta, H.R. Rezaie, M.R. Naimi-Jamal, The influence of 3-glycidyloxypropyl trimethoxysilane on the rheological and in-vitro behavior of injectable composites containing 64S bioactive glass, chitosan, and gelatin, Journal of Applied Polymer Science 138(38) (2021).

[273] R.R. Roesler, K. Danielmeier, Tris-3-(1-aziridino)propionates and their use in formulated products, Progress in Organic Coatings 50(1) (2004) 1-27.

[274] A. Fiorati, G. Turco, A. Travan, E. Caneva, N. Pastori, M. Cametti, C. Punta, L. Melone, Mechanical and Drug Release Properties of Sponges from Cross-linked Cellulose Nanofibers, Chempluschem 82(6) (2017) 848-858.

[275] G. Paladini, V. Venuti, L. Almasy, L. Melone, V. Crupi, D. Majolino, N. Pastori, A. Fiorati, C. Punta, Cross-linked cellulose nano-sponges: a small angle neutron scattering (SANS) study, Cellulose 26(17) (2019) 9005-9019.

[276] G. Paladini, V. Venuti, V. Crupi, D. Majolino, A. Fiorati, C. Punta, FTIR-ATR analysis of the H-bond network of water in branched polyethyleneimine/TEMPO-oxidized cellulose nano-fiber xerogels, Cellulose 27(15) (2020) 8605-8618.

[277] J.M. Zhang, X.F. Zhang, Y.R. Tian, T.Y. Zhong, F.Y. Liu, Novel and wet-resilient cellulose nanofiber cryogels with tunable porosity and improved mechanical strength for methyl orange dyes removal, Journal of Hazardous Materials 416 (2021).

[278] N. Husing, U. Schubert, Aerogels airy materials: Chemistry, structure, and properties, Angewandte Chemie-International Edition 37(1-2) (1998) 23-45.

[279] H.P. Cong, X.C. Ren, P. Wang, S.H. Yu, Macroscopic Multifunctional Graphene-Based Hydrogels and Aerogels by a Metal Ion Induced Self-Assembly Process, Acs Nano 6(3) (2012) 2693-2703.

[280] S. Lombardo, W. Thielemans, Thermodynamics of adsorption on nanocellulose surfaces, Cellulose 26(1) (2019) 249-279.

[281] B. Yan, C.Y. He, S. Chen, L. Xiang, L. Gong, Y.C. Gu, H.B. Zeng, Nanoconfining Cation-pi Interactions as a Modular Strategy to Construct Injectable Self-Healing Hydrogel, Ccs Chemistry 4(8) (2022) 2724-2737.

[282] L. Zhang, X.G. Liu, W.F. Rao, J.F. Li, Multilayer Dye Aggregation at Dye/TiO2 Interface via pi center dot center dot center dot pi Stacking and Hydrogen Bond and Its Impact on Solar Cell Performance: A DFT Analysis, Scientific Reports 6 (2016).

[283] S. Kim, A. Faghihnejad, Y. Lee, Y. Jho, H.B. Zeng, D.S. Hwang, Cation-pi interaction in DOPA-deficient mussel adhesive protein mfp-1, Journal of Materials Chemistry B 3(5) (2015) 738-743.

[284] Q.Y. Lu, D.X. Oh, Y. Lee, Y. Jho, D.S. Hwang, H.B. Zeng, Nanomechanics of Cation Interactions in Aqueous Solution, Angewandte Chemie-International Edition 52(14) (2013) 3944-3948.

[285] D.M. Guo, Q.D. An, Z.Y. Xiao, S.R. Zhai, Z. Shi, Polyethylenimine-functionalized cellulose aerogel beads for efficient dynamic removal of chromium(VI) from aqueous solution, RSC Adv. 7(85) (2017) 54039-54052.

[286] L.L. Hao, N.N. Wang, C. Wang, G.J. Li, Arsenic removal from water and river water by the combined adsorption - UF membrane process, Chemosphere 202 (2018) 768-776.

[287] Z.J. He, H. Song, Y.N. Cui, W.X. Zhu, K.F. Du, S. Yao, Porous Spherical Cellulose Carrier Modified with Polyethyleneimine and Its Adsorption for Cr(III) and Fe(III) from Aqueous Solutions, Chinese Journal of Chemical Engineering 22(9) (2014) 984-990.

[288] A. Fiorati, G. Grassi, A. Graziano, G. Liberatori, N. Pastori, L. Melone, L. Bonciani, L. Pontorno, C. Punta, I. Corsi, Eco-design of nanostructured cellulose sponges for sea-water decontamination from heavy metal ions, Journal of Cleaner Production 246 (2020).

[289] G. Liberatori, G. Grassi, P. Guidi, M. Bernardeschi, A. Fiorati, V. Scarcelli, M. Genovese, C. Faleri, G. Protano, G. Frenzilli, C. Punta, I. Corsi, Effect-Based Approach to Assess Nanostructured Cellulose Sponge Removal Efficacy of Zinc Ions from Seawater to Prevent Ecological Risks, Nanomaterials 10(7) (2020).

[290] X.C. Jin, Z.Y. Xiang, Q.G. Liu, Y. Chen, F.C. Lu, Polyethyleneimine-bacterial cellulose bioadsorbent for effective removal of copper and lead ions from aqueous solution, Bioresource Technology 244 (2017) 844-849.

[291] D. Setyono, S. Valiyaveettil, Functionalized paper-A readily accessible adsorbent for removal of dissolved heavy metal salts and nanoparticles from water, Journal of Hazardous Materials 302 (2016) 120-128.

[292] R.R. Si, Y.H. Chen, D.Q. Wang, D.M. Yu, Q.J. Ding, R.G. Li, C.J. Wu, Nanoarchitectonics for High Adsorption Capacity Carboxymethyl Cellulose Nanofibrils-Based Adsorbents for Efficient Cu2+ Removal, Nanomaterials 12(1) (2022).

[293] X.Y. Xing, W.Q. Li, J. Zhang, H. Wu, Y. Guan, H. Gao, TEMPO-oxidized cellulose hydrogel for efficient adsorption of Cu2+ and Pb2+ modified by polyethyleneimine, Cellulose 28(12) (2021) 7953-7968.

[294] Z.Z. Chu, P.T. Zheng, Y. Yang, C.Y. Wang, Z.H. Yang, Compressible nanowood/polymer composite adsorbents for wastewater purification applications, Composites Science and Technology 198 (2020).

[295] C.Z. Zhang, J.J. Su, H.X. Zhu, J.H. Xiong, X.L. Liu, D.X. Li, Y.M. Chen, Y.H. Li, The removal of heavy metal ions from aqueous solutions by amine functionalized cellulose pretreated with microwave-H2O2, Rsc Advances 7(54) (2017) 34182-34191.

[296] S. Deng, G.S. Zhang, S.W. Chen, Y.N. Xue, Z.L. Du, P. Wang, Rapid and effective preparation of a HPEI modified biosorbent based on cellulose fiber with a microwave irradiation method for enhanced arsenic removal in water, Journal of Materials Chemistry A 4(41) (2016) 15851-15860.

[297] H. Cheng, Y.Z. Li, B.J. Wang, Z.P. Mao, H. Xu, L.P. Zhang, Y. Zhong, X.F. Sui, Chemical crosslinking reinforced flexible cellulose nanofiber-supported cryogel, Cellulose 25(1) (2018) 573-582.

[298] Y.C. Tang, Q.L. Ma, Y.F. Luo, L. Zhai, Y.J. Che, F.J. Meng, Improved synthesis of a branched poly(ethylene imine)-modified cellulose-based adsorbent for removal and recovery of Cu(II) from aqueous solution, Journal of Applied Polymer Science 129(4) (2013) 1799-1805.

[299] J.Q. Wang, X.K. Lu, P.F. Ng, K.I. Lee, B. Fei, J.H. Xin, J.Y. Wu, Polyethylenimine coated bacterial cellulose nanofiber membrane and application as adsorbent and catalyst, Journal of Colloid and Interface Science 440 (2015) 32-38.

[300] M. Ahmad, J.Q. Wang, J. Xu, Q.Y. Zhang, B.L. Zhang, Magnetic tubular carbon nanofibers as efficient Cu(II) ion adsorbent from wastewater, Journal of Cleaner Production 252 (2020).

[301] X.Z. Xu, M.X. Zhang, H. Lv, Y.J. Zhou, Y.Y. Yang, D.G. Yu, Electrospun polyacrylonitrile-based lace nanostructures and their Cu (II) adsorption, Separation and Purification Technology 288 (2022).

[302] Z.A. Sutirman, E.A. Rahim, M.M. Sanagi, K.J. Abd Karim, W.A.W. Ibrahim, New efficient chitosan derivative for Cu(II) ions removal: Characterization and adsorption performance, International Journal of Biological Macromolecules 153 (2020) 513-522.

[303] Y. Kuang, Z.Y. Zhang, D.Y. Wu, Synthesis of graphene oxide/polyethyleneimine sponge and its performance in the sustainable removal of Cu(II) from water, Science of the Total Environment 806 (2022).

[304] S.M. Anush, H.R. Chandan, B.H. Gayathri, Asma, N. Manju, B. Vishalakshi, B. Kalluraya, Graphene oxide functionalized chitosan-magnetite nanocomposite for removal of Cu(II) and Cr(VI) from waste water, International Journal of Biological Macromolecules 164 (2020) 4391-4402.

[305] X.K. Wu, T. Guo, Z.Y. Chen, Z.H. Wang, K. Qin, Z.K. Wang, Z.Q. Ao, C. Yang, D.K. Shen, C.F. Wu, Facile and green preparation of solid carbon nanoonions via catalytic co-pyrolysis of

lignin and polyethylene and their adsorption capability towards Cu(ii), Rsc Advances 12(8) (2022) 5042-5052.

[306] L. Yang, Y.F. Zhan, Y.J. Gong, E.H. Ren, J.W. Lan, R.H. Guo, B. Yan, S. Chen, S.J. Lin, Development of eco-friendly CO2-responsive cellulose nanofibril aerogels as "green" adsorbents for anionic dyes removal, Journal of Hazardous Materials 405 (2021).

[307] W.J. Zhu, L. Liu, Q. Liao, X. Chen, Z.Q. Qian, J.Y. Shen, J.L. Liang, J.M. Yao, Functionalization of cellulose with hyperbranched polyethylenimine for selective dye adsorption and separation, Cellulose 23(6) (2016) 3785-3797.

[308] W. Wang, Q. Bai, T. Liang, H.Y. Bai, X.Y. Liu, Two-Sided Surface Oxidized Cellulose Membranes Modified with PEI: Preparation, Characterization and Application for Dyes Removal, Polymers 9(9) (2017).

[309] T. Anitha, Novel chitosan blended polymers for the removal of Rose Bengal dye: adsorption isotherms, kinetics and mechanism, International Journal of Environment and Waste Management 22(1-4) (2018) 87-110.

[310] V. Vaid, R. Jindal, An efficient pH-responsive kappa-carrageenan/tamarind kernel powder hydrogel for the removal of brilliant green and rose bengal from aqueous solution, Journal of Applied Polymer Science 139(21) (2022).

[311] Y.H. Ding, C.H. Song, W.L. Gong, L. Liu, M.B. Wu, L.D. Li, J.M. Yao, Robust, sustainable, hierarchical multi-porous cellulose beads via pre-crosslinking strategy for efficient dye adsorption, Cellulose 28(11) (2021) 7227-7241.

[312] M.C. Stanciu, M. Nichifor, Influence of dextran hydrogel characteristics on adsorption capacity for anionic dyes, Carbohydrate Polymers 199 (2018) 75-83.

[313] U. Habiba, T.A. Siddique, J.J.L. Lee, T.C. Joo, B.C. Ang, A.M. Afifi, Adsorption study of methyl orange by chitosan/polyvinyl alcohol/zeolite electrospun composite nanofibrous membrane, Carbohydrate Polymers 191 (2018) 79-85.

[314] L.L. Zhai, Z.S. Bai, Y. Zhu, B.J. Wang, W.Q. Luo, Fabrication of chitosan microspheres for efficient adsorption of methyl orange, Chinese Journal of Chemical Engineering 26(3) (2018) 657-666.

[315] C. Karaman, O. Karaman, P.-L. Show, Y. Orooji, H. Karimi-Maleh, Utilization of a double-cross-linked amino-functionalized three-dimensional graphene networks as a monolithic adsorbent for methyl orange removal: equilibrium, kinetics, thermodynamics and artificial neural network modeling, Environmental research 207 (2022) 112156.

[316] R.K. Ibrahim, A. El-Shafie, L.S. Hin, N.S.B. Mohd, M.M. Aljumaily, S. Ibraim, M.A. AlSaadi, A clean approach for functionalized carbon nanotubes by deep eutectic solvents and their performance in the adsorption of methyl orange from aqueous solution, Journal of Environmental Management 235 (2019) 521-534.

[317] Y.Q. Zheng, B. Cheng, W. You, J.G. Yu, W.K. Ho, 3D hierarchical graphene oxide-NiFe LDH composite with enhanced adsorption affinity to Congo red, methyl orange and Cr(VI) ions, Journal of Hazardous Materials 369 (2019) 214-225.

[318] L. Wu, J. Sun, M. Wu, Modified cellulose membrane prepared from corn stalk for adsorption of methyl blue, Cellulose 24 (2017) 5625-5638.

[319] K. Polley, J. Bera, Adsorptive removal of methyl blue dye through magnetically retrievable BaFe12O19-activated charcoal-chitosan composite powder: kinetics, isotherms and thermodynamics studies, International Journal of Environmental Analytical Chemistry (2022) 1-18.

[320] T. Luo, H. Liang, D. Chen, Y. Ma, W. Yang, Highly enhanced adsorption of methyl blue on weakly cross-linked ammonium-functionalized hollow polymer particles, Applied Surface Science 505 (2020) 144607.

[321] D. Li, K. Chai, X. Yao, L. Zhou, K. Wu, Z. Huang, J. Yan, X. Qin, W. Wei, H. Ji, β-Cyclodextrin functionalized SBA-15 via amide linkage as a super adsorbent for rapid removal of methyl blue, Journal of Colloid and Interface Science 583 (2021) 100-112.

[322] W. Konicki, A. Hełminiak, W. Arabczyk, E. Mijowska, Adsorption of cationic dyes onto Fe@ graphite core–shell magnetic nanocomposite: Equilibrium, kinetics and thermodynamics, Chemical Engineering Research and Design 129 (2018) 259-270.

[323] S.K. Mani, R. Bhandari, Microwave-assisted synthesis of self-assembled network of Graphene oxide-Polyethylenimine-Polyvinyl alcohol hydrogel beads for removal of cationic and anionic dyes from wastewater, Journal of Molecular Liquids 345 (2022) 117809.

[324] M.B. Ahmed, J.L. Zhou, H.H. Ngo, W. Guo, N.S. Thomaidis, J. Xu, Progress in the biological and chemical treatment technologies for emerging contaminant removal from wastewater: a critical review, Journal of hazardous materials 323 (2017) 274-298.

[325] Y. Ma, Q. Zhou, A. Li, C. Shuang, Q. Shi, M. Zhang, Preparation of a novel magnetic microporous adsorbent and its adsorption behavior of p-nitrophenol and chlorotetracycline, Journal of Hazardous Materials 266 (2014) 84-93.

[326] M.J. Ahmed, S.K. Theydan, Adsorptive removal of p-nitrophenol on microporous activated carbon by FeCl3 activation: equilibrium and kinetics studies, Desalination and Water Treatment 55(2) (2015) 522-531.

[327] B. Zhang, F. Li, T. Wu, D. Sun, Y. Li, Adsorption of p-nitrophenol from aqueous solutions using nanographite oxide, Colloids and Surfaces A: Physicochemical and Engineering Aspects 464 (2015) 78-88.

[328] Q. Qu, J. Pan, Y. Yin, R. Wu, W. Shi, Y. Yan, X. Dai, Synthesis of macroporous polymer foams via pickering high internal phase emulsions for highly efficient 2, 4, 5-trichlorophenol removal, Journal of Applied Polymer Science 132(6) (2015).

[329] N. Djebri, M. Boutahala, N.-E. Chelali, N. Boukhalfa, Z. Larbi, Adsorption of bisphenol A and 2, 4, 5-trichlorophenol onto organo-acid-activated bentonite from aqueous solutions in single and binary systems, Desalination and Water Treatment 66 (2017) 383-393.

[330] H. Chakhtouna, H. Benzeid, N. Zari, R. Bouhfid, Functional CoFe2O4-modified biochar derived from banana pseudostem as an efficient adsorbent for the removal of amoxicillin from water, Separation and Purification Technology 266 (2021) 118592.

[331] R. Zandipak, S. Sobhanardakani, Novel mesoporous Fe 3 O 4/SiO 2/CTAB–SiO 2 as an effective adsorbent for the removal of amoxicillin and tetracycline from water, Clean technologies and environmental policy 20 (2018) 871-885.

[332] O. Köklükaya, F. Carosio, L. Wågberg, Tailoring flame-retardancy and strength of papers via layer-by-layer treatment of cellulose fibers, Cellulose 25(4) (2018) 2691-2709.

[333] X. Huang, B. Li, S. Wang, X. Yue, Y. Zhengguo, X. Deng, J. Ma, Facile in-situ synthesis of PEI-Pt modified bacterial cellulose bio-adsorbent and its distinctly selective adsorption of anionic dyes, Colloids and Surfaces A: Physicochemical and Engineering Aspects 586 (2020) 124163.

[334] H.-J. Hong, J. Ryu, Synthesis of copper nanoparticles from Cu2+-spiked wastewater via adsorptive separation and subsequent chemical reduction, Nanomaterials 11(8) (2021) 2051.

[335] N. Li, H. Zhang, Y. Xiao, Y. Huang, M. Xu, D. You, W. Lu, J. Yu, Fabrication of cellulose-nanocrystal-based folate targeted nanomedicine via layer-by-layer assembly with lysosomal pH-controlled drug release into the nucleus, Biomacromolecules 20(2) (2019) 937-948.

[336] Y. Jia, H. Yu, Y. Zhang, F. Dong, Z. Li, Cellulose acetate nanofibers coated layer-by-layer with polyethylenimine and graphene oxide on a quartz crystal microbalance for use as a highly sensitive ammonia sensor, Colloids and Surfaces B: Biointerfaces 148 (2016) 263-269.

[337] H.-Y. Mi, X. Jing, Q. Zheng, L. Fang, H.-X. Huang, L.-S. Turng, S. Gong, High-performance flexible triboelectric nanogenerator based on porous aerogels and electrospun nanofibers for energy harvesting and sensitive self-powered sensing, Nano Energy 48 (2018) 327-336.

[338] L. Riva, A.D. Lotito, C. Punta, A. Sacchetti, Zinc-and copper-loaded nanosponges from cellulose nanofibers hydrogels: New heterogeneous catalysts for the synthesis of aromatic acetals, Gels 8(1) (2022) 54.

[339] X.Z. Tang, B. Yu, R.V. Hansen, X. Chen, X. Hu, J. Yang, Grafting low contents of branched polyethylenimine onto carbon fibers to effectively improve their interfacial shear strength with an epoxy matrix, Advanced Materials Interfaces 2(12) (2015) 1500122.

[340] R. Baselt, Encyclopedia of toxicology, Oxford University Press, 2014.

[341] C. Zhang, J. Su, H. Zhu, J. Xiong, X. Liu, D. Li, Y. Chen, Y. Li, The removal of heavy metal ions from aqueous solutions by amine functionalized cellulose pretreated with microwave-H 2 O 2, RSC advances 7(54) (2017) 34182-34191.

[342] L. Mo, H. Pang, Y. Tan, S. Zhang, J. Li, 3D multi-wall perforated nanocellulose-based polyethylenimine aerogels for ultrahigh efficient and reversible removal of Cu (II) ions from water, Chemical Engineering Journal 378 (2019) 122157.

[343] S.S. Lal, S.T. Mhaske, TEMPO-oxidized cellulose nanofiber/kafirin protein thin film crosslinked by Maillard reaction, Cellulose 26 (2019) 6099-6118.

[344] D. Gomez-Maldonado, I. Filpponen, L.S. Johansson, M.N. Waters, I.B. Vega Erramuspe, M.S. Peresin, Environmentally dependent adsorption of 2, 4-dichlorophenol on cellulose-chitosan self-assembled composites, Biopolymers 112(8) (2021) e23434.

[345] J.A. Hernandez, B. Soni, M.C. Iglesias, I.B. Vega Erramuspe, C.E. Frazier, M.S. Peresin, Soybean hull pectin and nanocellulose: tack properties in aqueous pMDI dispersions, Journal of Materials Science 57(8) (2022) 5022-5035.

[346] A. Cassales, P.B. de Souza-Cruz, R. Rech, M.A.Z. Ayub, Optimization of soybean hull acid hydrolysis and its characterization as a potential substrate for bioprocessing, Biomass and bioenergy 35(11) (2011) 4675-4683.

[347] H.-M. Liu, H.-Y. Li, Application and conversion of soybean hulls, Soybean-the basis of yield, biomass and productivity, IntechOpen2017.

[348] M.C. Iglesias, F. Hamade, B. Aksoy, Z. Jiang, V.A. Davis, M.S. Peresin, Correlations between rheological behavior and intrinsic properties of nanofibrillated cellulose from wood and soybean hulls with varying lignin content, BioResources 16(3) (2021) 4831.

[349] P. Lu, Y. Yang, R. Liu, X. Liu, J. Ma, M. Wu, S. Wang, Preparation of sugarcane bagasse nanocellulose hydrogel as a colourimetric freshness indicator for intelligent food packaging, Carbohydrate Polymers 249 (2020) 116831.

[350] T. Saito, M. Hirota, N. Tamura, S. Kimura, H. Fukuzumi, L. Heux, A. Isogai, Individualization of nano-sized plant cellulose fibrils by direct surface carboxylation using TEMPO catalyst under neutral conditions, Biomacromolecules 10(7) (2009) 1992-1996.

[351] A. Salama, N. Shukry, M. El-Sakhawy, Carboxymethyl cellulose-g-poly (2-(dimethylamino) ethyl methacrylate) hydrogel as adsorbent for dye removal, International Journal of Biological Macromolecules 73 (2015) 72-75.

[352] J. Li, K. Zuo, W. Wu, Z. Xu, Y. Yi, Y. Jing, H. Dai, G. Fang, Shape memory aerogels from nanocellulose and polyethyleneimine as a novel adsorbent for removal of Cu (II) and Pb (II), Carbohydrate Polymers 196 (2018) 376-384.

[353] B. Qiu, J. Guo, X. Zhang, D. Sun, H. Gu, Q. Wang, H. Wang, X. Wang, X. Zhang, B.L. Weeks, Polyethylenimine facilitated ethyl cellulose for hexavalent chromium removal with a wide pH range, ACS applied materials & interfaces 6(22) (2014) 19816-19824.

[354] D. Hu, T. Zhang, S. Zhang, J. He, X. Dong, Diffusion of polyethyleneimine with different molecular weights into cotton fibers at low concentration, Cellulose 28 (2021) 3997-4008.

[355] P. Lu, R. Liu, X. Liu, M. Wu, Preparation of self-supporting bagasse cellulose nanofibrils hydrogels induced by zinc ions, Nanomaterials 8(10) (2018) 800.

[356] C. Wang, S. Okubayashi, Polyethyleneimine-crosslinked cellulose aerogel for combustion CO2 capture, Carbohydrate polymers 225 (2019) 115248.

[357] X. Wang, V. Schwartz, J.C. Clark, X. Ma, S.H. Overbury, X. Xu, C. Song, Infrared study of CO2 sorption over “molecular basket” sorbent consisting of polyethylenimine-modified mesoporous molecular sieve, The Journal of Physical Chemistry C 113(17) (2009) 7260-7268.

[358] L. Wang, C. Shi, L. Pan, X. Zhang, J.-J. Zou, Rational design, synthesis, adsorption principles and applications of metal oxide adsorbents: a review, Nanoscale 12(8) (2020) 4790-4815.

[359] N.M. Alves, C. Picart, J.F. Mano, Self assembling and crosslinking of polyelectrolyte multilayer films of chitosan and alginate studied by QCM and IR spectroscopy, Macromolecular bioscience 9(8) (2009) 776-785.

[360] K. Junka, J. Guo, I. Filpponen, J. Laine, O.J. Rojas, Modification of cellulose nanofibrils with luminescent carbon dots, Biomacromolecules 15(3) (2014) 876-881.

[361] Hokkanen, Sanna, Bhatnagar, Amit, Sillanpaa, Mika, Sillanpää, A review on modification methods to cellulose-based adsorbents to improve adsorption capacity, Water Res. 91 (2016) 156-173.

[362] B. Thomas, M.C. Raj, K.B. Athira, M.H. Rubiyah, J. Joy, A. Moores, G.L. Drisko, C. Sanchez, Nanocellulose, a Versatile Green Platform: From Biosources to Materials and Their Applications, Chem. Rev 118(24) (2018) 11575-11625.

[363] A.H. Nordin, S. Wong, N. Ngadi, M. Mohammad Zainol, N.A.F. Abd Latif, W. Nabgan, Surface functionalization of cellulose with polyethyleneimine and magnetic nanoparticles for efficient removal of anionic dye in wastewater, J. Environ. Chem. Eng 9(1) (2021).

[364] S. Liu, Preparation of nanocellulose grafted molecularly imprinted polymer for selective adsorption Pb (II) and Hg (II), Chemosphere (2023) 137832.

[365] J. Xue, E. Zhu, H. Zhu, D. Liu, H. Cai, C. Xiong, Q. Yang, Z. Shi, Dye adsorption performance of nanocellulose beads with different carboxyl group content, Cellulose 30(3) (2023) 1623-1636.

[366] Y. Nan, D. Gomez-Maldonado, M.C. Iglesias, D.C. Whitehead, M.S. Peresin, Valorized soybean hulls as TEMPO-oxidized cellulose nanofibril and polyethylenimine composite hydrogels and their potential removal of water pollutants, Cellulose 30(6) (2023) 3639-3651.

[367] Y. Nan, D. Gomez-Maldonado, D. Whitehead, M. Yang, M.S. Peresin, Comparison between nanocellulose-polyethyleneimine composites synthesis methods towards multiple water pollutants removal: A review, Int. J. Biol. Macromol (2023) 123342.

[368] M.V. Lorevice, P.I. Claro, N.A. Aleixo, L.S. Martins, M.T. Maia, A.P. Oliveira, D.S. Martinez, R.F. Gouveia, Designing 3D fractal morphology of eco-friendly nanocellulose-based composite aerogels for water remediation, Chem. Eng. J 462 (2023) 142166.

[369] C. Zhu, Y. Xia, Y. Zai, Y. Dai, X. Liu, J. Bian, Y. Liu, J. Liu, G. Li, Adsorption and desorption behaviors of HPEI and thermoresponsive HPEI based gels on anionic and cationic dyes, Chem. Eng. J 369 (2019) 863-873.

[370] D. Hu, T. Zhang, S. Zhang, J. He, X. Dong, Diffusion of polyethyleneimine with different molecular weights into cotton fibers at low concentration, Cellulose 28(7) (2021) 3997-4008.

[371] R.R. Pasupuleti, P.C. Tsai, V.K. Ponnusamy, Low-cost disposable Poly(ethyleneimine)-Functionalized Carbon Nanofibers Coated Cellulose Paper as efficient solid phase extraction sorbent material for the extraction of Parahydroxybenzoates from environmental waters, Chemosphere 267 (2021) 129274.

[372] M.A. Al-Ghouti, D.A. Da'ana, Guidelines for the use and interpretation of adsorption isotherm models: A review, J. Hazard. Mater. 393 (2020) 122383.

[373] J. Wang, X. Guo, Adsorption isotherm models: Classification, physical meaning, application and solving method, Chemosphere 258 (2020) 127279.

[374] T. Chen, Z. Zhou, R. Han, R. Meng, H. Wang, W. Lu, Adsorption of cadmium by biochar derived from municipal sewage sludge: impact factors and adsorption mechanism, Chemosphere 134 (2015) 286-293.

[375] D. Li, K. Chai, X. Yao, L. Zhou, K. Wu, Z. Huang, J. Yan, X. Qin, W. Wei, H. Ji, β-Cyclodextrin functionalized SBA-15 via amide linkage as a super adsorbent for rapid removal of methyl blue, 583 (2020) 100-112.

[376] S. Xie, Y. Yang, W. Gai, Z. Deng, Oxide modified aluminum for removal of methyl orange and methyl blue in aqueous solution, RSC Advances 11(2) (2021) 867-875.

[377] Y. Shu, Y. Shao, X. Wei, X. Wang, Q. Sun, Q. Zhang, L. Li, Synthesis and characterization of Ni-MCM-41 for methyl blue adsorption, Microporous Mesoporous Mater. 214 (2015) 88-94.

[378] M.-X. Huo, Y.-L. Jin, Z.-F. Sun, F. Ren, L. Pei, P.-G.J.C.p. Ren, Facile synthesis of chitosan-based acid-resistant composite films for efficient selective adsorption properties towards anionic dyes, 254 (2021) 117473.

[379] C. Liu, R.-N. Jin, X.-k. Ouyang, Y.-G.J.A.S.S. Wang, Adsorption behavior of carboxylated cellulose nanocrystal—polyethyleneimine composite for removal of Cr (VI) ions, 408 (2017) 77-87.

[380] C. Tang, P. Brodie, Y. Li, N.J. Grishkewich, M. Brunsting, K.C. Tam, Shape recoverable and mechanically robust cellulose aerogel beads for efficient removal of copper ions, Chem. Eng. J 392 (2020).

[381] D.-M. Guo, Q.-D. An, Z.-Y. Xiao, S.-R. Zhai, Z.J.R.a. Shi, Polyethylenimine-functionalized cellulose aerogel beads for efficient dynamic removal of chromium (VI) from aqueous solution, 7(85) (2017) 54039-54052.

[382] L. Wu, J. Sun, M.J.C. Wu, Modified cellulose membrane prepared from corn stalk for adsorption of methyl blue, 24(12) (2017) 5625-5638.

[383] L. Yang, Y. Zhan, Y. Gong, E. Ren, J. Lan, R. Guo, B. Yan, S. Chen, S. Lin, Development of eco-friendly CO_2-responsive cellulose nanofibril aerogels as "green" adsorbents for anionic dyes removal, J. Hazard. Mater. 405 (2021) 124194.

[384] K. Polley, R. Kundu, J. Bera, Adsorption and sunlight-induced photocatalytic degradation of methyl blue by $BaFe_{12}O_{19}$ ferrite particles synthesised through co-precipitation method, Int J Environ Anal Chem (2021) 2038-2057.

[385] T. Luo, H. Liang, D. Chen, Y. Ma, W. Yang, Highly enhanced adsorption of methyl blue on weakly cross-linked ammonium-functionalized hollow polymer particles, Appl. Surf. Sci 505 (2020) 144607.

[386] A.S. Elsherbiny, M.E. El-Hefnawy, A.H. Gemeay, Linker impact on the adsorption capacity of polyaspartate/montmorillonite composites towards methyl blue removal, Chem. Eng. J 315 (2017) 142-151.

[387] W. Cheng, F. Rechberger, M. Niederberger, Three-dimensional assembly of yttrium oxide nanosheets into luminescent aerogel monoliths with outstanding adsorption properties, ACS nano 10(2) (2016) 2467-2475.

[388] B. Yan, C. He, S. Chen, L. Xiang, L. Gong, Y. Gu, H. Zeng, Nanoconfining cation-π interactions as a modular strategy to construct injectable self-healing hydrogel, CCS Chemistry 4(8) (2022) 2724-2737.

[389] L. Zhang, X. Liu, W. Rao, J. Li, Multilayer dye aggregation at dye/TiO2 interface via π… π stacking and hydrogen bond and its impact on solar cell performance: a DFT analysis, Scientific reports 6(1) (2016) 35893.

[390] S. Kim, A. Faghihnejad, Y. Lee, Y. Jho, H. Zeng, D.S. Hwang, Cation–π interaction in DOPA-deficient mussel adhesive protein mfp-1, J Mater Chem B 3(5) (2015) 738-743.

[391] Q. Lu, D.X. Oh, Y. Lee, Y. Jho, D.S. Hwang, H. Zeng, Nanomechanics of cation–π interactions in aqueous solution, Angew. Chem. 125(14) (2013) 4036-4040.

[392] S. Wong, H.H. Tumari, N. Ngadi, N.B. Mohamed, O. Hassan, R. Mat, N.A.S. Amin, Adsorption of anionic dyes on spent tea leaves modified with polyethyleneimine (PEI-STL), J. Clean. Prod 206 (2019) 394-406.

[393] J.D. Sheehan, E. Ebikade, D.G. Vlachos, R.F. Lobo, Lignin-Based Water-Soluble Polymers Exhibiting Biodegradability and Activity as Flocculating Agents, ACS Sustain. Chem. Eng. 10(34) (2022) 11117-11129.

[394] J. Sirviö, A. Honka, H. Liimatainen, J. Niinimäki, O. Hormi, Synthesis of highly cationic water-soluble cellulose derivative and its potential as novel biopolymeric flocculation agent, Carbohydr. Polym 86(1) (2011) 266-270.

[395] M. Zhu, L. Lee, H. Wang, Z. Wang, Removal of an anionic dye by adsorption/precipitation processes using alkaline white mud, J. Hazard. Mater. 149(3) (2007) 735-741.

[396] K. Lin, M. Qin, X. Geng, L. Wang, H. Wu, $ZnCo_2O_4$ nanorods as a novel class of high-performance adsorbent for removal of methyl blue, Adv Powder Technol 29(8) (2018) 1933-1939.

[397] T. Shirafuji, J. Hieda, O. Takai, N. Saito, T. Morita, O. Sakai, K. Tachibana, FTIR study of methylene blue plasma degradation products through plasma treatment on water, TENCON 2010-2010 IEEE Region 10 Conference, IEEE, 2010, pp. 1938-1942.

[398] R. Chen, J. Yu, W. Xiao, Hierarchically porous MnO_2 microspheres with enhanced adsorption performance, J. Mater. Chem. A 1(38) (2013) 11682-11690.

[399] R. Reshmy, E. Philip, A. Madhavan, A. Pugazhendhi, R. Sindhu, R. Sirohi, M.K. Awasthi, A. Pandey, P. Binod, Nanocellulose as green material for remediation of hazardous heavy metal contaminants, J. Hazard. Mater. 424 (2022) 127516.

[400] H. Wu, L.T. Tufa, J. Kwon, Y. Choi, J.B. Lee, Facile one-pot synthesis of polyethyleneimine functionalized alpha-FeOOH nanoraft consisted of single-layer parallel-aligned ultrathin nanowires for efficient removal of Cr (VI): Synergy of reduction and adsorption, Science of the Total Environment 857 (2023).

[401] Y. Kim, J. Bang, J. Kim, J.H. Choi, S.W. Hwang, H. Yeo, I.G. Choi, H.J. Jin, H.W. Kwak, Cationic surface-modified regenerated nanocellulose hydrogel for efficient Cr(VI) remediation, Carbohydrate Polymers 278 (2022).

[402] W.H. Zhang, L.Y. Wang, E. Makila, S. Willfor, C.L. Xu, Ultralight and porous cellulose nanofibers/polyethyleneimine composite aerogels with exceptional performance for selective anionic dye adsorption, Industrial Crops and Products 177 (2022).

[403] X.Y. Wang, P.B. Xie, L. He, Y.W. Liang, L. Zhang, Y.Y. Miao, Z.B. Liu, Ultralight, Mechanically Enhanced, and Thermally Improved Graphene-Cellulose-Polyethyleneimine Aerogels for the Adsorption of Anionic and Cationic Dyes, Nanomaterials 12(10) (2022).

[404] Y.Y. Fang, H. He, K.Q. Dong, J.S. Yang, Z.Y. Qin, Preparation and adsorption properties of hyperbranched polyethyleneimine-cellulose nanofiber aerogel, New Journal of Chemistry 46(13) (2022) 5954-5965.

[405] N. Li, H. Zhang, Y. Xiao, Y.S. Huang, M.D. Xu, D.L. You, W. Lu, J.H. Yu, Fabrication of Cellulose-Nanocrystal-Based Folate Targeted Nanomedicine via Layer-by-Layer Assembly with Lysosomal pH-Controlled Drug Release into the Nucleus, Biomacromolecules 20(2) (2019) 937-948.

[406] Q.H. Wang, M. Li, Z. Zheng, Y. Niu, X.L. Xue, C.H. Ao, W. Zhang, C.H. Lu, Polyethylenimine-Functionalized Nanofiber Nonwovens Electrospun from Cotton Cellulose for

Wound Dressing with High Drug Loading and Sustained Release Properties, Polymers 14(9) (2022).

[407] Y.Y. Liu, Q. Fan, Y. Huo, M. Li, H.B. Liu, B. Li, Construction of nanocellulose-based composite hydrogel with a double packing structure as an intelligent drug carrier, Cellulose 28(11) (2021) 6953-6966.

[408] H. He, M.X. Cheng, Y.T. Liang, H.X. Zhu, Y.P. Sun, D. Dong, S.F. Wang, Intelligent Cellulose Nanofibers with Excellent Biocompatibility Enable Sustained Antibacterial and Drug Release via a pH-Responsive Mechanism, Journal of Agricultural and Food Chemistry 68(11) (2020) 3518-3527.

[409] S.W. Wang, Z.Y. Yu, Y.M. He, C. Li, L.L. Wang, M.H. Wu, A fabric-based electrode for wearable piezoelectric nanogenerators to distinguish sense human motions, Applied Surface Science 610 (2023).

[410] Y.Q. Li, Q. Gong, L. Han, X.H. Liu, Y. Yang, C. Chen, C.H. Qian, Q.S. Han, Carboxymethyl cellulose assisted polyaniline in conductive hydrogels for high-performance self-powered strain sensors, Carbohydrate Polymers 298 (2022).

[411] L. Riva, C. Punta, A. Sacchetti, Co-Polymeric Nanosponges from Cellulose Biomass as Heterogeneous Catalysts for amine-catalyzed Organic Reactions, Chemcatchem 12(24) (2020) 6214-6222.

[412] L. Riva, A.D. Lotito, C. Punta, A. Sacchetti, Zinc- and Copper-Loaded Nanosponges from Cellulose Nanofibers Hydrogels: New Heterogeneous Catalysts for the Synthesis of Aromatic Acetals, Gels 8(1) (2022).

[413] L. Riva, G. Nicastro, M.C. Liu, C. Battocchio, C. Punta, A. Sacchetti, Pd-Loaded Cellulose NanoSponge as a Heterogeneous Catalyst for Suzuki-Miyaura Coupling Reactions, Gels 8(12) (2022).

[414] Y. Nan, D. Gomez-Maldonado, D. Whitehead, M. Yang, M.S. Peresin, Comparison between nanocellulose-polyethyleneimine composites synthesis methods towards multiple water pollutants removal: A review, International Journal of Biological Macromolecules 232 (2023) 123342.

[415] C. Liu, R.N. Jin, X.K. Ouyang, Y.G. Wang, Adsorption behavior of carboxylated cellulose nanocrystal-polyethyleneimine composite for removal of Cr(VI) ions, Applied Surface Science 408 (2017) 77-87.

[416] S. Chatterjee, W.-T. Ke, Y.-C. Liao, Elastic nanocellulose/graphene aerogel with excellent shape retention and oil absorption selectivity, Journal of the Taiwan Institute of Chemical Engineers 111 (2020) 261-269.

[417] Y. Nan, D. Gomez-Maldonado, D. Whitehead, M. Yang, M.S. Peresin, Comparison between nanocellulose-polyethyleneimine composites synthesis methods towards multiple water pollutants removal: A review, International Journal of Biological Macromolecules (2023) 123342.

[418] B.I. Escher, H.M. Stapleton, E.L. Schymanski, Tracking complex mixtures of chemicals in our changing environment, Science 367(6476) (2020) 388-392.

[419] P.J. Landrigan, J.J. Stegeman, L.E. Fleming, D. Allemand, D.M. Anderson, L.C. Backer, F. Brucker-Davis, N. Chevalier, L. Corra, D. Czerucka, Human health and ocean pollution, Annals of global health 86(1) (2020).

[420] G.N. Hlongwane, P.T. Sekoai, M. Meyyappan, K.J.S.o.T.T.E. Moothi, Simultaneous removal of pollutants from water using nanoparticles: A shift from single pollutant control to multiple pollutant control, 656 (2019) 808-833.

[421] X. Zheng, W. Sun, A. Li, B. Wang, R. Jiang, Z. Song, Y. Zhang, Z. Li, Graphene oxide and polyethyleneimine cooperative construct ionic imprinted cellulose nanocrystal aerogel for selective adsorption of Dy(III), Cellulose 29(1) (2021) 469-481.

[422] F. Jiang, W. Zhao, Y. Wu, Y. Wu, G. Liu, J. Dong, K. Zhou, A polyethyleneimine-grafted graphene oxide hybrid nanomaterial: Synthesis and anti-corrosion applications, Applied Surface Science 479 (2019) 963-973.

[423] X. Qiu, X. Wang, S. Chen, A stable and easily regenerable solid amine adsorbent derived from a polyethylenimine-impregnated dialdehyde-cellulose/graphene-oxide composite, New Journal of Chemistry 46(15) (2022) 6956-6965.

[424] F. Arshad, M. Selvaraj, J. Zain, F. Banat, M.A. Haija, Polyethylenimine modified graphene oxide hydrogel composite as an efficient adsorbent for heavy metal ions, Separation and Purification Technology 209 (2019) 870-880.

[425] H. Dong, J.F. Snyder, K.S. Williams, J.W.B. Andzelm, Cation-induced hydrogels of cellulose nanofibrils with tunable moduli, 14(9) (2013) 3338-3345.

[426] J. Geng, Y. Yin, Q. Liang, Z. Zhu, H. Luo, Polyethyleneimine cross-linked graphene oxide for removing hazardous hexavalent chromium: Adsorption performance and mechanism, Chemical Engineering Journal 361 (2019) 1497-1510.

[427] E. Aliyari, M. Alvand, F. Shemirani, Modified surface-active ionic liquid-coated magnetic graphene oxide as a new magnetic solid phase extraction sorbent for preconcentration of trace nickel, Rsc Advances 6(69) (2016) 64193-64202.

[428] S. Nikkhah, H. Tahermansouri, F. Chekin, Synthesis, characterization, and electrochemical properties of the modified graphene oxide with 4, 4′-methylenedianiline, Materials Letters 211 (2018) 323-327.

[429] J. Mondal, S.K. Srivastava, δ-MnO2 nanoflowers and their reduced graphene oxide nanocomposites for electromagnetic interference shielding, ACS Applied Nano Materials 3(11) (2020) 11048-11059.

[430] N. Sharma, V. Sharma, Y. Jain, M. Kumari, R. Gupta, S. Sharma, K. Sachdev, Synthesis and characterization of graphene oxide (GO) and reduced graphene oxide (rGO) for gas sensing application, Macromolecular Symposia, Wiley Online Library, 2017, p. 1700006.

[431] S. Chaiyakun, N. Witit-Anun, N. Nuntawong, P. Chindaudom, S. Oaew, C. Kedkeaw, P.J.P.E. Limsuwan, Preparation and characterization of graphene oxide nanosheets, 32 (2012) 759-764.

[432] S. Ruiz, J.A. Tamayo, J. Delgado Ospina, D.P. Navia Porras, M.E. Valencia Zapata, J.H. Mina Hernandez, C.H. Valencia, F. Zuluaga, C.D. Grande Tovar, Antimicrobial films based on nanocomposites of chitosan/poly (vinyl alcohol)/graphene oxide for biomedical applications, Biomolecules 9(3) (2019) 109.

[433] A.P. Papavlu, V. Dinca, M. Filipescu, M. Dinescu, Matrix-assisted pulsed laser evaporation of organic thin gilms: Applications in biology and chemical sensors, Laser Ablation—From Fundamentals to Applications; Itina, TE, Ed.; InTech: Rijeka, Croatia (2017) 171-189.

[434] Y. Pang, G. Zeng, L. Tang, Y. Zhang, Y. Liu, X. Lei, Z. Li, J. Zhang, G. Xie, PEI-grafted magnetic porous powder for highly effective adsorption of heavy metal ions, Desalination 281 (2011) 278-284.

[435] P. Ding, S. Su, N. Song, S. Tang, Y. Liu, L. Shi, Influence on thermal conductivity of polyamide-6 covalently-grafted graphene nanocomposites: varied grafting-structures by controllable macromolecular length, Rsc Advances 4(36) (2014) 18782-18791.

[436] Y. Yu, Y. Liang, Y. Zhang, Z. Xie, J. Chen, Z. Zheng, J. Kang, F. Yang, Y. Cao, M. Xiang, Characterizations and performances of polysulfone/graphene oxide with structural defects repaired by cellulose nanocrystals, Polymer Composites 43(6) (2022) 3446-3456.

[437] H. Liu, J. Guo, Y. Zhou, J. Qian, Preparation and Adsorption Performance of Efficient Adsorbent for Heavy Metal Copper (II) Using Graphene-Oxide-Based Composites, ChemistrySelect 5(36) (2020) 11354-11360.

[438] F. Arshad, M. Selvaraj, J. Zain, F. Banat, M.A.J.S. Haija, P. Technology, Polyethylenimine modified graphene oxide hydrogel composite as an efficient adsorbent for heavy metal ions, 209 (2019) 870-880.

[439] V. Bruder, T. Ludwig, S. Opitz, R. Christoffels, T. Fischer, H. Maleki, Hierarchical Assembly of Surface Modified Silk Fibroin Biomass into Micro-, and Milli-Metric Hybrid Aerogels with Core-Shell, Janus, and Composite Configurations for Rapid Removal of Water Pollutants, Advanced Materials Interfaces 8(5) (2021) 2001892.

[440] V.T. Nguyen, L.Q. Ha, T.D. Nguyen, P.H. Ly, D.M. Nguyen, D. Hoang, Nanocellulose and graphene oxide aerogels for adsorption and removal methylene blue from an aqueous environment, ACS omega 7(1) (2021) 1003-1013.

[441] A. Pal, A. Kondor, S. Mitra, K. Thu, S. Harish, B.B. Saha, On surface energy and acid–base properties of highly porous parent and surface treated activated carbons using inverse gas chromatography, Journal of industrial and engineering chemistry 69 (2019) 432-443.

[442] Z. Yao, L. Ge, W. Yang, M. Xia, X. Ji, M. Jin, J. Tang, J.r. Dienstmaier, Finite dilution inverse gas chromatography as a versatile tool to determine the surface properties of biofillers for plastic composite applications, Analytical chemistry 87(13) (2015) 6724-6729.

[443] I.A. Sacui, R.C. Nieuwendaal, D.J. Burnett, S.J. Stranick, M. Jorfi, C. Weder, E.J. Foster, R.T. Olsson, J.W. Gilman, Comparison of the properties of cellulose nanocrystals and cellulose nanofibrils isolated from bacteria, tunicate, and wood processed using acid, enzymatic, mechanical, and oxidative methods, ACS applied materials & interfaces 6(9) (2014) 6127-6138.

[444] P.V. Kelly, S. Shams Es-haghi, M.E. Lamm, K. Copenhaver, S. Ozcan, D.J. Gardner, W.M. Gramlich, Polymer-Grafted Cellulose Nanofibrils with Enhanced Interfacial Compatibility for Stronger Poly (lactic acid) Composites, ACS Applied Polymer Materials 5(5) (2023) 3661-3676.

[445] W. Bai, H. Yu, L. Liu, E. Pakdel, B. Tang, H. Su, C. Hurren, L. Liu, J. Wang, X. Wang, The adsorption kinetics and mechanism of odorous gases onto textile fibers, RSC Sustainability 1(2) (2023) 357-367.

[446] Y.N. Hwang, H. Kim, Y. Lee, S.-C. Park, Evolution of the surface energy of BaTiO3 nanoparticles in the course of dispersant coating; An inverse gas chromatography study, Colloids and Surfaces A: Physicochemical and Engineering Aspects (2023) 131888.

[447] J. Wang, Functionalization of Graphene Oxide with Polysilicone: Synthesis, Characterization, and Its Flame Retardancy in Epoxy Resin, Polymers 13(21) (2021) 3857.

[448] H. Ruomeng, J. Ying, L. Xiaomeng, H. Yuanzheng, S. Keke, Adsorption and photocatalytic degradation of gas-phase UDMH under simulated sunlight by AgBr/TiO 2/rGA, RSC advances 11(21) (2021) 12583-12594.

[449] J.V.D. Perez, E.T. Nadres, H.N. Nguyen, M.L.P. Dalida, D.F. Rodrigues, Response surface methodology as a powerful tool to optimize the synthesis of polymer-based graphene oxide nanocomposites for simultaneous removal of cationic and anionic heavy metal contaminants, RSC advances 7(30) (2017) 18480-18490.

[450] C. Tang, P. Brodie, Y. Li, N.J. Grishkewich, M. Brunsting, K.C.J.C.E.J. Tam, Shape recoverable and mechanically robust cellulose aerogel beads for efficient removal of copper ions, 392 (2020) 124821.

[451] H.B. Slama, A. Chenari Bouket, Z. Pourhassan, F.N. Alenezi, A. Silini, H. Cherif-Silini, T. Oszako, L. Luptakova, P. Golińska, L. Belbahri, Diversity of synthetic dyes from textile industries, discharge impacts and treatment methods, Applied Sciences 11(14) (2021) 6255.

[452] S.K. Sen, S. Raut, S. Raut, Mycoremediation of anthraquinone dyes from textile industries: a mini-review, BioTechnologia 104(1) (2023) 85.

[453] H. Liu, S. Yang, Y. Ni, Comparison of dye behavior from aspen HYP: Dyes added in the HYP manufacturing process versus dyes added at the papermaking wet end, Journal of wood chemistry and technology 30(2) (2010) 118-128.

[454] Z. Liu, T.A. Khan, M.A. Islam, U. Tabrez, A review on the treatment of dyes in printing and dyeing wastewater by plant biomass carbon, Bioresource Technology 354 (2022) 127168.

[455] E. Guerra, M. Llompart, C. Garcia-Jares, Analysis of dyes in cosmetics: challenges and recent developments, Cosmetics 5(3) (2018) 47.

[456] S. Kobylewski, M.F. Jacobson, Toxicology of food dyes, International journal of occupational and environmental health 18(3) (2012) 220-246.

[457] A. Ahmad, S.H. Mohd-Setapar, C.S. Chuong, A. Khatoon, W.A. Wani, R. Kumar, M. Rafatullah, Recent advances in new generation dye removal technologies: novel search for approaches to reprocess wastewater, RSC advances 5(39) (2015) 30801-30818.

[458] J. Sharma, S. Sharma, V. Soni, Classification and impact of synthetic textile dyes on Aquatic Flora: A review, Regional Studies in Marine Science 45 (2021) 101802.

[459] C.B. Godiya, Y. Xiao, X. Lu, Amine functionalized sodium alginate hydrogel for efficient and rapid removal of methyl blue in water, International journal of biological macromolecules 144 (2020) 671-681.

[460] H. Zhu, E. Zhu, Y. Xie, D. Liu, Y. Hu, Z. Shi, C. Xiong, Q. Yang, Hydrangea-like nanocellulose microspheres with high dye adsorption and drug encapsulation prepared by emulsion method, Carbohydrate Polymers 296 (2022) 119947.

[461] K. Jain, A.S. Patel, V.P. Pardhi, S.J.S. Flora, Nanotechnology in wastewater management: a new paradigm towards wastewater treatment, Molecules 26(6) (2021) 1797.

[462] V.K. Upadhyayula, S. Deng, M.C. Mitchell, G.B. Smith, Application of carbon nanotube technology for removal of contaminants in drinking water: a review, Science of the total environment 408(1) (2009) 1-13.

[463] J.H. Chung, N. Hasyimah, N. Hussein, Application of carbon nanotubes (CNTs) for remediation of emerging pollutants-a review, Tropical Aquatic and Soil Pollution 2(1) (2022) 13-26.

[464] X. Pan, J. Ji, N. Zhang, M. Xing, Research progress of graphene-based nanomaterials for the environmental remediation, Chinese Chemical Letters 31(6) (2020) 1462-1473.

[465] X. Wang, R. Yin, L. Zeng, M. Zhu, A review of graphene-based nanomaterials for removal of antibiotics from aqueous environments, Environmental Pollution 253 (2019) 100-110.

[466] M.S. Bichave, A.Y. Kature, S.V. Koranne, R.S. Shinde, A.S. Gongle, V.P. Choudhari, N.S. Topare, S. Raut-Jadhav, S.A. Bokil, Nano-metal oxides-activated carbons for dyes removal: A review, Materials Today: Proceedings 77 (2023) 19-30.

[467] M. Hua, S. Zhang, B. Pan, W. Zhang, L. Lv, Q. Zhang, Heavy metal removal from water/wastewater by nanosized metal oxides: a review, Journal of hazardous materials 211 (2012) 317-331.

[468] A.M. Abdelfatah, M. Fawzy, A.S. Eltaweil, M.E. El-Khouly, Green synthesis of nano-zero-valent iron using ricinus communis seeds extract: Characterization and application in the treatment of methylene blue-polluted water, ACS omega 6(39) (2021) 25397-25411.

[469] H.N. Banavath, N.K. Bhardwaj, A. Ray, A comparative study of the effect of refining on charge of various pulps, Bioresource Technology 102(6) (2011) 4544-4551.

[470] R.K. Mishra, A. Sabu, S.K. Tiwari, Materials chemistry and the futurist eco-friendly applications of nanocellulose: Status and prospect, Journal of Saudi Chemical Society 22(8) (2018) 949-978.

[471] H. Qiao, Y. Zhou, F. Yu, E. Wang, Y. Min, Q. Huang, L. Pang, T. Ma, Effective removal of cationic dyes using carboxylate-functionalized cellulose nanocrystals, Chemosphere 141 (2015) 297-303.

[472] R. Batmaz, N. Mohammed, M. Zaman, G. Minhas, R.M. Berry, K.C. Tam, Cellulose nanocrystals as promising adsorbents for the removal of cationic dyes, Cellulose 21 (2014) 1655-1665.

[473] X. He, K.B. Male, P.N. Nesterenko, D. Brabazon, B. Paull, J.H. Luong, Adsorption and desorption of methylene blue on porous carbon monoliths and nanocrystalline cellulose, ACS Applied Materials & Interfaces 5(17) (2013) 8796-8804.

[474] D. Wang, H. Yu, X. Fan, J. Gu, S. Ye, J. Yao, Q. Ni, High aspect ratio carboxylated cellulose nanofibers cross-linked to robust aerogels for superabsorption–flocculants: paving way from nanoscale to macroscale, ACS applied materials & interfaces 10(24) (2018) 20755-20766.

[475] X. Yang, H. Liu, F. Han, S. Jiang, L. Liu, Z. Xia, Fabrication of cellulose nanocrystal from Carex meyeriana Kunth and its application in the adsorption of methylene blue, Carbohydrate polymers 175 (2017) 464-472.

[476] H. Wang, J.J. Zhu, Q. Ma, U.P. Agarwal, R. Gleisner, R. Reiner, C. Baez, J. Zhu, Pilot-scale production of cellulosic nanowhiskers with similar morphology to cellulose nanocrystals, Frontiers in Bioengineering and Biotechnology 8 (2020) 565084.

[477] P.M.M. da Silva, N.G. Camparotto, T.F. Neves, V.R. Mastelaro, B. Nunes, C.S.F. Picone, P. Prediger, Instantaneous adsorption and synergic effect in simultaneous removal of complex dyes through nanocellulose/graphene oxide nanocomposites: Batch, fixed-bed experiments and mechanism, Environmental Nanotechnology, Monitoring & Management 16 (2021) 100584.